GEOLOGICAL AND GEOCHEMICAL STUDIES OF THE GOLD-BEARING QUARTZ-FUCHSITE VEIN AT THE DOME MINE, TIMMINS AREA

By

ROBERT PETER MORITZ

Lic. ès Sc. Terre, Ing.-Géol. Dipl.

A Thesis
Submitted to the School of Graduate Studies
in Partial Fulfilment of the Requirements
for the Degree
Doctor of Philosophy

McMaster University
September 1988

GENESIS OF A GOLD-BEARING QUARTZ-FUCHSITE VEIN,
DOME MINE, TIMMINS

DOCTOR OF PHILOSOPHY (1988) McMASTER UNIVERSITY

(Geology) Hamilton, Ontario

TITLE:	Geological and Geochemical Studies of the Gold-Bearing Quartz-Fuchsite Vein at the Dome Mine, Timmins Area
AUTHOR:	Robert Peter Moritz Licence ès Sciences de la Terre (Université de Genève, Suisse) Diplôme d'Ingénieur-Géologue (Université de Genève, Suisse)
SUPERVISOR:	Dr. J.H. Crocket
NUMBER OF PAGES:	xviii, 280

ABSTRACT

The Quartz-Fuchsite vein at the Dome Mine, Timmins area, has been the subject of an integrated field, petrographic, geochemical, and fluid inclusion study to characterize the site and the cause of ore deposition, and to establish the source of ore components in Archean lode gold deposits.

The vein lies in a zone of carbonatized komatiites at the contact with a unit of slates. The wall rock alteration that accompanied ore genesis is centered around a porphyry lens located in the zone of carbonatized rocks. The location of the Quartz-Fuchsite vein is coincident with the outer rim of the alteration envelop.

A high pore fluid regime that developed in the carbonatized komatiites in proximity to the slates resulted in hydraulic fracturing and genesis of the Quartz-Fuchsite vein. Massive and barren quartz was deposited during protracted stages of fracture growth, while banded and gold-bearing quartz was formed during repetitive and brief periods of crack-seal vein growth. Quartz veining took place before the compressional deformation which has affected the Timmins area.

Fluid inclusion studies indicate that the hydrothermal fluid contemporaneous with quartz veining and gold deposition was a low salinity CH_4-rich H_2O-CO_2 fluid that underwent intermittent unmixing. Phase separation was promoted during pressure drops in fractures that accompany the crack-seal vein growth mechanism. The strong partitioning of CO_2 and CH_4 into the vapor during unmixing resulted in a shift in the remaining fluid toward higher pH and fO_2. As a consequence, gold complexes were probably destabilized in the hydrothermal fluid and deposited with quartz in crack-seal veins.

Lead isotope studies of whole rocks and galenas associated with gold in the Quartz-Fuchsite vein suggest a genetic link between the gold mineralization and the quartz-feldspar porphyries of the Dome Mine environment, although other source reservoirs cannot be ruled out on the basis of lead isotopes alone. Sulfur isotope compositions of pyrites and galenas from the Quartz-Fuchsite vein are compatible with a magmatic or a metamorphic fluid.

The weight of evidence indicates that the development of the gold mineralization in the Quartz-Fuchsite vein is genetically related to the emplacement of quartz-feldspar porphyries in the Dome Mine environment. The ultimate source of gold and the mineralizing fluid is probably a deeper seated magma, or possibly the lower crust.

ACKNOWLEDGEMENTS

I would like to thank the many people who have helped me during the preparation of this thesis. I would like to express my sincere gratitude to Dr. J.H. Crocket who suggested the present topic and introduced me to the Timmins gold mining camp. His supervision, encouragement, and his helpful criticism of the draft of this dissertation are greatly appreciated. Thanks are also due to Dr. D.M. Shaw whose critical questions throughout this study, and comments on the manuscript helped me to clarify parts of the present thesis. I am also indebted to Dr. A.P. Dickin who introduced me to the magic and frustrations of lead isotopes. His advice, enthusiasm and great accessibility are more than appreciated. Dr. J. Copley and Dr. J.C. Waddington are thanked for acting as external departmental members of my supervision committee.

Special thanks go to D.S. Rogers (Chief geologist, Dome Mine) for arranging the field work, for his helpful guidance and discussions, and for providing valuable information. Dr. R. Mason (Queen's University) is also thanked, his pertinent remarks about the local geology and his advice helped me considerably in understanding many field observations.

Many aspects of this study would not be possible without the expertise and the professionalism of O. Murdoch (XRF, LOI), L. Zwicker (thin section preparation), A. Kabir (NAA), J. Whorwood (preparation of plates), and Dr. R.M. McNutt, D. Jones and J. McAndrew (lead isotopes), and C. Jaeger (sulfur and lead isotopes). I would like to thank them for their help.

The support of my friends and colleagues is gratefuly appreciated. Comments by and stimulating discussions with F. Ghazban, F. Marcantonio, W.Lee, N. Blum and J. Inman helped me to improve the content of this thesis. I owe a special note of appreciation to S. Zymela who is also thanked for his great expertise and advice in computer software.

This dissertation is dedicated to my wife Catherine. Her presence, continuous encouragement, and help made it possible to accomplish this thesis in time.

Financial support that came from NSERC funding to Dr. J.H. Crocket and Dr. D.M. Shaw, and an OGR grant to Dr. J.H. Crocket is greatly appreciated.

TABLE OF CONTENTS Page

LIST OF FIGURES

LIST OF TABLES Page

LIST OF PLATES

CHAPTER 1

INTRODUCTION

1.1. AIM OF STUDY

Archean lode gold deposits have contributed approximately 20% to the cumulative world gold production (Phillips, 1985; Roberts, 1987). They have been one of the major sources of gold up to the present, and they represent a large ore potential for the future. However, the mechanisms of formation of these deposits are still highly controversial. No unique genetic model has yet been agreed upon on a world wide basis.

The essential geological and geochemical features critical to ore genesis need to be identified and understood, in order to generate a global and accurate model. The basic requirements in ore genesis modeling are to :

1) establish the source of the mineralizing components;
2) define the environment and the mode of ore deposition;
3) characterize the nature of the ore-bearing fluid.

The problem of ore genesis can be approached in two ways : either with a rigorous and intensive study of the details of individual deposits, or by comparing geological and geochemical characteristics of similar deposits on a broad scale. The latter approach has contributed significantly in defining the general features of Archean lode gold deposits, and in providing valuable working hypotheses. Nevertheless, the models developed so far fail to explain many of the variable geological and geochemical characteristics of these deposits observed on a local scale. Additional investigations on individual deposits are required. The interpretation of such observations and the processes of ore formation deduced from them will in turn contribute to the general knowledge required for broad conceptual models.

Thus, the objectives of the present study are to :

1) define the basic geological setting of an individual Archean lode gold-ore body;

2) characterize the site and the cause of ore deposition;

3) establish the source of gold, and of the ore-bearing fluid for the particular mineralization under study.

These findings will then be integrated in order to:

1) work out a reasonable genesis for the investigated ore body;

2) select the most appropriate and plausible Archean lode gold deposit model(s), which would suit the genesis of the mineralization in the present case study;

3) constrain and refine the particular "preferred"

conceptual model in the light of the new findings of the present research.

1.2. PRESENT STATE OF KNOWLEDGE

The current state of knowledge of Archean lode gold deposits will be briefly reviewed, so that the relevance to the research topic of the field area and the methods of study employed can be fully appreciated.

Extensive recent reviews of Archean lode gold deposits can be found in Colvine (1983), Colvine et al. (1984), Hutchinson and Burlington (1984), Groves and Phillips (1987), Hutchinson (1987), and Roberts (1987).

Lode deposits occur mainly within the volcanic-sedimentary rock sequences of greenstone belts from Archean shield areas. The predominant host lithologies in mining camps are mafic volcanic rocks, with significant amounts of komatiite, greywacke and shale. Other lithologies that are also important hosts to gold deposits are chemical sediments, such as iron formations (e.g., Fyon et al., 1983a; Macdonald, 1983, 1984; Phillips et al., 1984), and felsic intrusives. The latter host lithology appears to be mainly typical of Canadian greenstone belts, where gold deposits may be located in, or adjacent to felsic porphyry intrusions (e.g., Hodgson and MacGeehan, 1982; Cherry, 1983; Marmont, 1983). The porphyries are considered as a key to the discovery of new gold deposits, albeit volumetrically, they are not a major lithological component of greenstone belts. For instance, most of the larger gold producing mines in the Superior Province of the Canadian shield are spatially associated with felsic porphyries (Hodgson and MacGeehan, 1982). Felsic volcanic rocks are generally unimportant as gold hosts. Although ore bodies might be stratabound, they do not appear to be stratigraphically controlled.

The possible role of intrusions in the genesis of Archean lode gold deposits has been the subject of much controversy. Three scenarios are commonly proposed : either felsic intrusions contributed both metals and fluids to the mineralization; or they acted only as a heat pump driving an ore-forming hydrothermal system; or the spatial relationship is purely coincidental, in that both gold-bearing fluids and intrusives have followed the same structurally prepared pathway (Cherry, 1983; Marmont, 1983).

Archean lode gold deposits are often located in, or adjacent to, faults or shear zones of regional extent. In recent years, research has been focused on this particular relationship, in order to unravel the geological evolution of the structural discontinuities and the gold deposits contained therein. The facts are that these zones are the location of anomalously high strain. They indicate a compressional deformation. It is commonly regarded to be one of the latest events, which has affected the gold hosting environment. This deformation often results in the development of a penetrative linear and planar fabric in the wall rocks. Ore bodies appear often to be strained and highly distorted as well. Lately, it has been common practice to interpret gold-bearing quartz veins in the shear zones as Riedel-, R'-, P-, and D-type fractures, which are developed during simple shear (Tchalenko, 1968; Ramsay and Graham, 1970; Gamond, 1983; Hancock, 1985). Significant displacements are, however, never recorded along the gold-hosting shear zones. The localization of gold deposits in brittle-ductile shear zones suggests to many researchers that mineralization is structurally controlled (e.g., Kerrich and Allison, 1978; Robert et al., 1983; Colvine et al., 1984; Robert and Brown, 1986a; Groves and Phillips, 1987).

The host rock sequences of the gold deposits have been metamorphosed to variable degrees, ranging from sub-greenschist up to amphibolite facies. Ore bodies are usually accompanied by wall rock alteration. In greenschist facies rocks, ferromagnesian minerals and oxides are commonly hydrolyzed and carbonatized. Alteration of the wall rocks is less well documented in amphibolite-grade rocks. The time relationship between these two metasomatic events is also not clearly established. For instance, in the Timmins area, Mason and Melnik (1986a) place the alteration associated with mineralization before greenschist metamorphism. Fyon (1986) also argues for carbonatization of wall rocks that either predated or was coeval with metamorphism; on the other hand many authors suggest that wall rock alteration was synchronous with and/or postdated peak-metamorphism (e.g. Colvine et al., 1984; Robert and Brown, 1986b; Andrews et al., 1986; Clark et al., 1986; Thomson, 1986; Groves and Phillips, 1987).

Archean lode gold deposits display diverse morphologies. An ore body may consist of an individual vein, a complex vein structure, or disseminated mineralization in the wall rock. Ore deposits are frequently developed over large depth intervals. Gold occurs as the native metal visible to the naked eye, as microscopic grains located in sulfides, such as pyrite, pyrrhotite, galena, or arsenopyrite, or as gold-bearing tellurides. Besides sulfides and tellurides, other ore indicators and associated minerals are scheelite, tourmaline, K-V-Cr-mica, chlorite, carbonaceous material, and of course carbonates (Boyle, 1979).

Fluid inclusions and stable isotope studies have been used to characterize the nature and the source of the mineralizing fluid, and the mechanisms of ore deposition. Fluid inclusions are predominantly composed of carbon dioxide and water, with minor methane. Low salinities are typical. Phase separation into a carbon dioxide-rich vapor and a water-rich liquid is occasionally reported. Homogenization temperatures commonly range from 200° to 400°C (e.g., Guha et al., 1982; Smith et al., 1984; Ho et al., 1985; Wood et al., 1986a; Robert and Kelly, 1987). Such a fluid may have been derived from a metamorphic environment (Touret, 1971, Crawford, 1981b), a magmatic system (Holloway, 1976; Cameron and Hattori, 1987), or by degassing of the mantle (Crawford, 1981b; Touret, 1981).

Ambiguity also prevails in the interpretation of isotope data. Hydrogen and oxygen isotope values fall within the range of metamorphic and magmatic fluids (Colvine et al., 1984; Kerrich, 1987). The tight clustering of carbon isotopes around -3‰ suggests a magmatic signature to Burrows et al. (1986), whereas Fyon et al. (1984), Fyon (1986), Cameron (1988), and Groves et al. (1988) favor a mantle origin for carbon on isotopic grounds. Kerrich et al. (1987) advocate that carbon finds its source in outgassing of the lower crust. Sulfur isotope values of pyrite and pyrrhotite range predominantly between 0 and +10‰. Sulfur of this composition can be interpreted as of magmatic or metamorphic origin (Colvine et al., 1984; Kerrich, 1987).

To the knowledge of the author, there have been a few studies that have applied radiogenic isotopes as tracers of the source of ore components in Archean lode gold deposits. Kerrich et al. (1987) noted that large scale rock reservoirs did not develop distinctly different strontium-isotope signatures in the Archean. Hence the use of strontium isotopes as a tracer is limited. However, Kerrich et al. (1987) suggest that a source of strontium more radiogenic than komatiites or the contemporaneous mantle is required to explain their data. No unique gold source could be defined with lead isotope studies on sulfides and tellurides that are associated with Archean lode gold mineralizations. Kramers and Foster (1984) propose an upper crustal environment, in particular banded iron formations, or the mantle as the source of lead, and possibly gold, in deposits from Zimbabwe. Browning et al (1987) concluded from a study in Western Australia that lead, and by inference gold, were derived from a mafic-ultramafic rock sequence. These authors found no evidence for a multistage lead evolution. In contrast, Saager and Köppel (1976) report multistage histories for some galena lead in gold deposits from South Africa. The later authors found lead isotope patterns which suggest cogenetic evolutions of leads from vein-type deposits and "porphyry-type" ores. Lead isotope compositions of sulfides from gold deposits from the Abitibi Greenstone belt (Ontario) commonly show one of two compositional trends. One group of sulfide lead compositions have model ages that cluster around 2700 m.y., and a second group of sulfides that defines secondary isochrons (Franklin et al., 1983). The development of these secondary isochrons is attributed to addition of radiogenic lead to lead of preexisting sulfides in the gold deposits during metamorphism (Thorpe et al., 1981; Franklin et al., 1983). It appears that no attempt has been made to compare the lead isotopes of an individual Archean lode gold ore body with respect to its host rocks.

The inconclusive fluid inclusion and isotope data, and the conflicting interpretations on the timing of mineralization, metamorphism, and wall rock alteration have lead to the development of contrasting Archean lode gold deposit models.

Hutchinson and Burlington (1984) advocate a complex multistage volcanic syngenetic-remobilization model. They argue that auriferous exhalite sediments formed during initial sea-floor hydrothermal activity. This first stage was followed by several types of metamorphogenic remobilizations to form the shear-hosted veins, discordant vein systems, or stockworks, which host major gold deposits.

Another model, recently refined by Groves and Phillips (1987), proposes that metamorphic ore-bearing fluids were generated by devolatilization of volcanic rocks deep in the greenstone pile. These fluids were then focussed and channelled upwards along regional lineaments, i.e. shear zones or faults. Pressure and temperature drops across the amphibolite-greenschist facies boundary partially controlled ore deposition. Reactions between auriferous fluids and iron-rich wall rock is believed to be another mechanism of ore deposition.

As mentioned above, the genesis of lode deposits has been interpreted by some investigators to be related to magmatic intrusions. On the one hand, Mason and Melnik (1986a,b) suggest a gold-rich porphyry copper-type model for the generation of the ore bodies associated with the Pearl Lake porphyry in the Timmins area. They favor an emplacement of the mineralization in a tensional environment, preceding regional deformation. On the other hand, Spooner et al. (1985), Burrows and Spooner (1986), and Wood et al. (1986a,b) argue that the spatial association of the gold mineralization with the Pearl Lake porphyry is purely structural, and that no genetic relationship exists between them. The latter authors conclude that ore deposition post-dates regional deformation, and that a more distant magma is the source of the gold. Wood et al. (1986a), for instance, suggest that "...domal tonalite gneiss-granodiorite-quartz-monzonite-type material which intrudes the lower parts of Archean greenstone belts...might be a possible indirect, or direct, source region...". Hodgson (1986) believes that gold ore formed in conjunction with late stage intrusives, during the last compressional event which affected the Abitibi greenstone belt.

Colvine et al. (1984), Fyon et al. (1984), Fyon (1986), and Cameron (1988) integrate granulitization of the lower crust due to mantle degassing of carbon dioxide, melting of the lower crust, and large ion lithophile element redistribution within the crust to explain the formation of Archean lode gold deposits. This later model includes a magmatic component.

The models noted above call upon a variety of gold sources. Intrusives are cited as a specific source by Mason and Melnik (1986a), Wood et al. (1986a), Cameron and Hattori (1987), and Hattori (1987). Researchers advocating the metamorphic model (e.g. Groves and Phillips, 1987) find komatiites to be a convenient source. This choice is mainly based on the fact that there is a close spatial relationship between komatiites and gold deposits (Pyke, 1976). Keays (1984, 1987) suggested that komatiites might be a favorable protolith enriched in gold above normal background. Such gold could be leached out and transferred into interflow sediments at the sea-floor alteration stage. Subsequent metamorphism would then remobilize gold and concentrate it into ore bodies. However, unaltered primary igneous rocks, ranging in composition from ultramafic to felsic, commonly have low abundances (about 2 ppb) of gold (Tilling et al., 1973; Kwong and Crocket, 1978). In particular, a recent study by Crocket and MacRae (1986) has shown that relatively fresh komatiites from Munro Township

(Ontario) contain an average of 2.5 ppb gold. There is no lithology which can be shown to be a more propitious local source rock than another.

Sites of deposition which are suggested include structurally prepared sites (shear zones), chemically susceptible host rocks (e.g., banded-iron formations, iron-tholeiites), and submarine discharge zones. The cause of deposition is usually attributed to fluid destabilization due to pressure and/or temperature decrease, to fluid-wall rock interaction, and hydraulic fracturing.

Seward (1973, 1984) has demonstrated experimentally that thio-complexes are very stable and generate high gold solubility in hydrothermal fluids. Currently, there seems to be a consensus that these are the main complexes carrying gold in Archean hydrothermal fluids. Alternatively, gold chloride complexes are stable in certain types of hydrothermal fluids (Henley, 1973); however, fluid inclusions indicate that salinities were low in hydrothermal systems that formed Archean lode gold deposits, placing into doubt the possible presence of such complexes. Kerrich and Fyfe (1981) suggested that some of the gold may be transported as carbonyl or carbonate complex, since the hydrothermal fluid responsible for alteration is carbon dioxide-rich.

1.3. AREA AND METHODS OF STUDY

The Dome Mine in the Timmins area (Ontario) presents all the ingredients of an environment that is typical of Archean lode gold deposits (Holmes, 1968; Rogers, 1982a,b) (see chapter 3). With a production of 54 million ounces, the Timmins area (Porcupine mining camp) has one of the largest gold productions in the world. The Dome Mine is one of the three largest mines in the Timmins gold camp (Hodgson and MacGeehan, 1982). The ore body selected for the present study is a gold-bearing Quartz-Fuchsite vein, known to be the highest ore grade vein in the mine. For convenience, the term Quartz-Fuchsite vein will be shortened in QFV.

Several features of the QFV make it an attractive target for an ore genesis study, which adresses the objectives of the present research. From a practical aspect, the QFV is fairly easily accessible underground in both vertical and horizontal dimensions. Since it is nearly mined out, it is possible to gain a complete view of this particular ore body. The QFV consists of mineralized and barren areas. This provides an opportunity to undertake a comparative study to determine ore-related geological and geochemical features.

The QFV is located in what is thought to be a fault zone, and in spatial association with felsic porphyry lenses and two of the major quartz-feldspar porphyry intrusions of the Timmins area, namely the Preston and the Paymaster porphyries. This setting permits a study, in time and space, of the relationship between mineralization, a fault (i.e. a structural site) and local intrusions.

For most of its length, the immediate wall rock of the QFV is a single strongly carbonatized rock unit, which is probably an altered komatiite. The QFV commonly lies very close to the lithological contact with another rock unit, namely slate. This presents the opportunity to evaluate several factors including the chemical influence, if any, that a given wall rock exerted on ore deposition, the significance of the stratabound character of the mineralization, and the particular relationship of komatiite to gold mineralization.

Gold is consistently associated with galena and with fuchsite and chlorite banding in the QFV. The lead and sulfur isotope composition of galena (lead sulfide) may possibly be used to trace the source of gold. Banded quartz, also called ribbon- or laminated-quartz, is of high ore grade in gold deposits. Its importance on ore deposition may also be evaluated in the Dome Mine geological setting.

Besides lead and sulfur isotope studies, the methods of investigation which were used include :

- field geology, particularly structural geology aspects;
- petrographical studies;

- major and trace element geochemistry;
- microthermometric studies of fluid inclusions.

CHAPTER 2

METHODOLOGY

2.1 INTRODUCTION

The multidisciplinary approach adopted in the present research combines field observations with petrographic, geochemical and fluid inclusion investigations. The field work and the maps provided by the Dome Mine were used to establish the geologic framework for the interpretation of the subsequent petrographic and analytical data.

2.2. FIELD STUDY

The field study was undertaken to map the essential structural elements of the QFV, and to investigate its relationship with characteristic features or structures present in the wall rock, such as foliation, quartz veining or alteration. The essential geological characteristics related to mineralization were identified with a comparative description of gold-producing and barren domains of the QFV. Finally, the QFV and the wall rocks were sampled for further petrographic, geochemical and fluid inclusion studies.

Geological mapping of the lithological units was not carried out, since excellent maps at a scale of 1 inch to 30 feet (1:360) were provided by the Geology Department of the Dome Mine. All additional information collected by the author was recorded on these maps at a 1:360 scale.

The QFV extends from the 6th level of the Dome Mine downwards to the 17th level. Levels are separated by 150 feet (46 m). Mapping and sampling was possible on levels 8, 10, 12, 13, 15, 16, and 17, as well as in producing stopes. Description of the vein and sampling is biased towards ore zones, since mining is concentrated in gold-producing zones. Thus, barren domains of the vein were only accessible along drives on the levels, and never on their full length. Access to the wall rock of the QFV was limited to its immediate vicinity, usually at the most 1 to 2 m away from the vein. This restriction is imposed by the cut and fill stoping method (Thomas, 1978) used to mine out the ore zones. Only a few cross-cuts on the levels 8, 12, 13, and 17 permitted access to the wall rocks at a greater distance from the QFV. Diamond drilling is widely used as an exploration tool in the Dome Mine (Rogers, 1982a); unfortunately, all the cores are assayed, thus eliminating a further possibility for examination of the wall rocks at some distance from the QFV.

The shape of the QFV has been represented with the help of a Conolly contour diagram (Conolly, 1936; see also

Garnett, 1966; Taylor, 1966). Gold grades have also been contoured, and superimposed onto the Conolly diagram. Unfortunately, the width of the QFV is highly irregular, and not enough maps from stopes were available to trace a reliable vein-thickness contour diagram. The method of constructing a Conolly diagram is summarized in Appendix I.

2.3. MINERALOGY

Samples from the QFV and the wall rocks were examined petrographically in both transmitted and reflected light mode, in order to identify their mineralogy and describe their texture.

The carbonate mineralogy of the wall rocks was determined by X-ray diffraction (XRD). This method was found to be the most efficient in identifying carbonates from altered rocks in gold camps from the Abitibi belt (Tihor, 1978). However, it does not allow dolomite, ferroan dolomite and ankerite to be differentiated, because their diagnostic X-ray reflection peaks are virtually identical at 30.9° 2θ. Fryer et al. (1979) published microprobe analyses of similar carbonate material from the Dome Mine, which shows that this phase is a ferroan dolomite. Thus, the presence of a peak at 30.9° 2θ is arbitrarily referred to as ferroan dolomite in this study. XRD was also used to identify the type of mica and chlorite present in the banding of the QFV. Whole rock powders for the carbonates, and mineral powder for the micas and the chlorites, were crushed to pass 200 mesh. The powder was slurred onto a glass slide using acetone and scanned from 25° to 33° 2θ for carbonates, and from 0° to 90° 2θ for micas and chlorites, using CuK radiation produced at 30 kV and 16 mA.

The optical identification of some opaque minerals, particularly tellurides, was verified by scanning electron microscopy (SEM). The possible presence of gold within pyrite was also examined using SEM.

2.4. GEOCHEMISTRY

2.4.1. Sample preparation preceding chemical analysis

Whole rocks were broken with a jaw crusher, and then ground to -200 mesh using a ceramic disk grinder, and a tungsten carbide shatter box. Chlorites, micas and galenas were sorted out by handpicking from rock fragments of the QFV. Pyrites were separated from the QFV and wall rock samples by digestion in concentrated hydrofluoric acid (HF) (Neuerburg, 1975). Purity of mineral separates was checked with a binocular microscope. Chlorites and micas were ground to pass 200 mesh using a steel mortar. Galenas and pyrites were pulverized with an agate mortar, cleaned with nitric acid (HNO_3) between each grinding.

2.4.2. X-ray fluorescence (XRF) analysis

Concentrations of major and trace elements were determined on fusion (Norrish and Hutton, 1969) and pressed powder (Marchand, 1973) pellets, respectively. Analyses were carried out on a PW 1450 Philips automatic sequential spectrometer. Analytical procedures involved the following five routines : major elements, Rb - Sr - Y - Zr - Nb, Ni - Co - Cr - V - Zn - Cu, Pb, and S.

Accuracy of analyses was monitored using international rock standards, including PCC-1, JG-1, JB-1, NIM-P, NIM-D, SCo-1, NIM-G, Mica-Mg, and Mica-Fe. Machine variation was corrected using a drift monitor standard with each set of three samples. Precision, accuracy and detection limit estimates of XRF analyses are presented in Appendix II.1.

The Co concentrations have not been used throughout the present study, because of possible contamination from the tungsten carbide shatter box (Thompson and Bankston, 1970).

2.4.3. Neutron activation analysis (NAA)

Instrumental and radiochemical NAA was used to determine trace element concentrations in whole rock samples and mineral separates. Polystyrene vials were used as sample containers for all irradiations, except for Ir concentration determinations. Irradiations were carried out in a high flux position in the McMaster University reactor. Analytical procedures involved four separate routines :

1) Rare earth elements (REE) :

The procedure generally follows that of Jacobs et al. (1977). Each irradiation package consisted of 14 whole rock or mineral separate samples of approximately 1 g weight and two 0.5 g rock standards (STM-1, AC(Open University Rock Standard: OURS)). La and Sm were determined three days after a first irradiation of 2 MW hours. After one month cooling,the samples were irradiated a second time for 7 MW hours. Following a decay period of 13 days, the abundances of the remaining REE (Ce, Nd, Eu, Tm, Tb, Lu, Yb) and Th were then determined. The majority of samples analyzed were komatiites. Komatiites are known to have low REE content (e.g., Sun and Nesbitt, 1978). Thus, Eu was the only REE which could be detected after an additional two months of decay. REE abundances were normalized to chondrite values from Haskin et al. (1968).

2) Au - W - As - Sb (short lived elements) :

Each irradiation package consisted of 12 whole rock samples of approximately 0.6 g weight, 2 international standards (Sco-1, SGR-1) weighing approximately 0.5 g, and 2 chemical standards (i.e., silica powder doped with known amounts of metal, kindly prepared by A.Kabir, McMaster University) weighing approximately 0.2 g. Samples were counted 3 days after a 2 MW hour irradiation.

3) Rb - Zr - Ba - Th - Hf - Cs - Ta - Ni - Cr - Sc - Sb-Co (long lived elements) :

Each irradiation package consisted of 14 whole rock or mineral separate samples, and 2 international standards (STM-1, NIM-D). Samples were irradiated for 7 MW hours. A 15 days cooling period elapsed before counting.

4) Ir :

Ir abundances of 10 whole rock samples and mineral separate samples were obtained by A.Kabir by radiochemical NAA following the procedure described by Crocket et al. (1968). Approximately 200 mg of sample were irradiated in a quartz vial. Standards were prepared by A.Kabir.

Counting was carried out on a 10% efficient, coaxial intrinsic germanium detector (Aptec Engineering Limited, Toronto, Model C510), linked to a Canberra, Series 80, multichannel analyzer. An account of analytical errors is included in Appendix II.2.

Due to possible contamination during grinding in the tungsten carbide shatter box (Thompson and Bankston, 1970), W and Co abundances are not considered reliable.

Rb, Zr, Cr, and Ni abundances were obtained by both XRF and NAA. Values obtained by XRF are used in the present study, in order to compare them to data published in the literature. Abundances of these elements are commonly obtained by XRF analysis. However, Cr, Ni and Rb abundances obtained by NAA are used when discussing the geochemistry of the banding present in the QFV, since no pressed powder pellets were made for samples from this banding.

2.4.4. Determination of volatiles

Loss on ignition (LOI) was measured by firing approximately 3 g of powdered sample at 1000°C for 30 minutes in an electric furnace.

Fusion of approximately 0.3 g of powdered sample in a LECO induction furnace yielded total carbon which was calculated as carbon dioxide (CO_2).

Since the whole rock samples consist predominantly of carbonate- and hydroxyl-bearing minerals, total water (H_2O) is given by the difference between LOI and CO_2.

2.4.5. Sulfur isotopes

Pyrite and galena samples were converted to sulfur dioxide (SO_2) by burning at 1350°C, in the presence of copper monoxide (CuO). In some cases pyrite was previously converted to silver sulfide (Ag_2S), and then oxidized to SO_2 (Thode et al., 1961). Sulfur isotope analyses were performed on a double-collector mass spectrometer (Thode and Rees, 1971; Rees, 1978). The $\delta^{34}S$ data are given with respect to the Canyon Diablo Troilite standard (CDT). Precision expressed as the standard deviation of a single determination is ± 0.2 °/∞.

2.4.6. Lead isotopes

Rock sample splits weighing approximately 300 mg were digested in HF for four days, followed by a twelve hour dissolution in HNO_3 and finally another twelve hour digestion in hydrochloric acid (HCl). The dry residue was dissolved in 1 M hydrobromic acid (HBr). Pb was separated by anionic exchange in HBr columns, and collected with 6 M HCl solution. Galenas were dissolved in 0.01 M HNO_3, and Pb was purified by electrodeposition on a Pt-electrode (Arden and Gale, 1974).

Isotopic ratios were measured on a VG 365 mass spectrometer. The accuracy of the Pb isotopic composition measurements was assessed by replicate analyses of the NBS SRM 981 standard. The two main errors that affect the analyses are mass dependent isotopic fractionation in the mass spectrometer and accuracy in measurement of the small ^{204}Pb peak. Both of these parameters can be estimated from day-to-day variation of analyses of a particular sample (Doe et al., 1966). This estimation was performed with replicate analyses of the NBS SRM 981 standard. Within-run precision averaged 0.056% (2σ) and 0.006% (2σ) for whole rocks and galenas, respectively. Between-run precision is estimated to be 0.1% (1σ) for both whole rocks and galenas. Analytical errors are discussed in more detail in Appendix II.3. Total processing blanks were below 1.5 ng.

2.5. FLUID INCLUSIONS

Microthermometric measurements were performed on quartz samples from the QFV and from quartz veins present in the wall rocks. Samples consisted of doubly polished, unmounted 100 μm to 200 μm thick sections prepared by Vancouver Petrographics Ltd. Fragments of about 25 mm square were most easily handled.

The fluid inclusions were examined with a Nikon AFX-II petrographic microscope equipped with a U.S. Geological Survey gas flow heating-freezing stage (Werre et al.,1979; Woods et al., 1981). A Leitz L32 long focus objective was used, with which a maximum magnification of 480 times was obtained. Most inclusions were too small (≤2 μm) to be adequately viewed at this magnification. Only a few inclusions were large enough (between 2 and 10 μm) to permit precise measurements. Calibration of the heating-freezing stage, and accuracy and precision of the analytical results are discussed in Appendix II.4.

The approximate composition of the fluids in the inclusions is determined by direct observation of phase changes in individual inclusions and by comparing the observed temperatures with experimentally determined phase equilibria for appropriate synthetic chemical systems. Most fluids in the earth's crust fall in the C-O-H-S + salt system (Holloway, 1981). A large fraction of all fluid inclusions consist almost entirely of H_2O, CO_2, and NaCl (smaller concentrations of KCl, $CaCl_2$, and other chlorides may also be present, but salinities are commonly given in equivalent NaCl wt %). The interpretation of microthermometric measurements of fluid inclusions is therefore essentially founded upon the knowledge of simple binary systems, such as H_2O-CO_2, H_2O-NaCl, and CO_2-CH_4 (Roedder, 1984).

The use of the microthermometric technique allows one to measure the following phase changes (Hollister and Burruss, 1976; Ramboz, 1980) :

- $TmCO_2$ = temperature of melting of CO_2.
- TmI = temperature of melting of ice.
- TmC = temperature of melting of CO_2 and/or CH_4 clathrate hydrate.
- $ThCO_2$ = temperature of homogenization of CO_2.
- Th = temperature of homogenization of the fluid inclusion.

CHAPTER 3

GEOLOGICAL SETTING

3.1. REGIONAL GEOLOGY

The geology of the Timmins area has been discussed by Dunbar (1948), Ferguson et al. (1968), Davies (1977), Roberts (1981), Pyke (1981,1982), Hodgson (1983), and Mason and Brisbin (1987).

With the exception of a few diabase dikes and minor Middle Precambrian sedimentary rocks, the bedrock in the area is of Archean age (Fig. 3-1). Two cycles of volcanic rocks are recognized. The older Deloro Group is confined to the southern area of the mining camp. It is largely a calc-alkaline sequence, composed mainly of andesite and basalt flows in the lower part, grading to dacitic flows with dacitic and rhyolitic pyroclastic rocks towards the top. Iron formations are common at or near the top of the group. A major change in volcanism marks the beginning of the younger Tisdale Group. Its basal formation consists largely of ultramafic volcanic rocks and basaltic komatiites. These rocks are in turn overlain by a thick sequence of tholeiitic basalts. The uppermost formation is largely volcaniclastic units of a calc-alkaline dacite composition

Figure 3-1
A: Generalized geology of the Timmins area (after Ferguson et al.; Davies, 1977; Roberts, 1981; Pyke, 1982; Hodgson, 1983).

B: Distribution of stratigraphic units in the Timmins area (after Pyke, 1982).

1: Preston porphyry,
2: Paymaster porphyry,
3: Preston West porphyry,
4: Pearl Lake porphyry,
D.F.: Dome fault,
P.S.: Porcupine syncline,
C.T.A.: Central Tisdale anticline,
S.T.A.: South Tisdale anticline,
I: Deloro Group,
II: Tisdale Group.

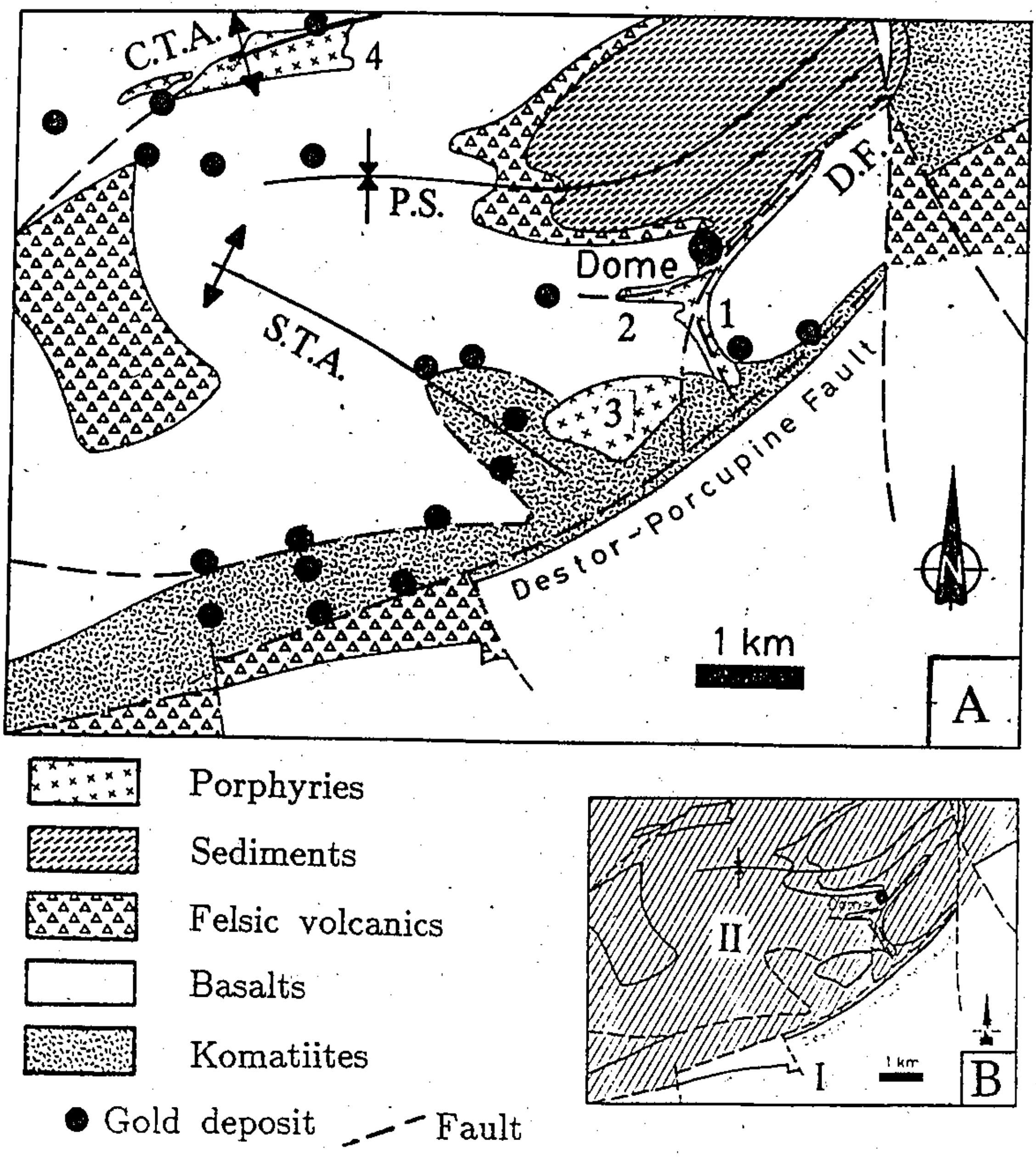
C.T.A.
4
P.S.
D.F.
Dome
1
2
S.T.A.
3
Destor-Porcupine Fault
1 km
A
Porphyries
Sediments
Felsic volcanics
Basalts
Komatiites
Gold deposit
Fault
II
I
1 km
B

(Pyke, 1982). Metasediments, mainly a turbidite sequence, consist dominantly of interlayered wacke, siltstone, and conglomerate. According to Pyke (1982), this sediment sequence is time equivalent to the upper part of the Deloro Group and the entire Tisdale Group. A thin unit of fluvial deposits is developed at the top of the clastic sequence (Pyke, 1982). Hodgson (1983) has questioned the aforementioned stratigraphic interpretation, and places the deposition of the turbidite sequence after the formation of the Tisdale Group.

Small quartz-feldspar porphyry bodies are a distinctive lithological component of the Timmins mining camp. The largest porphyry bodies are the Pearl Lake porphyry, with the adjacent Gillies Lake, Miller Lake, Crown and Corniaurum porphyries in the northwestern part of the mining camp, and the Paymaster, Preston and Preston West porphyries in the southeastern part (Ferguson et al., 1968) (Fig. 3-1). The mode of emplacement of many porphyry bodies, either intrusive or extrusive, is still not resolved and remains controversial (Pyke, 1982).

No faults are observed in surface mapping (Ferguson et al., 1968). Thus, in the Timmins area, proposed faults and their precise location vary according to the interpretation of one author or another. The most widely accepted fault is the major northeast striking Destor-Porcupine Fault, which separates volcanic rocks of the

Tisdale Group and younger sedimentary rocks from the predominantly volcanic rocks of the Deloro Group to the south. The Burrows-Benedict Fault is the most prominent of a number of late northwest striking faults (Davies, 1977; Roberts, 1981; Pyke, 1982). Various other minor faults have been proposed such as the Hollinger Fault, the Vipond Fault, and the Dome Fault (Ferguson et al., 1968; Davies, 1977; Hodgson, 1983, 1986).

One of the dominant structures north of the Destor-Porcupine Fault is the Porcupine Syncline, which closes in the west and plunges to the northeast (Fig. 3-1). It is flanked on the northwest by the Central Tisdale Anticline and on the southwest by the South Tisdale Anticline. Davies (1977), Roberts (1981) and Pyke (1982) interpret these structures to represent two periods of folding, with the Porcupine Syncline as the younger structure. Alternatively, Hodgson (1983, 1986) proposed that following Tisdale volcanism and deposition of the lower sediment formations, the strata were rotated into subvertical attitudes along listric normal faults. Erosion followed and the upper sediment formations were deposited. Both sequences were then folded, after which they were cut by major faults. Following folding, a penetrative east-west foliation and strong east plunging lineation was imparted to the volcanic, sedimentary and intrusive rocks (Roberts et al., 1978; Roberts, 1981; Hodgson, 1983, 1986).

U-Pb zircon ages of 2725 ± 2 and 2703 ± 2 million years (m.y.), (Nunes and Pyke, 1980, 1981) have been obtained for the felsic volcanic rocks at the top of the Deloro and Tisdale Groups, respectively. The Pearl Lake and Preston porphyries have a U-Pb zircon age of 2685 ± 3 m.y. (S.Marmont in Masliwec et al., 1986; S.Marmont in Fyon, 1986). On the basis of K-Ar ages, Leech (in Ferguson et al., 1968) determined that the diabase dikes crosscutting the Archean volcanic rocks in the immediate Timmins area (Tisdale Township) are of Middle to Late Precambrian age. Pyke (1982) also believes that some of the dikes are of Early Precambrian age.

The rocks in the Timmins area have undergone several overlapping events of metamorphism and alteration (Fyon, 1986). Initial seawater alteration was overprinted by burial metamorphism to prehnite-pumpellyite grade (Jolly, 1978, 1980, 1982). Some areas were locally affected by hydrothermal alteration (Ferguson et al., 1968; Davies and Luhta, 1978; Karvinen, 1982; Fyon and Crocket, 1982; Pyke, 1982; Fyon, 1986; Mason and Melnik, 1986a,b), and by contact metamorphism to greenschist and amphibolite facies (Jolly, 1978, 1980, 1982). The temporal relationship between the alteration types cannot be easily deciphered due to contact metamorphism. Fyon (1986) has shown that carbonate alteration of the volcanic rocks from the Tisdale Group occurred in several stages. Precipitation of hydrothermal calcite started when the volcanic sequence underwent low temperature seawater alteration. It was overprinted by a more intense carbonate alteration, characterized by ferroan dolomite-rich assemblages. According to Fyon (1986), the intense carbonatization event either predated or developed synchronously with the regional deformation and greenschist metamorphism.

Most of the gold deposits are located in the Tisdale Group, north of the Destor-Porcupine Fault (Fig. 3-1). Virtually all the gold production from the area has been from quartz-carbonate veins in the volcanic, sedimentary and intrusive rocks (Ferguson et al., 1968; Pyke, 1982). Although gold mineralization may occur within zones of carbonate alteration (Ferguson et al., 1968; Fyon and Crocket, 1982; Karvinen, 1982; Pyke, 1982), not all zones of carbonate alteration are associated with gold mineralization (Hodgson, 1983; Fyon, 1986). It has long been recognized that many auriferous quartz veins are in close proximity to quartz-feldspar porphyry stocks (Ferguson et al., 1968).

The time of gold-ore formation in the geological evolution of the Timmins area is still a matter of debate. On the one hand, Roberts et al. (1978), Roberts (1981), Hodgson (1983, 1986), and Brisbin and Mason (1987) argue for the emplacement of gold mineralization before the development of the penetrative east-west foliation and the strong east plunging lineation. This is also favored by Mason and Melnik (1986a,b), who interpret the small porphyry copper deposit hosted by the Pearl Lake porphyry (Davies and Luhta, 1978) as an Archean gold dominated porphyry copper system, emplaced before the development of any penetrative fabric. On the other hand, Fryer et al. (1979), Kerrich and Fryer (1979), Spooner et al. (1985), Burrows and Spooner (1986), and Wood et al. (1986a,b) advocate a late introduction of gold, postdating the development of the penetrative foliation and the lineation.

3.2. DOME MINE GEOLOGY

The geology of the Dome Mine has been described by Holmes (1968) and Rogers (1982a,b). Some specific geological, petrographic and geochemical aspects of the Dome Mine were studied by Fryer et al. (1979), Kerrich and Fryer (1979), Roberts (1981), Roberts and Reading (1981), Reading et al. (1982), and McAuley (1983). A simplified map of the geology of the Dome Mine is presented in figure 3-2.

The Dome Mine lies on the south limb of the Porcupine Syncline (Fig. 3-1). In the central part of the mine, volcanic rocks are overlain by metamorphosed slates and conglomerates. This folded assemblage plunges northeasterly and creates the structure referred to as the "Greenstone Nose". To the north of the "Greenstone Nose" lies a body of felsic pyroclastic rocks called "Gold Center

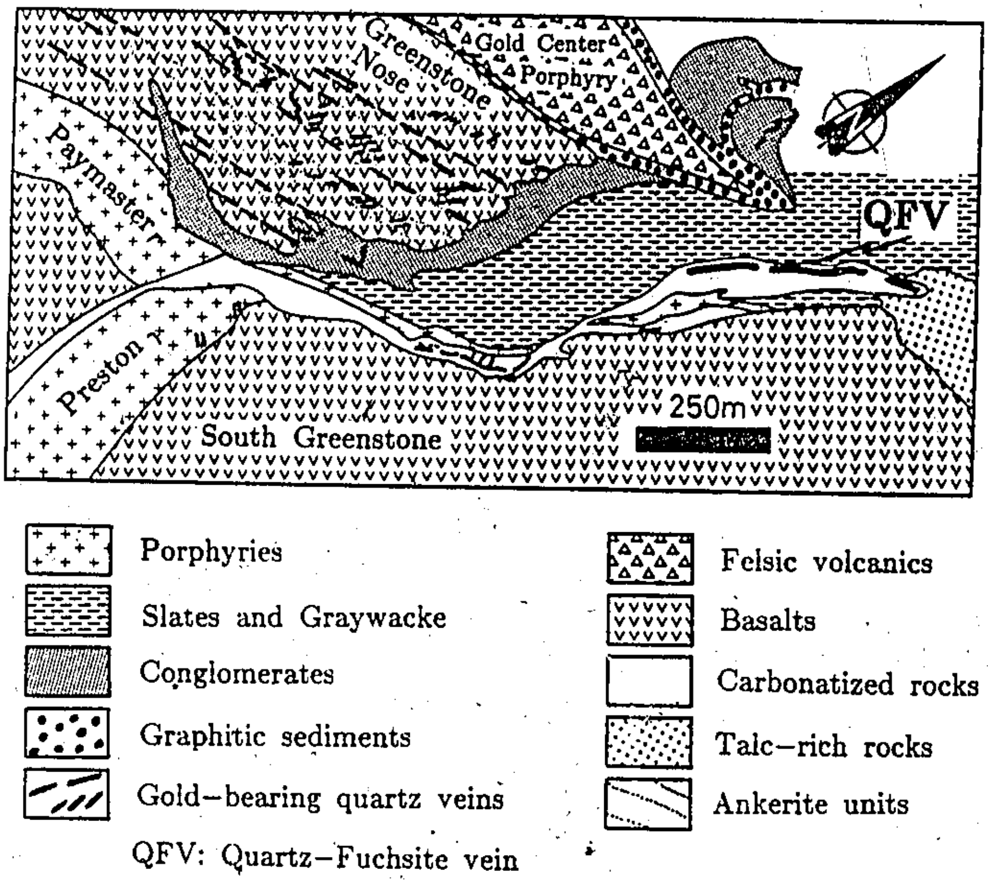

Fig. 3-2 Generalized geology of the Dome Mine, 12th level (after maps provided by the Geology Department of the Dome Mine, and Roberts, 1981).

Porphyry" in mine terminology. This latter unit is surrounded by a band of carbonaceous slates. South of the sedimentary rocks lie the "South Greenstone", a series of south-dipping massive mafic flows. The "South Greenstone" are bounded on the southeast by the Destor-Porcupine Fault, and on the northwest by a zone of carbonatized rocks and altered porphyries trending northeast (Holmes, 1968; Rogers, 1982a,b). This latter zone hosts the QFV.

On the mine plans, rocks of this zone are mapped as "Porphyry", "Carbonate Rock", and "Highly Altered" (Holmes, 1968). Each rock type forms bodies usually elongated parallel to the zone, but irregularly arranged within it. Lenses of slates are present as well. To the east, the rocks of the zone between the "South Greenstones" and the sediments change to talcose rocks. To the west the zone of carbonatized rocks and altered porphyry lenses bends southward between the two major quartz-feldspar porphyries of the Dome Mine environment, the Preston and the Paymaster porphyries. The "Carbonate Rock" is composed dominantly of magnesite, dolomite, quartz, and chlorite. It is often coarse grained, and massive, but locally schistose. "Highly Altered" rocks have the same mineralogical characteristics as the "Carbonate Rock", with the difference that fuchsite (chrome-bearing muscovite) is present in variable amounts. This zone of altered rocks is presumed to occupy a fault zone, namely the Dome Fault, which is thought to be a branch of the major Destor-Porcupine Fault (Holmes, 1968; Davies, 1977; Rogers, 1982a; Hodgson, 1983). However, according to Roberts (1981) and Roberts and Reading (1981) there is no evidence for major displacements along this zone, and they suggest that the metasediments, the altered rocks and the "South Greenstones" are a continuous sequence. In this latter interpretation the zone of altered rocks and the "South Greenstones" constitute a volcanic sequence that progresses from komatiites at the base, through mafic komatiites, to magnesium-rich tholeites at the top (Roberts and Reading, 1981). Fryer et al. (1979) also favor a komatiitic protolith for the carbonatized rocks.

The Preston and Paymaster porphyries, as well as the porphyry lenses from the zone of altered rocks were studied by McAuley (1983). Their mineralogy is dominated by phenocrysts of albitic feldspar and quartz in a matrix of quartzo-feldspathic minerals, sericite and carbonate. Late stage veins containing quartz, carbonate, albite, sericite, pyrite and tourmaline cut the previous mineral phases. The porphyry lenses from the altered rock zone are petrographically similar to the Preston porphyry. The main difference is that these porphyry lenses are apt to be much more schistose and carbonatized. Two metasomatic events have affected the porphyries : a sericite alteration, pre- or syn-kinematic to regional folding, which was followed by albitization. This latter metasomatic event developed after regional deformation and metamorphism (McAuley, 1983). The effects of the two metasomatic events have obliterated primary textures and little is known about their original nature. Holmes (1968) and McAuley (1983) indicate that the Paymaster and Preston porphyries are discordant with respect to the volcanic stratigraphy, which suggests an intrusive nature. McAuley (1983) also concludes that all porphyries are cogenetic and predate regional metamorphism.

Gold ore is found in a number of different rock types and in association with various structural settings (Holmes, 1968; Rogers, 1982a,b) (Table 3-1). As mentioned above, Roberts et al. (1978), Roberts (1981) and Hodgson (1983) propose that the majority of the ore bodies were formed before the development of the penetrative planar and linear fabric, whereas Fryer et al. (1979) and Kerrich and Fryer (1979) favor an emplacement following foliation and lineation development. The ankerite veins (Table 3-1, type Ia) have for some time been interpreted as chemical sediments of volcanic exhalative origin, and thus have been used as one of the key arguments for the early introduction of gold in the Timmins area (Fryer et al., 1979; Kerrich and Fryer, 1979; Roberts, 1981; Karvinen, 1982; Reading et al., 1982). However, the sedimentary origin of the ankerite veins has been placed into doubt by Hodgson (1983) and

Macdonald (1984); additionally, Roberts (1987) has reinterpreted the ankerite units as shear zones.

A crystallization age of 2685 ± 3 m.y. was obtained by U-Pb dating of zircon for the Preston porphyry (S.Marmont in Masliwec et al., 1986). Masliwec et al. (1986) obtained an $^{40}Ar/^{39}Ar$ age of 2633 ± 6 m.y. for fuchsite associated with gold mineralization in the Dome Mine. This latter age represents the minimum estimate of the age of the mica. Thus, Masliwec et al. (1986) place the age of formation of the Dome Mine gold deposits between 2633 ± 6 m.y. and 2685 ± 3 m.y., since they consider gold emplacement to be syn- or pre-fuchsite, and post-dating the porphyries.

TYPE OF ORE BODY	COMMON HOST ROCK
Type I : Long narrow veins in schist, parallel to the general trend of the formations.	
I(a) - Ankerite veins	Metavolcanic rocks of the "Greenstone Nose"
I(b) - Quartz-tourmaline veins	Mainly in "Highly altered" rocks
I(c) - Quartz-fuchsite vein	Carbonate rock
Type II : Lenticular or irregular "tension" veins in both massive and schistose rocks	
II(a) - Quartz veins arranged en echelon (Dacite ore)	Metavolcanic rocks of the "Greenstone Nose"
II(b) - Stockworks	Porphyry and "Highly altered" rocks
II(c) - Stockworks	Generally in conglomerates, between the Paymaster porphyry and the "Greenstone Nose"
Type III: Mineralized rock	In conglomerates along the "Greenstone Nose", some are inside the "Greenstone Nose"
Type IV : Silicified Greenstone	"South Greenstone"

Table 3-1. Classification of ore deposits at the Dome Mine (after Holmes (1968) and Rogers (1982a)).

CHAPTER 4

WALL ROCKS OF THE QUARTZ-FUCHSITE VEIN

4.1. INTRODUCTION

The QFV is located in the zone of carbonatized rocks and altered porphyries, at the contact between the carbonate rocks and slates (Figs. 3-2 and 5-1). In order to understand the genesis of the gold mineralization hosted by the QFV, the mineralogy and the lithochemistry of the immediate wall rocks need to be documented. In particular, the pattern of wall rock alteration has to be elucidated.

As mentioned earlier, the rocks of the Timmins area have undergone several superimposed stages of metamorphism and alteration. It can probably be assumed that all rocks have suffered the same degree of burial metamorphism, and seawater alteration. Alteration due to ore-bearing or other hydrothermal fluids was probably more localized. Thus, a comparison of altered wall rocks of the QFV and relatively "fresher" counterparts should allow one to evaluate the changes in element distribution associated with the ore-bearing fluid. This approach is valid, provided that any subsequent metamorphic event did not modify the element distribution resulting from the hydrothermal alteration.

It can be expected that slates and carbonate rocks reacted differently to the various metasomatic events, since their original mineralogy, texture and chemical composition were certainly different. The original nature and chemistry of both rock types will be established first, so that the effects of hydrothermal alteration can be evaluated.

4.2. SLATES

4.2.1. Mineralogy and texture

The slates are composed chiefly of quartz, chlorite, and muscovite. With minor pyrite and carbonates. They are fine-grained and well-bedded. Black dense argillaceous beds alternate with light-coloured beds and frequently show grain size gradation by which the tops can be determined (Holmes, 1968).

No changes in texture or mineralogy can be observed on approaching the contact with the carbonate rocks or the QFV. Visible alteration zones are absent.

4.2.2. Lithochemistry

Major and trace element geochemistry of the slates from the Dome Mine is fairly typical of Archean shales (Table 4-1). Various factors control the composition of shales (Taylor and McLennan, 1985; Wronkiewicz and Condie, 1987). Among these, mobilization of elements during metamorphism and grain-size effect (mineralogical control) have to be taken into consideration, before the effects of hydrothermal alteration associated with the QFV can be evaluated.

The effects of metamorphism on the mobility of elements in slates is poorly understood. Some studies indicate that major and trace element changes are minimal during regional metamorphism (Shaw 1954, 1956; Condie and Martell, 1983). In contrast, mobility of some elements (large ion lithophile and high field strength elements (HFSE)), as well as fractionation among rare earth elements (REE) has been suggested by some workers, especially during low-grade metamorphism (Hower et al., 1976; Merriman et al., 1986). Comparative studies on the North American Shale Composite and its metamorphosed equivalent show that element abundance variations between the two composites are relatively small (<15% for REE, Rb, SiO_2, TiO_2 and Al_2O_3; between 15 and 25% for Zr, Cs, Ba, Hf, Ta and Th) (Gromet et al., 1984). Furthermore, Taylor and McLennan (1985) indicate that REE have very large mineral-aqueous fluid distribution coefficients, and suggest that very high water-rock ratios would be necessary to cause important changes in REE patterns during metamorphism. Despite differing opinions in the literature, it appears that metamorphism does not greatly affect the composition of shales.

Small resistate phases such as zircon, magnetite, monazite and tourmaline might be present in shales and might be responsible for variations in REE and HFSE between samples (Gromet et al., 1984). The fairly consistent chemical composition and inter-element ratios between the slate samples suggest that there is no significant mineralogical control due to irregularly distributed accessory phases (Table 4-1, fig.4-1).

Thus, a possible reaction between the slates and the ore-bearing fluid might be revealed by distinctive compositional variations at their contact with the carbonate rocks and the QFV.

Kerrich and Fryer (1979) suggested a genetic link between the slates and the porphyries of the Dome Mine environment based on REE patterns. This suggestion is partially substantiated in the present study. However, the REE patterns obtained for the slates in the present study are less depleted in heavy REE than the average patterns obtained for the quartz-feldspar porphyries from the Dome Mine environment (Fig. 4-1). A second component other than the porphyries is called for. Taylor and McLennan (1985) suggested that the geochemistry of Archean sedimentary rocks is best explained by a mixture of mafic volcanics and felsic rocks. This observation probably applies to the slates of the Dome Mine, that is the slates were derived from local porphyries and mafic volcanics.

	10001A	10001B	10001C	12532	12534	12535	12537
Dist. (m)	2	1	0.1	0.1	5	10	35
SiO2	60.56	56.56	69.49	63.32	65.90	61.98	66.61
Al2O3	18.85	20.72	14.46	18.18	15.97	18.93	15.27
Fe2O3	6.97	7.27	5.78	6.58	6.21	6.57	5.42
MgO	2.90	3.78	2.55	3.16	2.75	2.70	3.38
CaO	0.50	0.18	0.23	0.06	0.19	0.36	1.38
Na2O	2.10	1.72	2.10	4.10	2.53	2.40	1.99
K2O	3.13	4.26	1.20	1.25	2.58	3.13	2.04
TiO2	0.71	0.77	0.50	0.72	0.62	0.74	0.54
MnO	0.06	0.06	<0.01	0.04	0.06	0.04	0.06
P2O5	0.15	0.16	0.13	0.09	0.07	0.10	0.08
LOI	4.06	4.53	3.57	2.50	3.12	3.04	3.23
TOTAL	99.99	100.01	100.01	100	100	99.99	100
CO2	0.70	1.01	0.24	0.46	0.89	0.58	1.85
S				0.04	0.05	0.02	0.04
Rb	80	118	24	31	70	93	72
Sr	110	72	104	131	90	143	309
Y	24	26	17	22	23	29	25
Zr	147	149	153	189	160	180	181
Nb	10	12	13	11	6	8	5
Ba				122.8	204.1	175.2	170.0
Th				8.5	6.0	6.8	5.9
Hf				4.0	3.4	3.5	3.4
Cs				0.5	0.9	1.2	1.2
Ta				0.8	0.8	0.8	0.9
Ni	96	102	67	93	75	84	59
Cr	261	295	185	165	143	153	143
Sc				25	22	28	19
V	156	183	82	159	125	163	107

Table 4-1. Chemical analyses of slates from the Dome Mine.
Samples were collected on two cross-sections (10000 and 12500 suites).
Distance indicates sample location with respect to the contact with the carbonate rock, thus with the Quartz-Fuchsite vein. Ratios in column A correspond to inter-element ratios typical of Archean slates (Taylor and McLennan, 1985).

	10001A	10001B	10001C	12532	12534	12535	12537	
	2	1	0.1	0.1	5	10	35	A
Pb	18	10	11	16	18	13	22	
Zn	108	85	82	79	77	84	74	
Cu	43	48	56	36	25	32	34	
As				44	36	37	27	
Sb				0.7	1.1	0.7	1.4	
La				26.99		31.49	21.60	
Ce				59.92		68.42	50.70	
Nd				25.39		31.13	23.11	
Sm				4.90		5.72	4.35	
Eu				1.21		1.36	1.01	
Tb				0.32		0.33	0.23	
Tm				0.24		0.20	0.19	
Yb				1.64		1.61	1.07	
Lu				0.23		0.25	0.18	
K2O/Na2O	1.5	2.5	0.6	0.3	1.0	1.3	1.0	
SiO2/Al2O3	3.2	2.7	4.8	3.5	4.1	3.3	4.4	
K/Rb	162.3	149.8	207.4	167.3	152.9	139.6	117.6	
Rb/Sr	0.7	1.6	0.2	0.2	0.8	0.7	0.2	
Ba/Rb				4.0	2.9	1.9	2.4	
Ba/Sr				0.9	2.3	1.2	0.6	
Th/Sc				0.3	0.3	0.2	0.3	0.43+/-0.7
La/Sc				1.1		1.1	1.1	1.3+/-0.2
Zr/Y	6.1	5.7	9.0	8.6	7.0	6.2	7.2	
Ti/Zr	2.9	3.1	2.0	2.3	2.3	2.5	1.8	
La/Th				3.2		4.6	3.7	3.5+/-0.3
Cr/V	1.7	1.6	2.3	1.0	1.1	0.9	1.3	1.5+/-0.3
V/Ni	1.5	1.8	1.2	1.7	1.7	1.9	1.8	1.7+/-0.7
Cr/Zr	1.8	2.0	1.2	0.9	0.9	0.9	0.8	

Table 4-1. cont'd

Figure 4-1. REE-chondrite normalized patterns of slate samples from the Dome Mine.

See sample location in figure 4-2.
Dashed patterns correspond to average REE content of quartz-feldspar porphyries from the Dome Mine environment (Unpublished data provided by Dr. J.H.Crocket, 1988).

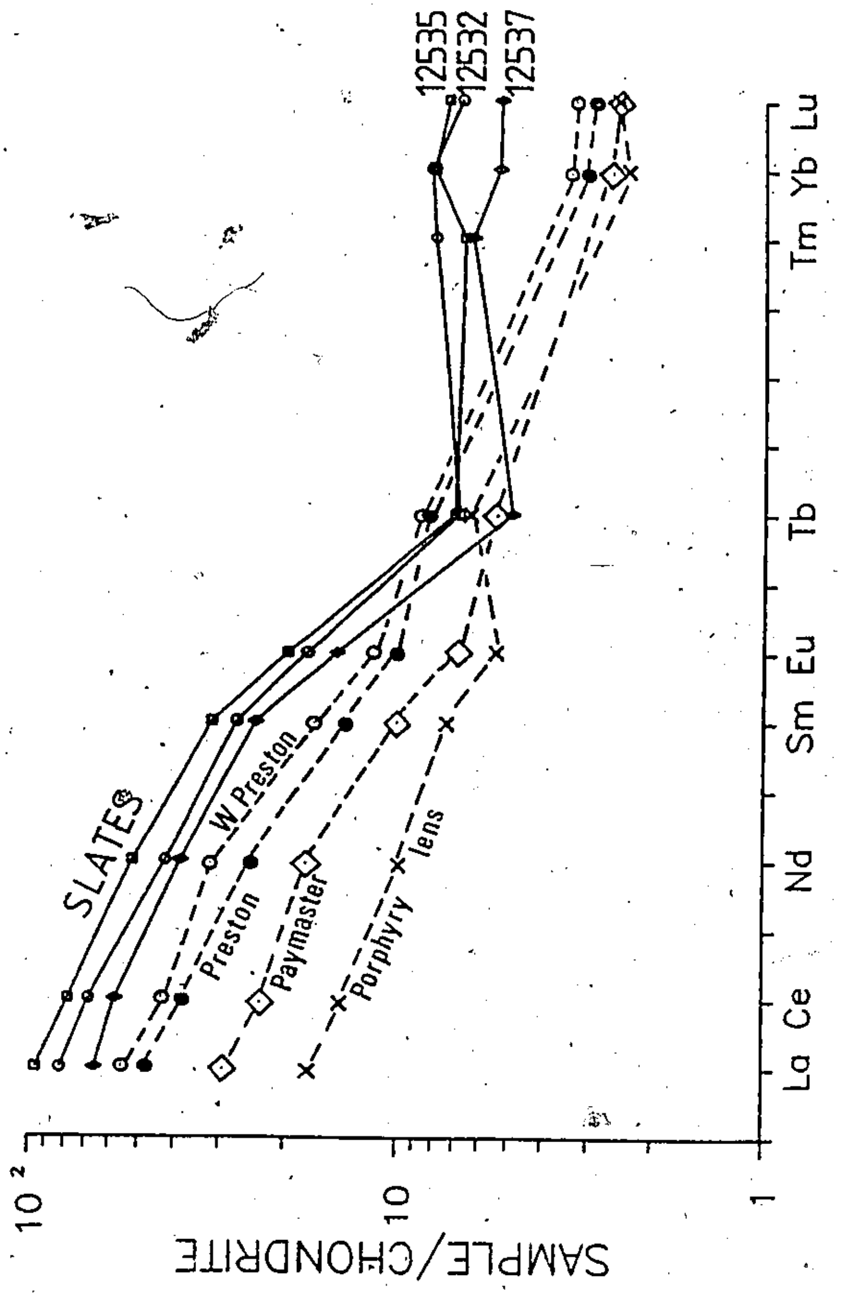
SAMPLE/CHONDRITE
10 2
10
1
La
Ce
Nd
Sm
Eu
Tb
Tm
Yb
Lu
SLATES
12535
12532
12537
W. Preston
Preston
Paymaster
Porphyry lens

4.2.3. Alteration

Slate samples collected in proximity to the contact with the carbonate rocks show depletions in K_2O, Rb, Ba and Cs, as well as in CO_2 and CaO (Table 4-1). Na_2O is the only constituent which seems to be enriched in one instance (Table 4-1, sample #12532). This alteration will be discussed in more detail in section 4.4. (Pattern of alteration).

4.3. CARBONATE ROCKS

4.3.1. Mineralogy and texture

The mineralogy of the carbonate rocks is dominated by carbonates, quartz, chlorite and chromian-muscovite, commonly referred to as fuchsite. Accessory minerals are pyrite, rutile, and rarely chalcopyrite and melonite ($NiTe_2$). XRD-analyses of whole rock powder show that the carbonates are magnesite and ferroan dolomite. Chlorite microprobe analysis indicates that it is the clinochlore species (Fryer et al., 1979).No inclusions of gold were observed in pyrites from the wall rock during microscopic and SEM analyses. Fuchsite crosscuts the other phases, and replaces the carbonates.

The carbonate rocks are coarse-grained and massive to schistose. Textures resembling flow top breccia can be observed locally (Fig. 5-1), and carbonatized rocks on the surface, south of the Dome Mine, show polyhedral jointing. The carbonate rocks are intensely veined. Veinlets are usually small, their width and their length are in the millimeter and centimeter range, respectively. Quartz and carbonates compose the vein material.

The spatial distribution of minerals and textures in the carbonate rocks can be illustrated by a drift, crosscutting the QFV on the 12th level (Figs. 4-2 and 4-3). Close to the QFV, the carbonate rocks are composed of carbonates, quartz, and chlorite. Pyrite and fuchsite are secondary minerals. This rock type corresponds to the "Carbrock" in the mine terminology. Melonite is only present in the immediate vicinity of the QFV. In contrast, the carbonate rock on both sides of the porphyry lens becomes fuchsite- and pyrite-richer, as the contact between the two rock types is approached. This fuchsite-rich carbonate rock is referred to as "Highly Altered" rock in the mine legend.

A planar penetrative fabric is occasionally present in the carbonate rock. It is commonly more intensely developed around the QFV. The penetrative fabric is sparse to almost absent around the porphyry lens, where the carbonate rock is rather fragmental in nature. Its texture progresses from massive to highly fragmented towards the porphyry lens, with a concomitant decrease in size of the fragments. Quartz veining of the carbonate rock also

Figure 4-2. Pattern of wall rock alteration and distribution of textures and mineralogy in the zone of carbonate rocks and altered porphyries. Part I.

See text for discussion. Crosscutting drift on the 12 level (see fig. 5-1 for location). Except for sample 12537, the three first digits of the sample number have been omitted. For instance, 02 should be read 12502, 15 corresponds to 12515, etc.

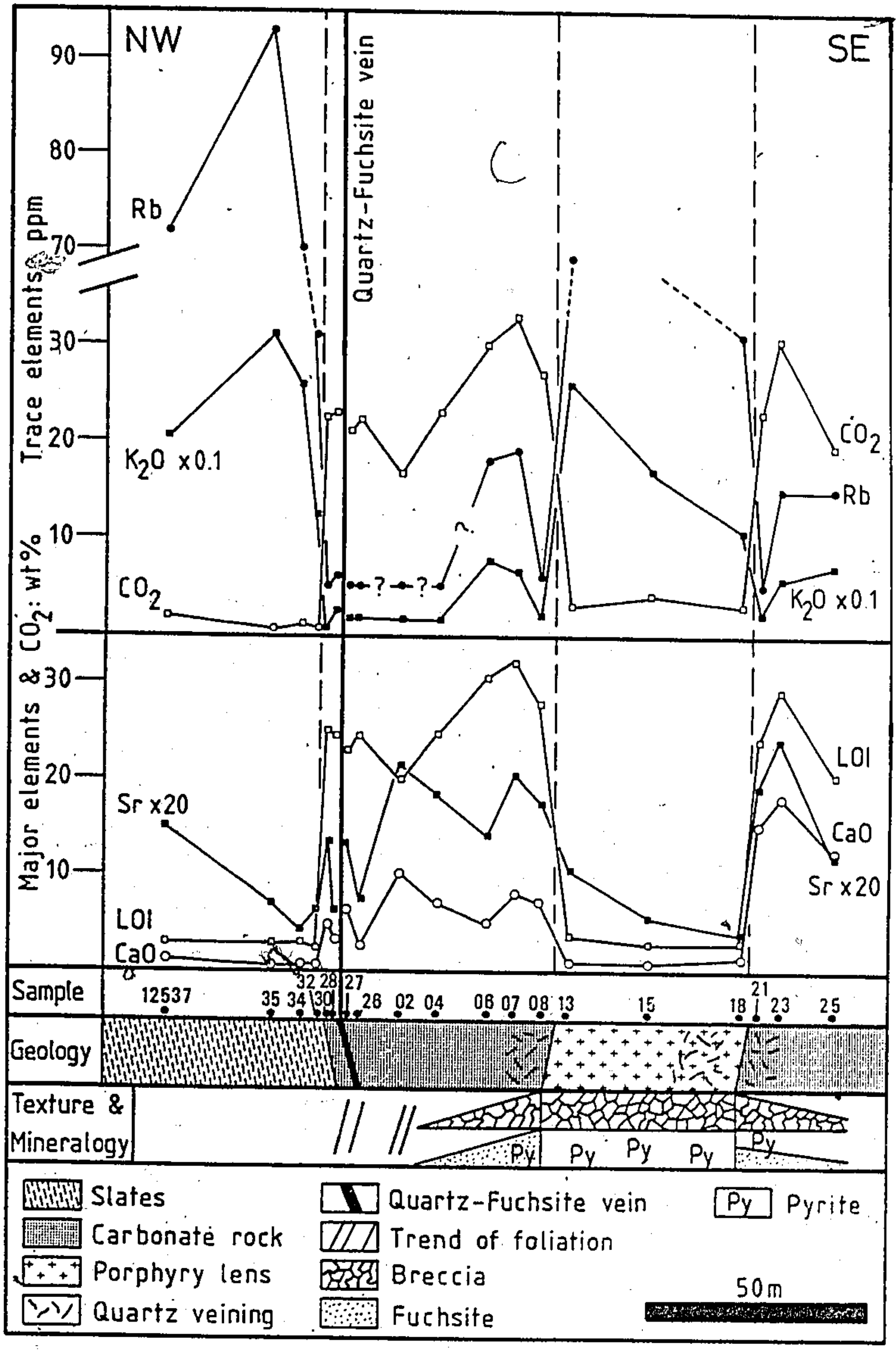
NW
SE
Quartz-Fuchsite vein
Trace elements ppm
Major elements & CO$_2$: wt%
90
80
70
30
20
10
Rb
K$_2$O x0.1
CO$_2$
?
Sr x20
LOI
CaO
Sample
12537
35
34
32
30
28
27
26
02
04
06
07
08
13
15
18
21
23
25
Geology
Texture & Mineralogy
Py
Slates
Carbonate rock
Porphyry lens
Quartz veining
Quartz-Fuchsite vein
Trend of foliation
Breccia
Fuchsite
Pyrite
50m

Figure 4-3. Pattern of wall rock alteration and distribution of textures and mineralogy in the zone of carbonate rocks and altered porphyries. Part II.

See text for discussion. Crosscutting drift on the 12 level (see fig. 5-1 for location). Except for sample 12537, the three first digits of the sample number have been omitted. For instance, 06 should be read 12506, 23 corresponds to 12523, etc.

A: CaO/Al_2O_3 ratio around 1 typical of komatiites (Nesbitt et al., 1979).
B: Ti/Zr range of ratios (between 110 and 160) typical of komatiites (see table 4-3).
C: Ti/Y range of ratios (between 180 and 280) typical of komatiites (see table 4-3).

Gold contents have been averaged at each sample location from muck sample analyses provided by the Dome Mine.

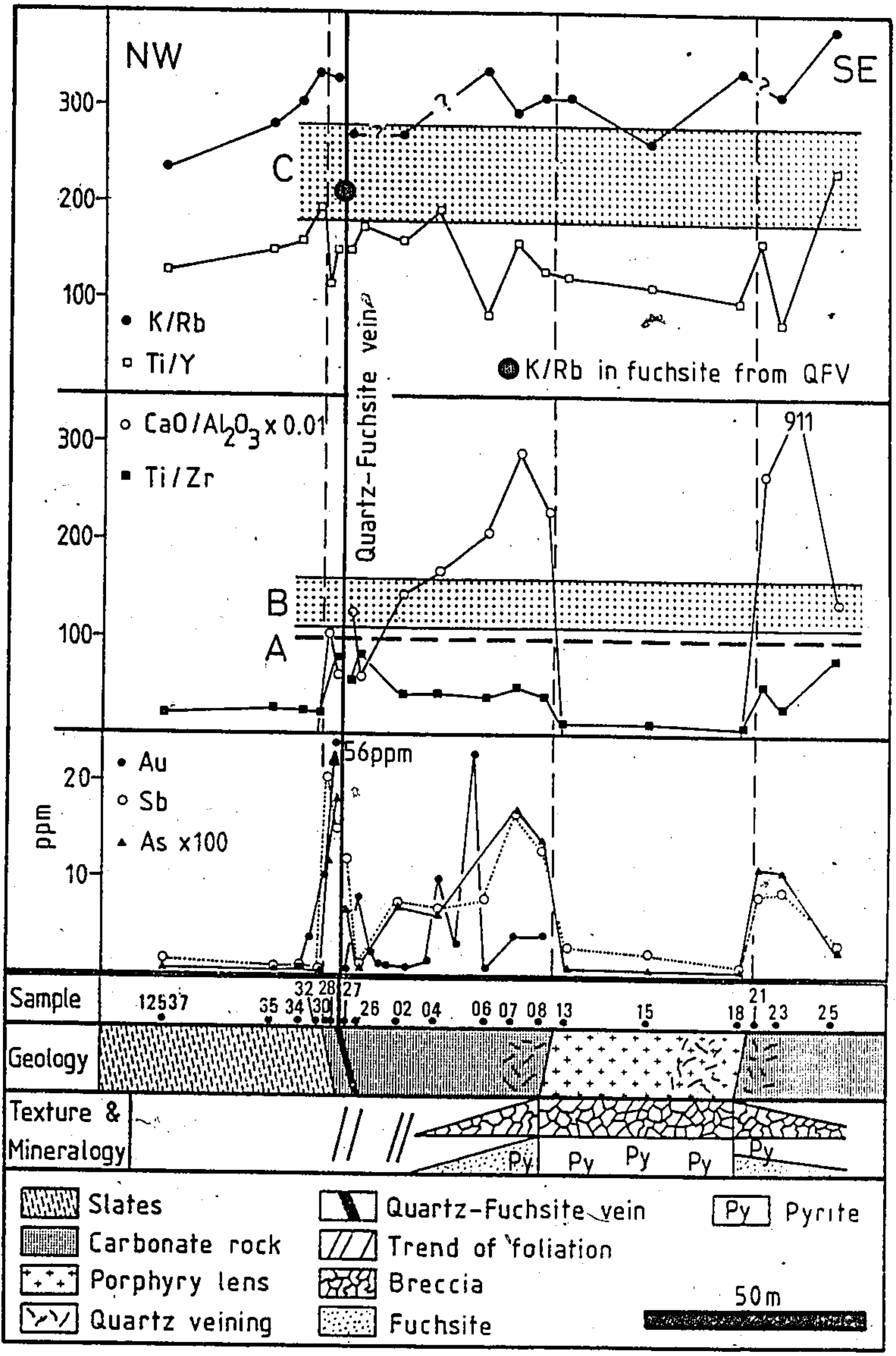
NW
SE
300
200
100
C
K/Rb
Ti/Y
K/Rb in fuchsite from QFV
Quartz-Fuchsite vein
CaO/Al$_2$O$_3$ x 0.01
Ti/Zr
911
B
A
ppm
20
10
Au
Sb
As x100
56ppm
Sample
12537
35 34
32 28 27
30
26 02 04 06 07 08 13 15 18 21 23 25
Geology
Texture & Mineralogy
Py
Slates
Carbonate rock
Porphyry lens
Quartz veining
Quartz-Fuchsite vein
Trend of foliation
Breccia
Fuchsite
Py Pyrite
50m

becomes more important in the neighborhood of the porphyry, accompanying the trend of increasing fuchsite and pyrite abundances, and intensity of fragmentation. This textural and mineralogical zonation of the carbonate rock in the vicinity of porphyry lenses can be observed on several levels (12th, 13th, and 17th levels). Rogers (personal communication, 1984) mentioned that a zonation often observed in the Dome Mine is a porphyry lens enveloped successively by "Highly Altered" rock and "Carbrock". The fragmental nature of the carbonate rock around the porphyry lens can be interpreted either as a tectonic or fault breccia, as advocated by McAuley (1983), or as a result of hydraulic fracturing during hydrothermal activity. The combination of muscovite and pyrite alteration, fracturing of the wall rock and development of intense quartz veining close to the porphyry lens is similar to alteration patterns observed around porphyry copper deposits (Beane and Titley, 1981). Thus, the fragmental nature of the carbonate rock in the proximity of porphyry lenses can probably be attributed in part to hydrothermal fracturing. However, it cannot be ruled out that the brecciated nature is of tectonic origin, since faults and shears are often present at contacts between porphyries and their carbonate host rocks. Alternatively, such deformation might have been superimposed on fractures formed during hydrothermal activity. The presence of heterolithic breccias and intense fracturing has been noted around other porphyries in the Timmins area, in association with sericite and pyrite alteration (Mason and Melnik, 1986a,b; Brisbin and Mason, 1987; Mason and Brisbin, 1987).

Variations in both mineralogical and texture zonations exist. Fuchsite development can be important in the vicinity of the QFV, especially at upper stoping levels of the QFV. However, fuchsite zonation around the QFV is not consistently associated with high ore grades in the vein. The planar penetrative fabric is sometimes completely absent near the QFV. For instance, undeformed and well preserved flow top breccias can be found in the immediate proximity of the vein (Fig. 5-1).

4.3.2. Origin of the carbonate rocks

The original character of the carbonate rocks may be deduced from remnant primary textures, and from diagnostic chemical features. Fryer et al. (1979) classified the carbonate rocks as komatiites on the basis of Ti/Zr ratios, Mg, Cr, and Ni abundances. Roberts and Reading (1981) suggested a komatiitic protolith as well, using the cation plot developed by Jensen (1976) and REE pattern.

The present study substantiates these conclusions. Chemical analyses of the carbonate rocks recalculated to 100% on a volatile-free basis are similar to those of komatiites from Munro (Ontario), Dundonald-Clergue (Ontario) and Lamotte (Québec) Townships, and to komatiites located south of the Dome Mine (Table 4-2). Al_2O_3, Fe_2O_3, MgO, TiO_2, MnO, Ni, Cr, Sc, V, and some of the REE (Sm, Yb, Lu) are present in comparable abundances in both komatiites and carbonate rocks. High MgO content of carbonate rocks, and presence of flow top breccias and polyhedral jointing are compatible with Arndt's and Nisbet's (1982) definition of a komatiite. Ratios of TiO_2 to Al_2O_3 are within the range of komatiites (Table 4-3).

The Ir content of the carbonate rocks, ranging from 1.63 to 4.69 ppb (on a volatile-free basis), is similar to that of ultramafic rocks which range between 1 and 10 ppb (Crocket, 1981). These abundances are comparable to those of komatiites from Western Australia, Munro Township and Alexo (Ontario) (Table 4-4). The Ir content of 4.69 ppb in sample #12530 is however slightly anomalous with respect to Ir concentrations in komatiites. The anomaly presented by this particular sample will be addressed after alteration of the komatiites has been discussed.

Carbonatized rocks, sampled near the "South Greenstone", have relatively lower MgO, Cr and Ni concentrations, and higher Al_2O_3, TiO_2, and REE abundances than samples taken further away from the "South Greenstone" (Table 4-5, figs. 4-3 and 4-4). This is characteristic of a komatiitic sequence, in which rocks of ultramafic composition grade into rocks of mafic composition (Naldrett and Smith, 1980). This type of progression in the Dome Mine was noted previously by Roberts and Reading (1981). Sample #8506 (Table 4-5), which shows a mafic composition, lies close to the northern contact between the slates and the carbonate rocks (Fig. 5-3 and 5-7). This suggests that the ultramafic portion of the carbonate rocks gradually pinches out towards shallower depth.

4.3.3. Alteration

Beswick (1982) recently reviewed the literature on alteration of komatiites. Various methods have been suggested to identify and evaluate alteration in metavolcanic rocks.

A common practice is to grade samples with respect to the degree of alteration for a given rock suite. This is based on choosing samples which show the best preservation of primary mineralogy and textures as "least altered" samples (e.g., Sun and Nesbitt, 1978). Their chemistry is then compared with "more altered" samples. Any attempt to designate a particular sample from the zone of carbonate rock in the QFV setting as "least" altered is doomed to failure. The volatile content of the carbonate rocks (combined H_2O and CO_2) is around 25% (Table 4-2). This level of volatiles, together with the presence of magnesite, corresponds to the most altered rocks which can be found in

Table 4-2. Major and trace element analyses of the carbonate rocks from the Dome Mine compared to komatiites from Timmins (area south of the Dome Mine, fig. 3-1), Munro Township (Ontario), Lamotte Township (Québec), and Alexo (Dundonald-Clergue Townships, Ontario).

Major elements in weight percent. Trace elements in ppm. The data has been recalculated to 100 per cent on a volatile-free basis. SD = one standard deviation. n = number of samples.

Carbonate rocks and samples 801B and 807 were analyzed in the course of the present study. Individual carbonate rock analyses can be found in Appendix IV.
1 - Spinifex-textured peridotitic komatiite, average of samples 3 and 4 from Arndt et al. (1977, table 7).
2 - Spinifex-textured peridotitic komatiite, sample 42 (422/95) from Sun and Nesbitt (1978, tables 1A and 2).
3 - Peridotitic komatiite, sample 31 (422/93) from Nesbitt et al. (1979, table 1).
4 - Komatiites, average of samples DC107, NFT5156, DC112 and DC114 from Canil (1987, table 1).
5 - Komatiites, average of samples 1 and 2 from Ludden and Gelinas (1982, table 21.2).
6 - Flow top breccia, sample M667 from Arndt (1986, tables 2 and 3).
7 - Random and chevron spinifex-textured komatiite, average of samples M651, M654, M663, and M664 from Arndt (1986, tables 2 and 3).
8 - Plate spinifex-textured komatiite, average of samples M656, M657, and M668 from Arndt (1986, tables 2 and 3).
9 - Cumulate zone in komatiite, sample M661 from Arndt (1986, tables 2 and 3).

ELEMENTS	CARBONATE ROCK			KOMATIITES SOUTH OF THE DOME MINE		MUNRO TOWNSHIP				LAMOTTE TOWNSHIP	ALEXO AREA (DUNDONALD-CLERGUE TOWNSHIPS)			
	Mean	SD	n	801B	807	1	2	3	4	5	6	7	8	9
SiO_2	41.01	5.69	31	45.63	46.41	45.3	45.85	44.07	45.95	47.0	45.1	44.9	44.6	43.7
Al_2O_3	6.74	2.21	31	5.61	4.76	7.42	8.35	5.47	9.50	6.9	6.64	6.35	8.6	3.2
Fe_2O_3	12.45	1.98	31	12.11	10.64	12.6	12.17	10.54	12.55	10.1	12.0	11.4	12.8	9.1
MgO	26.31	3.86	31	26.82	32.26	26.8	23.45	33.92	21.51	27.6	30.4	30.4	22.3	42.1
CaO	12.29	5.35	31	0.98	5.08	7.01	8.74	5.20	8.72	6.9	4.80	5.80	10.40	0.99
Na_2O	0.55	0.16	5	<0.20	<0.20	0.45	0.83	0.32	0.96	0.22	0.03	0.26	0.08	0.01
K_2O	0.28	0.26	24	<0.05	<0.05	0.07	0.15	0.13	0.06	0.01	0.03	0.07	0.03	0.01
TiO_2	0.37	0.11	31	0.41	0.34	0.32	0.35	0.21	0.51	0.35	0.33	0.32	0.45	0.19
MnO	0.24	0.07	31	0.15	0.16	0.24	0.22	0.19	0.22		0.18	0.15	0.18	0.12
P_2O_5	0.05	0.06	30	0.03	0.08		0.02	0.02	0.07	0.02				
H_2O	2.07	1.38	31	4.96	6.93	5.3	3.63	5.00		5.7	10.1	8.3	5.9	12.7
CO_2	23.26	4.24	31	0.91	0.22					0.4	0.47	0.21	0.12	0.29
Rb	7	6	31	<5	<5			2	1		5	4	2	
Sr	423	159	31	22	14			18	19	34	16	19	11	3
Y	16	3	31	10	11			7	13	8	8	7	11	4
Zr	45	8	16	17	13			12	38	17	14	13	21	9
Nb	7	4	26	<2	4			1	4					
Ba	45	27	15	30	1			7	15					
Ni	1308	343	31	1409	1645	787		1530	903		1490	1735	936	2600
Cr	3355	767	31	2512	2646	1505		2290	2038		2710	2545	2977	1920
Sc	24	21	31	36	30			20		25	25	23	33	13
V	167	46	31	37	144			103			147	128	182	66
La	0.98	0.48	8		0.80		0.46			0.5	0.41	0.53	0.86	
Ce	3.89	2.06	11		1.72		1.47			3.3	1.33	1.61	2.29	
Nd	3.16	2.10	2				1.66				1.42	1.55	2.31	
Sm	0.73	0.40	11		0.70		0.77				0.61	0.64	0.91	
Eu	0.66	0.85	11		0.26		0.33				0.23	0.25	0.38	
Tb	0.26	0.19	9											
Yb	0.84	0.20	11		0.77		1.08			0.7	0.79	0.78	1.10	
Lu	0.16	0.05	11		0.11						0.12	0.11	0.17	

ROCK TYPES AND LOCATION	Ti/Zr	Ti/Y	Zr/Y	Ti/Sc	Zr/Sc	Al_2O_3/TiO_2	CaO/Al_2O_3	Ref.
Host rock of the QFV : Carbonate rock.								
Mean	53	145	3.2	55	1.2	18.5	2.1	1
SD	18	44	0.8	6	0.4	3.7	1.6	
n	16	31	16	19	15	31	31	
Range	25-83	75-285	1.9-4.3	45-67	0.7-2.3	10.3-29.2	0.6-9.1	
Komatiites, south of the Dome Mine : 801B	146	260	1.8	69	0.5	13.6	1.6	1
807	160	192	1.2	69	0.4	13.8	1.1	
Komatiites, Munro Township.	105	180	1.7	63	0.6	26.0	1.0	2
Komatiites, Lamotte Township.	110-160	214-230		98-105	0.7-0.9	16-19	0.8-1.3	3
Flow top breccia.	141	261	1.8	81	0.6	20.1	0.7	4
Random and spinifex-textured komatiites.	138	272	2.0	83	0.6	19.5	0.9	5
Plate spinifex-textured komatiites.	126	253	2.0	84	0.7	19.2	1.2	6
Cumulate zone in komatiites.	131	300	2.3	89	0.7	16.8	0.3	7
Alexo (Dundonald-Clergue Township).								
Spinifex-textured komatiites. Yilgarn bloc, Western Australia.	111	265	2.4			20.7	1.0	8

Table 4-3. Element ratios of carbonate rocks (MgO > 18%, volatile-free basis) compared to primary element ratios in komatiites.

QFV: Quartz-Fuchsite vein. SD: one standard deviation. n: number of samples.
References :
1 - Present study.
2 - Peridotitic komatiite. Sample 31 (422/93) from Nesbitt et al. (1979, table 1).
3 - Komatiite: range of ratios from Lamotte I (K) and Lamotte II (K) from Ludden and Gelinas (1982, table 21.3).
4 - Sample M667 from Arndt (1986, table 2).
5 - Average of samples M651, M654, M663, and M664 from Arndt (1986, table 2).
6 - Average of samples M656, M657, and M668 from Arndt (1986, table 2).
7 - Sample M661 from Arndt (1986, table 2).
8 - Average of samples 1 to 7 from Nesbitt and Sun (1976, table 1).

SAMPLE PROVENANCE, TYPE AND NUMBER	Ir ABUNDANCES (ppb)	REFERENCE
Dome Mine, Timmins:		1
807 (Komatiite)	3.21	
12504 (Carbrock)	1.97	
12525 (Carbrock)	1.75	
12526 (Carbrock)	2.57	
12527 (Carbrock)	1.63	
12530 (Carbrock)	4.69	
Mt Clifford (Western Australia):		2
Spinifex-textured	2.99 2.22	
Cumulate-textured	2.10 2.37	
Pyke Hill (Munro Township):		3
Spinifex-textured	0.97 0.77	
Cumulate-textured	0.97 2.04	
Alexo (Dundonald-Clergue Townships):		4
Plate spinifex	2.08	
Random spinifex	2.6	

Table 4-4. Comparison of Ir abundances between carbonate rocks (carbrock), a komatiite from the Dome Mine (Timmins), and komatiites from Western Australia and Ontario (Pyke Hill and Alexo).

Data is presented on a volatile-free basis.
The data for Mt Clifford and Pyke Hill represent the analyses of two different flows in each locality.
References: 1 - this study; 2 - Keays (1982); 3 - Crocket and MacRae (1986); 4 - Bruegman et al. (1987), (sample locations from Arndt (1986)).

	CARBONATE ROCK			KOMATIITES SOUTH OF THE DOME MINE		CARBONATE ROCKS WITH A TREND TOWARDS MAFIC COMPOSITION			
	Mean	SD	n	801B	807	8506	12525	17103A	17536
SiO_2	41.01	5.69	31	45.63	46.41	47.53	35.78	49.85	50.88
Al_2O_3	6.74	2.21	31	5.61	4.76	6.92	11.37	10.66	10.00
Fe_2O_3	12.45	1.98	31	12.11	10.64	10.87	18.54	13.29	16.99
MgO	26.31	3.86	31	26.82	32.26	17.74	15.29	13.96	9.00
CaO	12.29	5.35	31	8.98	5.08	15.90	15.80	10.87	10.40
Na_2O	0.55	0.16	5	<0.20	<0.20	<0.20	0.93	<0.20	0.31
K_2O	0.28	0.26	24	<0.05	<0.05	<0.05	0.88	0.21	1.34
TiO_2	0.37	0.11	31	0.41	0.34	0.41	0.74	0.63	0.64
MnO	0.24	0.07	31	0.15	0.16	0.30	0.57	0.28	0.42
P_2O_5	0.05	0.06	30	0.03	0.08	0.02	0.10	0.02	0.02
H_2O	2.07	1.38	31	4.96	6.93	0.00	0.94	3.90	10.94
CO_2	23.26	4.24	31	0.91	0.22	19.18	19.61	10.52	7.66
Rb	7	6	31	<5	<5	<5	15	6	28
Sr	423	159	31	22	14	468	241	68	98
Y	16	3	31	10	11	11	16	17	17
Zr	45	8	16	17	13	43	44	51	57
Nb	7	4	26	<2	4	3	3	3	2
Ba	45	27	15	30	1	18	37	40	51
Ni	1308	343	31	1409	1645	717	503	715	1314
Cr	3355	767	31	2512	2646	1927	1810	2592	1880
Sc	24	21	31	36	30	31	50	50	50
V	167	46	31	37	144	130	290	211	201
La	0.98	0.48	8		0.80		2.04	0.34	1.30
Ce	3.89	2.06	11		1.72		3.44	2.63	4.28
Nd	3.16	2.10	2				3.72		
Sm	0.73	0.40	11		0.70		1.15	1.34	1.23
Eu	0.66	0.85	11		0.26		0.58	0.51	0.45
Tb	0.26	0.19	9				0.47		
Yb	0.84	0.20	11		0.77		0.87	1.30	1.00
Lu	0.16	0.05	11		0.11		0.15	0.23	0.14

Table 4-5. Mafic komatiites in the zone of carbonate rocks.

The location of sample 12525 is given in figure 4-2, and of sample 8506 in figure 5-3. Carbonate rocks of ultramafic composition, and komatiites from the Timmins area (south of the Dome Mine) are given for comparison purpose.

Major elements in weight percent. Trace elements in ppm. The data has been recalculated to 100 per cent on a volatile-free basis.

SD = one standard deviation. n = number of samples.

the Timmins area (Fyon and Crocket, 1981; Fyon et al., 1983b). The carbonate rocks have most certainly been thoroughly recrystallized, concomitant with important chemical changes. These rocks are probably the result of carbonatization of komatiites. In the course of such metasomatism, large amounts of CO_2 are introduced into the original silicate rock, and transform it into a rock whose mineralogy is dominated by carbonates (Johannes, 1969; Harte and Graham, 1975; Fyon et al., 1983). "Least altered" komatiites from other localities have to be selected for comparison purposes (e.g., Alexo area, Munro and Lamotte Townships).

Gresens (1967) (see also Babcock, 1973; Grant, 1986) suggested that volume changes during metasomatic processes must be considered to adequately quantify element enrichment or depletion. However, this method may lead to erroneous results, if the rocks being compared were not identical in chemical composition before metasomatism. Detailed chemical studies by Beswick (1983), Arndt (1986) (see also table 4-2), Crocket and MacRae (1986), and Blais et al. (1987) attest that element abundances can be fairly variable between different zones of a komatiitic flow. Gresens' method cannot be used for the carbonate rocks of the Dome Mine, since no textural or chemical criteria allow them to be related to a particular zone of a komatiitic flow; and, as mentioned above, no unaltered counterparts are present.

Beswick and Soucie (1978) and Beswick (1982) argue for an analysis of the degree of alteration through molecular proportion ratio (MPR) diagrams. However, great caution must be taken in the use of MPR diagrams, because of possible introduction of spurious and enhanced correlations (Butler, 1986; Rollinson and Roberts, 1986); moreover according to Pearce (1987), the extent of element mobility cannot be deduced from such diagrams.

Thus, it seems that only a qualitative assessement of element mobility in the carbonate rocks can be made by a broad comparison on a volatile-free basis with equivalent rocks from other localities, as illustrated for instance in table 4-2.

On the one hand, it is generally accepted that elements such as Na, K, Rb, Sr, and Ba are very mobile during alteration and metamorphism of metavolcanic rocks (e.g., Nesbitt and Sun, 1976; Sun and Nesbitt, 1978; Nesbitt et al., 1979; Naldrett and Smith, 1980; Beswick, 1982; Arndt, 1986; Canil, 1987). On the other hand, however, disagreement prevails as to the mobility of many other elements.

If a komatiitic protolith is a correct choice for the carbonate rocks, then the comparative approach can be used to determine relative element enrichment or depletion in the carbonate rock zone. It is assumed that the carbonate rocks and the comparative komatiite suites underwent fairly similar seawater alteration and burial metamorphism. The difference in chemical composition is then attributed mainly to interaction with hydrothermal fluids. Since carbonatization of the komatiites probably predated or was coeval with regional deformation and greenschist metamorphism (Fyon, 1986), it is further assumed that metamorphism did not severely alter element distribution patterns after hydrothermal alteration. The following conclusions can be reached from table 4-2 :

1) Substantial amounts of CaO, K_2O, CO_2, Sr, Zr, Nb, and Ba have been added to the carbonate rocks.

2) Na_2O, MnO, Rb, and Y are increased in the carbonate rocks with respect to "fresher" komatiites; however, this increase is less pronounced for these elements than for the elements from the first group (CaO to Ba, point 1).

3) SiO_2 and H_2O are the only constituents significantly depleted in the zone of carbonate rocks. The question can be raised whether silica-depletion is real or not. Large quartz veins, which are not abundant, were avoided during sampling of the wall rocks. Small quartz veins could not be avoided during sampling. These are most certainly an integral part of the carbonatization process of the komatiites. Breakdown of Ca, Mg, and Fe silicates and introduction of CO_2 results in the formation of Ca, Mg, and

Fe carbonates and an excess of silica (Johannes, 1969; Harte and Graham, 1975). Excess silica was thus available for formation of quartz veins, or might have been removed from the carbonate rock environment. It is believed that the lower silica content of the carbonate rocks relative to komatiites is real and not an artefact due to sampling procedures, i.e. some silica was certainly removed from the komatiites during the carbonatization process.

4) La, Ce, Nd and Eu are present in higher abundances in the carbonate rocks than in the komatiites while Sm, Yb, and Lu are present in similar abundances. Chondrite-normalized REE diagrams of the carbonate rocks are shown in figures 4-4 and 4-5. The LREE display the largest variations between samples. Most of the samples show positive Eu anomalies. Carbonate rocks and komatiites display similar trends for HREE, whereas LREE are enriched in the carbonate rocks with respect to komatiites (Fig. 4-6). The Eu anomaly is only present in the carbonate rocks. REE patterns obtained in the present study are comparable to those of Roberts and Reading (1981). They differ however from those obtained by Kerrich and Fryer (1979) for the same rock types from the Dome Mine. The latter show patterns strongly depleted in HREE. This discrepancy is attributed to different analytical methods (i.e. NAA in the present study and XRF by Kerrich and Fryer (1979)). Since NAA is thought to be a more reliable technique for

Figure 4-4. REE chondrite normalized patterns of carbonate wall rocks from the crosscutting drift on the 12 level.

For sample location see figure 4-2, and for drift location see figure 5-1.

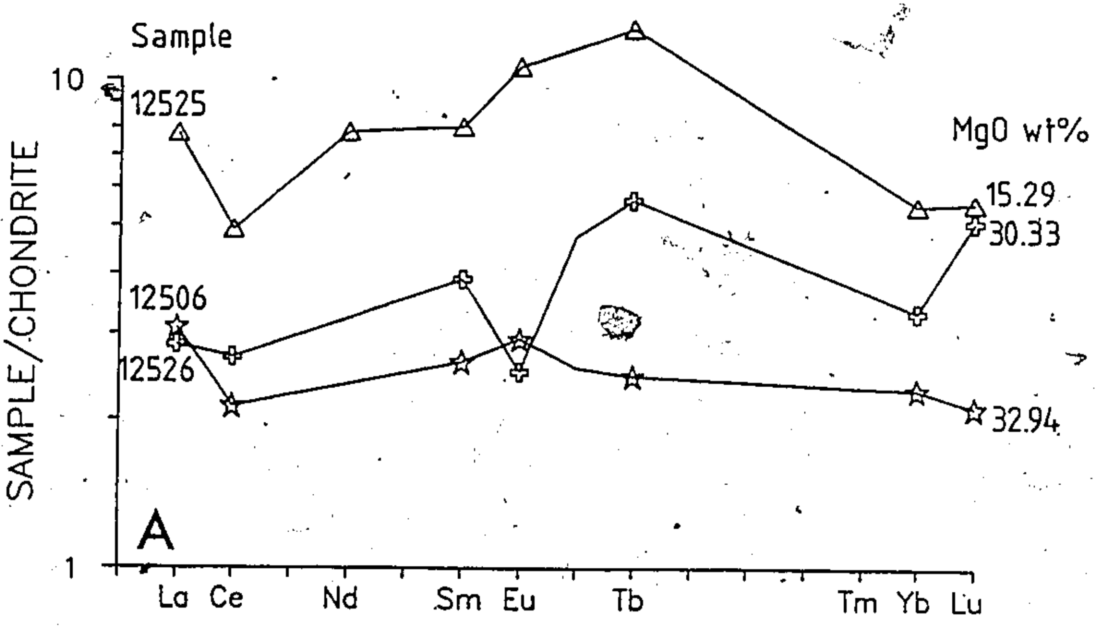
Sample
10
12525
12506
12526
1
SAMPLE/CHONDRITE
A
MgO wt%
15.29
30.33
32.94
La
Ce
Nd
Sm
Eu
Tb
Tm
Yb
Lu

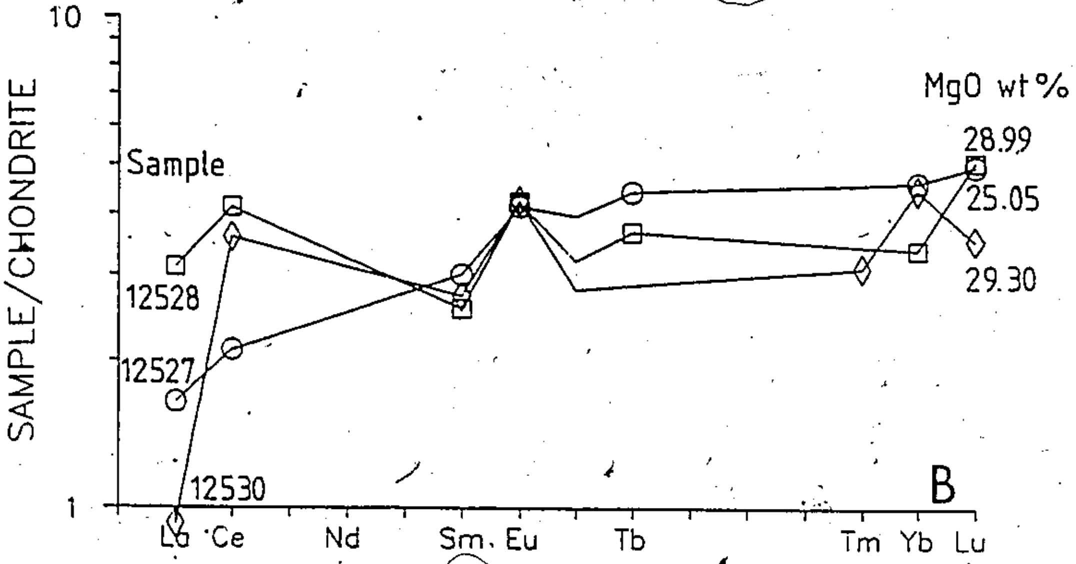
10
Sample
12528
12527
12530
1
SAMPLE/CHONDRITE
B
MgO wt%
28.99
25.05
29.30
La
Ce
Nd
Sm
Eu
Tb
Tm
Yb
Lu

Figure 4-5. REE-chondrite normalized patterns of carbonate wall rock samples other than the samples from the crosscutting drift on the 1/2 level..

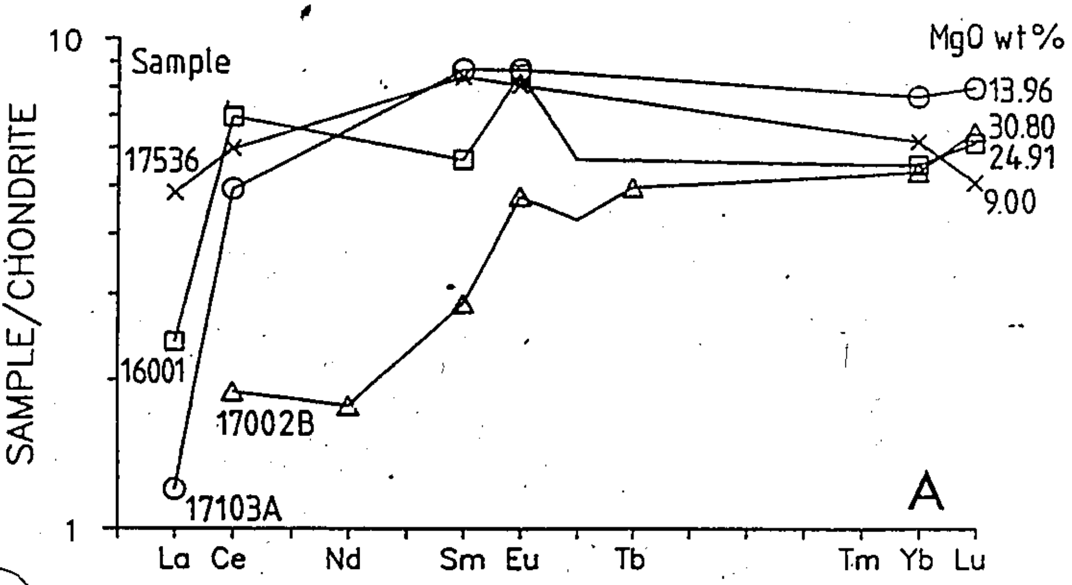
10
Sample
MgO wt%
17536
16001
17002B
17103A
13.96
30.80
24.91
9.00
SAMPLE/CHONDRITE
A
1
La
Ce
Nd
Sm
Eu
Tb
Tm
Yb
Lu

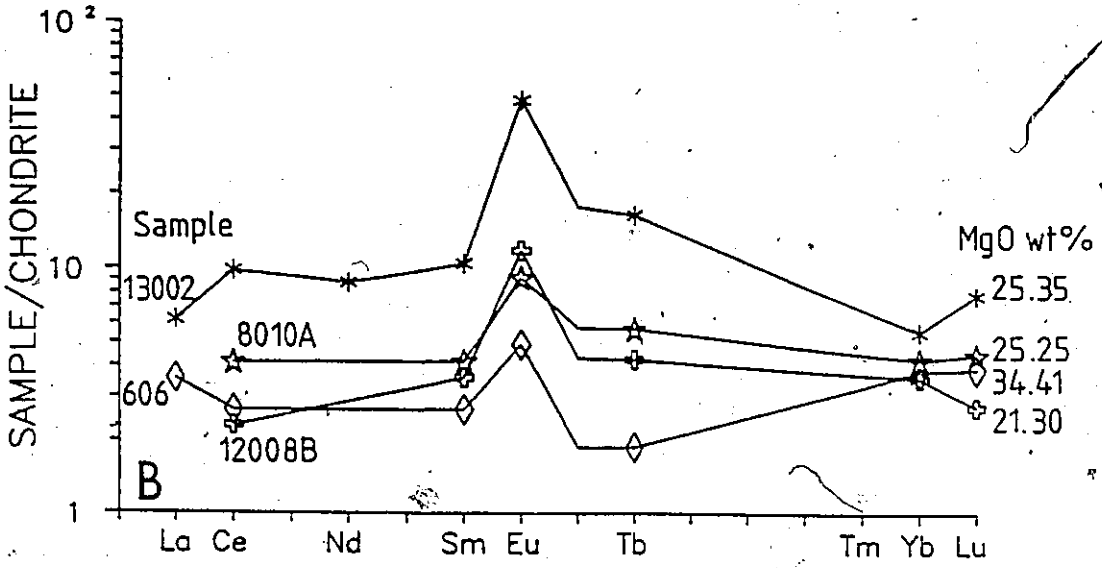
10 2
Sample
MgO wt%
13002
8010A
606
12008B
25.35
25.25
34.41
21.30
SAMPLE/CHONDRITE
10
B
1
La
Ce
Nd
Sm
Eu
Tb
Tm
Yb
Lu

Figure 4-6. REE-chondrite normalized patterns of carbonate rocks from the Dome Mine compared to patterns of komatiites from the Abitibi Greenstone belt.

a: Envelop for carbonate rock samples from the Dome Mine depicted in figure 4-2.
b: Envelop for carbonate rock samples from the Dome Mine depicted in figure 4-3.
c: Sample 807. Spinifex-textured komatiite from area south of the Dome Mine.
d: Envelop for Upper komatiites from Munro Township (Naldrett and Smith, 1980).
e: Envelop for lower peridotitic komatiites from Munro Township (Naldrett and Smith, 1980).
1: Plate-spinifex textured komatiite from the Alexo area (Arndt, 1986), column #8 in table 4-2.
2: Random and chevron spinifex textured komatiite from the Alexo area (Arndt, 1986), column #7 in table 4-2.
3: Flow top breccia from the Alexo area (Arndt, 1986), column #6 in table 4-2.
4: Spinifex-textured komatiite from Munro Township (Sun and Nesbitt, 1978), column #2 in table 4-2.

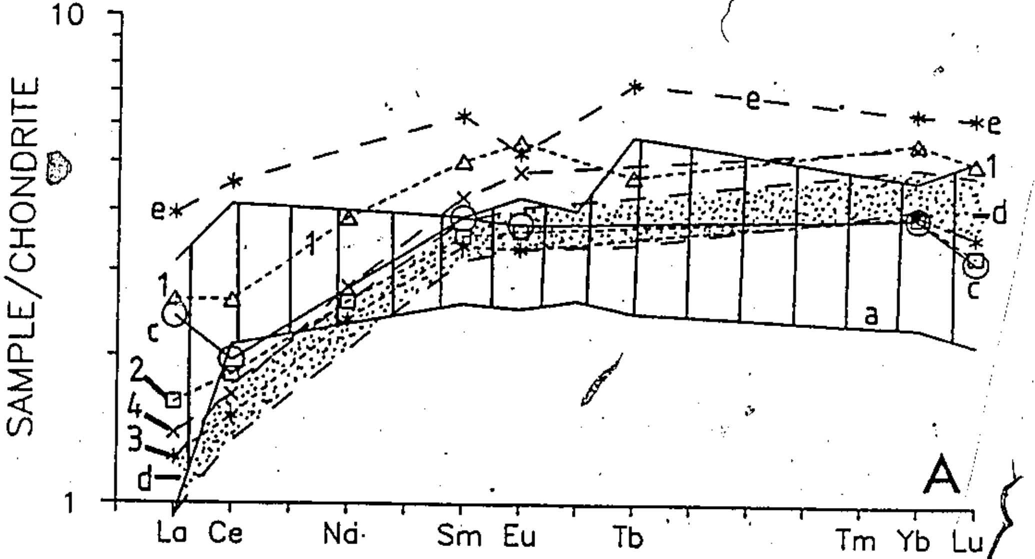
10
1
SAMPLE/CHONDRITE
La
Ce
Nd
Sm
Eu
Tb
Tm
Yb
Lu
e
1
c
2
4
3
d
a
A

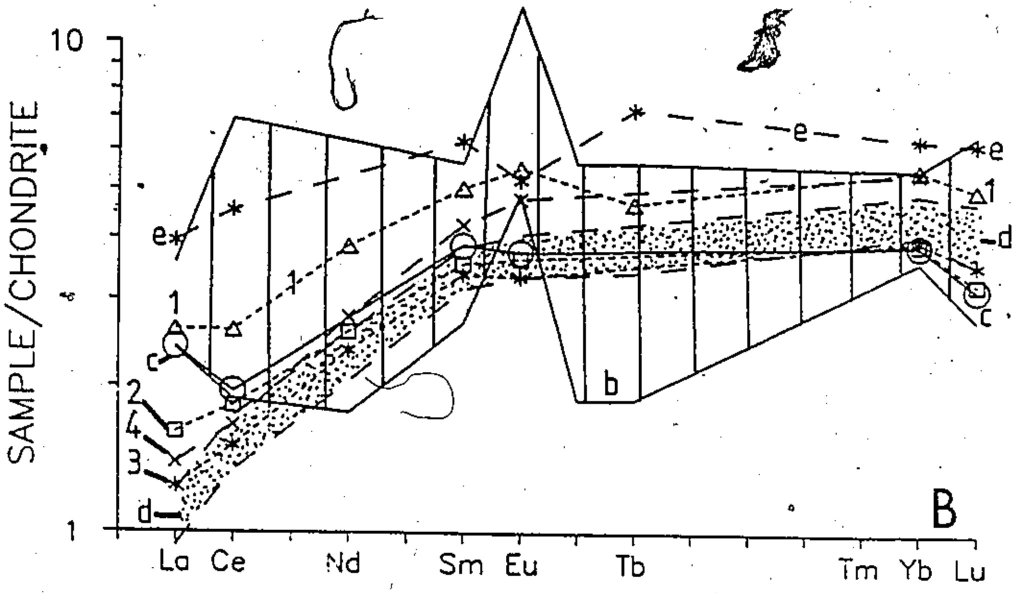
10
1
SAMPLE/CHONDRITE
La
Ce
Nd
Sm
Eu
Tb
Tm
Yb
Lu
e
1
c
2
4
3
d
b
B

analyzing REE, especially at low abundance levels (Henderson and Pankhurst, 1984), more confidence is placed in the patterns obtained in the present work, and these will be used subsequently.

From this comparative study it appears that on average Al_2O_3, Fe_2O_3, MgO, TiO_2, Ni, Cr, Sc, V, Sm, Yb, and Lu are substantially the same in the carbonate rocks and a komatiitic protolith. However, these elements may have been mobile within the carbonate rock zone. Nesbitt et al. (1979) suggested that consistent inter-element ratios may be diagnostic of a primary magmatic character as they cannot be duplicated by metasomatic processes. Nesbitt and Sun (1976) noted that Ti/Zr, Ti/Y, Zr/Y, TiO_2/P_2O_5 and Zr/Nb ratios were relatively constant in komatiites from Western Australia, Canada, and South Africa. Consistency of these ratios and similarity to chondrite values lead to the assumption that they represent primary petrogenetic characteristics. Remobilization during metamorphism was implied to be insignificant. Using this approach, Ludden and Gélinas (1982) concluded that Ti, Y, Sc and HREE were essentially immobile in komatiites from Lamotte and Destor Townships (Québec), and that variations in their ratios could be attributed to heterogeneous magma source regions. In contrast, mobility of Zr, Y, Hf was suggested by Beswick (1982, 1983) in a study of an altered komatiite flow in Val d'Or (Québec). Inter-element ratios between Ti, Zr, Y, Sc, and Al_2O_3 are presented in table 4-3 for the carbonate rocks from the Dome Mine, and are compared to those from komatiites from the Abitibi belt and from Western Australia. It can be noted that :

1) The spread in ratios is greater for the carbonate rocks than for the komatiites.

2) Excluding Al_2O_3/TiO_2, ratios of the carbonate rocks usually do not correspond to values typical of komatiites.

3) Differences in ratios exist between various localities and within a single flow (e.g. Alexo area); however differences are greater between the carbonate rocks and komatiites from Timmins, than they are between the Timmins komatiites and komatiites from more or less remote localities in the Abitibi belt.

These observations substantiate the conclusion that Zr and Y are mobile in the carbonate rock environment. The difference of the Ti/Sc ratio with respect to komatiitic values, and the large spread of the Al_2O_3/TiO_2 ratio also lead to the assumption that Ti, Sc, and Al might have been mobile to varying degrees.

These considerations indicate that the hydrothermal alteration responsible for the development of the carbonate rocks involved the remobilization of many, if not all, elements within the carbonate rock unit and within surrounding rock sequences. Even elements such as Zr, Y, Ti, and Al commonly regarded as immobile have been redistributed to some extent. Other examples are known where carbonatization has redistributed so called immobile elements : Hynes (1980), Ludden et al. (1984) and Murphy and Hynes (1986) have described mobility of Ti, Y, Zr, Al, Hf, Sc, P, and Nb in metabasalts and felsic rocks affected by carbonatization.

A general consensus seems to exist about the behavior of REE during alteration and metamorphism of komatiites. LREE and Eu are thought to be more susceptible to redistribution than HREE (Sun and Nesbitt, 1978; Beswick, 1982, 1983). However, Whitford and Arndt (1978), Arndt (1986) and Blais et al. (1987) state that differences in REE abundances and minor variations in LREE patterns are consistent with primary chemical characteristics.

The non-carbonatized komatiite sample from the Timmins area (Fig. 4-6; sample #807) has an REE pattern which is comparable to komatiites from the Upper Cycle in Munro Township, and strikingly similar to the random and chevron spinifex-textured zone of the Alexo komatiite. It can be assumed that the carbonatized komatiites (carbonate rocks) from the Dome Mine had comparable LREE-depleted pattern before the alteration event. Thus, carbonatization resulted in introduction of LREE and Eu. The overall variation in absolute REE abundances (spread in chondrite normalized patterns) of the carbonate rocks can be attributed to primary covariance of REE abundances with MgO content (e.g. Whitford and Arndt, 1978; Arndt, 1986; Blais et al., 1987), or to erratic redistribution of REE. This later point is suggested by the lack of correlation between REE and MgO concentrations (Figs. 4-4 and 4-5). The vertical spread is probably a result of both primary and secondary processes.

It has been experimentally demonstrated that REE can be extremely mobile in CO_2-rich fluids under crustal conditions (Wendlandt and Harrison, 1979). Empirical observations show that HREE form stronger carbonate complexes than LREE (Kosterin, 1959; Taylor and Fryer, 1982). Thus, the LREE enrichment in the carbonate rocks can be explained by preferential breakdown of the weaker LREE-carbonate complexes from a CO_2-rich fluid, whether or not enriched in LREE.

The Eu anomalies could be attributed to either low oxygen-fugacities of the hydrothermal fluid or interaction with a solution enriched in Eu. Fryer et al. (1979) found a high ferrous to ferric iron ratio for the carbonate rocks (Fe^{2+}/Fe^{3+} = 0.85 - 0.97), which they regarded as evidence for the reducing nature of the hydrothermal fluid. However, a high Fe^{2+}/Fe^{3+} ratio need not indicate a reduced hydrothermal fluid. For instance, Eckstrand (1975) has shown that carbonatization indicates oxidizing conditions rather than a reducing environment. Thus, the Eu anomaly is not necessarily due to a reducing fluid altering the komatiites which host the QFV. Another alternative is that the fluid which carbonatized the komatiites was enriched in Eu relative to the other REE. This could be the case if the hydrothermal fluid was derived from decomposition of a rock containing feldspars. McAuley (1983) describes the presence of remnant primary feldspars grains in the porphyries of the Dome Mine environment. Thus, at least some of the Eu might be derived from the local porphyries, and its subsequent deposition in the carbonate rocks might have contributed to the Eu anomaly. Moreover, Ca was introduced in the komatiites as they were carbonatized. Ca-bearing carbonates would be likely hosts for any bivalent Eu present in solution.

4.4. PATTERN OF ALTERATION

The cross-cutting drift on the 12th level through the QFV and adjacent lithologies permits an examination of the pattern of element distribution in the alteration zone. The komatiites and the porphyries (McAuley, 1983) have been more affected by the carbonate alteration than the slates. This is a common observation in alteration halos around gold-bearing quartz veins, where slates usually remain largely unaffected by the hydrothermal ore-bearing fluid (Boyle, 1979).

Most of the elements show no particular distribution trend in any of the rock types. Nevertheless,

CO_2 and LOI are higher in the carbonate rocks in the vicinity of the porphyry lens (Fig. 4-2), as are K_2O, Rb, CaO and Sr (Fig. 4-2). These patterns correspond to the mineralogical and textural zonation observed in the carbonate rocks around the porphyries (Fig. 4-2). It appears that the alteration pattern is centered around the porphyry lens, rather that around the QFV. Fuchsite development is a direct result of the higher K_2O abundances around the porphyry lens. Sb and As, which are commonly good gold indicators (Boyle, 1981; Fyon and Crocket, 1982) are, together with gold, the only elements which show a significant enrichment around the QFV. Au, As, and Sb are also enriched in the neighborhood of the porphyry lens (Fig. 4-3). The gold concentration in the carbonate rocks is far higher than in unaltered komatiites, which usually contain around 2 ppb gold, suggesting that gold must have been added to the komatiites during the hydrothermal alteration. Thus, it appears very unlikely that the carbonatized komatiites were the gold-source of the mineralization present in the QFV.

The porphyries in the zone of altered rocks have been extensively sericitized (McAuley, 1983). The carbonate rocks are commonly rich in fuchsite in the vicinity of the porphyries. It is inferred from this observation that the fluid which sericitized the porphyries is certainly also responsible for the development of fuchsite in the immediate host rock. This implies that some kind of fluid circulation was active from the porphyry lens towards the komatiitic host rock.

In contrast, depletion of K_2O, Rb, Cs and Ba can be recognized in the slates immediately adjacent to the carbonate rocks (Fig. 4-2, and Table 4-1). The K/Rb ratio of the slates increases sharply towards the slate-carbonate rock contact (Fig. 4-3). This trend is a typical result of rock-hydrothermal fluid interaction during which Rb is preferentially removed relative to K, leaving an altered rock with a higher K/Rb ratio and a fluid enriched in Rb (Armbrust and Ganicott, 1980). Due to very low K- and/or Rb-concentrations in most of the carbonate rocks, it was not possible to profile the distribution of K/Rb ratios along the complete cross-section depicted in figure 4-3.

The formation of fuchsite, i.e. introduction of K and Rb in the carbonate rocks in proximity to the porphyry lens, and the removal of K and Rb in the slates at the contact with the carbonate rocks suggests two interpretations :

1) Two independent hydrothermal fluids might be responsible for this alteration pattern. One fluid sericitized the porphyry lens and deposited fuchsite in the carbonate rocks, and then a second fluid migrated along the QFV, and removed both K and Rb from the slates and the carbonate rocks in the vicinity of the gold-bearing vein.

2) Alternatively, a single fluid may account for this alteration pattern as follows : the fluid which sericitized the porphyry lens migrated into the carbonate host rock. Since it was oversaturated in K (and Rb), it formed the Cr-muscovite in the country rock. At a certain distance from the porphyry lens, the hydrothermal fluid became too depleted in K-content to stabilize fuchsite. When it reached the slates, it started to leach such elements as K, Rb, Cs, and Ba.

The second scenario seems to be more likely in the view of the distribution of Ti/Zr, Ti/Y, and CaO/Al_2O_3 ratios in the alteration zone (Fig. 4-3). Since komatiites are the original protolith of the carbonate rocks, the Ti/Zr and Ti/Y ratios would be expected to range between 110 and 160, and between 190 and 280, respectively (Table 4-3). The carbonate rocks, however, show Ti/Zr and Ti/Y ratios which are lower than komatiitic values. It was argued that this resulted from introduction of Zr and Y into the komatiites during carbonatization. Figure 4-3 displays a trend of increasing Ti/Zr ratio in the carbonate rocks towards values characteristic of komatiites, with increasing sample distance from the porphyry lens. This may indicate that the source of Zr was the porphyry lens. Zr content of the hydrothermal fluid was higher near the porphyry lens, thus resulting in lower Ti/Zr ratios near it. The more remote carbonate rocks near the slates were progressively less enriched in Zr. An analogous observation is that of Ludden et al. (1984) who noted that Zr was leached from felsic rock during carbonatization. Thus, it seems plausible in the present case that the hydrothermal fluid which carbonatized the porphyry lens removed some Zr, and deposited it in the adjacent komatiites. It is believed that the slates did not contribute Ti or Zr to the carbonate rocks. There is no noticeable depletion of TiO_2 or Zr in the slates at the contact with the carbonate rocks. The Ti/Y ratio shows a similar trend to the Ti/Zr ratio (Fig. 4-3). However, the slates seem to have contributed some Y to the carbonate rocks as well. The Ti/Y ratio in the slates increases towards the carbonate rocks, and this trend can be attributed to Y-leaching. The CaO/Al_2O_3 ratio is usually close to 1 in "fresh" komatiites from the Abitibi belt (Nesbitt et al., 1979). In the carbonate rocks there is a constant decrease of this ratio from 3 to 1 as one progresses from the porphyry outwards to the QFV and the slate contact (Fig. 4-3). This trend together with the CaO halo around the porphyry lens (Fig. 4-2), suggests that CaO was added to the komatiites, and that it was brought in by a fluid migrating out of the porphyry lens.

Thus, there was probably one single fluid which was responsible for the alteration pattern in the zone of carbonatized rocks and altered porphyries. The path of fluid migration was probably from the porphyry lens outwards into the carbonate country rock and up to the less permeable slates. The fluid did not penetrate very far into the slates, and left only a slight signature by removing such elements as K_2O, Rb, Ba, and Cs.

It seems highly unlikely that two successive fluids first modified primary magmatic ratios in the komatiites, and then altered these rocks a second time to return these ratios close to the original magmatic ratios.

4.5. IRIDIUM ANOMALY

As mentioned above, one sample in the carbonate rocks has a higher Ir content than usual for a komatiitic protolith (Table 4-4, sample #12530). Conflicting opinions exist about the distribution and the control of Ir in rock forming minerals. A positive correlation of Ir abundances with Cr or Ni concentrations is often observed in ultramafic rocks. For instance, Agiorgitis and Wolf (1978) and Razin and Khomenko (1969) found a high correlation between Cr and platinum group elements (PGE), particularly Ir, Os and Ru, in chromites from ophiolites and Alaska-type complexes. These authors argued that PGE substituted for Cr^{3+} in spinel. However, recent studies have described inclusions of platinum-group minerals (PGM) in chromites from ophiolites (e.g., Stockman and Hlava, 1984; Augé, 1985, 1986), leading to the inference that PGE occur in discrete sulfide or alloy phases, rather than in the crystal structure of major oxides and silicates. Crocket (1979) and Naldrett et al. (1979) suggested that, in sulfur-poor rocks, olivine might constitute a sink for Ir, whereas Keays (1982) and Barnes (1983, in Crocket and MacRae, 1986) contend that sulfides and refractory metal phases are the major Ir-concentrators in komatiites. In a study on the Pyke Hill komatiite flow (Munro Township, Ontario), Crocket and MacRae (1986) found no affinity between Ir and sulfides, but accepted the possibility of an Ir-concentrator phase (i.e., a metallic alloy) mechanically incorporated in olivine.

The covariance of Ir with respect to Cr and Ni is shown in figure 4-7. Overall, there is a positive correlation between Ir, Cr, and Ni in samples from the wall rock and from mineral separates from the banding of the QFV. The geochemistry of the chlorite and fuchsite separates will be addressed in chapter 6. Among the wall rock samples, the covariance seems to be better for Ir and Ni than for Ir and Cr (Table 4-6). Samples from the wall rocks show a good correlation between Ir and Ni (r=0.83), but it is weaker than the correlation between Ni and MgO (r=0.93). Moreover, the correlation between MgO and Ir is also weak (r=0.66) suggesting that Ir was probably not incorporated in the structure of olivine in the original komatiites. The association of Ir and Ni possibly results

Figure 4-7A. Covariance diagram for Ir and Cr in the carbonate wall rocks, a spinifex textured komatiite from the Timmins area, and chlorite and fuchsite separates from the Quartz-Fuchsite vein.

Figure 4-7B. Covariance diagram for Ir and Ni in the carbonate wall rocks, a spinifex textured komatiite from the Timmins area, and chlorite and fuchsite separates from the Quartz-Fuchsite vein.

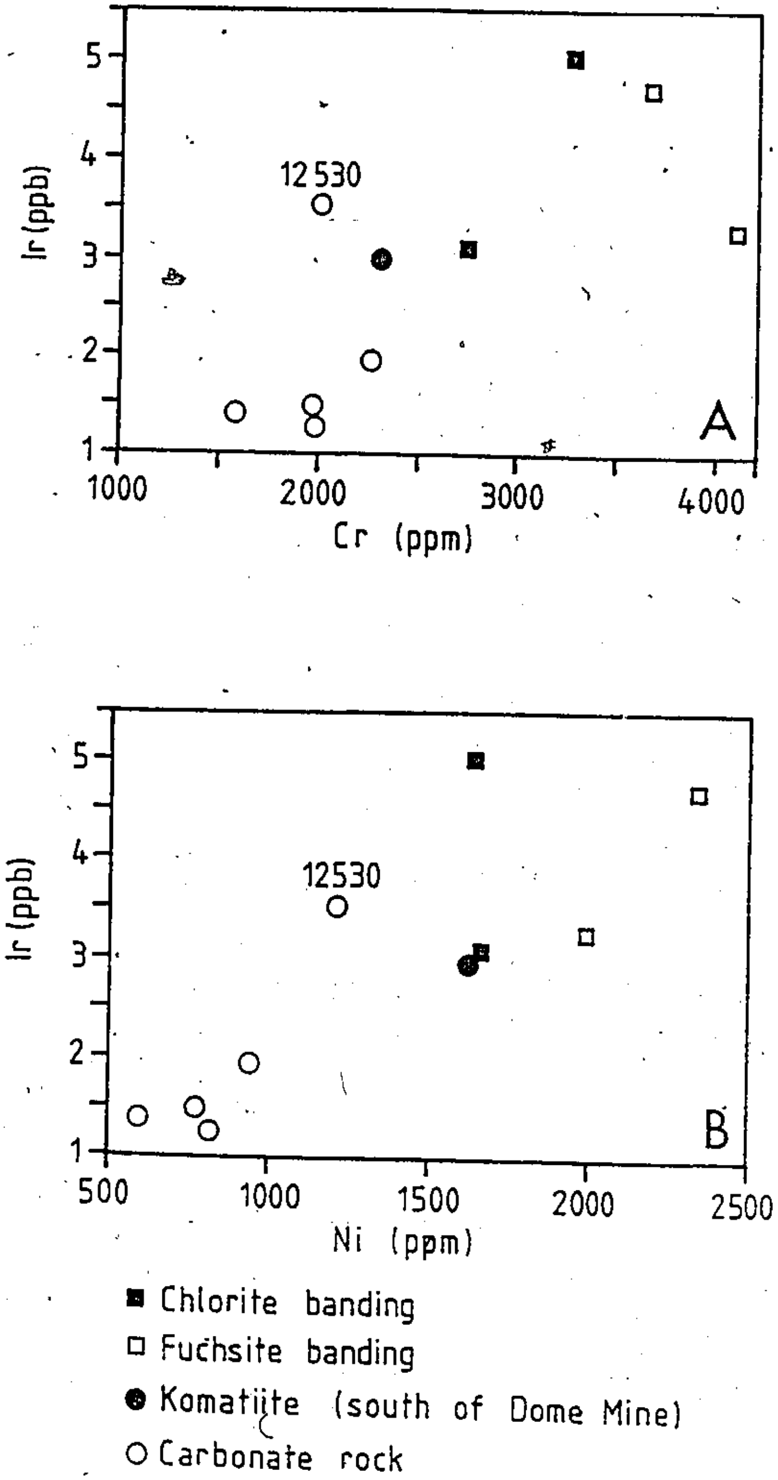
Ir (ppb)
5
4
3
2
1
12530
A
1000
2000
3000
4000
Cr (ppm)
Ir (ppb)
5
4
3
2
1
12530
B
500
1000
1500
2000
2500
Ni (ppm)
■ Chlorite banding
□ Fuchsite banding
● Komatiite (south of Dome Mine)
○ Carbonate rock

	Ni	Cr	Ir	MgO	S
Cr	0.74	—			
Ir	0.83	0.45			
MgO	0.93	0.93	0.66		
S	-0.51	-0.82	-0.36	-0.71	
Cu	-0.42	-0.67	-0.44	-0.57	0.96

Table 4-6. Interelement correlation matrix for carbonate rocks from the Dome Mine, and a komatiite located south of the Dome Mine.

Sample numbers: 807, 12504, 12525, 12526, 12527, and 12530. For sample location see figure 4-2.

from the presence of mineral inclusions in olivine which concentrate Ir. As suggested by the low correlation coefficient (r=0.45) between Ir and Cr, substitution of Ir for Cr-bearing minerals is not important. The role of sulfides as Ir-carriers is probably also minimal as no relationship exists between Ir and S or Cu. Thus, in the wall rocks of the QFV, Ir may have been carried in a refractory metal phase, conceivably as an inclusion in olivine. As noted previously, the wall rocks were severely altered, resulting in the mobility of many elements from the protolith. Alteration might have modified the inter-element correlations on which the present discussion is based. Nevertheless, Crocket and MacRae (1986) reached similar conclusions on much less altered komatiites from Pyke Hill (Ontario).

Due to higher Ir content, sample #12530 stands out from the linear trend displayed by the other samples (Fig. 4-7). In this particular sample, Ir may be concentrated by some other phase rather than a remnant refractory carrier in olivine. As mentioned above, sulfides are probably not important Ir-carriers in the environment of the QFV. Ir appears to be fairly immobile during alteration processes (e.g., Glasson and Keays, 1978; Mitchell and Keays, 1981; Oshin and Crocket, 1982; Barnes et al., 1985). Thus, it is presumed that Ir behaved like all the elements that are present in comparable abundances in the carbonate rocks relative to komatiites (Al_2O_3, TiO_2, Cr, Ni, MgO, etc.); that is, it was probably mobile to some extent in the altered komatiite, and no Ir was added from an extraneous source.

Excluding PGM, arsenides and sulfarsenides act as majors concentrators of PGE (Crocket, 1981). Sample #12530 was collected in very close proximity to the QFV (Fig. 4-2). This sample has the highest As content of all the samples analyzed for Ir (Fig. 4-8). It is possible that the introduction of As in the komatiites during alteration resulted in crystallization of an arsenide-sulfarsenide mineral which concentrated Ir. The presence of an arsenide-sulfarsenide in the immediate QFV-environment will be substantiated furthermore in chapter 6.

4.6. CONCLUSIONS

The wall rocks of the QFV have been altered to various degrees. The slates were altered only in the immediate vicinity of the QFV. The alteration pattern suggests that K_2O, CaO, CO_2, Rb, Ba, and Cs were removed from the slates while Na_2O seems to be the sole constituent that was added to the slates.

The carbonate rocks are probably the completely altered counterparts of komatiites. A komatiitic protolith is suggested by high MgO, Cr, Ni, and Ir abundances, as well as flow top breccias and polygonal jointing. Al_2O_3,

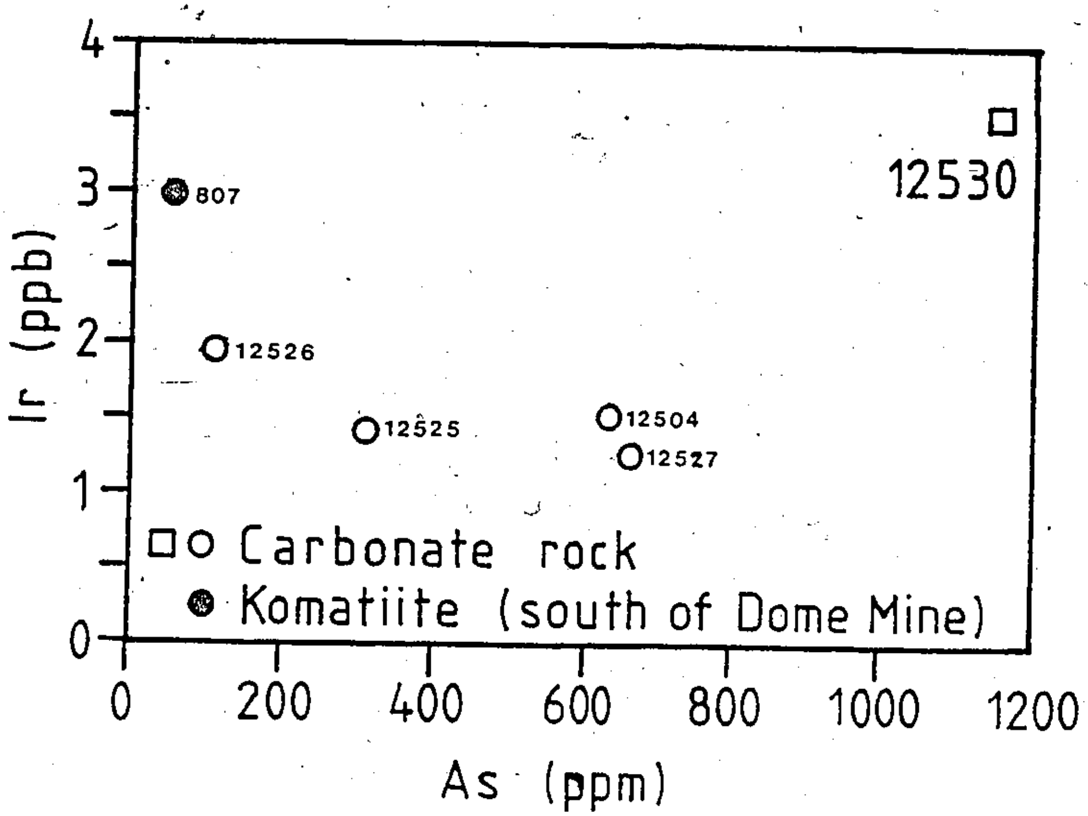

Figure 4-8. Covariance between Ir and As in carbonate rock samples from the Dome Mine and a spinifex-textured komatiite from the Timmins area.

Fe_2O_3, TiO_2, MnO, Sc, V, and some REE (Sm, Yb, Lu) are present in the carbonate rocks in similar abundances to "fresher" komatiites from the Abitibi belt. Carbonatization of the komatiites resulted in the introduction of CaO, K_2O, Sr, Zr, Nb, Ba, Na_2O, MnO, Rb, Y, As, Sb, Au, and of course CO_2. The altered rocks are also enriched in LREE, and most display a positive Eu anomaly. The latter might reflect a reducing hydrothermal fluid. However, more likely they represent a hydrothermal fluid that was spiked with Eu after reaction with a rock containing plagioclase. SiO_2 and H_2O appear to be the only constituents that have been partially lost from the carbonate rocks.

The large variation in Al_2O_3/TiO_2 ratio, and Ti/Zr, Ti/Y, Zr/Y, Ti/Sc, and Zr/Sc ratios inconsistent with values typical of komatiites, suggest high element mobility. Elements were probably mobile within the carbonate rocks to some extent, and exchange of certain elements with surrounding lithologies was important. This precludes the use of quantitative mass-balance calculations to evaluate element mobility in these rocks.

Alteration of the carbonate rocks is centered around the porphyry lens in proximity to the QFV, rather than around the QFV itself. The mineralogical and textural zonation around the porphyry lens on the 12th level is analogous to the alteration pattern that can be found in the periphery of porphyry copper deposits. The geochemical alteration follows the trends displayed by texture and mineralogy. Elements that are enriched in the carbonate rocks relative to komatiites were probably introduced into the latter via a single alteration event. The hydrothermal fluid migrated outwards from the porphyry lens into the komatiitic host rocks. This fluid probably did not penetrate very far in the less permeable slates, and did not greatly alter them. Thus, it seems that most of the extraneous major and trace elements in the carbonate rocks were derived from the immediate neighboring lithologies, mainly the porphyries, and to a lesser extent the slates.

Gold is enriched in all host rocks. It appears unlikely that carbonatization of the komatiites supplied gold to the QFV, since the komatiites are themselves enriched.

CHAPTER 5

ANATOMY AND MECHANISM OF FORMATION OF THE QUARTZ-FUCHSITE VEIN

5.1. INTRODUCTION

Gold mineralization in Archean greenstone belts is commonly located in, or adjacent to, shear zones and faults (e.g., Gustafson and Miller, 1937; Dunbar, 1948; Henderson, 1948; Thomson, 1948; Travis et al., 1971; Robert et al., 1983; Colvine et al., 1984; Bernasconi, 1985; Clark et al., 1984; Robert and Brown, 1986a; Groves and Phillips, 1987). This observation led many researchers to conclude that Archean gold deposits are structurally controlled by faults or shear zones. The deformation affecting host rocks of gold deposits is often one of the latest recorded events. Thus, caution is needed in suggesting a genetic link between the late deformation event and the emplacement of the ore body. The question is whether the structure controlled the development of the ore body, or whether the ore body was a zone of weakness which controlled the localization of higher strain.

The choice of one or the other of these alternatives will have major implications on the interpretation of the geochemical and fluid inclusion data, and the interpretation of ore genesis. In this context, it is important for the Dome Mine study to: determine the mechanism of formation of the QFV, distinguish features related to vein formation from features related to deformation, place the vein genesis into the geological evolution of the Timmins area, determine the distribution of gold within the QFV, and understand how the ore distribution ties into vein development and deformation.

5.2. LOCATION AND GENERAL STRUCTURE OF THE QUARTZ-FUCHSITE VEIN

The QFV is located in the zone of carbonatized komatiites and altered porphyries (Fig. 5-1). It has a NE-SW trend and commonly dips towards the SE (Fig. 5-2A). It is subparallel to the northern contact of the altered rocks and the slates (Fig. 5-3), and for most of its extension, the immediate wall rocks are the carbonatized komatiites. However, the QFV sometimes marks the boundary between the carbonate rocks and the slates. The gold mineralization is entirely hosted within the 500 m by 550 m by 3.5 m average width QFV, although in the upper 6th and 8th levels, economic concentrations are also found in the immediate carbonate wall rock. The structure and the thickness of the vein is highly variable along strike and dip. The vein is a chain of quartz lenses, often bounded by faults of variable orientations (Figs. 5-1, 5-5, and 5-7). For the sake of simplicity, the chain of quartz lenses is referred to as QFV. Two main types of quartz veins can be distinguished along the strike of the QFV : quartz veins in the wall rock and quartz material forming the QFV.

Figure 5-4 represents the shape of the QFV with the help of a Conolly contour diagram (Conolly, 1936). The strike and dip of the reference plane are 045 (N45°E) and 75°SE, respectively. Measurements of the distance between the reference plane and the vein are at 15' intervals. Overall, the QFV has a convex shape towards the NW (Fig. 5-4). According to the Conolly diagram (Fig. 5-4), the QFV can be broadly separated in two domains. The western part of the vein has a very regular shape. The distance between the vein and the reference plane increases regularly from east to west, as well as from bottom to top. The eastern domain has a more irregular shape, and structurally speaking, seems to be more complex than the western extension of the vein. The irregular shape is also reflected in the greater difficulty in following and mining the eastern part of the vein. In this area, the contouring values show a sharp break between the 10th level and the 12th level. This jump in the values can also be noticed on the cross-section in figure 5-3. On the 12th and 13th levels, the vein is located at the lower carbrock - slate contact, whereas on the 8th and 10th levels the vein lies

Figure 5-1. Local geology of the Quartz-Fuchsite vein on the 12 level (adapted from maps provided by the Geology Department of the Dome Mine).

A - B, C - D, E - F: location of cross-sections A-B, C-D, and E-F depicted in figure 5-3.
a: location of plate 5-3A.
b: location of plates 5-1B and 5-3B.
c: area where C-S fabric is present in the carbonate wall rock.
d: location of the mine drift crosscutting the Quartz-Fuchsite vein and the geological units. It corresponds to the sample location for the wall rock alteration study shown in figures 4-2 and 4-3.
e: location of map in figure 5-9.
I: high grade ore zone in the Quartz-Fuchsite vein characterized by strong fuchsite and chlorite banding.
II: low grade ore zone in the Quartz-Fuchsite vein with rare chlorite banding.
III: high grade ore zone in the Quartz-Fuchsite vein characterized by strong chlorite banding.
1: sample location of slates for composite sample COMP4 analyzed for whole rock lead isotope composition (chap. 8).
2: sample location of galena samples 12003 and 12031 analyzed for lead isotope composition.
3: sample location of porphyry lens sample 12515 analyzed for whole rock lead isotope composition.

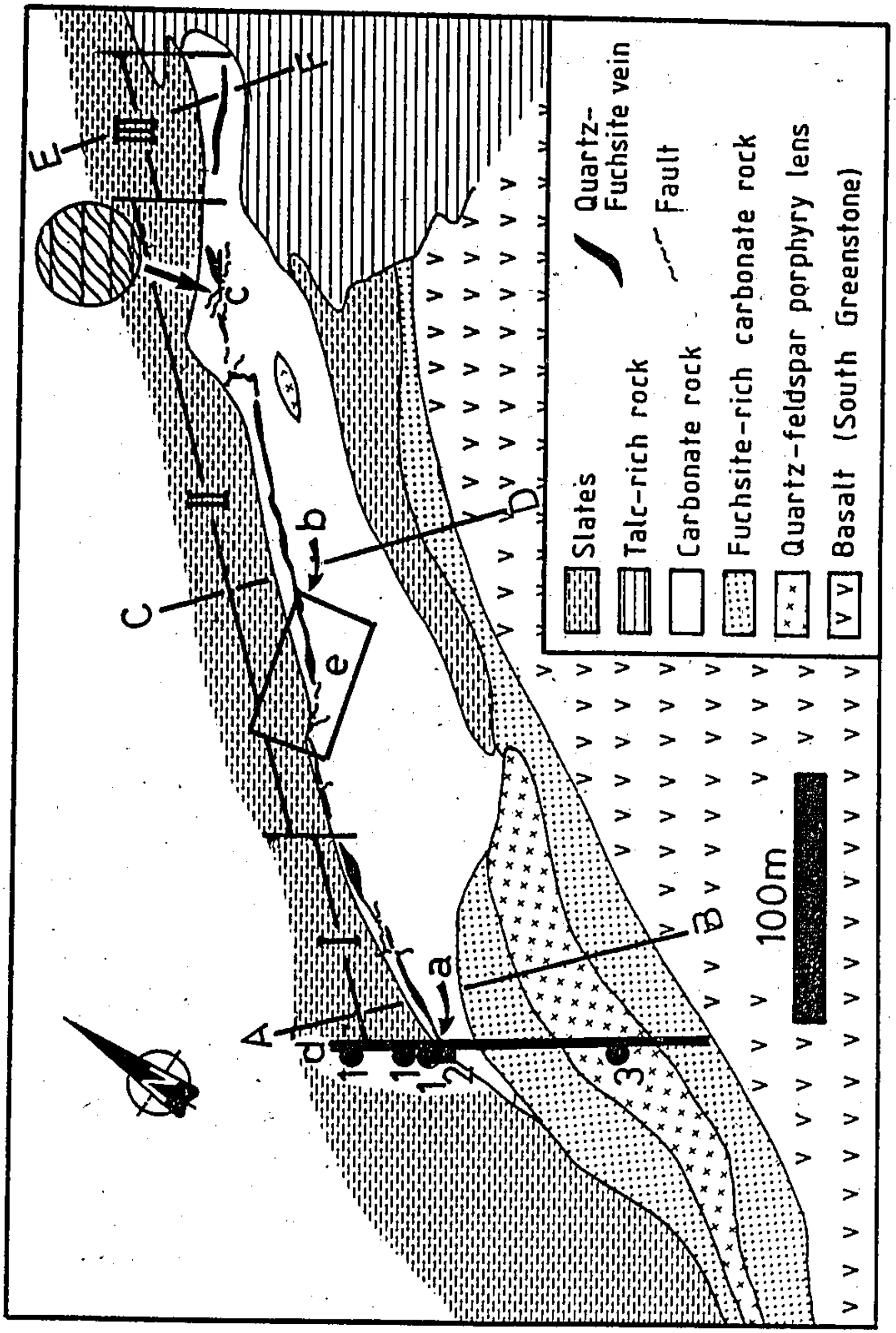
A
B
C
D
E
F
I
II
III
a
b
c
d
e
1
1
1
2
3
100m
Slates
Talc-rich rock
Carbonate rock
Fuchsite-rich carbonate rock
Quartz-feldspar porphyry lens
Basalt (South Greenstone)
Quartz-Fuchsite vein
Fault

Figure 5-2. Stereographic projection of structural elements of the Quartz-Fuchsite vein and of its wall rocks (Wulff stereographic net).

A: orientation of the Quartz-Fuchsite vein and the foliation in the carbonate wall rock.

B: orientation of the slickenside striations in the Quartz-Fuchsite vein, and the two high grade ore zones in the Quartz-Fuchsite vein.

C: orientation of relatively undeformed quartz veins in the carbonate wall rocks.

D: theoretical orientation of fractures associated with strike-slip simple shear and concomitant development of a foliation in the wall rock. Orientation of second order fractures has been taken from Hancock (1985). The orientation of the theoretical foliation in D has been visually estimated to represent the average orientation of the foliation of the carbonate wall rock depicted in A.

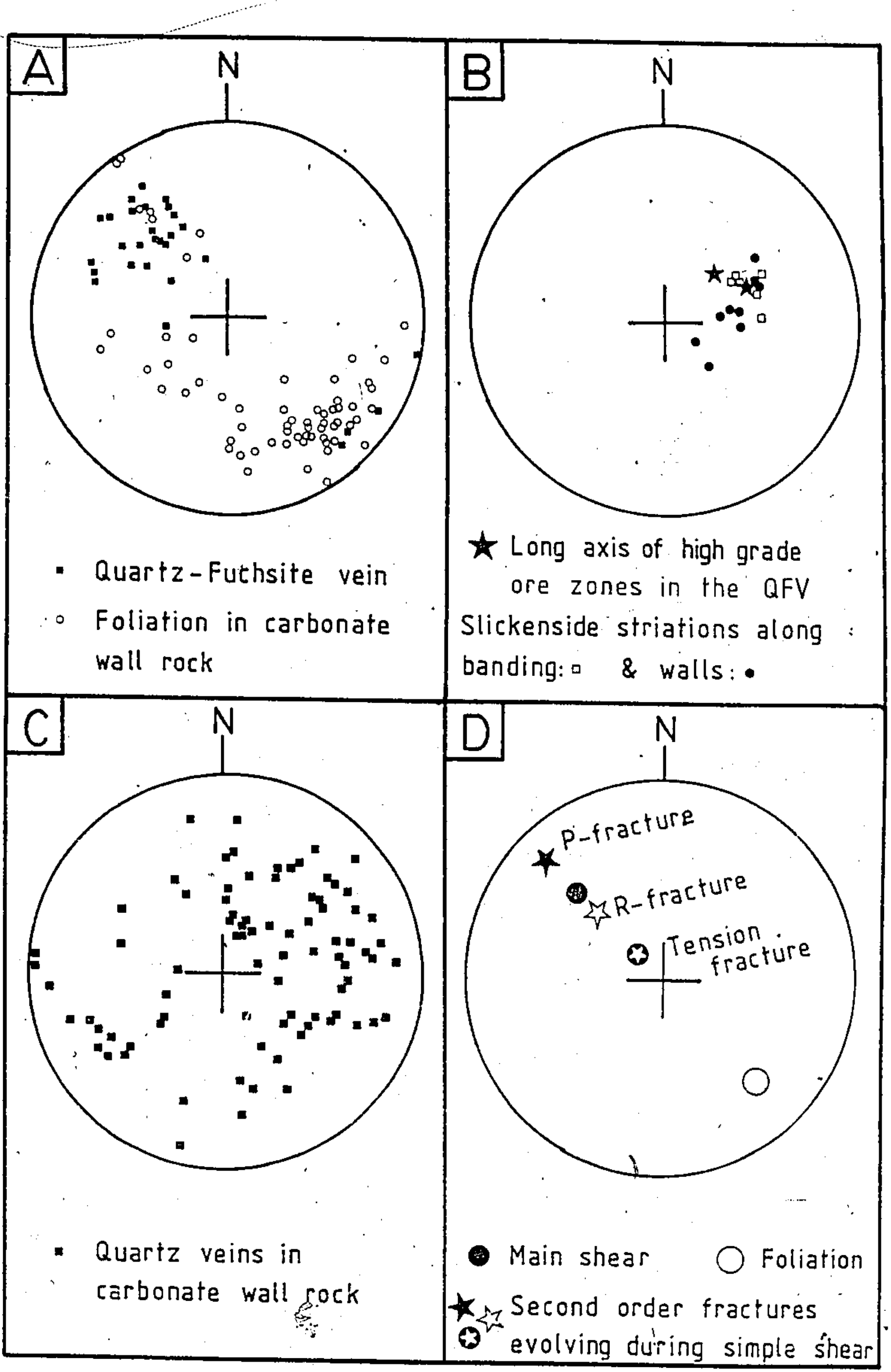
A
N
▪ Quartz-Futhsite vein
○ Foliation in carbonate wall rock
B
N
★ Long axis of high grade ore zones in the QFV
Slickenside striations along banding: ▫ & walls: •
C
N
▪ Quartz veins in carbonate wall rock
D
N
P-fracture
R-fracture
Tension fracture
● Main shear
○ Foliation
★ ☆ ✪ Second order fractures evolving during simple shear

Figure 5-3. Cross-sections through the zone of carbonatized rocks hosting the Quartz-Fuchsite vein.

A - B: section in the western extremity of the vein.
C - D: section in the central part of the vein.
E - F: section in the eastern extremity of the vein.
Location of sample 8506 from table 4-5, and the crosscutting drift studied for the pattern of wall rock alteration are also indicated.

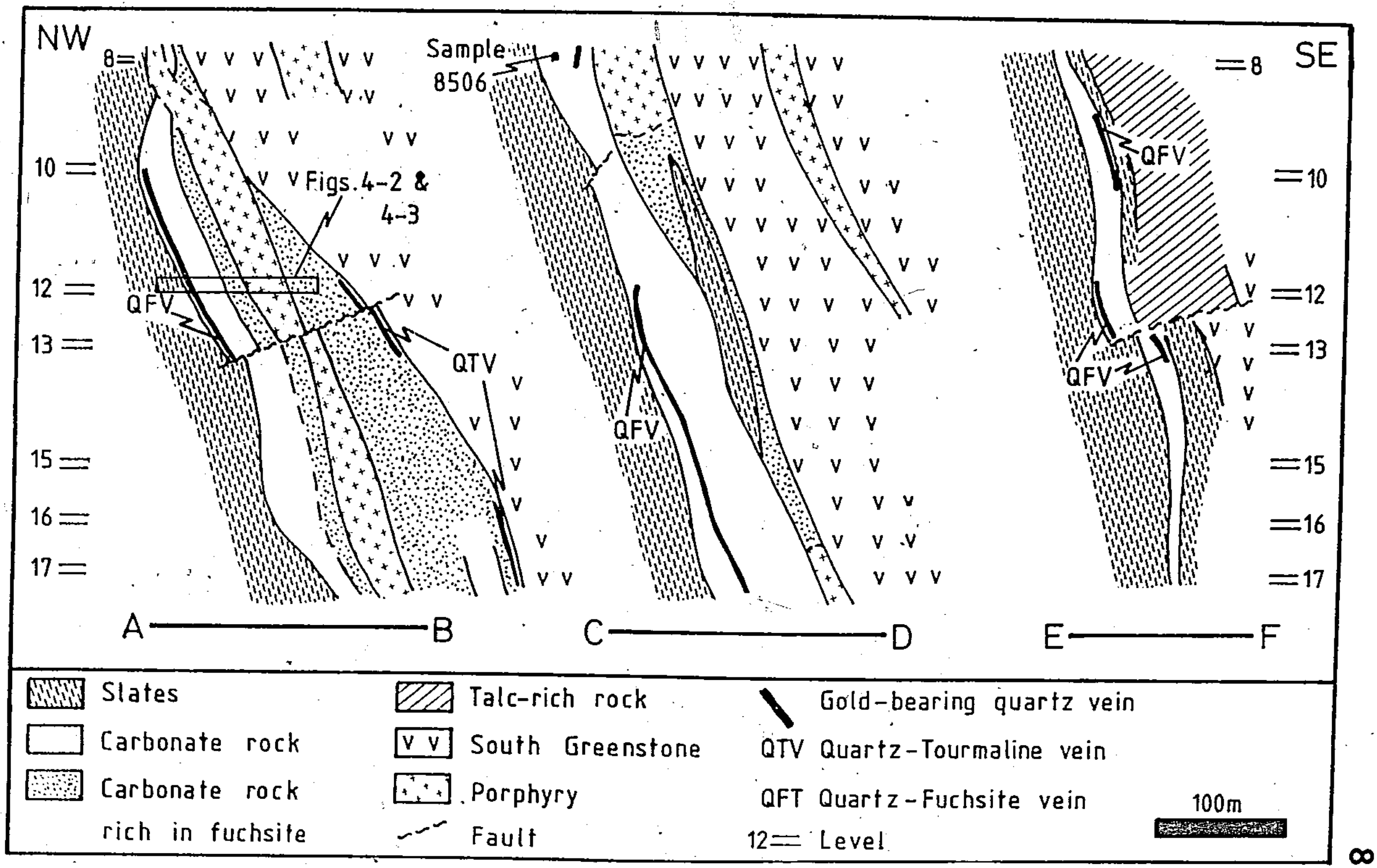
NW
SE
8=
=8
10
=10
12
=12
13
=13
15
=15
16
=16
17
=17
Sample 8506
Figs. 4-2 & 4-3
QFV
QTV
QFV
QFV
QFV
A
B
C
D
E
F
Slates
Carbonate rock
Carbonate rock rich in fuchsite
Talc-rich rock
South Greenstone
Porphyry
Fault
Gold-bearing quartz vein
QTV Quartz-Tourmaline vein
QFT Quartz-Fuchsite vein
12 Level
100m

Figure 5-4. Conolly contour diagram, with superimposed distribution of gold grades in the Quartz-Fuchsite vein.

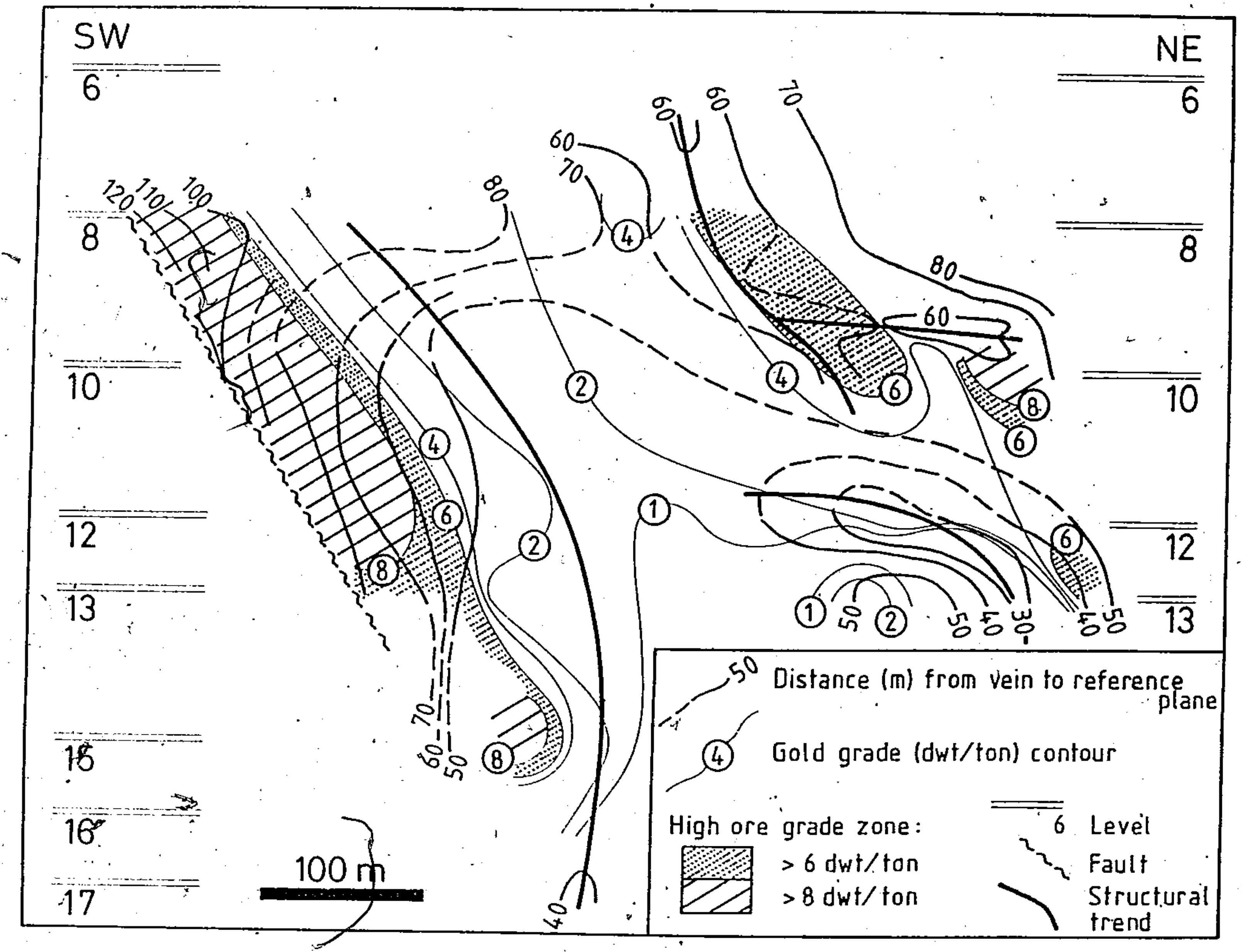
SW
NE
6
8
10
12
13
15
16
17
6
8
10
12
13
120
110
100
80
70
60
50
40
30
1
2
4
6
8
100 m
Distance (m) from vein to reference plane
Gold grade (dwt/ton) contour
High ore grade zone:
> 6 dwt/ton
> 8 dwt/ton
Level
Fault
Structural trend

along the upper contact between the carbrock and the slates. At its western extremity, the vein has a NNE-SSW trend, while it strikes NE-SW at the eastern end. Two main structural trends can be observed: one which is nearly horizontal, and another which is subvertical, dipping steeply to the NE. The horizontal trend is only present in the eastern domain of the vein.

5.3. TIMING OF THE QUARTZ-FUCHSITE VEIN IN THE GEOLOGICAL EVOLUTION OF THE TIMMINS AREA

The most distinctive deformation event in the Timmins area is the development of an eastward striking foliation and plunging lineation, defined as D_1 by Roberts et al. (1978) and Roberts (1981). It is important to establish the time relationship between this penetrative deformation and the QFV to understand the development of the vein and its gold mineralization within the geological evolution of the Timmins area.

In the vicinity of the QFV, foliation is indicated by preferential alignment of chlorite and mica. It commonly strikes NE and dips steeply to the NW (Fig. 5-2A), identical with the trend of the planar fabric in the D_1 deformation event (Roberts et al., 1978; Roberts, 1981). The foliation appears to be discordant with the orientation of the QFV. Mapping of the behavior of the foliation across the QFV also shows the discordancy between foliation and the vein (Figs. 4-2, 5-5, 5-6). The vein becomes parallel to the foliation only in the upper levels (Fig. 5-7) where it bends into a vertical orientation and dips to the NW (Fig. 5-3). For most of the extension of the QFV, it strikes parallel to the strike of the foliation (Fig. 5-2A). This parallelism often gives the impression in stopes and drifts, that both the foliation and the QFV are parallel. However, the important vertical dimension is not available in these situations so that a full view of the relationship between the vein and the planar penetrative fabric cannot be obtained.

The presence of a fracture cleavage in the QFV (Plate 5-1A), and crenulations at the contact between the vein and the wall rock (Plate 5-1B), indicate that formation of the QFV preceded the development of the foliation. Moreover, the foliation can vary in an irregular fashion across the QFV (Fig. 5-5 and 5-6), or may be present in one wall and absent in the opposite wall suggesting that the foliation is irregularly refracted through the QFV. Holmes (1968, p.91) noted this seemingly puzzling behavior of the foliation in the proximity of ore bodies : "...The degree and attitude of the schisting are difficult to establish. Frequently the dip appears considerably different on the wall and on the adjacent back; it is also common for the rock to appear moderately schisted on the wall and perfectly massive on the back...".

The quartz veins present in the wall rock predate the foliation as well. Some veinlets are tightly folded, and the foliation is axial planar to the isoclinally folded veins (Plates 5-5A and 5-7A). This indicates that these veins were present before the foliation was imparted to the rocks, and presumably at a high angle to it.

The orientation of the foliation in wall rock inclusions in the QFV is similar to that of the wall rock (Fig. 5-8). The immediate inference from such a relationship is that foliation antedates quartz veining. However, this is most unlikely, since :

1) the contact between wall rock and quartz material is jagged or crenulated, whether one considers the wall rock inclusions inside the QFV, or quartz veins in the wall rock (Plates 5-2A and 5-2B);

2) a fracture cleavage, which is the refracted counterpart of the host rock foliation, is easily recognized in veins extending from the QFV into the wall rock (Plate 5-2B).

In conclusion, the bulk of the quartz material present in the QFV or in the wall rock was precipitated before the foliation developed. The only veins which seem to be coeval with the foliation are small en-échelon quartz veins, sometimes sigmoidal in shape (Plates 5-4A and 5-4B). This type of quartz veining is however poorly represented in the carbonatized rocks, and is volumetrically

Figure 5-5. Orientation of the foliation in the carbonate wall rock on the 17 level.

Note the discordant relationship between the foliation and the Quartz-Fuchsite vein. The foliation dips constantly to the NW, whereas the Quartz-Fuchsite vein plunges to the SE.

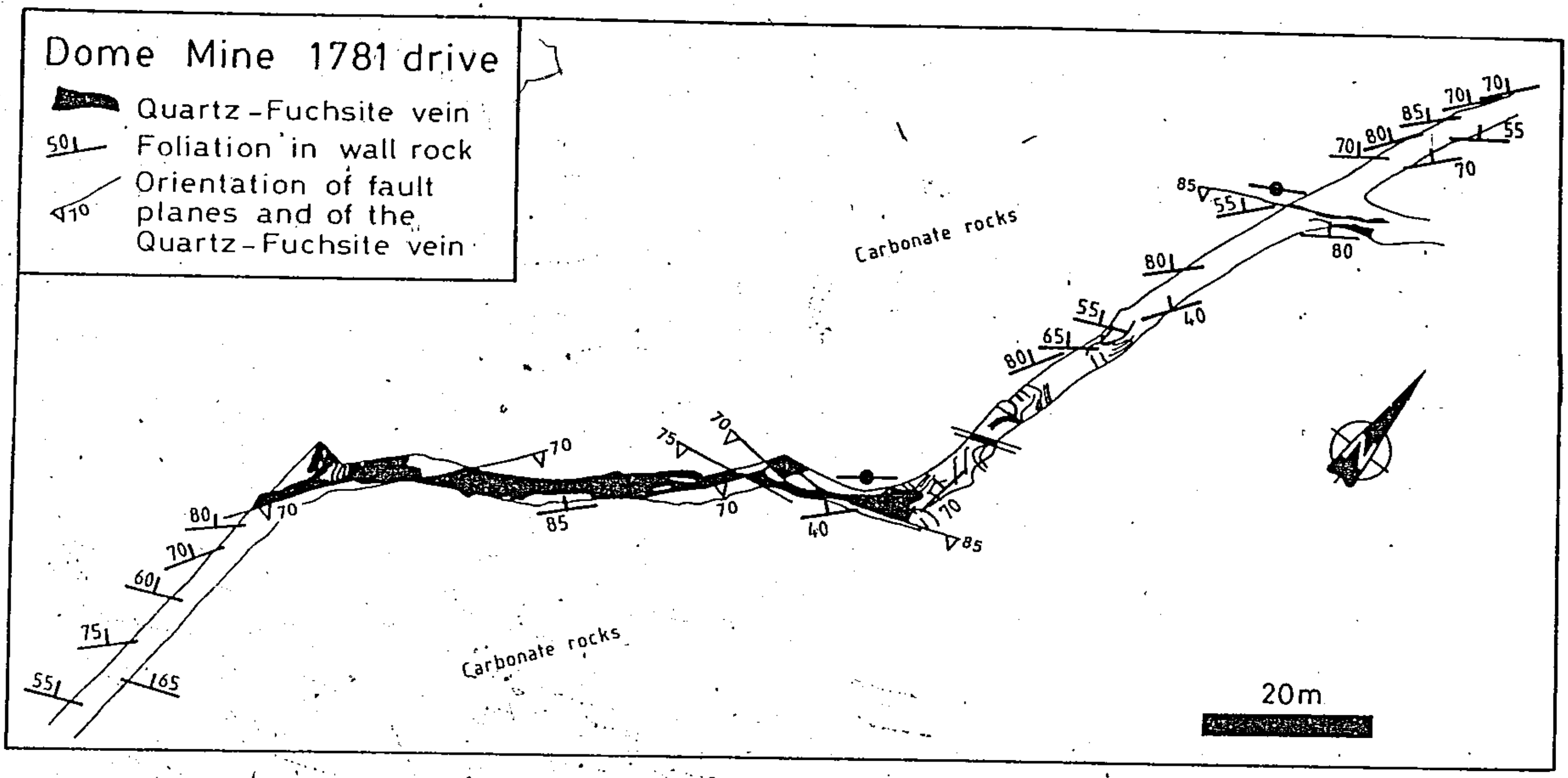
Dome Mine 1781 drive
Quartz-Fuchsite vein
50 Foliation in wall rock
70 Orientation of fault planes and of the Quartz-Fuchsite vein
Carbonate rocks
Carbonate rocks
20m
70
70
85
80
55
70
70
85
55
80
80
40
55
65
80
70
85
70
75
70
40
70
85
70
80
70
60
75
65
55

Figure 5-6. Orientation of the foliation in the wall rock between the 10 and 12 levels.

Note the discordant relationship between the foliation and the Quartz-Fuchsite vein. The foliation appears to be irregularly arranged along the Quartz-Fuchsite vein.

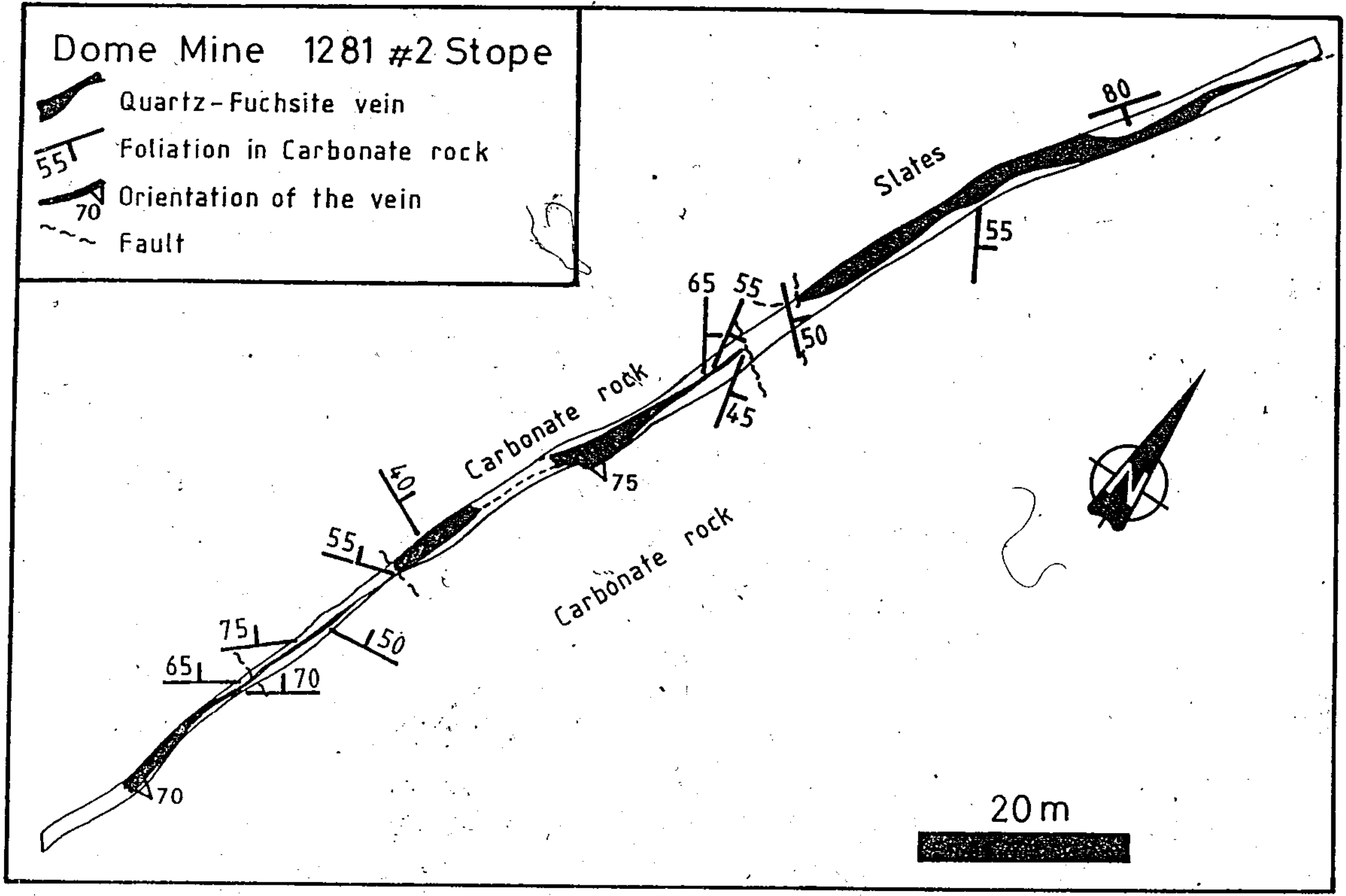
Dome Mine 1281 #2 Stope
Quartz-Fuchsite vein
55 Foliation in Carbonate rock
70 Orientation of the vein
Fault
Slates
Carbonate rock
Carbonate rock
80
55
65
55
50
45
75
40
55
75
65
70
50
70
20 m

Figure 5-7. Orientation of the foliation in the wall rock on the 8 level.

The foliation in the wall rocks has the same constant orientation as in deeper levels (see fig. 5-5). The parallelism of the Quartz-Fuchsite vein with the foliation is due to the overall change in dip of the vein at shallower mine levels (see figs. 5-3 and 5-4). Location of sample 8506 (Table 4-5) is also indicated.

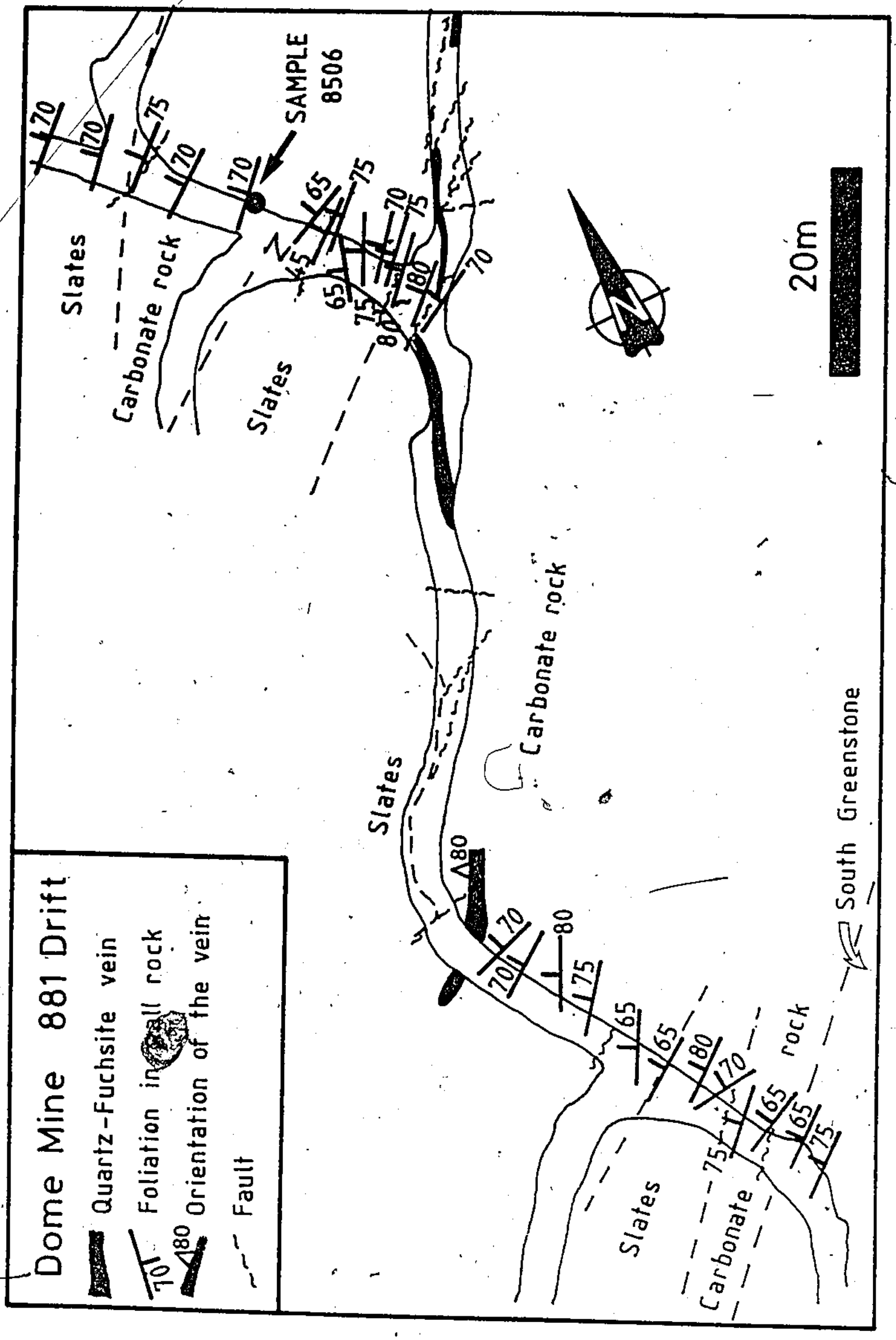
Dome Mine 881 Drift
Quartz-Fuchsite vein
Foliation in wall rock
Orientation of the vein
Fault
70
80
SAMPLE
8506
Slates
Carbonate rock
Slates
Carbonate rock
Carbonate rock
Slates
South Greenstone
rock
Slates
Carbonate
20m
70
75
65
45
80
180

Figure 5-8. Time relationship between the foliation in the carbonate wall rock, the Quartz-Fuchsite vein and quartz veins in the wall rock.

Location: mine face on the 16 level, barren and massive quartz. The foliation has been imparted to the composite rock mass after emplacement of the Quartz-Fuchsite vein and the quartz veins in the wall rock. This is evidenced by the crenulations at the contact between vein material and the host rock, and the fracture cleavage present in the vein material. See plates 5-2A and 5-2B for a more detailed description of these relationships. This mine face also shows the ambiguous time relationship between quartz veins emplaced in the wall rock and the quartz material forming the Quartz-Fuchsite vein. In fact at this site, the Quartz-Fuchsite vein appears to have been build up by progressive accretion of large, massive and barren quartz veins in the wall rock from left to right.

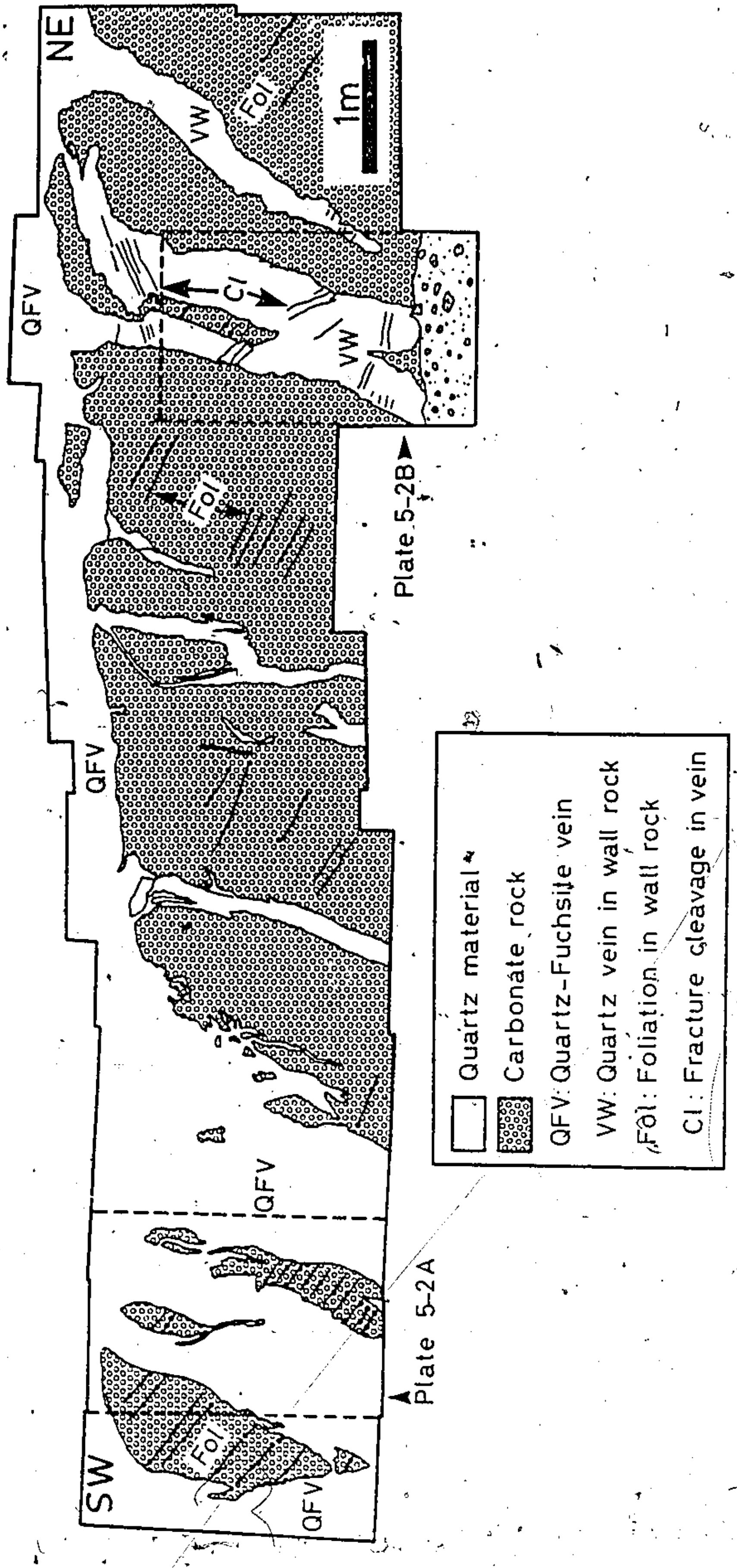
NE
1m
Fol
VW
QFV
Cl
VW
Fol
Plate 5-2B
QFV
QFV
Plate 5-2A
SW
Fol
QFV
Quartz material
Carbonate rock
QFV: Quartz-Fuchsite vein
VW: Quartz vein in wall rock
Fol: Foliation in wall rock
Cl: Fracture cleavage in vein

Plate 5-1A. Fracture cleavage and contractional fault in the Quartz-Fuchsite vein.

a: fracture cleavage,
b: foliation in carbonate wall rock,
c: chlorite and fuchsite banding outlining a contractional fault.
Location: 16 level, back of the drift.
The foliation of the wall rock runs from the lower right corner to the upper left corner of the plate. It is refracted through the Quartz-Fuchsite vein where it becomes steeper and is developed as a fracture cleavage rather than a foliation. This relationship is evidence for quartz veining preceding development of the foliation in the wall rock. Since the plate shows the back of the mine drift, the contractional fault indicates a right-hand sense of motion in a horizontal plane. Note how the banding from the vein runs in the wall rock, and how some bands are truncated by a second group of banding (c).

Plate 5-1B. Crenulated Quartz-Fuchsite vein - wall rock contact.

a: crenulated contact between the Quartz-Fuchsite vein and the carbonate wall rock,
b: foliation in the carbonate wall rock.
Location: 12 level, back of drift (for location see figs. 5-1 and 5-9).
The crenulation along the wall of the Quartz-Fuchsite vein was formed as a consequence of foliation development in the wall rock. Note the fracture cleavage in the vein which extends subperpendicular from the crenulated wall of the vein (a).

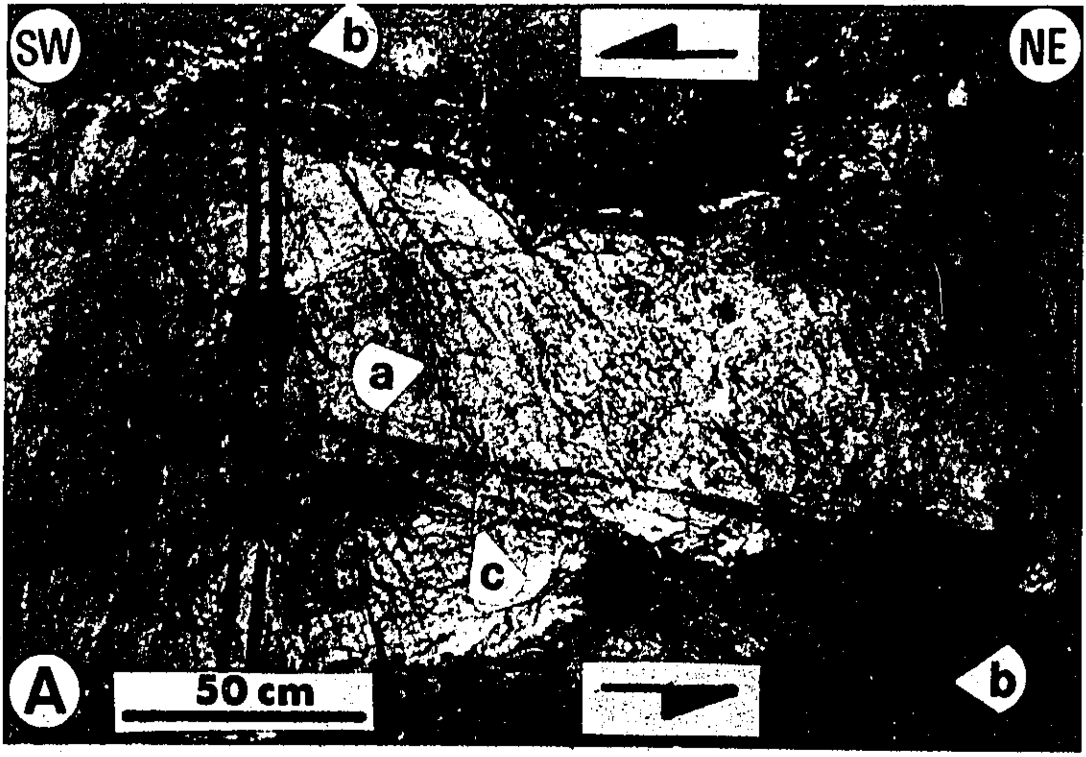
SW
b
NE
a
c
A
50 cm
b

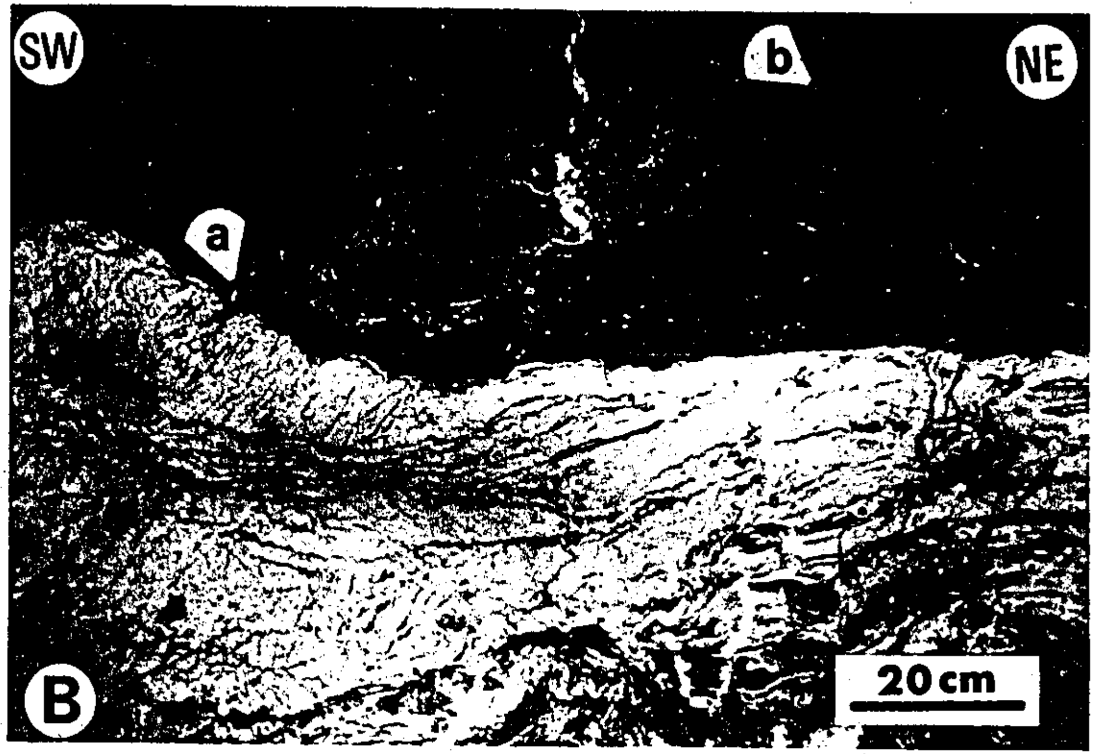
SW
b
NE
a
B
20 cm

Plate 5-2A. Foliated wall rock inclusions in the Quartz-Fuchsite vein.

a: foliation in carbonate wall rock inclusions,
b: crenulations at the contact between wall rock inclusions and the Quartz-Fuchsite vein.
Location: 16 level (see fig. 5-8).

Plate 5-2B. Fracture cleavage in quartz veins present in the carbonate wall rock.

a: crenulations at the contact between the vein and the carbonate wall rock,
b: fracture cleavage in the quartz vein,
c: foliation in the carbonate wall rock.
Location: 16 level (see fig. 5-8).

The fracture cleavage in the quartz veins in the wall rock and the crenulations at the contact between the quartz material indicate that development of the foliation in the wall rock postdates quartz veining.

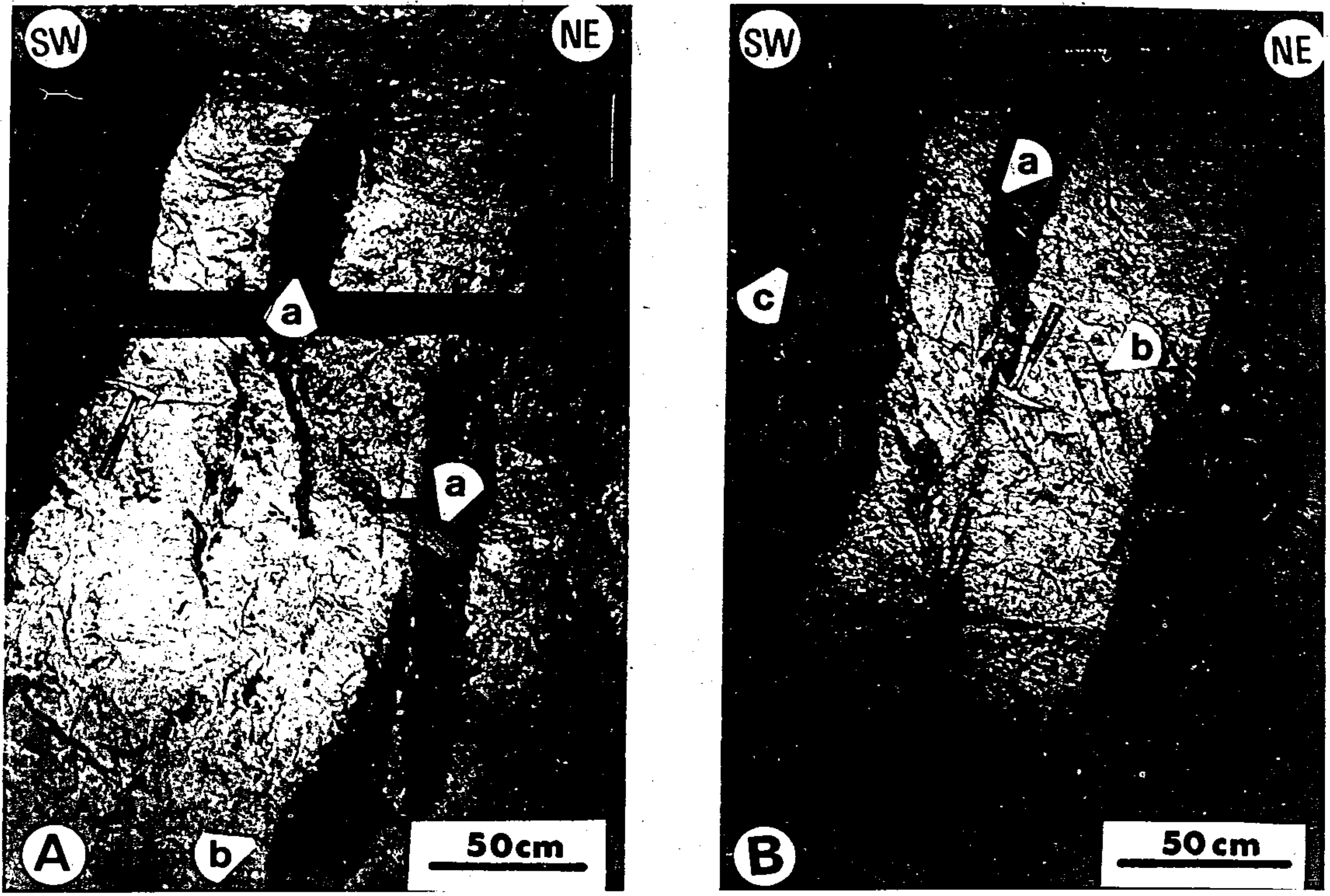
SW
NE
a
a
A
b
50cm
SW
NE
a
c
b
B
50 cm

Plate 5-3A. Typical ore-bearing zone in the Quartz-Fuchsite vein.

a: gold-bearing fuchsite and/or chlorite banding in the Quartz-Fuchsite vein,
b: massive and barren quartz zone in the Quartz-Fuchsite vein,
c: boudinage of banding,
d: relatively unstrained crosscutting quartz vein.
Location: 12 level (see fig. 5-1). Carbonate wall rock.

Plate 5-3B. Folded banding in the Quartz-Fuchsite vein.

a: isoclinal fold of the banding,
b: boudinage of the banding,
c: fracture cleavage in the Quartz-Fuchsite vein.
d: stylolitized banding.
Location: 12 level (see figs. 5-1 and 5-9). Carbonate wall rock.

The fold in the banding indicates that the banding was developed before deformation along the Quartz-Fuchsite vein took place. Pressure-solution in the Quartz-Fuchsite vein is indicated by the stylolitized banding.

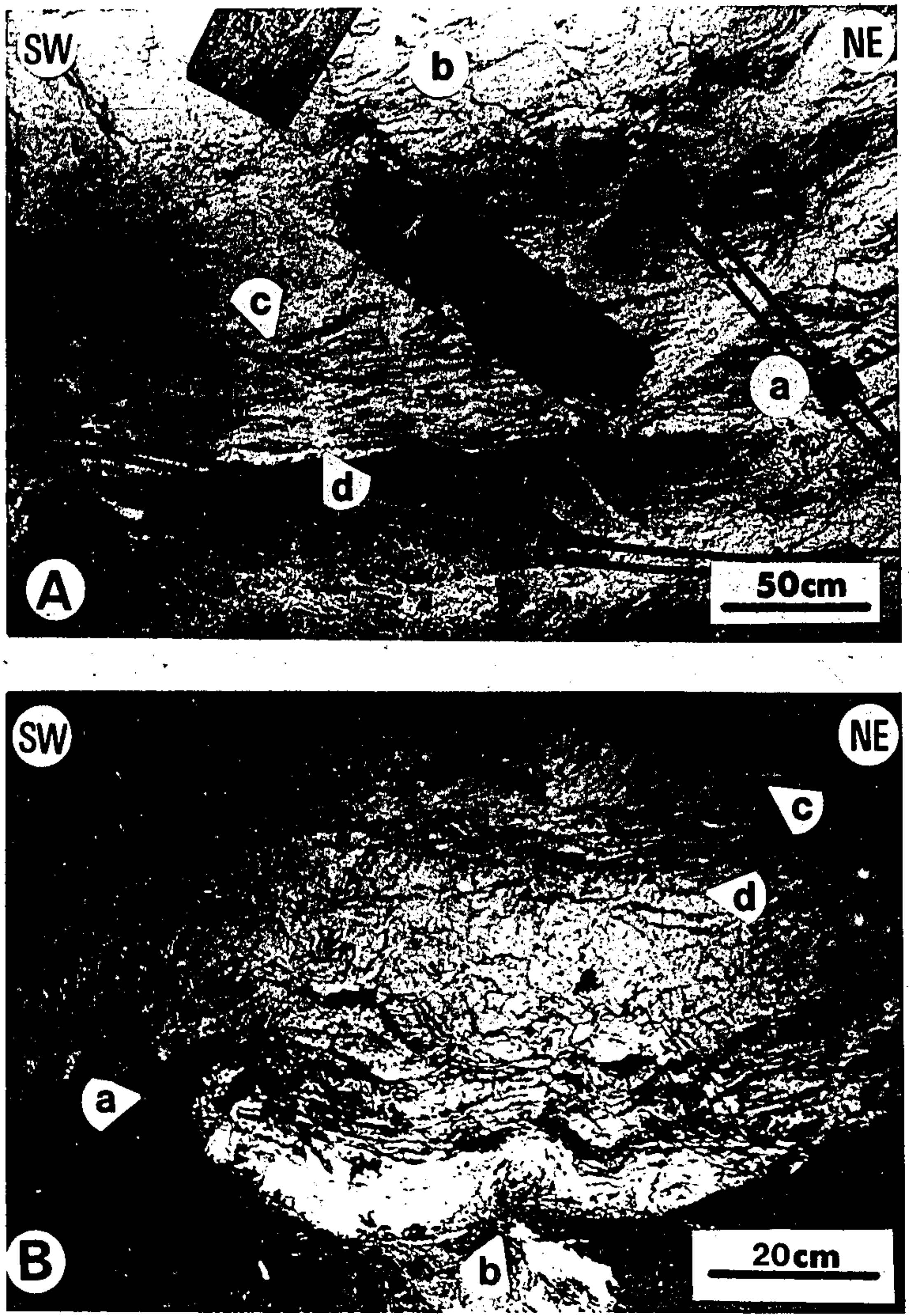
SW
b
NE
c
a
d
A
50cm
SW
NE
c
d
a
B
b
20cm

Plate 5-4A. En-échelon quartz veins in the carbonate wall rock.

a: en-échelon quartz veins,
b: quartz vein in the wall rock antedating foliation,
c: foliation in the carbonate wall rock.
Location: stope 1081#6.

The foliation in the carbonate wall rock is sub-vertical. The quartz vein running from the lower left corner to the upper right corner of the plate (b) antedates foliation. This is evidenced by the buckled appearance of the vein labelled b, the fracture cleavage running through it, and the crenulated vein-wall rock contact. The larger en-échelon and sigmoidal vein crosscuts vein b. The development of these en-échelon veins is probably contemporaneous with formation of the foliation.

Plate 5-4B. Boudinage of the Quartz-Fuchsite vein.

a: Quartz-Fuchsite vein,
b: en-échelon quartz vein in the pinch of the boudin,
c: foliation in carbonate wall rock.
Location: 15 level.

The sigmoidal en-échelon quartz vein probably formed as a consequence of boudinage of the Quartz-Fuchsite vein. A fracture in the pinch of the boudin acted as a sink for silica removed by pressure-solution from the swells of the boudinage structure.

Plate 5-4C. Folded banding in the Quartz-Fuchsite vein on a microscopic scale.

a: isoclinal fold,
b: recrystallized quartz,
c: pressure-solution contact between quartz grains (stylolite).

The folding of the banding indicates that deformation followed development of the banding. Pressure-solution contacts between quartz grains and recrystallized quartz are typical textures of banded zones from the Quartz-Fuchsite vein.

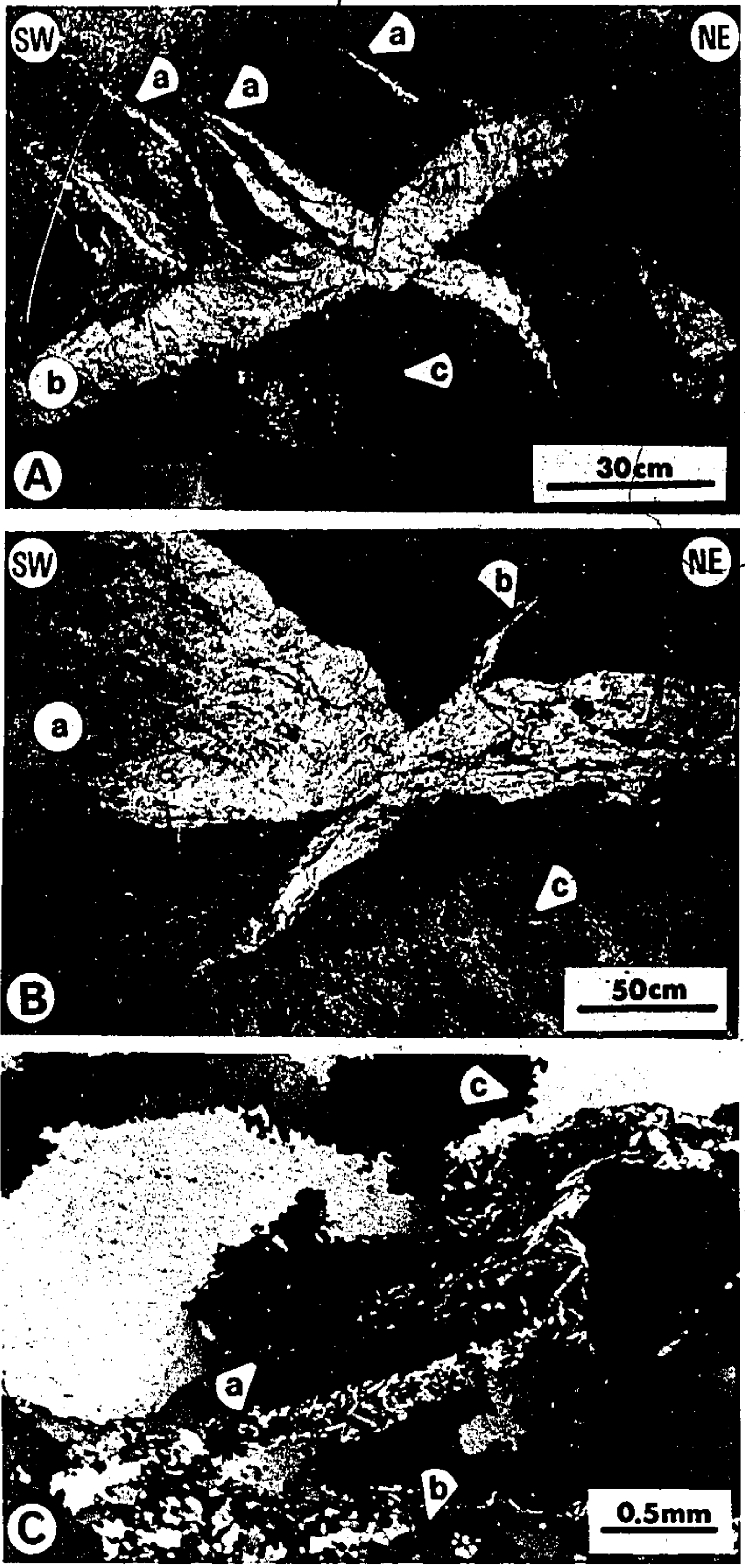
SW
NE
a
a
a
b
c
A
30cm
SW
NE
b
a
c
B
50cm
c
a
b
C
0.5mm

unimportant with respect to the veins which predate the foliation.

5.4. QUARTZ MATERIAL AND STRUCTURES PRESENT WITHIN THE QUARTZ-FUCHSITE VEIN

The QFV is composed of two main quartz types : one which is massive, and consists almost entirely of relatively unstrained quartz, and is usually of low gold grade; and a second type which consists of alternating bands of quartz and phyllosilicates and/or wall rock, and which contains high gold concentration (Plate 5-3A). The banding is mainly present in both eastern and western extremities of the QFV (Fig. 5-1). Fuchsite is dominant in the western domain of the vein, whereas chlorite is the main banding component in the eastern part of the QFV.

Banding is subparallel to the walls of the vein (Plates 5-3A and 5-7B). The width of the bands is in the millimeter range. Thicker bands can be recognized as slivers or inclusions of carbonatized komatiites or slates. The thin banding sometimes grades into inclusions of wall rock. Bands tend to occur in domains of several subparallel individual of single bands. In detail, however the bands are highly irregular and discontinuous. The banding can be parallel to one wall of the vein, and bends towards the opposite wall. It may be oblique with respect to the general trend of the vein or it may run into the wall rock.

One band may be truncated by another band (Plate 5-1A). The banding is also highly deformed, boudinaged (Plates 5-3A and 5-3B), and folded on both a macroscopic and a microscopic scale (Plates 5-3B and 5-4C).

Quartz within the bands is largely recrystallized, and, to a lesser extent, fractured. Stylolites are also observed in the banded zones of the QFV (Plates 5-3B, 5-4C, 5-6A, and 5-6B). This contrasts with the coarser grained and less deformed texture of the massive vein quartz.

Discordant quartz veins crosscut the banding at high angle (Plate 5-3A). These veins range in width and length from a few millimeters to several centimeters, sometimes up to 2 or 3 meters. Some of the smaller crosscutting veins seem to be related to the boudinage of the banding (Plate 5-3A). The quartz in these small veins is less strained than the quartz within the banded parts of the QFV. Boudinage can also affect the entire QFV, where its width is small. A small sigmoidal vein often occupies the pinch of the boudinage structure (Plate 5-4B).

Contractional faults are present in the QFV. Most show a right hand motion (Plate 5-1A), while some indicate a left hand motion. Both the QFV and the wall rock foliation are occasionally folded. Faults and folds are more commonly observed in the eastern portion of the QFV. Slickenside striations are common along both the banding and the walls of the QFV. The majority of the slickenside striations plunge to the E and NE (Fig. 5-2B). This orientation is similar to that of all linear structures present in the Dome Mine (Holmes, 1968), as well as the orientation of the D_1 linear fabric of the Timmins area (Roberts et al., 1978; Roberts, 1981). The slickenside surfaces indicate a reverse movement along the bands and walls, i.e. the south-eastern block moved upwards and the north-western block downwards.

Phyllosilicate laminations have been observed in rare cases within quartz grains from the banded parts of the QFV (Plate 5-6A). These small laminae composed of fuchsite and/or chlorite are most certainly crack-seal inclusion bands, as defined by Ramsay (1980a) and Cox and Etheridge (1983). These laminations, together with some quartz fibers (Plate 5-6B), are probably the only intact features remaining from the initial development of the QFV.

Many areas of the QFV consist of massive, barren, and relatively unstrained quartz (Fig. 5-8, plates 5-2A, 5-5B and 5-7B). The mode of occurrence of this type of quartz is variable. In some instances, the QFV is entirely composed of such massive quartz. Where banding is present, lenses of massive quartz separate zones of banding. In other occurrences, individual quartz veins are outlined by wall rock inclusions.

The time relationship between the banded and the massive quartz types is ambiguous. Massive quartz veins crosscut banded quartz, or in turn they are found to be truncated by banding (Plate 5-5A).

5.5. QUARTZ VEINING IN THE WALL ROCK

Quartz material shows various configurations in the wall rock. Straight quartz veins of relatively uniform width are the most common (Plates 5-2B, 5-4A and 5-5B). However, systems of quartz pockets and anastomosing veinlets (Plate 5-7B), and breccias occur as well. Breccias consist of angular to subangular and centimeter to meter size carbonatized wall rock fragments, which are embedded in a matrix of quartz. These breccias are present as little pockets along the QFV (Fig. 5-9). Although it is difficult to quantify, it appears that the irregular quartz pockets which are connected by small quartz veins (Plate 5-7B), become more abundant towards the upper levels of the QFV, i.e. 12th level and upwards.

The quartz veins present in the wall rock display a state of deformation ranging from unstrained to tightly and isoclinally folded (Plates 5-5A and 5-7A). The most deformed veins are usually found in the immediate vicinity of the QFV. Besides isoclinal folding, deformation also consist of boudinage, fracturing and/or deflection of wall rock veins into parallelism with the QFV (Plate 5-5B).

Relatively undeformed veins in the wall rock

Figure 5-9. Contrasting orientations of quartz veins in the wall rock adjacent to the Quartz-Fuchsite vein.

The contrasting orientations of the quartz veins on the opposite sides of the Quartz-Fuchsite vein are incompatible with a shear zone model. It is rather suggested that they acquired their orientation before the compressional event. They are deflected into parallelism with the Quartz-Fuchsite, and together with slickenslide striations they indicate a reverse strike-slip fault movement along the Quartz-Fuchsite vein (Not shown here). The occasional presence of well preserved flow top breccias near the Quartz-Fuchsite vein shows that strain is heterogeneously distributed along the vein. Wall rock breccia embedded in quartz indicates sudden drops in pore fluid pressure and hydraulic fracturing along the Quartz-Fuchsite vein.

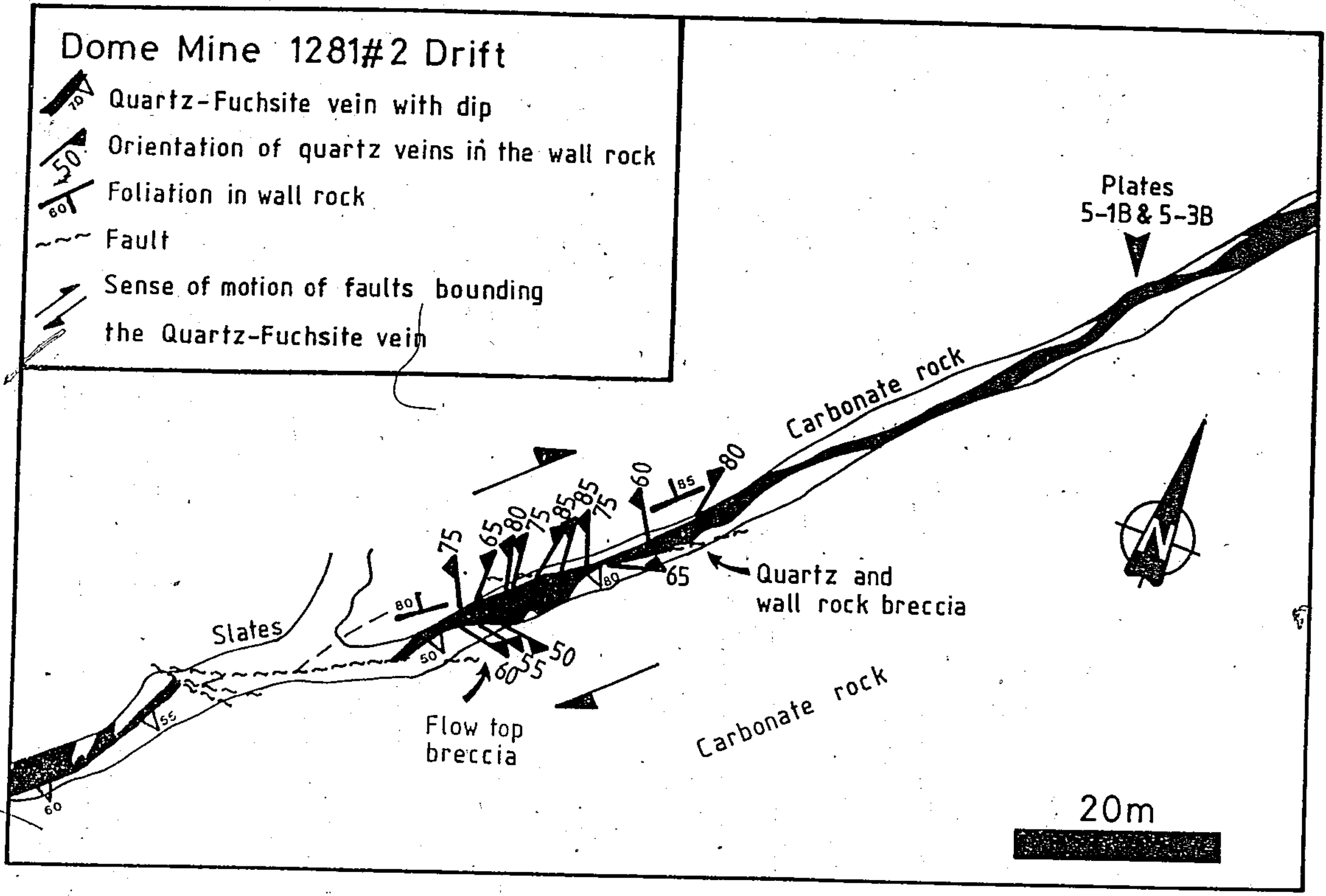
Dome Mine 1281#2 Drift
70
Quartz-Fuchsite vein with dip
50
Orientation of quartz veins in the wall rock
60
Foliation in wall rock
Fault
Sense of motion of faults bounding the Quartz-Fuchsite vein
Plates 5-1B & 5-3B
Carbonate rock
80
85
60
75
85
85
75
80
65
75
80
65
Quartz and wall rock breccia
80
50
50
55
60
Flow top breccia
Slates
55
60
Carbonate rock
20m

Plate 5-5A. Ambiguous time relationship between banded and massive quartz material in the Quartz-Fuchsite vein.

a: massive quartz vein,
b: isoclinally folded quartz vein in the carbonate wall rock.
Location: 13 level.

In the lower part of the plate, the quartz vein labelled a crosscuts the banding of the Quartz-Fuchsite vein running from left to right, whereas this same vein a is truncated by a second generation of banding in the central part of the Quartz-Fuchsite vein.

Plate 5-5B. Quartz veins in the wall rock deflected by fault movement along the Quartz-Fuchsite vein.

a: deflected quartz veins in the carbonate wall rock,
b: well developed boudinage in quartz veins of small width,
c: fracture cleavage running normal to the walls of the veins in the wall rock,
d: crenulations at the quartz vein-wall rock contact,
e: Quartz-Fuchsite vein.
Location: mine face on 16 level, barren domain of the Quartz-Fuchsite vein.

The deflection of the quartz veins in the wall rock indicates a left-hand motion along the Quartz-Fuchsite vein in a vertical plane.

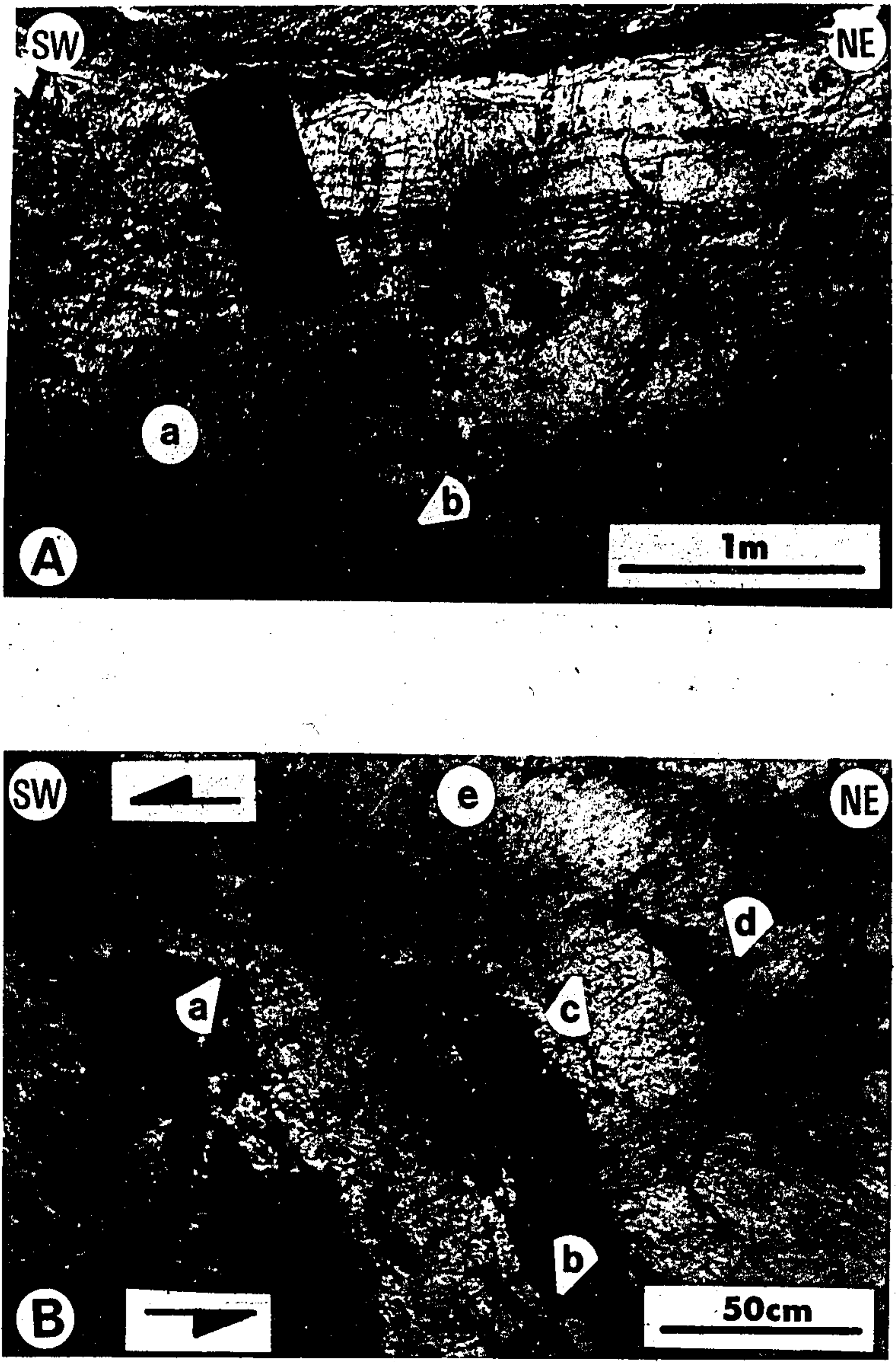
SW
NE
a
b
A
1m
SW
e
NE
d
a
c
b
B
50cm

Plate 5-6A. Phyllosilicate laminae in the Quartz-Fuchsite vein.

a: phyllosilicate laminae, or wall rock inclusion band (according to the terminology by Ramsay, 1980a),
b: wall rock inclusion trail (according to the terminology by Ramsay, 1980a).
c: pressure-solution surface (stylolite).

Phyllosilicate laminae and inclusion trails are original growth features of the Quartz-Fuchsite vein. They were developed during crack-seal vein growth when slivers of the wall rock were isolated from the main wall rock and were mechanically incorporated in the vein contemporaneously with quartz precipitation. These primary growth features were largely destroyed due to recrystallization of quartz and pressure-solution.

Plate 5-6B. Quartz fibers in the Quartz-Fuchsite vein.

a: chlorite banding,
b: quartz fiber,
c: pressure-solution surface (stylolite),
d: saw-tooth contact between quartz fibers (according to the terminology by Ramsay, 1980a).

This type of texture is typical of quartz growth perpendicular to the banding in a crack created by hydraulic fracturing. The saw-tooth contact between quartz fibers shows the competing effects of crystal growth.

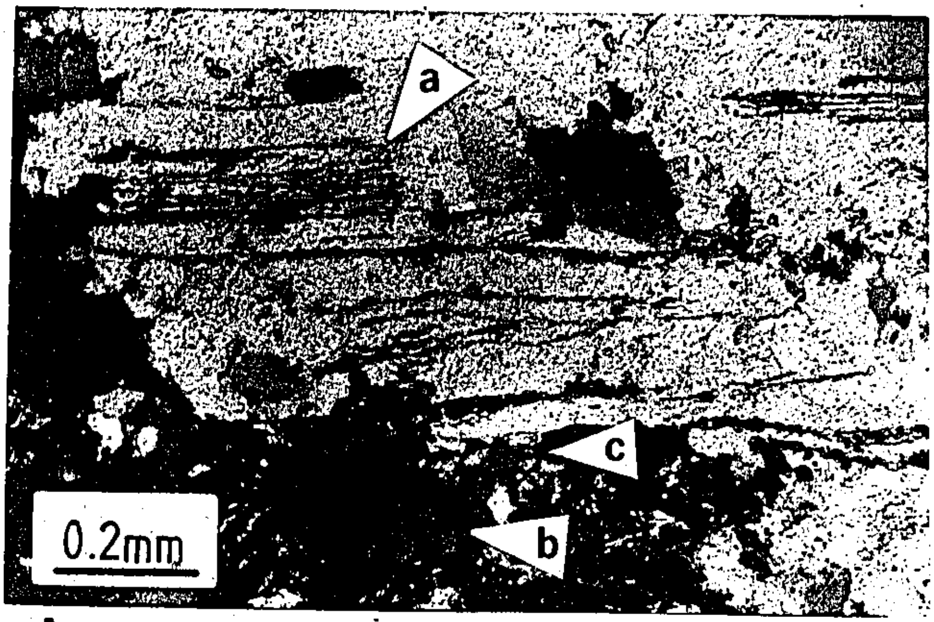

A

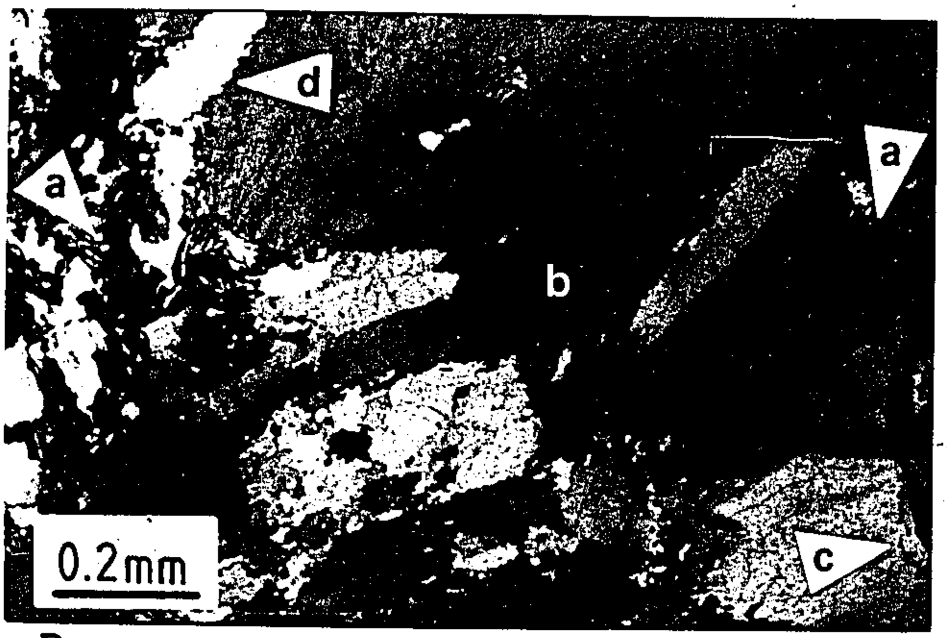

B

Plate 5-7A. Isoclinally folded quartz vein in the carbonate wall rock.

a: isoclinally folded quartz vein in the wall rock,
b: foliation in the carbonate wall rock,
c: Quartz-Fuchsite vein.
Location: 10level, back of the mine drift.

The small quartz vein in the wall rock was folded as a consequence of foliation development in the wall rock. The foliation is axial planar to the fold.

Plate 5-7B. Irregular quartz material in the carbonate wall rock.

a: irregular quartz material formed of pockets conected by veinlets.
b: banded and ore-bearing quartz in the Quartz-Fuchsite vein.
c: massive and barren quartz in the Quartz-Fuchsite vein.
Location: 1081#2 stope.

Irregular quartz veining becomes more frequent towards shallower mining levels of the Quartz-Fuchsite vein. This may indicate that the stress field was at certain times relatively isotropic, and probably more often at shallow depth.

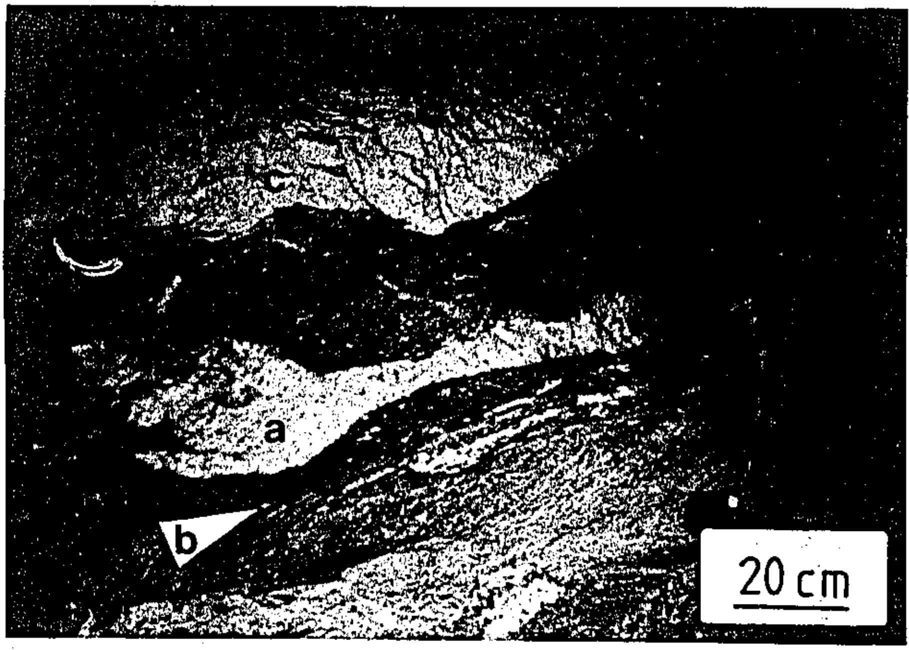

A

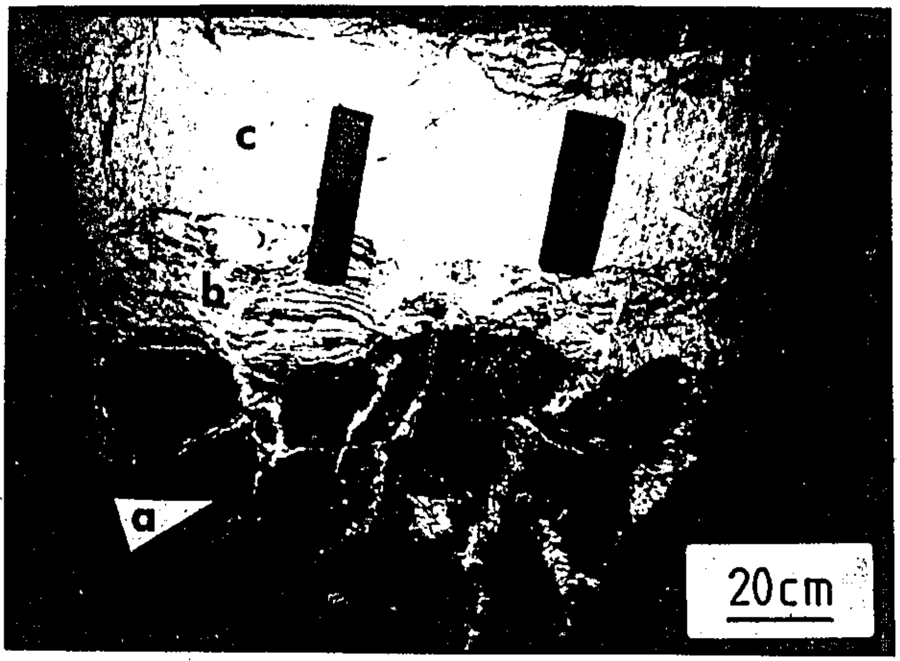

B

display variable orientations (Fig. 5-2C). In one instance, it was observed that veins present on one side of the QFV, show a diametrically different orientation in the opposite wall (Fig. 5-9). Veins on both sides however show a deflection which is consistent with the right-hand motion deduced from the slickenside surfaces along the banding.

Most of the veins in the wall rock are composed of only quartz. Banded veins have been recognized in some instances. Very few of the veins in the wall rock contain visible gold and galena.

The chronological relationship between the wall rock veins and the QFV is equivocal as well, since each one can be found to crosscut the other.

5.6. GROWTH FEATURES VS DEFORMATION FEATURES

5.6.1. Summary of textures and structures

The preceding description shows that two fundamental features can be recognized in the environment of the QFV : those that are related to vein formation, and those that are due to subsequent deformation. The purpose of this section is to summarize these textures and structures in order to "look through" the stage of deformation, and understand the mechanism of quartz deposition.

- Growth features related to quartz deposition are :

inclusions of wall rocks, banding and phyllosilicate laminae, quartz fibers, massive quartz veining, wall rock breccia embedded in quartz, and irregular quartz material.

Deformation features are : foliation in the wall rock, fracture cleavage in the QFV, crenulations at the QFV-wall rock contact, slickenside striations, contractional faults, folding of the QFV and foliation, boudinage of banding and the QFV, small crosscutting veinlets in the pinches of boudins, recrystallization of quartz, stylolites, folding, deflection, boudinage, and fracturing of veins present in the wall rock, and en-échelon quartz veins in the wall rock.

5.6.2. Consequences of the deformation event on primary growth features and location of strain

The orientation of the foliation with respect to the QFV (Fig. 5-2A) indicates that the maximum principal stress responsible for the development of the planar fabric was subperpendicular to the vein.

The difference in strain which can be observed in massive and banded quartz is striking. Quartz recrystallization and stylolites are common in banded parts, whereas massive quartz rarely displays these textures. Robin (1979) indicated that "...When a same strain rate is imposed on rocks which contain 'quartz' and differing amounts of 'mica', the rock which is richer in mica (other things being equal) will require a lesser differential stress, $\sigma_1-\sigma_3$, to cause the strain rate...". Thus, the same stress which was applied to the entire QFV resulted in highly strained areas, i.e. banded quartz, and relatively less deformed portions, i.e. massive homogeneous quartz.

Furthermore, Robin (1979) also noted how deformation can lead to segregation of bands or domains of different bulk composition. One of his conclusions is that under suitable conditions, variations in quartz-mica proportions will be accentuated due to stress induced diffusion transfer. As applied to the QFV, a maximum principal stress subperpendicular to the QFV would result in quartz dissolution in the phyllosilicate laminae and the banding. Silica would tend to migrate from the latter to the quartz layers so that the quartz layers became richer in quartz, and the phyllosilicate layers depleted in quartz.

The development of boudinage and crosscutting veins in the pinches of the banding are akin to the formation of boudins and extensional structures in anisotropic or foliated rocks (Platt and Vissers, 1980). Under compressional deformation, the banding limited ductile extension along the strike of the QFV. This caused brittle failure of the banding accompanied by the development of subperpendicular fractures. The cracks acted as sinks for the silica material removed by pressure solution in the banding, resulting in the formation of small crosscutting quartz veins. Subsequent shortening of the rock normal or oblique to the banding produced the pinch-and-swell structure.

Thus, the subhorizontal compression applied to the QFV resulted in the preferential location of strain in areas which were heterogeneous in composition to start with, i.e. banded quartz. As a consequence, quartz dissolution and recrystallization was more important in these areas. Delicate primary textures, such as phyllosilicate laminae and quartz fibers so characteristic of vein growth by crack-seal (Ramsay, 1980a; Cox and Etheridge, 1983), were largely destroyed.

5.6.3. Sense of motion along the Quartz-Fuchsite vein

Many of the deformation features described above are evidence for some displacement along the QFV. They allow the nature of the movement which took place along the QFV to be deduced. These features are summarized in figure 5-10. The motion along the QFV is a reverse dip-strike faulting, striking NE, with a sense of movement plunging approximately 60°NE, the SE block moving upwards and the NW block downwards. The occasional S-C fabric of the foliation in the wall rock is also in agreement with such a displacement history (Fig. 5-1).

Figure 5-10. Deformation features indicating reverse strike-dip fault movement along the Quartz-Fuchsite vein.

Many of the deformation features in and along the Quartz-Fuchsite vein indicate that it was the location of strike-dip faulting, striking NE, with a sense of movement plunging approximately 60°NE. The SE block moved upwards while the NW block moved downwards. However, this deformation event took place after the bulk of vein material was emplaced in the Quartz-Fuchsite vein.

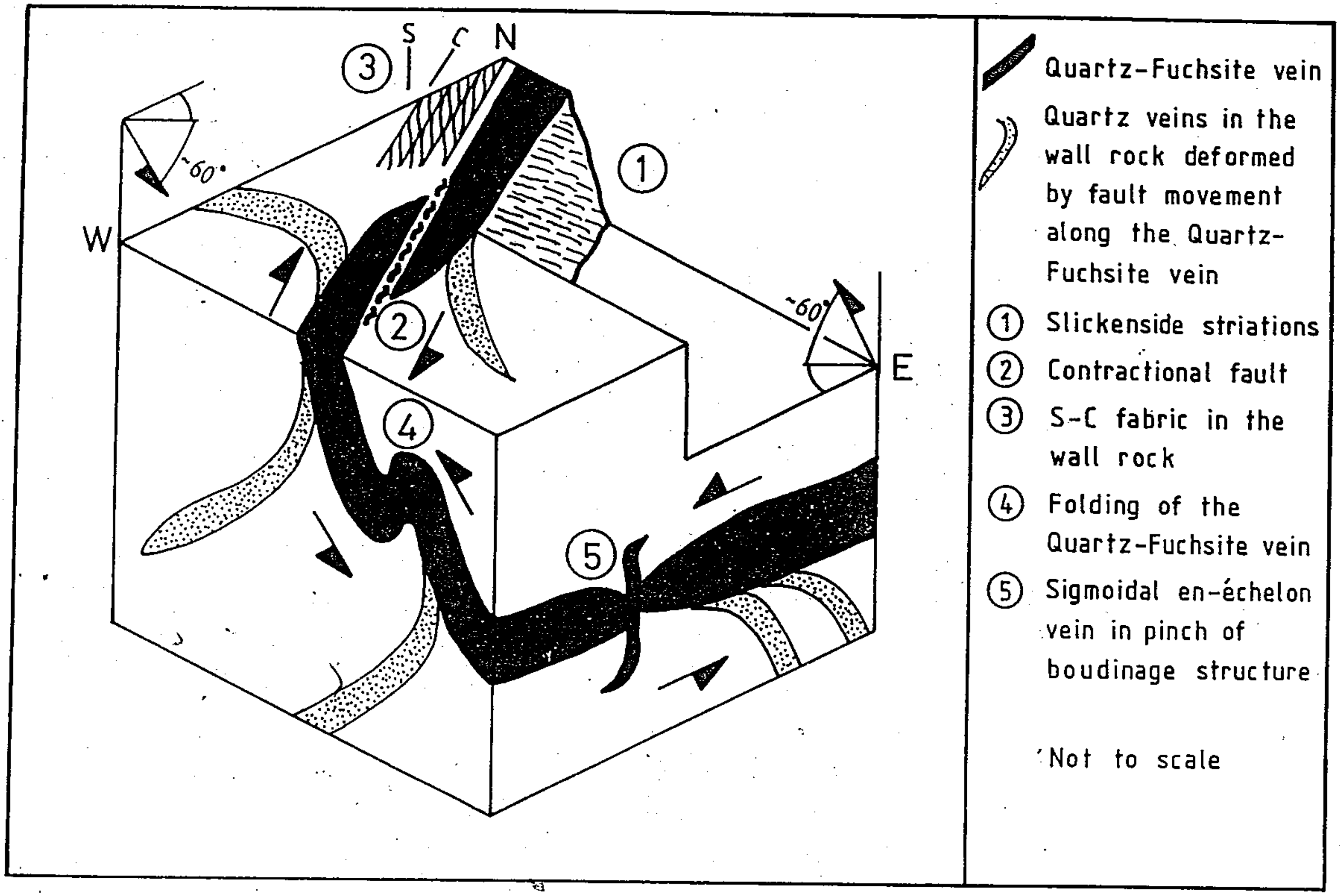
S
C
N
③
①
W
~60°
~60°
E
②
④
⑤
Quartz-Fuchsite vein
Quartz veins in the wall rock deformed by fault movement along the Quartz-Fuchsite vein
① Slickenside striations
② Contractional fault
③ S-C fabric in the wall rock
④ Folding of the Quartz-Fuchsite vein
⑤ Sigmoidal en-échelon vein in pinch of boudinage structure
Not to scale

5.7. MECHANISM OF FORMATION OF THE QUARTZ-FUCHSITE VEIN

5.7.1. Arguments against a shear zone model

A model of brittle-ductile shear zone development (Ramsay and Graham, 1970; Ramsay, 1980b; Ramsay and Huber, 1986) has been advocated by many researchers for the formation of Archean gold deposits (e.g., Kerrich and Allison, 1978; Robert et al., 1983; Colvine et al., 1984; Robert and Brown, 1986a; Groves and Phillips, 1987). However, the overall structural setting and anatomy of the QFV is not satisfactorily explained by such a model. The reasons for this are:

1) The deposition of most of the quartz material within the QFV and veins in the wall rock antedates the development of the foliation. The foliation cuts through the QFV which contains a fracture cleavage and crenulations occur at the QFV-wall rock contact. In a typical shear zone system, the foliation commonly makes an angle of 45° to the strike of the shear zone, and this angle progressively decreases towards the center of the shear zone (Ramsay and Graham, 1970; Ramsay, 1980b). Such a sigmoidal shape of the foliation has never been observed at the contact with the QFV.

2) The majority of the quartz veins in the wall rock do not display the en-échelon fractures, and Riedel, R' and P shears characteristic of strike-slip fault zones evolved

during simple shear (Tchalenko, 1968; Ramsay and Graham, 1970; Gamond, 1983; Hancock, 1985) (compare figures 5-2C and 5-2D). There are only a few small sigmoidal and en-échelon veinlets which might be contemporaneous and genetically related to the development of the foliation. The presence of veins in the wall rock with contrasting orientations on both sides of the QFV (Fig. 5-9) are very difficult to explain in a classical shear zone model.

3) The foliation is irregularly distributed along the strike of the QFV. It occurs predominantly in proximity of the banded parts of the QFV. Foliation is absent in some areas where primary textures can still be recognized in the carbonatized komatiites, i.e. flow top breccias (Fig. 5-9). Such irregularity in strain is difficult to explain within a shear zone model which implies increasing ductile strain up to brittle failure.

In brief, the deposition of the bulk of the quartz material in the QFV environment is unrelated to movement along a brittle-ductile shear zone concomitant with development of foliation in the wall rocks.

5.7.2. Mechanism of veining

An alternative mechanism to the shear zone model is presented in the following discussion, which might better integrate all the recorded field and thin-section observations. In this process of vein formation, hydrostatics plays a predominant role, and deformation is negligible.

Cox et al. (1987) recently reviewed fracture formation and vein growth processes. Two principal modes of failure can take place in rocks :

1) In high differential stress environments, when stress differences become approximately four times higher than the tensile strength of the intact rock ($\sigma_1-\sigma_3 \geq 4T$), failure will occur in a shear mode, regardless of the fluid pressure level.

2) In low differential stress environments ($\sigma_1-\sigma_3 < 4T$), extension failure can occur provided that pore fluid pressure is high. The effect of fluid pressure (P_F) is to decrease the effective normal stress (σ_{eff}) according to the following relation :

$$\sigma_{eff} = \sigma_N - P_F,$$

where σ_N is the normal stress acting on the wall of the vein. In a three-dimensional stress state , hydraulic fracturing can take place when :

$$P_F \geq \sigma_3 + T.$$

Thus, the conditions required for hydraulic extension failure are : low tensile strength of the rock, small minimum principal stress, and high fluid pressure.

In the QFV environment, there are two distinctive types of quartz material : banded quartz and massive quartz. The latter forms large veins or lenses, with thicknesses ranging from a few centimeters up to 3-4 meters, and lengths generally in the meter range. According to Cox et al. (1987), such massive textureless veins form usually during a prolonged stage of fracture growth and opening associated with continuous crystallization. If the fluid pressure within the fracture is sufficiently high to hold the vein walls apart ($P_F > \sigma_N$), and if the fluid remains supersaturated in certain components, then vein growth will persist. The vein will become sealed as soon as the fluid pressure drops below the normal stress acting on its walls ($P_F < \sigma_N$), or when mineral growth is faster than the rate of fracture-wall separation.

The presence of phyllosilicate laminae within the banded quartz suggests that this type of quartz veining occurred by a crack-seal growth mechanism (Ramsay, 1980a; Cox and Etheridge, 1983). Such vein growth involves many repeated increments of microcrack opening, followed by sealing due to crystallization of material from solution (Ramsay, 1980a). Wall rock inclusions can be mechanically incorporated in the vein, when microcrack opening and vein accretion occurs at the vein-host rock contact. As shown in plate 5-6A, repetitive crack-seal increments result in characteristic microstructures such as wall rock inclusion bands and trails in crystallographic continuous quartz. Numerous repeated increments of microcrack opening resulted in ripping off of wall rock selvages and their mechanical incorporation in the QFV concomitant with quartz precipitation from the hydrothermal fluid. This accretionary vein growth process is responsible for the formation of the characteristic banding in the ore-bearing zones of the QFV. For instance, Cox et al. (1987, p.77) mention that "...the growth of a vein about 100 mm thick generally involves several thousand crack-seal growth increments...". Etheridge et al. (1984) have modeled the operation of crack-seal systems (Fig. 5-11). A fracture in the rock is formed when local fluid pressure increases ($P_F > \sigma_3+T$). An instantaneous drop in fluid pressure results inside the crack. A fluid pressure difference is thus established between the surrounding rock and the fracture, resulting in fluid migration to the crack until fluid pressure is reequilibrated. Once this stress state is obtained, the vein seals. Increase in fluid pressure leads to another crack-seal sequence of fracture, fluid pressure drop, and precipitation. It has to be noted that the drop in fluid pressure inside the crack is small with respect to the total fluid pressure in the enclosing rock.

Figure 5-11. Operation of the crack-seal mechanism (after Etheridge et al., 1984).

1: Pore fluid pressure is too low to permit hydraulic fracturing. 2: Build up of pore fluid pressure results in the formation of a crack. A pressure gradient is created between the crack and the surrounding wall rock. This gradient drives the pore fluid towards the crack. Until fluid pressure is reequilibrated, the fluid in the fracture is in a lower state of pressure than the ambient pore fluid in the proximal wall rock.
3: Precipitation of material takes place in the crack as a result of the drop in fluid pressure. The crack is sealed once fluid pressure is reequilibrated.

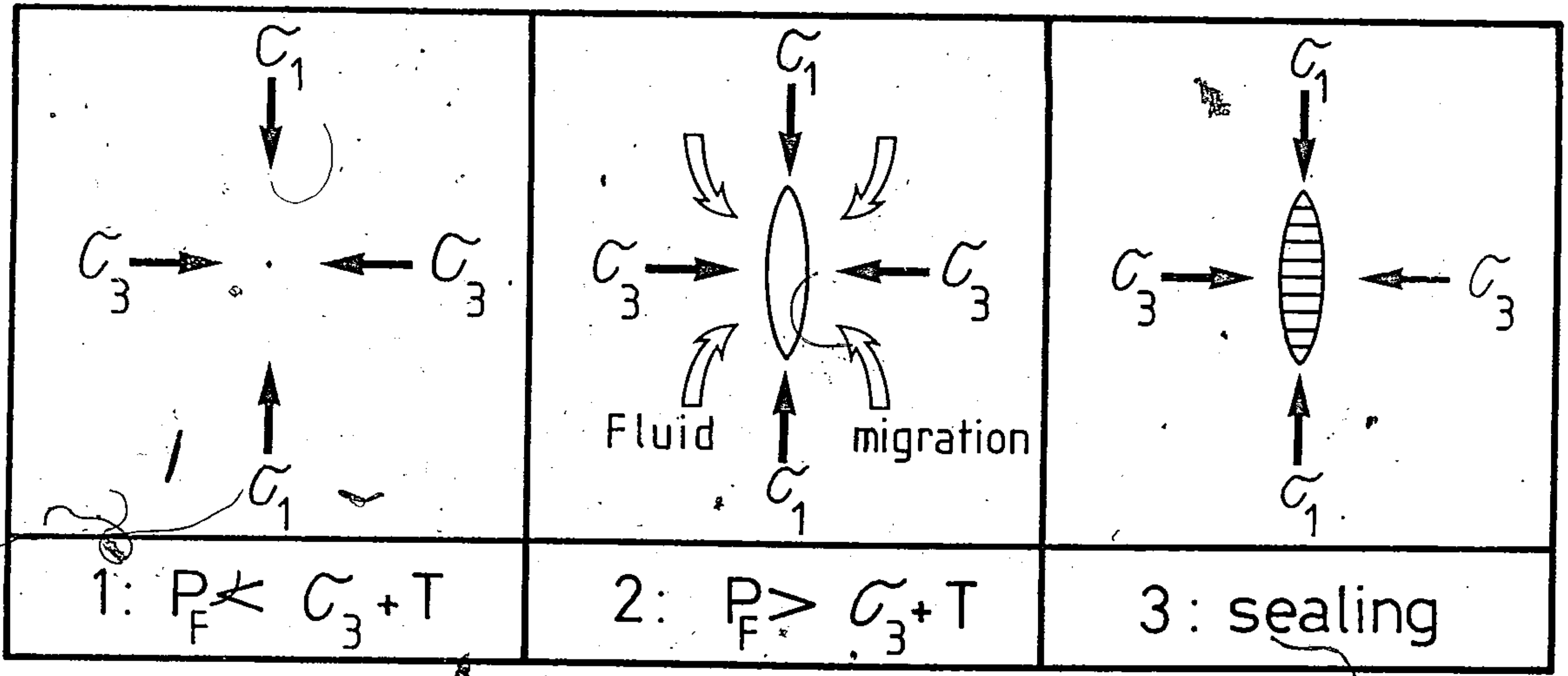

P_F : pore fluid pressure

T : tensile strength of rock

σ_1 : maximum principal stress

σ_3 : minimum principal stress

Consequently, only those fluid components which are strongly pressure sensitive will precipitate (Hobbs, 1987). Quartz, the main vein constituent in the present case, is such a mineral sensitive to sudden pressure drops (Fournier, 1985).

Wall rock and quartz breccias present along the strike of the QFV attest of sudden drops in fluid pressure as well (Phillips, 1972). The occurrence of quartz pockets connected by quartz veinlets is further evidence that hydraulic fracturing was predominant in the vicinity of the QFV.

In summary, low-stress differences and high fluid pressure would fully explain the presence of the various quartz types in and along the QFV. A high fluid pressure regime might have been developed by fluid migration in the carbonate rocks towards the contact with the slates (Fig. 5-12A) which represent a zone of low permeability, and may have hindered fluid migration. Increasing fluid pressure at the contact resulted in hydraulic fracturing. The orientation of the fracture was a function of the stress field present at the time of vein formation. The QFV and many veins in the wall rock have a subvertical attitude, which suggests that the maximum principal stress axis σ_1 was subvertical. Preexisting fractures or bedding planes in the slates, i.e. low tensile strength of the rock, probably also acted as controls for hydraulic fracturing, independent of the orientation of the main stress field (Haimson, 1981; Cornet, 1982).

Multiple cycles of fluid pressure increase, fracturing, and fluid pressure drop resulted in crack-seal type veins, which resulted in mechanical incorporation of wall rock slivers in the vein. In contrast, fractures held open by a high internal fluid pressure acted as open channel ways along which fluids moved, and formed the large, massive and unbanded quartz veins. These two processes of vein formation operated alternatly, thus resulting in the ambiguous and undefinable time relationship between both types of vein material.

The randomly oriented quartz pockets connected by quartz veins were developed under a near-isotropic stress field ($\sigma_1 \cong \sigma_2 \cong \sigma_3$). The observation, that this type of quartz material configuration is more frequent towards the upper levels of the QFV, might be evidence that the stress field was changing from low-stress differences at the bottom of the QFV to a near-isotropic stress field at the top of the QFV.

5.7.3. Geological evolution of the Quartz-Fuchsite vein

The present configuration of the QFV is the result of two independent geological events (Fig. 5-12) :

1) The bulk of quartz material was precipitated in cracks formed by hydraulic fracturing. The important controls on quartz deposition were : the presence of a lithological contact which acted as an impermeable barrier (slate-carbonate rock contact), high pore fluid pressure, and a low-stress difference environment, close to isotropic stress levels in some cases. The two types of banded and massive quartz were deposited in a single continuous event during fluctuating fluid pressures, and do not represent two separate episodes of quartz precipitation. The bulk chemical composition and the source of the fluid bringing the quartz into the fracture system was certainly identical for both quartz types.

2) Deformation was superimposed on the original growth features. The deformation features indicate that it was a compressional episode, with the maximum principal stress axis subhorizontal and subperpendicular to the orientation of the QFV. The foliation in the wall rock and the fracture cleavage in the quartz veins were developed at this stage. Strain was concentrated in zones of low competency, i.e. the banded parts of the QFV, which favored development of foliation around zones of banding. The banding was boudinaged and folded. Pressure-solution dissolved quartz

in the banded part of the vein. Fractures crosscut the banding and the dissolved silica was deposited therein. Sigmoidal veins were emplaced in the wall rock. As a result of higher strain, reverse movement took place along the QFV as indicated by the slickenside striations, contractional faults, folds and deflection of the veins present in the wall rock. Some of the wall rock veins were completely rotated into parallelism with the QFV and incorporated into it. Even the foliation was folded at this increasing stage of deformation.

Such a geological evolution explains the variable state of deformation displayed by the veins in the wall rock. Their deformation is a function of their orientation with respect to the principal stress field, their width, and their proximity to the QFV and zones of banding. For instance, small isoclinally folded veins in the wall rock do not represent an earlier generation of veins, but rather veins which due to their small width, and their unfavorable orientation were relatively easily deformed, whereas large and massive vein structures were less affected by the same strain.

The more complex structure of the QFV in its eastern extremity (Fig. 5-4) can be explained in the same manner. It is possible that this zone of the QFV was more unfavorably oriented with respect to the compressional event, and accommodated strain with a more complicated

Figure 5-12. Geological evolution of the Quartz-Fuchsite vein.

A: emplacement of quartz veins under high pore fluid pressure; the Quartz-Fuchsite vein was formed during this stage of accretionary vein growth.
1: massive barren unbanded quartz deposited during protracted stages of vein growth,
2: banded quartz formed during brief stages of crack-seal vein growth,
3: veins formed in the wall rock in preexisting fractures,
4: crack-seal vein growth along bedding planes of the slates.

B: deformation of the Quartz-Fuchsite vein under compressional stress. 1: crenulations at the vein-wall rock contact,
2: fracture cleavage in the Quartz-Fuchsite vein,
3: Folded banded quartz vein,
4: fold in the Quartz-Fuchsite vein,
5: folded vein in the wall rock,
6: sigmoidal tension vein in the pinch of the boudin of the Quartz-Fuchsite vein,
7: preferential development of the foliation in the wall rock in proximity to banded quartz,
8: boudinaged banding with quartz vein in the pinch.

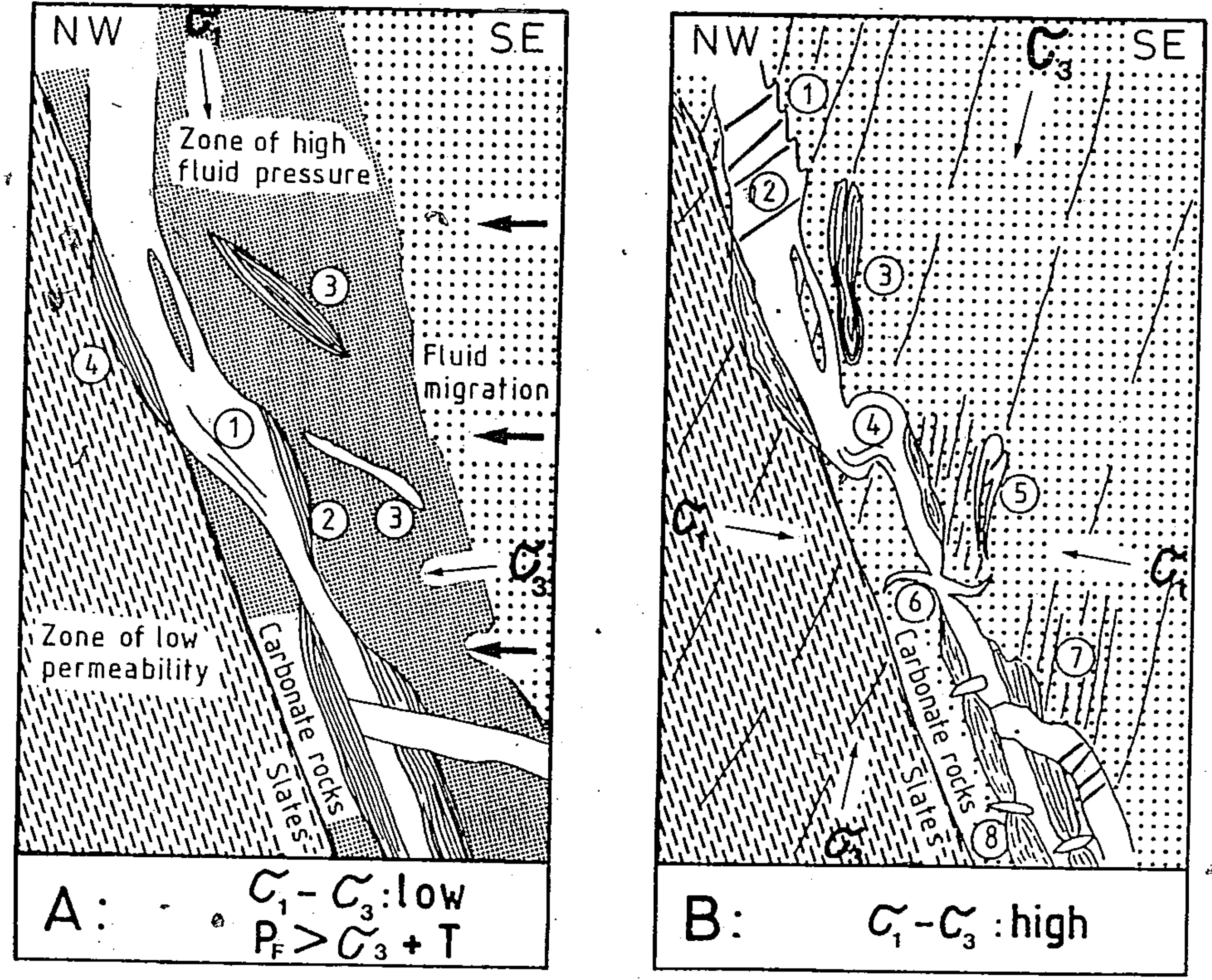
NW
SE
σ_1
Zone of high fluid pressure
Fluid migration
σ_3
①
②
③
③
④
Zone of low permeability
Carbonate rocks
Slates
A: $\sigma_1 - \sigma_3$: low
$P_F > \sigma_3 + T$
NW
SE
σ_3
σ_1
σ_1
σ_3
①
②
③
④
⑤
⑥
⑦
⑧
Carbonate rocks
Slates
B: $\sigma_1 - \sigma_3$: high

distortion. Field evidences in support of this argument is that folds and faults are more common in the eastern than in the western portion of the vein.

5.8. GOLD DISTRIBUTION WITHIN THE QUARTZ-FUCHSITE VEIN

5.8.1. Distribution of gold

The QFV is the highest ore grade vein in the Dome Mine (Rogers, 1982a,b). Visible gold and high ore grades are commonly associated with the characteristic fuchsite and/or chlorite banding of the vein. Massive and unbanded quartz is usually barren or of low ore grade. Veins crosscutting the banding do not contain any visible gold.

The gold content contour diagram has been superposed to the Conolly diagram (Fig. 5-4). Two high ore grade zones can be recognized. The highest grades are in the western portion of the QFV, while a second high grade zone is located in the upper part of the eastern extension. A further high grade ore zone seems to be present in the very eastern part of the QFV. Unfortunately, lack of information does not allow a clear contouring of the latter. Both high grade zones are ellipsoidal in shape. Their long axis plunges to the NE similar to the trend of the slickenside striations in the QFV (Fig. 5-2B), the D_1 stretch lineation (Roberts et al., 1978; Roberts, 1981), and the steeply northeast dipping structural trend apparent in the Conolly diagram (Fig. 5-4). However, ore grades show no particular affinity for width of the QFV.

Economic gold concentrations are typically present only in the QFV. However, in a stope below the 8th level (stope 1081#1), visible gold was observed in the wall rock adjacent to the vein. According to D.S. Rogers (chief geologist at the Dome Mine,; personal communication, 1985), this is a common observation at the shallower stoping levels of the QFV.

5.8.2. Relationship between gold distribution and the geological evolution of the Quartz-Fuchsite vein

Two scenarios can be envisaged, which may explain the consistent association of high ore grades and banding in the QFV : either gold was introduced in the QFV along with the bulk of quartz, or gold was introduced into the banded quartz during or after the compressional deformation event.

The second scenario is very unlikely, inasmuch as the deformation episode was accompanied by extensive pressure solution, especially in the banded zones of the QFV. Pressure solution is a mechanism during which rock porosity is drastically reduced, rather than increased (Sprunt and Nur, 1977). No evidence suggests that vein material was thoroughly fractured during deformation, so that enhanced permeability in the QFV was generated.

Thus, it appears that gold was introduced before the deformation event. The systematic affinity of gold for the banded quartz might be evidence for a genetic relationship between both. It has to be remembered that massive and textureless quartz is mainly barren. Multiple crack-seal vein growth must have been a very effective mechanism in removing gold and associated elements from the ore-bearing fluid. In such a case, gold is likely to have been deposited from a hydrothermal fluid which, like silica, was very pressure sensitive. The nature of this fluid will be discussed in chapter 7 dealing with fluid inclusions.

At shallower mine levels, the occurrence of gold in the carbonate wall rock adjacent to the QFV is further evidence for the fluid susceptibility to decreasing pressure. At about the depth of the 8th level, confining pressure was probably relatively low so that destabilization of metal complexes in the ore-bearing fluid occurred.

Hence, a vertical distribution can be recognized in the QFV. Below the 17th level, stress differences were too high and/or pore fluid pressure was too low to result in hydraulic extension fracture and no quartz and ore material could be deposited. Between the 17th level and the 6th level, hydraulic fracturing was important, and precipitation of quartz and gold during crack-seal vein growth took place. Towards shallower depths, i.e. 6th and 8th levels mainly, confining pressure was low enough to permit destabilization of the ore-bearing fluid and deposition of gold in the wall rock in the absence of crack-seal vein growth. The stress field probably also became more isotropic ($\sigma_1 \cong \sigma_2 \cong \sigma_3$) at shallower depths, as is indicated by the more frequent occurrence of quartz pockets connected by quartz veinlets. The latter type of quartz configuration and higher gold abundances in the wall rock is coincident with the presence of a large fuchsite halo around the QFV at these levels.

Visible gold in wall rock veins and high gold values in massive and textureless quartz are anomalies in the QFV environment. However, they are fully compatible within the mechanism of quartz and gold deposition described above, since occasional drops in fluid pressure might have occurred in these sites as well.

The ellipsoidal shape of the two high ore grade zones in the QFV can be ascribed to the deformation event which stretched the rocks in the Dome Mine (Holmes, 1968), parallel to the regional NE plunging D_1 linear fabric (Roberts et al., 1978; Roberts, 1981).

5.9. RECOMMENDATIONS FOR GOLD EXPLORATION

If the genetic model of the gold-bearing QFV is correct, then several ore guides applicable to the Dome Mine can be suggested. Indeed, the guides can probably also be applied to the entire Timmins mining camp, and perhaps universaly.

Other ore bodies like the QFV should be looked for at contacts between two rock types where a high pore fluid pressure regime might have been built up. The ideal situation is where a hydrothermal fluid could have circulated in a given rock type, but where further migration would have been hindered by a rock type of low permeability. The contact can be a lithological boundary, like the slate - carbonate rock contact where the QFV is located, or it could be a clear cut transition between a fractured and altered rock and its unaltered and massive counterpart, as is represented by the quartz-tourmaline vein, which lies at the boundary between the "Highly Altered" rocks and the "South Greenstone" (Fig. 5-3). In other words, prime targets are altered rocks, indicative of hydrothermal fluid circulation, at the contact with a relatively more impermeable rock type.

Of course, fluids which migrate parallel to the rock contact would not create a high pore fluid pressure environment. A mechanism has to operate which drives the fluids towards the contact. The later restriction is illustrated by the QFV and the quartz-tourmaline vein (Fig. 5-3). Both veins are more or less vertical and parallel to the transition from the altered rock zone to another rock type. This implies, at least partially, that fluid migration was lateral from the center of the altered rock zone towards its margins. The concept of fluid migration will be addressed in the chapter 10, where the genesis of the gold-bearing QFV will be considered in the light of the complete findings from the present research and conceptual models of Archean gold deposits.

Since gold precipitation appears to be related to crack-seal vein growth, veins with a high density of small alternating bands of quartz and wall rock laminae should be a good indicator of high ore grade. This type of quartz veining seems to be very productive in many Archean and younger terrains (e.g., Malcolm, 1929; Chace, 1949; McKinstry and Ohle, 1949; Coveney, 1981; Groves et al., 1985; Read and Meinert, 1986; Robert and Brown, 1986a,b; Vearncombe, 1986; Cox et al., 1987; Mawer, 1987). It is often described as ribbon- or laminated-quartz. Ore grades in many cases are dependent on the abundance of such veining, since it is recognized as generally being the richest in gold.

Most researchers in the Timmins area agree with an emplacement of gold-ore bodies before the regional compressional event (see chapter 3). The QFV under study fits such a geological evolution, as do banded veins from the McIntyre-Hollinger Mine near the Pearl Lake porphyry (Fig.3-1), since they are also folded (Plate 6 (figs. 18 and 19) in McKinstry and Ohle, 1946). During the regional compression, strain rates were higher in zones of heterogeneous composition, such as the banded parts of the QFV. This in turn resulted in preferential development of foliation in the wall rock adjacent to these zones, accompanied by a higher degree of recrystallization, quartz dissolution and redeposition. Rogers (1982a) mentioned that diamond drilling often intersects individual vein structures, but that assaying fails to yield any economic gold tenor. Degree of strain of quartz and intensity of foliation development in the host rock could be used as an indirect indicator of the proximity of high ore grade banding. Such a procedure can probably be applied to any ore present in banded quartz, which has undergone compressional deformation after its emplacement.

5.10. CONCLUSIONS

Deposition of quartz vein material took place before the compressional event labelled as D_1 by Roberts et al. (1978) and Roberts (1981).

Quartz was precipitated in cracks formed during hydraulic fracturing in a low differential stress and high pore fluid pressure environment. The high fluid pressure regime was developed at the carbonate rock-slates contact, where the slates acted as an impermeable barrier to fluid migration. Two types of vein material were deposited : massive unbanded quartz during protracted stages of fracture growth, opening and continuous crystallization, and banded quartz during repetitive stages of crack-seal vein growth. The characteristic banding of the QFV developed during these accretionary stages of vein growth, when wall rock slivers were mechanically incorporated in the QFV simultaneously with quartz precipitation from the hydrothermal fluid. Gold is consistently associated with banded quartz, suggesting that it was probably deposited from a hydrothermal fluid, which was sensitive to slight pressure drops characteristic of the crack-seal mechanism.

The subsequent deformation event was accompanied by important pressure-solution effects, which destroyed primary growth features to a large extent. Porosity was reduced, which rules out the possibility that gold was introduced at this or a later stage. Strain was mainly localized in and around zones of heterogeneous composition, that is the banded quartz. Thus, foliation is better developed in the wall rock adjacent to zones of banding. Contractional faults, folds and slickenside striations indicate that strike-slip displacement took place as deformation proceeded. The entire QFV and the ore zones contained therein were stretched parallel to the regional

D_1 lineation. In the view of field and petrographic evidence, the genesis of the gold mineralization in the QFV cannot be realistically explained within the development of a brittle-ductile shear zone model.

Structural and chemical controls are often invoked as the principal reasons for ore deposition. The geological setting of the QFV however clearly demonstrates that fluid hydrostatics and state of the stress field were predominant in the genesis of the ore body under study. These two concepts should at least deserve equal consideration to the two factors mentioned above in modeling ore deposition.

Hydrothermally altered rocks at the contact with impermeable rocks are a prime target in any search for ore bodies similar to the QFV. In this type of environment, banded quartz should be a good indicator of high ore grade. Additional guides are higher strained areas, where a deformation event may have been superimposed on crack-seal vein growth and ore deposition.

CHAPTER 6

MINERALOGY AND GEOCHEMISTRY OF THE QUARTZ-FUCHSITE VEIN

6.1. MINERALOGY

The mineralogy of the QFV is dominated by quartz. The remainder is composed of chromian-muscovite, chlorite, carbonates, and opaque minerals. The principal opaques are gold, galena, altaite (PbTe), and melonite ($NiTe_2$). Less abundant minerals are tellurobismuth (Bi_2Te_3), hessite (Ag_2Te), pyrite and tourmaline. Inclusions of wall rock fragments, either slates or carbonatized komatiites are present as well.

Multiple generations of milky, translucent to smoky quartz form the bulk of the QFV. Vein quartz can be massive or fractured and recrystallized. The latter texture is evidence for deformation following precipitation of quartz.

The crystallographic identity of the chrome-bearing muscovite was confirmed by its XRD-pattern. Using the same technique, chlorite was found to be clinochlore. Thin section evidence indicates that muscovite replaces both chlorite and wall rock carbonates. The chrome-bearing muscovite and chlorite form the characteristic banding of the QFV. These bands grade locally into tabular wall rock inclusions. The banding in the western part of the vein is due mainly to the chrome-bearing muscovite, whereas chlorite is predominant in the eastern section of the vein (Fig. 5-1). The distribution of the phyllosilicates in the vein is spatially associated with the porphyries in an analogous manner to the distribution of the chromian-muscovite in the carbonate wall rocks which is localized around the porphyry lens. To the west where the porphyry lenses are more prominent in the zone of carbonate rocks, the banding is predominantly muscovite, whereas to the east where porphyry bodies are rarely encountered, muscovite becomes secondary to chlorite, and is sometimes completely absent in the banding. Within the banded zones, quartz is commonly recrystallized and fractured to some extent, while parts of the vein lacking banding contain massive quartz. Latter generations of undeformed quartz veins crosscut the banding.

Galena and gold are consistently associated in the QFV (Plate 6-1A). Often they are accompanied by variable amounts of melonite and altaite (Plate, 6-1B). These minerals are intergrown. Small inclusions of altaite, tellurobismuth, and hessite are found in galena. Another opaque mineral is occasionally found in association with melonite. The mineral was too small to be adequately determined by optical means. SEM analyses of this mineral indicate the presence of Ni, Co, Fe, As, and S, suggesting the presence of a sulfarsenide (Plate 6-1B). No intermineral textures permit a temporal sequence of deposition between opaque minerals to be determined. It is assumed that these opaque minerals are coeval. Such age similarity has also been described for other gold deposits in the Timmins area (Hurst, 1935; Ferguson et al., 1968). The opaque minerals are found within fractures in quartz, between quartz grains, and along the banding. The banding is the predominant feature of gold-bearing areas in the vein. Opaque minerals are usually absent in areas where banding does not appear and only massive quartz is present.

The deformation sustained by the QFV precludes any detailed discussion of mineral paragenesis. In particular, it is not possible to decide whether the main opaque minerals, i.e. gold, galena, and tellurides, have been deposited contemporaneously with quartz, and mechanically remobilized into fractures and along grain boundaries during recrystallization of quartz or if minerals precipitated in a given sequence.

Late stage carbonates are present along fractures in quartz, and also replace quartz. Rutile and tourmaline, when occasionally present, are located within the banding. Pyrite is poorly represented in the QFV. Cubic pyrite is either present between quartz grains or along the banding.

Plate 6-1A. Typical gold-galena association in the Quartz-Fuchsite vein.

Gn: galena, Au: gold, Al: altaite, Qz: quartz.

Plate 6-1B. Telluride-gold association in the Quartz-Fuchsite vein.

Au: gold, Me: melonite, Al: altaite, ?: enigmatic mineral often associated with melonite containing Ni, Fe, Co, As and S (SEM analyses).

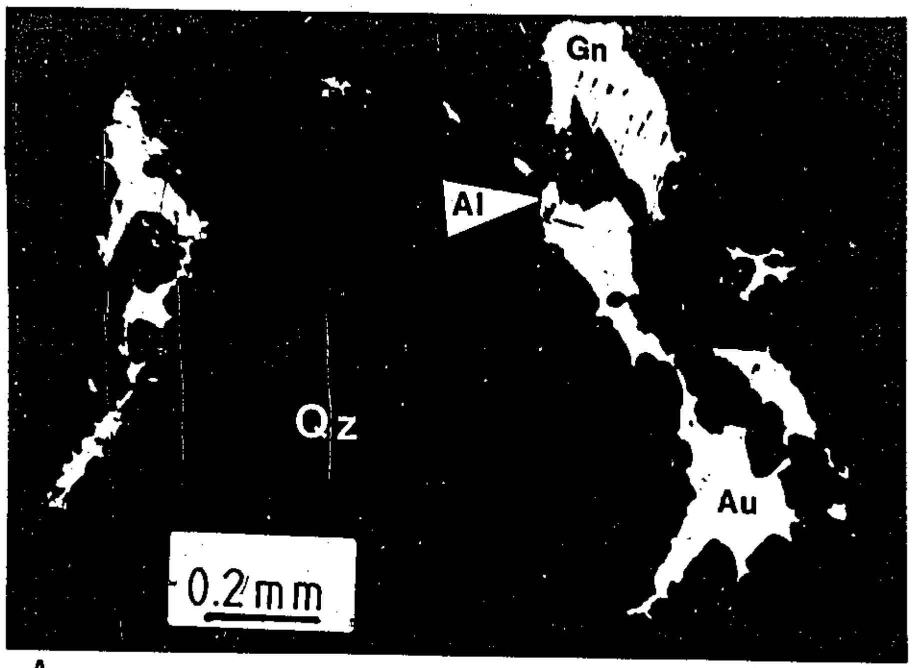

A

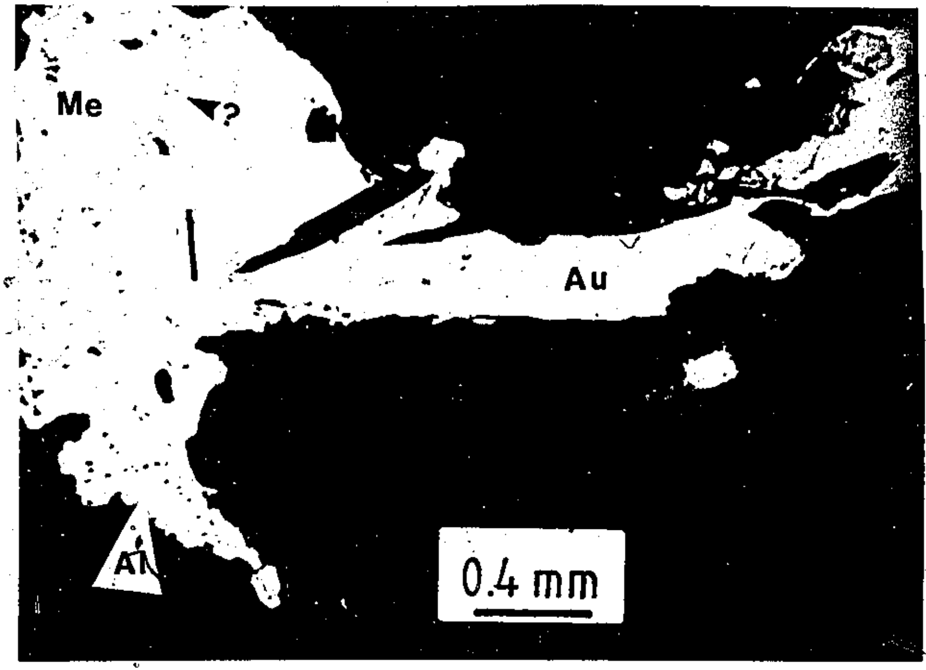

B

Komatiite wall rock inclusions in the QFV show the same state of alteration as the unveined wall rock. This suggests that carbonatization preceded quartz veining.

Although no exact mass-balance calculation can be made, the source of the large amounts of quartz present in the QFV can be speculated upon. In chapter 4, it was concluded that the komatiites were depleted in silica during the carbonatization event. The silica content of the carbonate rocks is lower by about 10% with respect to komatiites (Table 4-2). Thus, it is entirely possible that a major percentage of the quartz from the QFV is formed of silica of very local derivation, that was removed from the komatiites during carbonatization.

6.2. GEOCHEMISTRY

Chemical analyses of fuchsite and chlorite separates are presented in table 6-1. The major element chemistry of chlorite from the QFV is compatible with clinochlore composition (Deer et al., 1962). The higher SiO_2 value of sample #12019G can be attributed to quartz contamination. The chromian-muscovite, referred to as fuchsite, has SiO_2, Al_2O_3, Fe_2O_3, MgO, CaO, and LOI values which deviate from analyses of pure fuchsites (Whitmore et al., 1946; Deer et al., 1962). This can be ascribed to contamination from chlorite, quartz, or carbonates which were not completely separated from muscovite. The XRD-

	10010C Fuchsite HGC	13011 Fuchsite HGC	15003 Fuchsite HGC	17002C Fuchsite LGC	10005D Chlorite HGC	12019G Chlorite HGC	15003 Chlorite HGC	12009A Chlorite LGC	12024A Chlorite LGC	16001F Chlorite LGC
SiO_2		56.56		33.28	30.72	47.25				30.90
Al_2O_3		22.18		19.82	17.18	11.02				17.73
Fe_2O_3		2.21		5.77	14.58	10.06				15.17
MgO		2.76		9.53	22.99	14.99				24.17
CaO		1.78		5.32	0.08	3.06				0.25
Na_2O		1.01		0.16	1.06	0.39				0.07
K_2O		5.44		5.29	0.06	0.09				<0.05
TiO_2		0.28		0.42	0.60	0.20				0.22
MnO		0.02		0.08	0.01	0.03				0.01
P_2O_5		<0.01		0.04	<0.01	0.03				<0.01
Cr_2O_3	0.81	1.05	0.99	1.18	1.17	0.54	0.96	1.15	0.31	0.79
LOI		6.72		19.12	11.55	12.34				10.69
Rb	54	226	152	195						
Zr	33	63		34		85	87	196		
Ba	21	642	389	225		38			13	
Th									0.5	
Hf	0.7	0.8	0.9	1	0.9	0.3	0.3	0.7	0.3	0.8
Cs	2.1	3.7	2.8	2.3	0.3	0.3	0.8	0.2	0.8	0.[illegible]
Ta										
Ni	928	2338	1488	1994	2402	1003	1642	2374	575	1670
Sc	14	25	14	30	31	17	21	37	19	14
Sb	2.7	3.6	4.7	5.1	4.3	1.9	2.2	5.9	0.5	1.2
Ir		4.72		3.27			5.03			3.09

Table 6-1. Major and trace elements of fuchsite and chlorite separates from the Quartz-Fuchsite vein.

Major elements and Cr_2O_3 in wt.%. Trace elements in ppm, except Ir in ppb.
HGC: area of high gold content. LGC : area of low gold content.

pattern substantiate the presence of other phases in the chlorite and muscovite separates.

The Cr_2O_3 proportion in muscovite separates between 0.81 and 1.20 wt% confirms the desigation of the green mica in the QFV as fuchsite (Whitmore et al., 1949; Deer et al., 1962).

Ni appears to be an uncommon constituent of muscovites and chlorites (Deer et al., 1962). Its relatively high content in both mineral separates might indicate the presence of small melonite inclusions.

Ir concentrations are high in both fuchsite and chlorite separates (2.7-5.1 ppb). The controls on the distribution of Ir in rock forming minerals were discussed in chapter 4 (section 4-5). In the banding, Ir shows neither a well-defined affinity for Cr nor for Ni (Fig. 4-7). This raises the question whether the mineral phases controlling the Cr and Ni distribution in the banding, fuchsite and melonite, respectively, incorporate Ir in their lattice. It has been shown that Ir probably did not substitute for Cr or Ni in the original rock forming minerals in the wall rock. The association of an undetermined opaque phase with melonite is often observed in the banding (Plate 6-1B). The main components of this enigmatic mineral are Ni, Co, Fe, As, and S, and suggest the presence of a sulfarsenide. As mentioned above, arsenides and sulfarsenides act as major concentrators of

PGE (Crocket, 1981). For instance, the occurrence of Ir-arsenides within Co-Ni sulfarsenides has been described in several cases in nickel deposits from Finland (Häkli et al., 1976) and Western Australia (Hudson, 1986). Thus, it is suggested that Ir in the banding is not controlled by chlorite or fuchsite abundances, but rather by the presence of a sulfarsenide within or in close spatial relationship with melonite.

In brief, the development of fuchsite, melonite, and probably an arsenide-sulfarsenide mineral in the banding provide host phases for Cr, Ni, and Ir, elements which are typical constituents of ultramafic rocks, the probable protolith of the carbonatized rocks hosting the QFV. K, Te, and As were introduced into the QFV, perhaps with the Au- and Pb-bearing fluid. Wall rock slivers mechanically incorporated in the QFV during crack-seal increments probably reacted with the hydrothermal fluid that precipitated quartz and gold. As a result, relatively immobile elements from the slivers (Cr, Ni, Ir) were combined with constituents of the hydrothermal fluid (K, Te, As) to precipitate fuchsite , melonite, and an Ir-rich phase. This conclusion contrasts with that of Fryer et al. (1979), who suggested high mobilities of Cr and Ni in a hydrothermal fluid to explain their elevated concentrations in the banded quartz-fuchsite-tourmaline veins of the Dome Mine. It appears that fuchsite in the banding of the QFV is genetically related to deposition of gold since both were probably deposited in response to hydraulic fracturing and pressure drops during crack-seal vein growth. However, the capacity of the hydrothermal fluid to stabilize fuchsite in the QFV diminished as the distance from the porphyries, the most probable source, increased.

The K/Rb ratio of fuchsite from the banding is low (K/Rb = 205 - 228) with respect to that of the wall rocks (Fig. 4-2) and is characteristic of a late stage hydrothermal fluid enriched in Rb (Armbrust and Gannicott, 1978). It is very probable that the fluid which deposited fuchsite in the carbonate rocks in proximity to the porphyry lens, became enriched in Rb with respect to K. Further interaction with the slates decreased the K/Rb ratio of the fluid even more. The remaining fluid, which reacted with slivers of wall rock during the crack-seal hydraulic fracturing stages, was probably highly enriched in Rb relative to K. It is possible that K and Rb, which were added to the QFV, are derived from a local source, namely the adjacent slates, and more importantly the porphyries. For instance, McAuley (1983) suggested that the Preston porphyry and small lenses are relatively depleted in Rb and K with respect to normal intrusives.

Determination of REE in the banding was attempted. However, LREE were commonly below detection limits, and reproducibility was poor.

6.3. CONCLUSIONS

Wall rock selvages incorporated in the QFV during crack-seal episodes of vein growth probably reacted with the hydrothermal fluid that precipitated gold and quartz. Relatively immobile elements from the wall rock slivers, in particular Cr, Ni, and Ir, were combined with ore fluid components, in particular K, Te, and As, to form fuchsite, melonite, and an Ir-carrier (probably a sulfarsenide).

The K/Rb ratio of fuchsite from the banding suggests that the fluid, which deposited the Cr-muscovite, is the same fluid which previously interacted with the carbonate host rock and the slates. As concluded in chapter 4, this fluid was driven out of the porphyry lens towards the slate -carbonate rock contact.

Many of the components present in the QFV probably have a local source. Cr, Ni, and Ir are original components of the slivers that were isolated from the host rock during hydraulic fracturing. K and Rb could be derived from the porphyries to a large extent, and from the adjacent slates. Silica was possibly largely derived from the host komatiites during carbonatization.

Like the distribution of fuchsite in the carbonate rocks, fuchsite abundance in the QFV is a function of the proximity of the gold-bearing vein to porphyry bodies. Fuchsite is probably genetically related to deposition of gold in the QFV, but its presence is spatially controlled by porphyries.Carbonatization of the wall rock predates quartz veining.

CHAPTER 7

FLUID INCLUSIONS

7.1. INTRODUCTION

Fluid inclusion (FI) microthermometry is a direct method of studying the physical and chemical environment of mineral formation. FI studies can provide information about temperature, pressure, density, and composition of the fluid from which the host mineral was precipitated (primary FI), or that migrated through the mineral after its precipitation (secondary FI). Microthermometric studies may also provide evidence for mixing or unmixing of fluids, which may promote ore deposition. Fundamentals on FI studies can be found in Hollister and Crawford (1981) and Roedder (1984). FI microthermometry was applied to quartz samples from the QFV to characterize the nature of the ore-bearing fluid, and the processes of ore deposition.

7.2. REVIEW OF PREVIOUS FLUID INCLUSION STUDIES IN ARCHEAN LODE GOLD DEPOSITS

Recent microthermometric studies by Smith et al. (1984), LaKind (1984), Ho et al. (1985), Santosh (1986), Wood et al. (1986a), and Robert and Kelly (1987) indicate that the predominant components of fluids associated with Archean gold mineralization are H_2O and CO_2. Salinities are usually low, between less than 2 up to 12 equivalent NaCl wt % . FIs are either primary or secondary. Inclusions can be H_2O-rich, CO_2-rich, or mixtures of H_2O and CO_2. Unmixing of a parent H_2O-CO_2 fluid into a low-salinity aqueous liquid, and a CO_2-rich vapor is often recognized. CH_4 is occasionally associated with CO_2. Homogenization temperatures range between 150° and 400°C. Robert and Kelly (1987) reported very saline FIs with 25 to 34 wt% salt coexisting with CO_2-rich inclusions in gold-bearing fractures. Leachate analyses of FIs by Ho et al. (1985) for deposits from Western Australia, and by Robert and Kelly (1987) for the Sigma Mine, Québec, show that Na is the main cation in these fluids, accompanied by variable amounts of K and Ca, and to a lesser extent by Mg and Fe. Gas chromatography analyses of FIs from the Sigma Mine, Québec (Robert and Kelly, 1987) indicate that the principal gaseous components are H_2O and CO_2, and to a lesser extent CH_4. CO and N_2 were found to be present in very low abundances (less than 1 mole %). More importantly for the current study, in the Timmins area, Smith et al. (1984) and Spooner et al. (1987) found that H_2O, CO_2, and occasionally CH_4, are the most abundant species in the McIntyre-Hollinger mine. C_2H_6, CO, N_2, NO, and NO_2 were also recognized, although in minor concentrations.

It appears that most microthermometric FI data from Archean lode gold deposits can be adequately interpreted in the quaternary CO_2-CH_4-NaCl-H_2O system (Ramboz, 1980). Since CO_2 has a low solubility in H_2O at low temperatures (< 50°C), and CH_4 and salts are strongly partitioned in CO_2 and H_2O, respectively; phase changes occurring in FIs at temperatures below 50°C are adequately interpreted with respect to the much simpler H_2O-CO_2, CO_2-CH_4, NaCl-H_2O-CO_2, and H_2O-CO_2-CH_4 systems. A good and concise review of these systems can be found in Hollister and Burruss (1976), and a more detailed discussion in Burruss (1981), Crawford (1981a), and Roedder (1984, chap. 8). The CO_2-CH_4-H_2O-NaCl system has yet not been established to interpret quantitatively bulk homogenization phenomena of saline and CH_4-rich H_2O-CO_2 solutions. However, experimental data and thermodynamic calculations are available for the H_2O-NaCl-CO_2 system at high temperatures (Takenouchi and Kennedy, 1965; Hendel and Hollister, 1981; Hollister, 1981; Holloway, 1981; Bowers and Helgeson, 1983a) (Fig. 7-1). Although the effects of CH_4 on the H_2O-NaCl-CO_2 system have not been experimentally studied, it is generally suggested that, due to complete miscibility of CH_4 in CO_2, addition of CH_4 to an H_2O-NaCl-CO_2 solution will not significantly change the shape of that system (Hollister, 1981; Pichavant et al., 1982; Ramboz et al., 1982). Moreover, Hollister and Burruss (1976) suggested that addition of CH_4 to the H_2O-

Figure 7-1A. Data on the effect of NaCl on the position of the H_2O-CO_2 solvus (From Hollister, 1981).

Pressure conditions: 1 kb. Numbers are NaCl wt % in the aqueous solution. XCO_2: mole fraction of CO_2 in the aqueous solution. The two phase region lies on the low temperature side of a given curve. Note how addition of NaCl to the pure H_2O-CO_2 system widens the zone of immiscibility of such a solution.

Figure 7-1B. Pressure-temperature sections through the immiscibility volume in the H_2O-NaCl-CO_2 system (From Holloway, 1981).

The two phase region lies to the left of a given curve.
The curves are (in mole %):
a: 96.0 H_2O, 4.0 CO_2, 0.0 NaCl.
b: 94.1 H_2O, 4.0 CO_2, 1.9 NaCl.
c: 91.5 H_2O, 6.7 CO_2, 1.8 NaCl.
d: 88.6 H_2O, 9.7 CO_2, 1.7 NaCl.

6

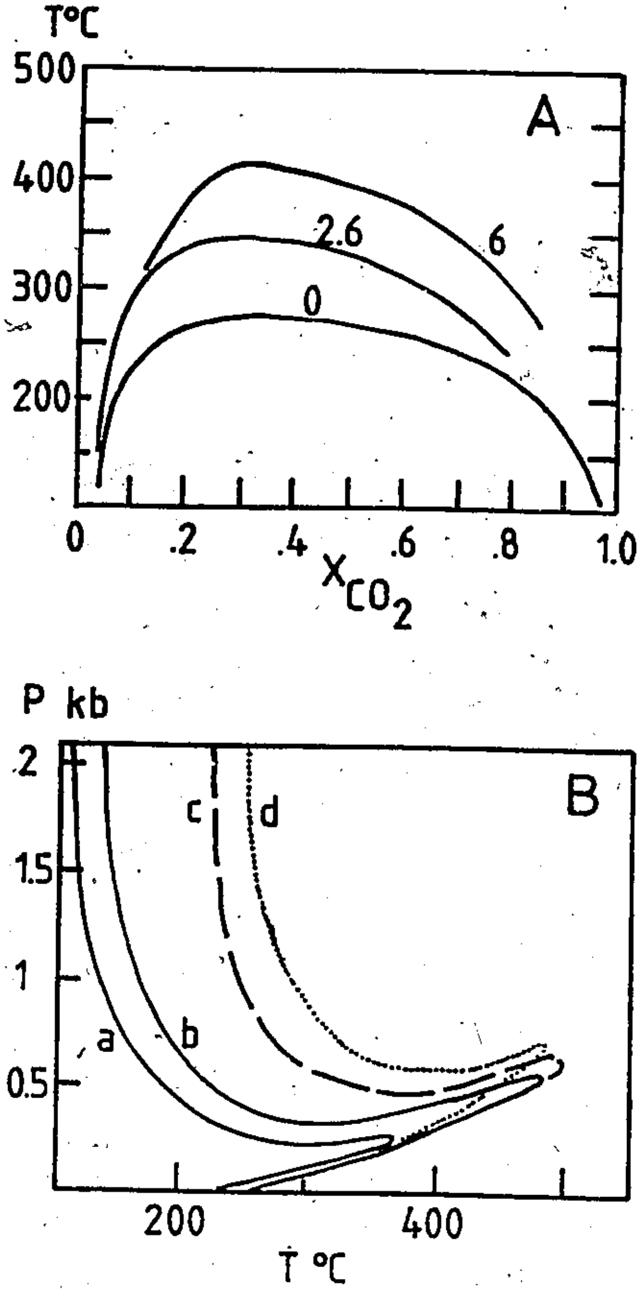
T°C
500
400
300
200
A
2.6
6
0
0
.2
.4
.6
.8
1.0
X_{CO_2}
P kb
2
1.5
1
0.5
B
c
d
a
b
200
400
T °C

$NaCl-CO_2$ system might raise its solvus to higher temperatures, and the miscibility gap of that system might therefore be widened. Thus, it appears that even if CH_4 is present in relatively high concentrations, the diagrams presented in figure 7-1 remain valid to explain at least qualitatively homogenization phenomena of low salinity CH_4-rich H_2O-CO_2 fluids. The important observation to make about the diagrams in figure 7-1 is that the low salinity H_2O-CO_2 fluids commonly described in Archean lode gold deposits are particularly sensitive to pressure and temperature variations in the 200° to 400°C temperature range and at pressures below 1 kb. Drops in temperature or pressure might promote unmixing of an aqueous fluid of moderate salinity and CO_2 content into a liquid with higher salinity and lower CO_2 content, and a vapor with lower salinity and higher CO_2 content (Ramboz et al., 1982). During unmixing of an $H_2O-NaCl-CO_2$ fluid, NaCl fractionates strongly into the H_2O-rich liquid phase which results in a higher salinity liquid (Bowers and Helgeson, 1983b), whereas CO_2 (and other volatiles such as CH_4, H_2S, N_2, etc.) are strongly partitioned into the vapor phase (Ramboz et al., 1982; Drummond and Ohmoto, 1985). Loss of CO_2 from the parent fluid to the vapor phase has the effect of increasing the pH of the fluid while partitioning of reduced gases such as CH_4 and H_2S into the vapor phase increases the oxygen fugacity (fO_2) of the remaining liquid (Drummond and Ohmoto, 1985).

7.3. EFFECTS OF DEFORMATION ON FLUID INCLUSIONS

In chapter 5, it was concluded that the bulk of quartz and gold were deposited in the QFV, before the latter underwent a severe compressional deformation event. Therefore, any FIs related to the mineralization event must have been affected by the same deformation episode. A brief review of the effects of changes in pressure-temperature conditions, deformation and recrystallization on inclusions is necessary to interpret FIs from the QFV, and their microthermometric data correctly.

Kerrich (1976), and Wilkins and Bargas (1978) recognized that deformation and recrystallization of quartz grains may lead to significant modifications of FI. These changes are :

1) A decrease in the number of primary FIs.

2) FIs in strained areas tend to be smaller in size (predominantly less than 2 µm), than primary FIs in undeformed domains.

3) A shift towards higher homogenization temperatures in deformed grains attributed to leakage of inclusions.

4) A more variable distribution of homogenization temperatures.

7

5) A clearing of FIs from the interior of quartz grains ("sweeping out"). Boundaries of newly recrystallized grains are often outlined by these expelled FIs.

In microthermometric studies of FIs, it is commonly assumed that the composition and the density of the fluid has not been altered since it has been trapped (Hollister, 1981). However, Pécher (1981) noted that densities of FIs, that are dependent on the pressure and the temperature of trapping, often disagree with pressure-temperature couples deduced by other geological means. Thus, it raises the question of density constancy in FIs. Pécher and Boullier (1984) have experimentally demonstrated that shape and density of FIs are changed under confining (experimental) pressure. Their main findings are :

1) At a given temperature, when confining pressure is lower than the pressure of the fluid inside the inclusion, FIs either decrepitate or their shape changes considerably (e.g. necking down). Homogenization temperatures of decrepitated or newly formed FIs are higher and very dispersed relative to initial homogenization temperatures of primary FIs. Homogenization temperatures of FIs that only changed in shape are still highly clustered, albeit higher than the homogenization temperature of inclusions measured prior to running the experiment.

2) At a given temperature, when confining pressure is higher than the internal pressure of the FI, only

modifications of shape and densities were recorded. Homogenization temperatures were shifted towards lower values after experimental runs.

The change of FI shape, in the absence of decrepitation, is attributed to the mechanism of pressure-solution (Gratier, 1982). However, this is not accompanied by a significant modification of the inclusion volume. According to Pécher and Boullier (1984), variation in homogenization temperatures, hence of densities, requires that diffusion of components such as OH⁻ and Si takes place. This process is poorly understood and remains controversial. Nevertheless, the experiments of Pécher and Boullier (1984) show that, under stress, densities or homogenization temperatures can be progressively modified towards higher or lower values.

Leroy (1979) pointed out that decrepitation of FIs is a function of the nature of the fluid, of the size and the shape of the inclusion, and of the degree of fracturing of the host mineral. Leroy (1979) experimentally demonstrated that small inclusions are able to sustain a larger difference between confining and internal pressures than larger inclusions.

These observations indicate that FIs can survive deformation and may still be suitable for microthermometric investigations. Nevertheless, care has to be taken in the selection of a particular inclusion for microthermometric runs. For instance, inclusions have to be carefully checked for absence of necking down, decrepitation, or leakage, especially in the case of larger inclusions. Size of FIs can be expected to be small. The data obtained in such a context should be taken with caution, in so far that temperature and composition might have been altered to a certain extent. These points are pertinent to the case of the QFV.

7.4. NATURE AND OCCURRENCE OF FLUID INCLUSIONS IN THE QUARTZ-FUCHSITE VEIN

Most of the FIs were too small (less than 2 µm) to be adequately studied with the heating-freezing stage at the maximum magnification of 480 times. Small FIs (less than 2µm) are predominantly present in healed fractures crosscutting large and relatively unstrained quartz grains, or were found to outline newly recrystallized quartz grains (Plate 7-1A).

FIs large enough to permit microthermometric studies (between 2 and 10 µm) are located in large quartz grains showing little or no recrystallization or deformation effects. Besides some low temperature and high salinity FIs (see below), large FIs have never been observed to crosscut recrystallized quartz grain-boundaries. In particular, these types of FIs "disappear" at the contact with recrystallized quartz (Plate 7-1B).

Plate 7-1A. Effects of quartz recrystallization and deformation on fluid inclusions.

a: small fluid inclusions outlining recrystallized quartz.
b: unstrained quartz with relatively larger aqueous-carbonaceous fluid inclusions than in a.

Recrystallization of quartz results in clearing off of fluid inclusions from quartz grains. Note how fluid inclusions from area b "disappear" in proximity to the area of recrystallized quartz.

Plate 7-1B. Chronological relationship between fluid inclusions.

a: trail of late stage saline aqueous inclusions (H_2O-salts) homogenizing between 110° and 150°C.
b: cluster of early CO_2-CH_4 inclusions.

The CO_2-CH_4 inclusions from an earlier aqueous-carbonaceous hydrothermal fluid stage are crosscut by the later stage lower temperature saline aqueous inclusions.

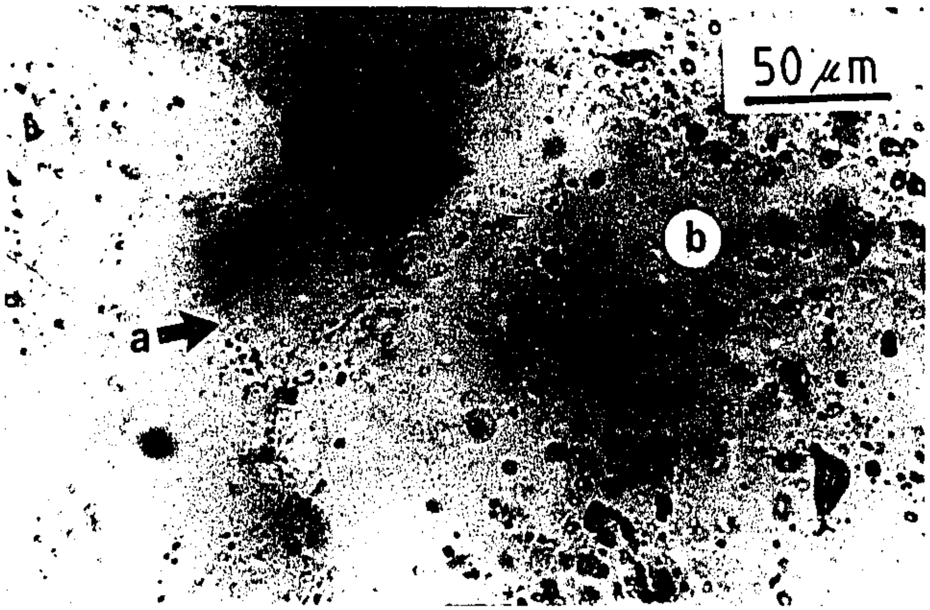

A

B

No primary inclusions were recognized. All inclusions seem to be secondary; that is, they were formed after their host quartz was precipitated. There are many FIs with variable degrees of filling. This can be attributed to necking down of older FIs in some cases. Inclusions for which necking down was recognized were not examined in heating and freezing runs. No difference in FI composition was observed between barren and ore zones of the QFV.

Four main types of FIs were recognized in quartz from the QFV. These are :

1) Aqueous CO_2- and CH_4-bearing inclusions (H_2O-CO_2-CH_4),
2) CO_2- and CH_4-rich inclusions (CO_2-CH_4),
3) low salinity aqueous inclusions (H_2O-NaCl),
4) high salinity aqueous inclusions (H_2O-Salts).

All inclusions occur in trails. Inclusions of type 1 and 2 occur in clusters as well. High salinity aqueous inclusions (type 4) are the only ones which were found to crosscut quartz sub-grain boundaries. Type 4 inclusions also crosscut CO_2- and CH_4-rich inclusions (Type 2) (Plate 7-1B). Each single type appears to have similar degrees of filling. Usually, only one type of FI occurs in a given cluster or along a given trail. An exception is a fifth type of inclusions with variable degrees of filling and compositions which showed no petrographic evidences of necking down.

Aqueous CO_2- and CH_4-bearing inclusions (Type 1) display negative crystal to subrounded shapes. Low salinity inclusions (Type 3) also display equant shapes, but tend to be more irregular, subrounded, and ellipsoidal. CO_2- and CH_4-rich inclusions (Type 2) are commonly irregular and subrounded, whereas the high salinity aqueous inclusions (Type 4) were found to be more angular in shape.

No solid phases were observed in any of the FI types. All inclusions contain two phases at room temperature including an inner vapor bubble, which is rimmed by a liquid phase.

7.5. FLUID INCLUSION MICROTHERMOMETRY

7.5.1. Type 1: Aqueous CO_2- and CH_4-bearing inclusions (H_2O-CO_2-CH_4)

An additional third phase appears in the inner bubble on cooling. The entire FI is frozen at approximately -100°C. On heating, four successive stages of melting or homogenization can be observed (Fig. 7-2A). Melting of CO_2 takes place between -63.9° and -61.2°C. Homogenization of CO_2 to the liquid phase occurs between -10.5° and -5.6°C. Melting of a further phase is recognized between +9.6° and +12.8°C, and indicates the presence of a clathrate hydrate. The inclusions often decrepitated before homogenization canbe reached. However, homogenization temperatures were obtained for three FIs at +344°C to the liquid, and at

Figure 7-2. Microthermometric data for quartz samples from the Quartz–Fuchsite vein.

TmCO2: melting temperature of CO_2. ThCO2: homogenization temperature of CO_2. TmC: melting temperature of clathrate. TmI: melting temperature of ice. Th: bulk homogenization temperature. n: number of analyses.
Homogenization is to the liquid unless stated otherwise.
Black squares: inclusion which decrepitated before homogenization. Cross-hatched squares: inclusion showing metastability behavior. V: homogenization to the vapor.

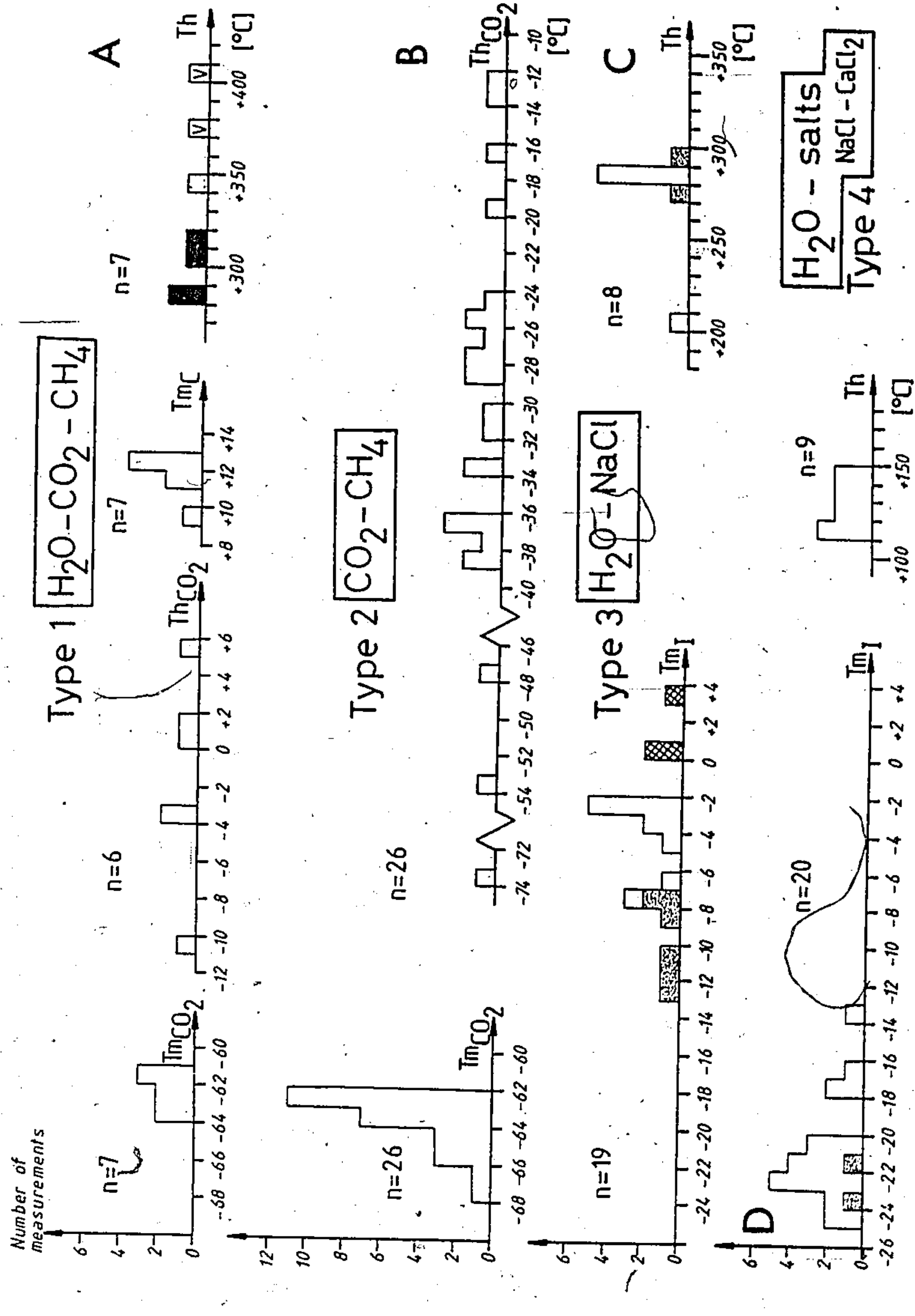
Number of measurements
Type 1 $H_2O-CO_2-CH_4$
Type 2 CO_2-CH_4
Type 3 $H_2O-NaCl$
H_2O - salts
NaCl - $CaCl_2$
Type 4
A
B
C
D
n=7
n=6
n=7
n=7
n=26
n=26
n=19
n=8
n=20
n=9
Tm_{CO_2}
Th_{CO_2}
Tm_C
Tm_I
Th
[°C]

+377.7° and +406.5°C to the vapor. No melting of ice could be observed in these FIs.

The presence of CH_4 is suspected because :

1) The melting temperature of CO_2 is shifted from -56.6°C towards lower temperatures.

2) The homogenization temperature of CO_2 is also anomalously low.

3) Melting of clathrate occurs predominantly above +10°C.

Addition of CH_4 to CO_2 is known to lower both melting and homogenization temperatures of the latter. Increasing CH_4 content in the CO_2-H_2O system shifts the melting temperature of the clathrate hydrate towards higher temperatures (Hollister and Burruss, 1976; Burruss, 1981; Roedder, 1984, chap. 8). CO_2 in these inclusions must contain a high proportion of CH_4, up to 25 to 30 mole%, according to either figure 3.10 in Burruss (1981, p.55), or figure 2 in Heyen et al. (1982, p.205), or figure 236.5 in Spooner et al. (1987, p.43). Non-detection of ice melting, and the counteracting effects of salt and CH_4 on clathrate melting preclude any measurement of salinity in these FIs (Hollister and Burruss, 1976; Collins, 1979).

7.5.2. Type 2: CO_2- and CH_4-rich inclusions (CO_2-CH_4)

Due to strong internal reflections, this type of inclusion appears to be very dark at room temperature, and thus is easily distinguished from the other types of FIs

(Fig. 7-2B). Melting temperatures of CO_2 range between -67.0° and -62.4°C, and homogenization temperatures between -82.6° and -12.5°C (Fig. 7-2B). No melting of ice or clathrate was observed. An outer rim of liquid (H_2O ?) is suspected in some cases, where a meniscus can be observed at sharp edges. According to figures 3.10 in Burruss (1981, p.55), 2 in Heyen et al. (1982, p.205), and 236.5 in Spooner et al. (1987, p.43), CO_2 must contain more than 30 mole % CH_4, and maybe as much as 50 mole % .

7.5.3. Type 3: low salinity aqueous inclusions (H_2O-NaCl)

Melting temperatures of ice range between -12.2° and -2.7°C for this type of FI (Fig. 7-2C). No melting was detected below about -20°C. This suggests that the main dissolved salt-species is NaCl, although the presence of KCl cannot be ruled out (Crawford, 1981a, table 4.1, p.83). Using the method of Potter et al. (1978), the range of melting temperatures of ice corresponds to 4.5 to 16.2 equivalent NaCl wt% . Besides salts, dissolved CO_2 in the liquid phase could be another component that can depress the freezing point of H_2O (Collins, 1979; Hedenquist and Henley, 1985). However, owing to the small size of the inclusions, the presence of CO_2 could not be detected. Homogenization temperatures cluster tightly between +260° and +300°C, with two inclusions yielding temperatures between +190° and +210°C (Fig. 7-2C). Homogenization is to the liquid.

Melting of ice at temperatures above 0°C is one problem that was often encountered with this type of FI (Fig. 7-2C). In these inclusions, the vapor bubble was eliminated on freezing. It reappeared suddenly on heating, at a temperature above 0°C, together with almost instantaneous melting of ice. Melting temperatures were not reproducible for a given inclusion. This type of phenomena can be attributed to metastable liquids in stretched inclusions (Roedder, 1984, p.298-299). It precluded the measurement of reliable microthermometric data for these particular inclusions.

7.5.4. Type 4: high salinity aqueous inclusions (H_2O-Salts)

This type of FI can be differentiated from the former type by ice melting and bulk homogenization temperatures. Melting of ice starts below -35°C, and final melting takes place between -24.4° and -13.6°C (Fig. 7-2D). According to Crawford (1981a, table 4.1, p.83), this type of behavior indicates that the major dissolved salts are NaCl and $CaCl_2$, although the presence of such components as $MgCl_2$ or KCl cannot be excluded. No solid phases were observed above melting temperatures of ice. Homogenization temperatures cluster between +110.9° and +144.4°C.

Homogenization is to the liquid. No CO_2 or CH_4 could be detected.

7.6. INTERPRETATION AND DISCUSSION

7.6.1. Anomalously high CH_4 content in CO_2

High abundances of CH_4 and CO_2 are incompatible in the same fluid. Either CO_2-rich aqueous fluids or CH_4-rich aqueous fluids can be stable in equilibrium with graphite (Holloway, 1984; Lamb and Valley, 1985; Kreulen, 1987). Thus, the high mole percentage of CH_4 in type 1 and type 2 inclusions seems to be anomalous. According to Kreulen (1987) several possibilities may account for such a discrepancy :

1) Reactions between gas species within the inclusions might lead to modifications of the original composition. This seems to be possible only in the presence of graphite (Dubessy, 1984). No graphite was detected by microscopic means in the inclusions under study. CH_4 might also be produced by reaction between CO_2 and NH_3. However, the resulting N_2 would have to be a dominant species in the inclusion. This seems unlikely, in so far as N_2 was not found to be a dominant species in the nearby McIntyre-Hollinger Mine (Smith et al., 1984; Spooner et al., 1987).

2) The fluids might have been in disequilibrium at the time of trapping. In other words, even if graphite was present in the rocks, the hydrothermal fluid might not have been in

equilibrium with it. H_2O and CO_2 seem to be the predominant species in ore-bearing fluids associated with Archean lode gold deposits (see section 7.2.). CH_4 appears to be insignificant in most cases. Therefore, it is possible that the original fluid which came into the QFV environment was mainly a CO_2-H_2O mixture, and that CH_4 came from another source. The most obvious source for such CH_4 is the adjacent slates (Fig. 5-1). In chapter 4, it was shown that the hydrothermal fluid which carbonatized the host komatiites came into contact with the slates, and that it leached out such elements as K, Rb, Cs, and Ba. Thus, the original H_2O-CO_2 fluid might have been reduced during interaction with the slates. According to Kreulen (1987), graphite could fail to nucleate for kinetic reasons. CH_4-rich FIs in Archean lode gold deposits seem to be predominantly encountered where carbonaceous sediments are present in the immediate ore environment (Ho et al., 1985; Spooner et al., 1987).

3) The real H_2O content might be higher than estimated by microscopic observations. H_2O preferentially wets the walls of FIs. For instance according to Kreulen (1987), more than 65 to 85 mole % of H_2O would have to be present to be detected in a 10 µm spherical inclusion. With the small size of the inclusions present in the QFV, this might be one of the main problems for the dark CO_2- and CH_4-rich inclusions (Plate 7-2B).

4) Hydrogen might have diffused out of the inclusions. This would result into a shift towards higher CO_2 content.

5) H_2O might have been lost after trapping. This is a process which is not fully understood, although experimental studies have shown that H_2O can diffuse through quartz. Kreulen (1987) suggests that deformation might remove H_2O from the inclusion as the host mineral recrystallizes, whereas other components stay behind. As we have seen above (see section 7.3.), the same reason has been invoked by Pécher and Boullier (1984) to explain changes of homogenization temperatures of inclusions, after they had undergone deformation.

In summary, four out of the five possibilities discussed by Kreulen (1987) can explain the apparent presence of high CH_4 and high CO_2 concentrations in the same inclusions. Large amounts of H_2O could easily go unnoticed in the small inclusions available. The deformation event that affected the QFV and its FIs, might have promoted diffusion of water and/or hydrogen through the quartz host resulting in an alteration of the originally trapped fluid. Finally, interaction of an H_2O-CO_2 fluid with the slates could have resulted in production of CH_4. The later possibility seems to be the most likely by analogy to other Archean lode gold deposits.

7.6.2. Chronological sequence

Type 1, 2, and 3 inclusions are commonly found in large and relatively unstrained quartz grains. They never crosscut recrystallized quartz grains (Plate 7-1A) whereas type 4 inclusions (high salinity, low temperature inclusions) are found to crosscut recrystallized quartz grains and FIs of type 2 (Plate 7-1B). Thus, it appears that two main hydrothermal stages were recorded in the QFV:

1) An early, probably high temperature, aqueous carbonaceous stage represented by type 1, 2, and 3 inclusions which predate recrystallization of quartz.

2) A later, low temperature and high salinity stage, represented by type 4 inclusions, which postdates recrystallization of quartz. This stage is certainly unrelated to gold mineralization, since ore formation took place before deformation.

No age relationships could be observed between FIs of type 1, 2, and 3.

7.6.3. Fluid immiscibility

Inclusions with variable degrees of filling may coexist in a given fracture or cluster. Composition of these inclusions are variable (Fig. 7-3), but show many similarities to the carbonaceous and aqueous inclusions of type 1, 2, and 3 (Figs. 7-2A, B, and C). These similarities are :

1) Melting temperature of CO_2 clusters around -63°C.

2) Homogenization temperatures of CO_2 vary between -42° and -5°C.

3) Low salinities between 4.5 and 8.7 equivalent NaCl wt% . Melting temperatures of ice cluster around -4°C (6.4 equivalent NaCl wt%).

4) Melting temperatures of clathrate are above +10°C, clustering around +13°C.

5) Bulk homogenization is to the liquid and to the vapor, mainly between +200° and +400°C.

Such heterogeneous fluid indicates either the presence of an immiscible fluid in the QFV, or that necking down took place (Ramboz et al., 1982). Necking down of inclusions certainly took place in some areas of the QFV, especially where strain was concentrated. But several features suggest that these heterogeneous FIs represent unmixing of a hydrothermal fluid :

1) No necking down could be recognized during microscopic observations. In particular, the sample studied in detail in figure 7-3 comes from a zone of massive and relatively unstrained quartz from the QFV.

2) Simultaneous trapping of all inclusions took place, since they are found in the same cluster and trails.

3) Highly variable degrees of filling.

Figure 7-3. Microthermometric data for cluster of inclusions showing heterogeneous trapping.

TmCO2: melting temperature of CO2. ThCO2: homogenization temperature of CO2. TmI: melting temperature of ice. TmC: melting temperature of clathrate. Th: bulk homogenization temperature. Black squares: inclusion which decrepitated before homogenization. Hatched squares: inclusion with critical homogenization.
Data points above the horizontal axis: bulk homogenization to the vapor. Data points below the horizontal axis: bulk homogenization to the liquid.

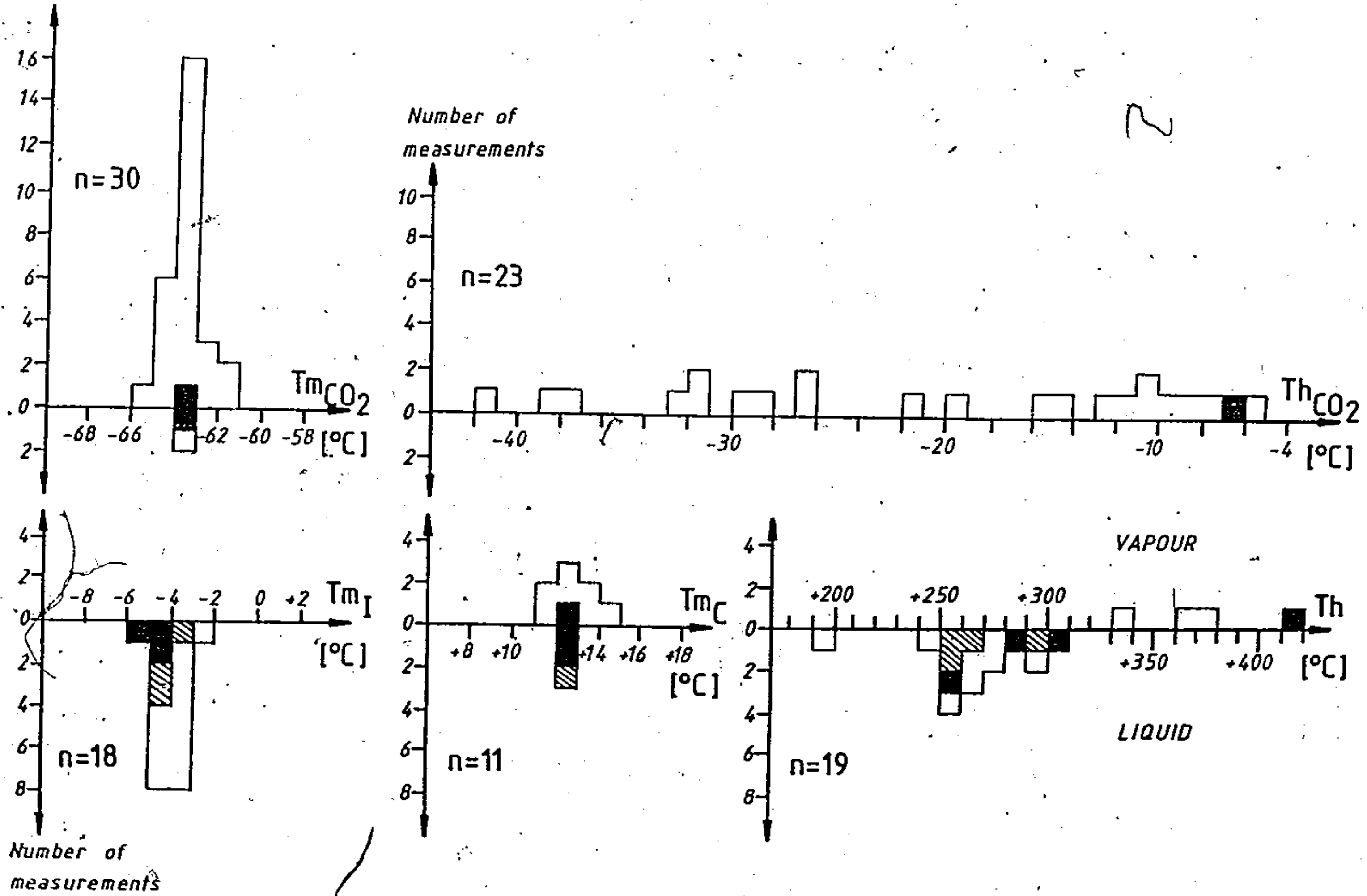
Number of measurements
n=30
16
14
12
10
8
6
4
2
0
2
Tm$_{CO_2}$
-68
-66
-62
-60
-58
[°C]
n=23
Th$_{CO_2}$
-40
-30
-20
-10
-4
[°C]
Tm$_I$
-8
-6
-4
-2
0
+2
[°C]
n=18
Tm$_C$
+8
+10
+14
+16
+18
[°C]
n=11
VAPOUR
LIQUID
Th
+200
+250
+300
+350
+400
[°C]
n=19
Number of measurements

4) Scattered temperatures of homogenization and hence variable densities. Low density FIs that homogenize to the vapor are present together with high density FIs that homogenize to the liquid.

5) Homogenization temperatures to the vapor are systematically higher than homogenization temperatures to the liquid. This is due to trapping of a film of fluid around the vapor bubble in the low density inclusions (Ramboz et al., 1982).

6) Vapor-rich inclusions, that are type 2 (CO_2-rich and CH_4-rich inclusions) are found in the absence of any liquid inclusions in single fractures. A fracture containing all vapor-rich inclusions could not result from necking down alone.

This evidence for unmixing of a carbonaceous and aqueous fluid suggests that type 1, 2, and 3 inclusions are related to each other. The vapor and liquid represented by FIs of type 2 (CO_2-CH_4) and type 3 (H_2O-NaCl), respectively, could be the result of unmixing of the fluid contained in type 1 inclusion (H_2O-CO_2-CH_4). The heterogeneous fluid, whose microthermometric data is displayed in figure 7-3, would represent the transition stage between the primary fluid (Type 1 FIs), and the unmixed vapor (Type 2 FIs) and liquid (Type 3 FIs). The coexistence in the QFV of inclusions containing the initial fluid before unmixing (Type 1), the liquid and the vapor after phase separation (Types 2 and 3), and the heterogeneous fluid, suggests that intermittent unmixing of an H_2O-CO_2 fluid took place in the QFV. As shown in figure 7-1, such unmixing may be due to pressure and/or temperature fluctuations back and forth through the solvus of such a fluid.

The strong partitioning of CH_4 for the vapor during unmixing is well illustrated in the case of the microthermometric data from the QFV. The increasing content of CH_4 in CO_2 with unmixing is shown by the positive correlation between the homogenization temperature of CO_2 and the melting temperature of CO_2, and the negative correlation between clathrate melting and the melting temperature of CO_2 (Fig. 7-4). Higher CH_4 content in CO_2 leads to lower melting and homogenization temperatures of CO_2, and to clathrate melting at higher temperatures (Hollister and Burruss, 1976; Burruss, 1981; Roedder, 1984, chap. 8). It is unlikely that deformation of the FIs would mimic an identical evolution trend as that displayed in figure 7-4.

Figure 7-4. Correlative variation of microthermometric data.

ThCO2: temperature of homogenization of CO2.
TmCO2: temperature of melting of CO2.
TmC : temperature of melting of clathrate.

Decreasing temperatures of homogenization and melting of CO2, and increasing melting temperature of clathrate as one progresses from the parent H_2O-CO_2-CH_4 fluid to the CO_2-CH_4-rich vapor indicates the strong partitioning of CH_4 to the vapor phase.

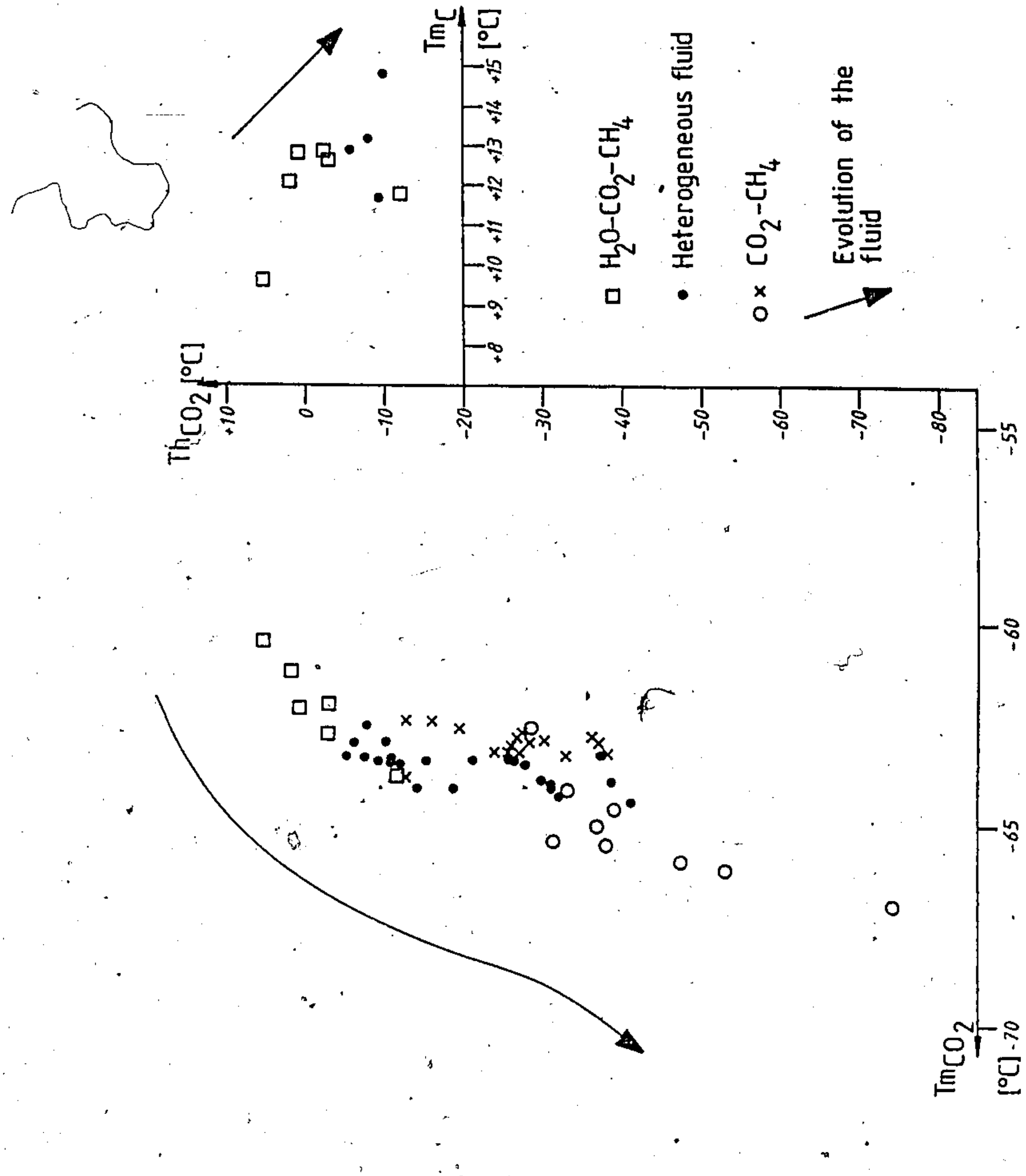
Tm$_C$ [°C]
+8
+9
+10
+11
+12
+13
+14
+15
Th$_{CO_2}$ [°C]
+10
0
-10
-20
-30
-40
-50
-60
-70
-80
Tm$_{CO_2}$ [°C]
-55
-60
-65
-70
□ H_2O-CO_2-CH_4
● Heterogeneous fluid
○ × CO_2-CH_4
Evolution of the fluid

7.6.4. Pressure-Temperature conditions at trapping

Since fluid unmixing took place, temperature conditions at trapping can be deduced from homogenization temperatures of the aqueous-carbonaceous FIs. Two fluids which are formed by phase separation of a common parent fluid at a given temperature, and which are trapped simultaneously in separate inclusions must homogenize to the same temperature of entrapment on heating. Thus, bulk homogenization temperatures obtained from microthermometric studies of these FIs equals the trapping temperature of the hydrothermal fluid (Pichavant et al., 1982; Ramboz et al., 1982; Roedder, 1984, chap. 9). In the case of the QFV, the two immiscible phases that resulted from unmixing are : type 2 FIs (CO_2-CH_4) and type 3 FIs (H_2O-NaCl). The most reliable trapping temperature is obtained from the inclusions homogenizing to the liquid that are type 3 FIs (H_2O-NaCl) (Fig. 7-2C), and which indicate that entrapment of the aqueous-carbonaceous fluid took place during episodes of unmixing around 280°C. The inclusions that trapped the heterogeneous fluid (Fig. 7-3) can be used as an additional indicator of the temperature of entrapment. This heterogeneous fluid was trapped at the instant when liquid and vapor were unmixing from a parent fluid. Only the homogenization temperatures to the liquid should be considered, since trapping of a thin film around a vapor bubble can result in anomalously high bulk homogenization temperature to the vapor (Ramboz et al., 1982; Roedder, 1984, p. 256 and 273). Trapping temperatures inferred from FIs containing the heterogeneous fluid range between 250° and 300°C. These temperatures are in concordance with the entrapment temperature of 280°C yielded by type 3 FIs (H_2O-NaCl). Provided that deformation did not greatly alter homogenization temperatures, the trapping temperatures for the QFV are very similar to the range of 277° ± 48°C obtained by Wood et al. (1986a) for the nearby McIntyre-Hollinger Mine, and to the range of 285° to 395°C obtained by Robert and Kelly (1987) for the Sigma Mine (Québec).

Figure 7-1B shows that the temperature of entrapment, the composition of the parent fluid before unmixing, and the position of the immiscibility surface of the chemical system pertinent to the fluid under study need to be known to define the pressure of trapping from microthermometric data of FIs. Unfortunately, it is not possible to determine the relative concentrations of H_2O, CO_2, CH_4 and NaCl in the parent fluid (Type 1 FIs: H_2O-CO_2-CH_4) with the freezing data of the present study; and more importantly, the effects of CH_4 on the position of the solvus in the H_2O-NaCl-CO_2 system are unknown. Thus, pressure of fluid entrapment cannot be established for the QFV. Nevertheless, Spooner et al. (1987) obtained homogenization temperatures for low salinity H_2O-CO_2 FIs with negligible CH_4 concentrations in gold-bearing quartz veins from the nearby McIntyre-Hollinger Mine. By using figure 7-1B, they were able to estimate a pressure and a depth of entrapment of 500 bars and 2 km, respectively. Since both the Dome Mine and the McIntyre-Hollinger Mine have similar geological settings, fluid inclusion types, and homogenization temperatures it is possible that these pressure and depth estimates are also valid for the QFV.

7.7. IMPLICATIONS FOR GOLD DEPOSITION IN THE QUARTZ-FUCHSITE VEIN

The carbonaceous and aqueous fluid observed in the QFV is very similar to the type of fluids observed in other Archean lode gold deposits (see section 7.2.). Occasional fluid unmixing is also noted in the McIntyre-Hollinger Mine (Timmins, Ontario) (Wood et al., 1986a; Spooner et al., 1987), and the Sigma Mine (Val d'Or, Québec) (Robert and Kelly, 1987). The carbonaceous and aqueous inclusions, like gold mineralization, predate the deformation event which has affected the QFV. Furthermore, the komatiite wall rock of the QFV has been extensively carbonatized during ingress of a CO_2-rich hydrothermal fluid, probably preceding quartz veining. These points suggest that FIs of type 1, 2, and 3, and the FIs with variable degrees of filling are probably the closest in composition to the ore-bearing fluid.

By analogy with other Archean lode gold deposits it can be inferred that the primary fluid before unmixing was a low salinity H_2O-CO_2 fluid (see section 7.2.). CH_4-rich fluids are usually only encountered in close proximity to carbonaceous sediments (Ho et al., 1985; Spooner et al., 1987). Thus, the fluid now present in the QFV probably acquired its CH_4-rich character only at the contact with the slates, although it may have been modified during later deformation (see sections 7.3. and 7.4.).

The aqueous-carbonaceous FIs can be found in either barren or ore zones of the QFV. This observation indicates that the fluid circulating along the QFV was of the same nature throughout the veining history, whether banded or massive quartz was precipitated. An identical conclusion was reached in chapter 5, where it was put forward that high ore grade banded quartz and low ore grade massive quartz veins were deposited from the same hydrothermal fluid. Since gold, with a few exceptions, is consistently associated with banded quartz, the destabilization of the gold complexes from the aqueous-carbonaceous fluid must be related to the crack-seal vein growth. As depicted in figure 5-11, when a crack was formed during hydraulic fracturing, the wall rock pore fluid migrated to the crack, thus resulting in a slight pressure drop within the fluid when it reached the fracture (Fig. 5-11). By analogy to figure 7-1B, the low salinity CH_4-rich H_2O-CO_2 fluid present in the QFV is very probably sensitive to pressure fluctuations at the pressure-temperature conditions determined in section 7.6.4. This aqueous-carbonaceous fluid may have undergone unmixing at each crack-seal event. Partitioning of CO_2 and CH_4 (plus other reduced volatile species) to the vapor would result in a shift in the remaining fluid toward higher pH and fO_2 (Drummond and Ohmoto, 1985). Assuming that gold was transported as a thio complex, pH and fO_2 will strongly affect the stability of such complexes (Seward 1973, 1984). Figure 7-5 shows how a simultaneous increase of both pH and fO_2 can result instantaneously in a dramatic drop of gold solubility. Partitioning of H_2S into the vapor also has the effect of destabilizing such thio complexes. The numerous crack-seal events that are required to generate the large width of the banded domains in the QFV were probably very efficient in removing gold from the ore-bearing solution.

Little gold, if any, was deposited in the massive and non-banded quartz material because the pressure of the hydrothermal fluid inside the vein had to be high enough to overcome the pressure acting on the walls. Therefore pressure conditions were such that no phase separation of the ore-bearing fluid could occur.

The absence of primary FIs does not invalidate the ore deposition modeling described above. The accretionary crack-seal vein growth process was operative during most of the quartz precipitation history of the QFV. Once quartz was deposited in a crack it became part of the composite

Figure 7-5. Gold solubility contours for $Au(HS)_2^-$ at 300°C (From Seward, 1984).

Solubility contours are in ppm and shown by the solid lines. Stability fields of pyrite (py), pyrrhotite (po), hematite (hm), and magnetite (mg) are given by the dashed lines. The vertical dotted lines give the pH stability fields for K-feldspar (kf), muscovite (musc), and kaolinite (ka) where $a_{K^+}=0.01$. The stippled area indicates the frequently encountered region of ore deposition (according to Seward, 1984).
A: total sulfur = 0.05 m, total chloride = 1.0 m.
B: total sulfur = 0.001 m, total chloride = 1.0 m.

The diagrams are given to illustrate qualitatively how the increase of both fO_2 and pH leads to a decrease in gold solubility (arrow). The exact position of the gold solubility contours cannot be given for the ore-bearing fluid in the Quartz-Fuchsite vein environment since the total sulfur content of that fluid is unknown. However, sulfides are relatively rare in the Quartz-Fuchsite vein, suggesting that diagram B based on low-sulfur concentrations is a better representation of the conditions prevailing in the Quartz-Fuchsite vein environment. The presence of pyrite and muscovite in the vein and its wall rocks constrains fO_2 and pH conditions to the intersection area of the stability fields of muscovite and pyrite (area 1 in diagram B). Thus, it is interesting to note that the shift of fO_2 and pH which is responsible for gold precipitation in the Quartz-Fuchsite vein takes place in the area of ore deposition that, according to Seward (1984), is commonly observed in gold mineralizations.

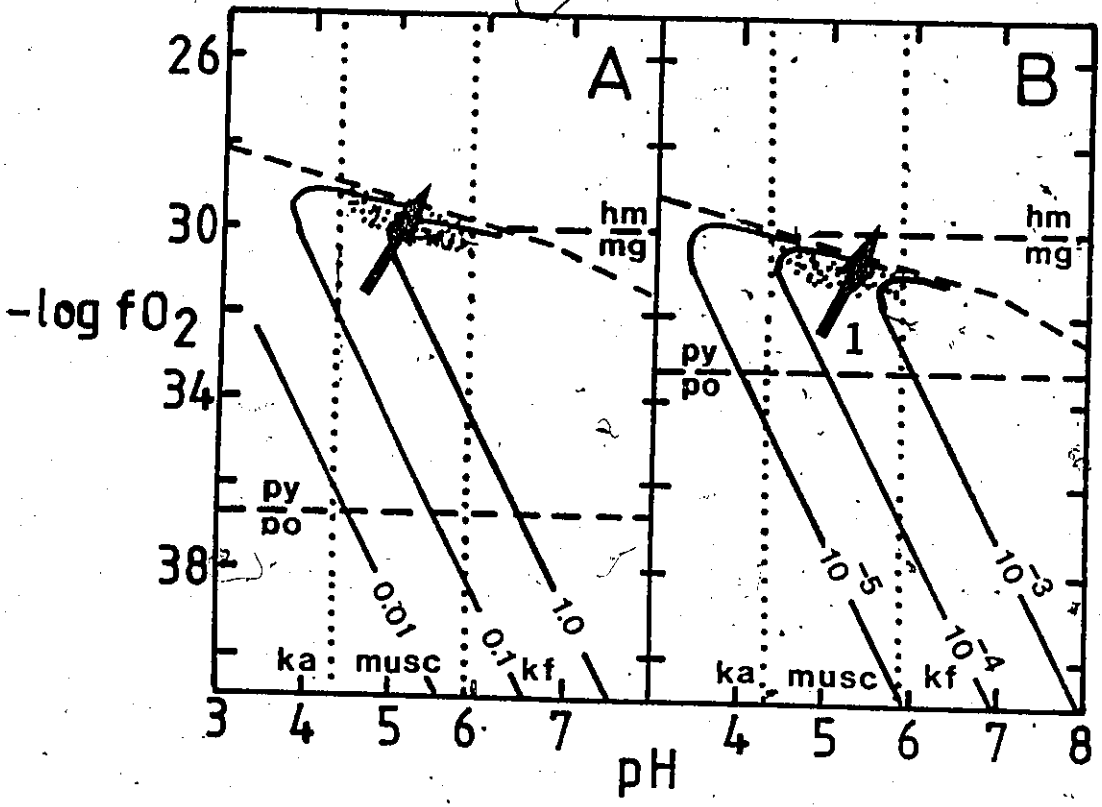
26
30
-log fO2
34
38
A
B
hm
mg
py
po
ka
musc
kf
0.01
0.1
1.0
10-5
10-4
10-3
1
3
4
5
6
7
8
pH

rock mass. Any subsequent crack-seal episode could have generated a fracture in previously deposited quartz. As described in figure 5-11, the pore fluid present in the adjacent wall rock would immediately migrate to such a fracture, deposit quartz therein, and possibly form a trail of secondary FIs on healing. As crack-seal was the predominant mechanism generating vein growth, secondary FIs can be expected to form in larger numbers than primary FIs. Together with the subsequent deformation event, crack-seal vein formation explains the apparent absence of, or the difficulty of recognizing, primary FIs in the QFV.

7.8. CONCLUSIONS

Two hydrothermal events were recorded in the FIs of the QFV : an early carbonaceous-aqueous and high temperature stage that predates deformation and recrystallization in the QFV; and a second high salinity and lower temperature stage that postdates deformation of the QFV, thus gold deposition.

The parent low salinity H_2O-CO_2 fluid of the first stage underwent intermittent unmixing, resulting in a low density CO_2-rich vapor, and a high density saline H_2O liquid. CO_2 contains up to 30 mole % CH_4 in the parent fluid, and probably as much as 50 mole % CH_4 in the vapor. The high CH_4 content in CO_2 is mainly attributed to interaction of the original low salinity H_2O-CO_2 fluid with slates, whereby the fluid was strongly reduced.

The mechanism of crack-seal vein growth probably created the small pressure drops inside fractures that triggered unmixing of the pressure sensitive low salinity CH_4-rich H_2O-CO_2 fluid. Strong partitioning of CO_2 and CH_4 (plus other volatiles) into the vapor phase resulted in an increase of pH and fO_2 of the remaining fluid.

The high temperature carbonaceous-aqueous fluid is most certainly the fluid that precipitated gold in the QFV. This conclusion follows from comparison with other Archean lode gold deposits, the observation that both gold and the carbonaceous-aqueous fluid predate deformation, and the fact that the observed wall rock alteration would be produced by the type of fluid present in the FIs. The temperature of this ore-bearing fluid was probably around 250° and 300°C, unless homogenization temperatures were strongly changed during deformation.

Assuming that gold was transported as a thio complex, then both the increase of pH and fO_2 during phase separation promoted gold deposition. Multiple crack-seal episodes in the QFV were an effective mechanism in the destabilization of gold complexes, and probably lead and telluride complexes, from a low salinity and CH_4-rich H_2O-CO_2 fluid.

The QFV is the highest grade ore vein in the Dome Mine. Therefore, the primary nature of the low salinity H_2O-CO_2 fluid, the presence of the slates which favored a build up of a high pore fluid pressure regime, and the crack-seal mechanism are probably optimum conditions to produce a high grade ore gold mineralization. Gold was not deposited in the massive quartz because phase separation could not take place during this type of vein formation, since fluid pressure was too high to permit phase separation.

CHAPTER 8

LEAD ISOTOPES

8.1. INTRODUCTION

Galena is intimately associated with native gold in the QFV. This relationship is so consistent that it can be assumed that both metals are coeval and deposited by the same hydrothermal. This inferred similarity in age has also been documented by earlier studies in the Timmins area (Hurst, 1935; Ferguson et al., 1968).

Any information obtained from the lead isotopic composition of the galenas may be directly relevant to the origin of the gold. Thus, lead isotopes could prove useful in constraining possible gold sources. In particular, the lead isotope signature may be evaluated in terms of local rock sources or lower crust and/or upper mantle sources.

8.2. SAMPLING

Eight galena samples were collected in the high grade ore zones of the QFV. All but one come from the banded parts. The galenas are typically in grain boundary contact with gold (Plate 6-1A). The one sample not from the banded part of the QFV comes from a quartz vein, in the wall rock, but in contact with the QFV (Fig. 5-1, sample #12003).

Whole rock lead isotope compositions were determined on various rocks from the Dome Mine environment, particularly the immediate host rocks of the QFV. Slates, carbonatized rocks, and a porphyry lens from a drift cutting the QFV on the 12th level (Fig. 5-1) were analyzed. The Preston porphyry was sampled on the 12th level, whereas the Paymaster and the Preston West porphyries, and an ultramafic flow were sampled at the surface south of the Dome Mine (Fig. 3-1).

8.3. DATA MANIPULATION AND INTERPRETATION

The treatment and interpretation of lead isotope data follows the procedures described by Faure (1986) and Gulson (1986, Chap.9). Model calculations, and constants and symbols used in lead-lead age and model calculations are given in Appendix III. The basic approach in a source rock investigation is to determine or infer the lead isotopic composition of the possible source rocks at the time of their formation, and compare these compositions with that of the ore, also at its time of formation.

The measured lead isotope compositions of the galenas do not need to be corrected for addition of radiogenic lead since their formation. Because of the far greater abundance of lead over uranium or thorium in galena, there is little concern about modification of the initial lead composition due to radioactive decay since the time of formation.

The situation is quite different for the whole rock samples. All the rocks contain some uranium, so that it is necessary to correct the observed lead isotope ratios for radioactive decay of uranium. Various approaches are used by which the starting lead composition can be defined (Lambert, 1985; Gulson, 1986, Chap.9). This can be achieved by utilizing K-feldspar, which usually has a very low uranium abundance with respect to lead. Unfortunately, no such K-feldspar can be found in any of the lithologies at the Dome Mine, so that this method cannot be applied. A similar procedure to determine the initial ratio is by correcting for in situ decay of uranium in the whole rock. However, studies by Rosholt et al. (1973) and Zielinski et al. (1981) have shown that uranium is very mobile under near-surface conditions making it difficult to obtain the initial isotopic composition. A further suggestion is to take the least radiogenic composition from galenas or another lead-rich mineral as the best approximation to the initial ratios. This procedure is redundant, since we want to determine whether or not a lithology from the Dome Mine had, at the time of its formation, a lead isotope composition similar to that of the lead from the galenas associated with gold in the QFV. Thus, as a first approach, the only remaining possibility is to obtain the initial ratio in a $^{207}Pb/^{204}Pb$ versus $^{206}Pb/^{204}Pb$ diagram by fitting a line through the array of whole rock data points of a given lithology (207/206 age), and extrapolating that same line until it intersects a model growth curve with a given μ value ($^{238}U/^{204}Pb$ ratio). The μ value is selected to give the same age for the lithology as deduced by other geochronological methods (e.g., U-Pb age).

In order to use the latter method, a lead evolution model has to be chosen. Several such models are proposed (e.g., Holmes, 1946; Houtermans, 1946; Cumming and Richards, 1975; Stacey and Kramers, 1975; Zartman and Doe, 1981; Thorpe, 1982). In the present study, Stacey's and Kramers' model (1975) and Thorpe's local Superior lead evolution model (1982) were opted for, because they yield lead-lead model ages for sulfides from a massive sulfide deposit (Kidd Creek mine, Timmins area) and for a komatiitic flow (Fred's flow, Munro Township), that are in good agreement with the most likely age of their host rocks (Table 8-1). Calculations with the single-stage Holmes-Houtermans model (Faure, 1986) are also given for comparison purposes.

The lead composition of the galenas from the Kidd Creek mine (Franklin et al., 1983; Tilton, 1983), and the chalcopyrites from Fred's Flow (Brévart et al., 1986) are also utilized to give an estimate of the μ value of

LOCALITY AND TYPE OF SULFIDE	LEAD ISOTOPE RATIOS			LEAD-LEAD MODEL AGES (m.y.) AND μ VALUES.						AGES (m.y.) OBTAINED BY OTHER METHODS ON THE HOST ROCKS.		
				Single-stage (Faure, 1986)		Two-stage (Stacey and Kramers, 1975)		Superior model (Thorpe, 1982)				
	$\frac{^{206}Pb}{^{204}Pb}$	$\frac{^{207}Pb}{^{204}Pb}$	Ref.	Age	μ	Age	μ	Age	μ	Age	Method	Ref.
Kidd Creek massive sulfide deposit : galenas	13.29	14.46	1	2640	7.67	2709	8.45	2715	8.62			
	13.27	14.47	1	2667	7.72	2757	8.77	2749	8.77	2717+/-4	U-Pb zircon	4
	13.28	14.47	2	2658	7.71	2743	8.69	2738	8.73			
Munro Township Fred's Flow : chalcopyrites	13.352	14.461	3	2585	7.60	2627	8.08	2652	8.44	Between 2703+/-2 and 2710+/-2	U-Pb zircon	5
	13.268	14.444	3	2646	7.65	2707	8.35	2717	8.57			
										2724+/-20	Lead-lead	3
										2662+/-120	Sm-Nd	6
										2726+/-93	Re-Os	7

Table 8-1. Comparison between lead-lead model ages obtained for sulfides from the Kidd Creek massive sulfide deposit and from the layered komatiitic Fred's Flow (Munro Township) and ages obtained by other means on their host rocks. μ values are also listed for each model.
References : 1 - Franklin et al., (1983), 2 - Tilton (1983), 3 - Brevart et al. (1986), 4 - Nunes and Pyke (1981), 5 - Nunes and Jensen (1980), 6 - Zindler (1982), 7 - Walker et al. (1988).

possible source rock reservoirs in the Archean. Galenas from the Kidd Creek massive sulfide deposit contain lead with a large crustal component, whereas chalcopyrites from Munro Township komatiites are representative of mantle type lead.

8.4. RESULTS AND DISCUSSION

8.4.1. Whole rock lead isotope ratios

Isotopic ratios were obtained for five porphyry samples, and one composite slate sample (Table 8-2). The carbonatized rocks and the ultramafic flow did not yield any reliable lead isotope results. In all probability this was due to low lead concentrations in these samples. Low concentration of lead are characteristic of unaltered komatiites (Table 2 in Brévart et al., 1986), and it is suggested that the komatiites of the Dome Mine were not greatly enriched in lead during subsequent alteration and metamorphic processes. It is doubtful that the carbonatized komatiitic wallrocks of the QFV contributed much of the lead now present in the galenas. Thus, the local carbonatized komatiites can be ruled out with great confidence as a major source rock reservoir for lead.

The lead isotope ratios of the three whole rock samples collected underground (Table 8-2, samples: COMP4, 12302, and 12515) are colinear (Fig. 8-1). In contrast, the

SAMPLE NUMBER	ROCK TYPE AND NAME OF LITHOLOGY	$\frac{206Pb}{204Pb}$	$\frac{207Pb}{204Pb}$	$\frac{208Pb}{204Pb}$
COMP4	Composite sample of slates lying north of the carbonate rock zone	18.171	15.381	38.537
608	Paymaster porphyry	19.320	15.547	38.501
609	Paymaster porphyry	18.317 18.283	15.238 15.236	37.073 37.040
709	Preston West porphyry	23.648	16.300	40.352
12302	Preston porphyry	18.822	15.508	37.861
12515	Porphyry lens in the carbonate rock zone	18.024 18.092	15.366 15.384	36.275 36.313

Table 8-2. Isotopic composition of whole rocks from the Dome Mine environment. All data are corrected for mass fractionation using SRM NBS 981.
Samples 608, 609, 709 were collected at the surface.
Samples COMP4, 12302, 12515 were collected on 12th level.

Figure 8-1. Whole rock lead isotope data of the porphyries and slates from the Dome Mine environment.

Black dots: underground samples of porphyries.
Open dot: underground slate composite sample.
Black triangles: surface samples of porphyries.

The position of the secondary isochron is constrained by its slope (calculated with the help of the 2685 m.y. U-Pb zircon age of the Preston porphyry, S.Marmont in Masliwec et al., 1986), and the distribution of the underground samples. The composition of the surface samples off the secondary isochron may be due to alteration, or may be a primary feature (see text for discussion). The intersection of the secondary isochron and the geochron at 2685 m.y. yields the initial isotope composition of the porphyries (open square). The composition of the intersection is model dependent as illustrated by the enlargement of the intersection area:

A: intersection between the secondary isochron and the geochron at 2685 m.y. in the single-stage model (1) (Faure, 1986).
B: intersection between the secondary isochron and the geochron at 2685 m.y. in the two-stage model (2) (Stacey and Kramers, 1975), and in the Superior model (3) (Thorpe, 1982).
I: growth-curve of the source reservoir of the porphyries according to the single-stage model (Faure, 1986), $\mu=7.79$.
II: growth-curve of the source reservoir of the porphyries according to the two-stage model (Stacey and Kramers, 1975) and the Superior model (Thorpe, 1982), $\mu=8.64$ and 8.71, respectively.

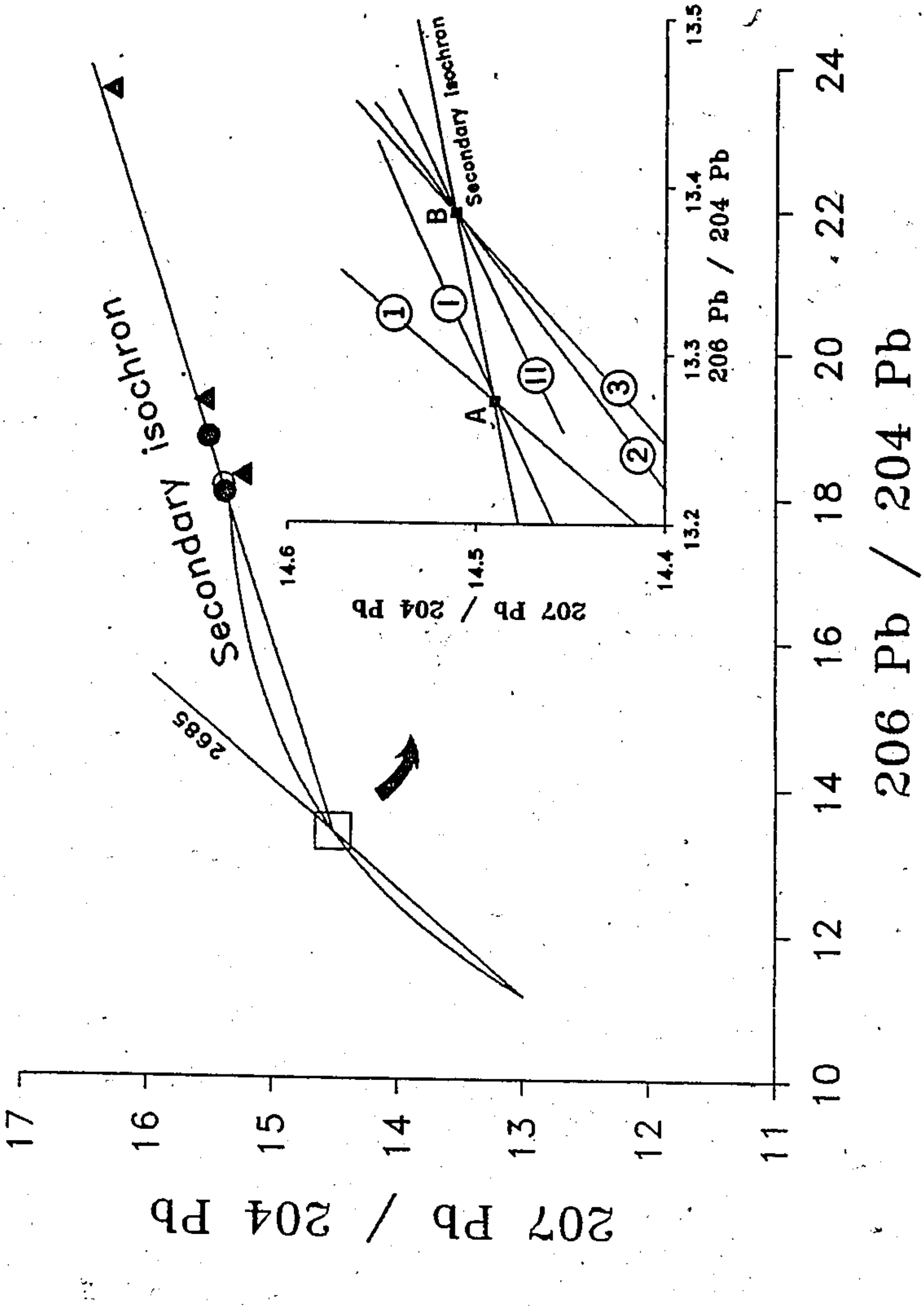
207 Pb / 204 Pb
17
16
15
14
13
12
11
206 Pb / 204 Pb
10
12
14
16
18
20
22
24
Secondary isochron
2685
207 Pb / 204 Pb
14.6
14.5
14.4
206 Pb / 204 Pb
13.2
13.3
13.4
13.5
Secondary isochron
A
B
①
②
③
I
II

surface samples (Table 8-2, samples: 608, 609, and 709) fall off this linear array (Fig. 8-1).

Assuming that all porphyries are cogenetic (McAuley, 1983) and that their evolution can be represented by a two-stage model, the crystallization age of the Preston porphyry, i.e. 2685 ± 3 m.y. (S.Marmont in Masliwec et al., 1986), can be used to calculate the slope of their theoretical secondary isochron. The calculated slope is 0.1835. The theoretical secondary isochron fits the lead isotope distribution of the colinear underground samples which yield a slope of 0.1822 ± 0.0545 (least square fitting method of York (1969)) (Fig. 8-1). The intersection of the geochron at 2685 m.y. and the secondary porphyry isochron gives the initial lead composition of the porphyries. The position of the 2685 m.y. geochron in the lead-lead diagram is a function of the parameters of the chosen model. These parameters are the $^{206}Pb/^{204}Pb$ and $^{207}Pb/^{204}Pb$ ratios at the initiation of the lead evolution, the starting time of the model, and variation in μ with time.

There is a good agreement between the initial ratios of the porphyries computed from Stacey's and Kramers' model (1975), and Thorpe's model (1982), whereas Holmes-Houtermans' single-stage model (Faure, 1986) yields lower initial ratios (Fig. 8-1, Table 8-3). The isotopic ratios corresponding to the intersection of the 2685 m.y. geochron

MODEL	INITIAL LEAD ISOTOPE RATIOS OF THE PORPHYRIES		μ VALUE OF THE SOURCE RESERVOIR
	$\frac{^{206}Pb}{^{204}Pb}$	$\frac{^{207}Pb}{^{204}Pb}$	μ
Single-stage (Faure, 1986)	13.271	14.489	7.79
Two-stage (Stacey and Kramers, 1975)	13.387	14.512	8.64
Superior model (Thorpe, 1982)	13.383	14.510	8.71

Table 8-3. Initial lead isotope ratios of the porphyries calculated with different lead evolution models. The corresponding μ values of the source reservoir are also given.

and the secondary porphyry isochron, and the lead isotope composition of the source at the initiation time of the model permits computation of the growth curve of the porphyry source reservoir and its μ value. These μ values are listed in table 8-3. μ values obtained by both the single-stage model and the two-stage model indicate a source reservoir for the porphyries which is depleted in uranium. The μ value of 8.64 calculated with Stacey and Kramers' model is lower than their terrestrial average μ value of 9.74. The value of ~~7.79~~ yielded by the single-stage model agrees well with μ values between 7.4 and 7.9 obtained by independent studies on the Archean mantle (e.g., Chauvel et al., 1987; Dupré and Arndt, 1987; Shirey and Carlson, 1987).

It is not surprising that the slate composite sample falls on the secondary isochron defined for the porphyries (Fig. 8-1, sample COMP4) since the slates in the Dome Mine environment are thought to be genetically related to the local porphyries (Kerrich and Fryer, 1979; present study, chapter 4).

Several reasons can be suggested to account for three porphyry samples lying off the secondary isochron. Alteration of the U-Pb ratio of the surface samples could be a possible cause. Alternatively, their discordant behavior might be an original feature of the porphyries. Reworking of ancient crust, or isotopic contamination from older crust might be the origin of the data scatter (e.g., Moorbath and Taylor, 1981). Depending on the proportions of different crustal and mantle material in the melt from which the porphyries crystallized, the source reservoir might have been fairly heterogeneous yielding highly variable initial ratios (e.g., Gariépy and Allègre, 1985). These different cases imply the presence of a relatively older crustal reservoir. Indirect evidence of an older sialic reservoir comes from the presence of zircons in detrital sediments from the Pontiac Group, which are at least 2940 m.y. old, while some could be as old as 3150 m.y. (Gariépy et al., 1984).

It is virtually impossible to decide whether one or the other above-mentioned scenarios is more likely. As illustrated by the galenas from the Kidd Creek mine, which contain mainly crustal lead, and the chalcopyrites from Fred's Flow (Munro Township), that have mainly mantle lead (Table 8-1, fig. 8-2), it may well be that in the Archean the various lead source reservoirs did not have significantly different µ values. This could be the result of a small age difference between production of older crustal source material from the mantle and the subsequent melting of either the crust or both the mantle and the crust to generate the porphyry magma. For instance, if the older crust was generated some 2940 m.y. ago (Gariépy et al., 1984), then the porphyries crystallized only some 250 m.y later, at about 2685 m.y. (S.Marmont in Masliwec et al., 1986).

In spite of the non-linearity of the whole rock data from the porphyries, the lead ratios can still be approximated by a two-stage model. In this case, it would be more accurate to call the secondary isochron a "scatterchron". If all whole rock data are used to compute the initial lead isotope ratio of the porphyries, then the µ values are not drastically affected and are 7.69, 8.27, and 8.51, instead of 7.79, 8.64, and 8.71 for the single-stage model, Stacey and Kramers' model, and the local Superior model, respectively. However, it adds another degree of uncertainty to the true initial lead isotope composition of the porphyries 2685 m.y. ago. The most appropriate lead evolution models to use are Stacey and Kramers' model (1975) and the local Superior model described by Thorpe (1982). The Holmes-Houtermans single-stage model (Faure, 1986) yields lead-lead ages too young for pyrites from the Kidd Creek massive sulfide deposit and chalcopyrites from Fred's Flow in comparison to the age of their host rocks (Table 8-1). The single-stage model probably gives lead compositions for the porphyries that are only a lower estimate of the true initial ratio.

8.4.2. Galena lead isotope ratios

The lead isotopic composition of the most likely reservoirs for the galenas from the QFV are known approximately. Chalcopyrites from Fred's Flow (Munro Township) provide an estimate of the lead isotope composition of the mantle beneath the Abitibi belt, and of a volcanic pile consisting predominantly of rocks derived from the mantle. Galenas from the Kidd Creek massive sulfide deposit contain lead with a large crustal component. The initial lead isotope ratio of the local porphyries has also been established. In addition, local carbonatized komatiites have been ruled out as a major lead source.

The lead isotopic compositions of galenas associated with gold are listed in table 8-4, and shown in figure 8-2, together with the composition of the major potential lead sources. Within the reproducibility of measurements, six out of eight galena samples cluster tightly near the origin of the secondary isochron of the local porphyries, as determined with the two-stage model (Stacey and Kramers, 1975) and the Superior model (Thorpe, 1982). The model ages of the galenas fall within a small range, and μ values indicate a source depleted in uranium relative to the terrestrial average value of 9.74 given by Stacey and Kramers (1975) (Table 8-4). The spread of this grouping is

SAMPLE NUMBER.	$^{206}Pb/^{204}Pb$	$^{207}Pb/^{204}Pb$	$^{208}Pb/^{204}Pb$	LEAD-LEAD MODEL AGES (m.y.) AND μ VALUES. Two-stage model		Superior model	
				Age	μ	Age	μ
8002D	13.725	14.638	33.376	2496	8.51	2502	8.64
8006G	13.611	14.606	33.304	2576	8.66	2575	8.72
	13.612	14.600	33.296	2563	8.57	2566	8.68
8010F	13.398	14.525	33.204	2692	8.74	2685	8.75
	13.389	14.513	33.158	2680	8.61	2679	8.70
10005D	13.400	14.531	33.183	2701	8.82	2691	8.79
	13.383	14.500	33.107	2663	8.46	2659	8.62
10017B	13.440	14.555	33.270	2694	8.92	2680	8.84
	13.418	14.535	33.203	2685	8.76	2677	8.77
12003	13.398	14.518	33.158	2678	8.63	2677	8.70
	13.387	14.518	33.179	2693	8.70	2688	8.74
12031	13.419	14.564	33.290	2739	9.22	2712	8.97
	13.408	14.538	33.234	2704	8.87	2691	8.82
13010	13.429	14.557	33.296	2713	9.03	2694	8.89

Table 8-4. Lead isotope compositions of galenas associated with gold in the Dome Mine Quartz-Fuchsite vein. Model ages and μ values are given as well for each sample. Errors on the ages are +18/-23 and +14/-19 m.y. for the two-stage model (Stacey and Kramers, 1975) and the Superior model (Thorpe, 1982), respectively.

All data are corrected for mass fractionation using SRM NBS 981.

Figure 8-2. Lead isotope composition of the galenas associated with gold in the Dome Mine Quartz-Fuchsite vein.

Black squares: galenas from the Quartz-Fuchsite vein.
Stars: chalcopyrites from the layered komatiitic Theo's Flow, Munro Township, Ont. (Brévart et al., 1986).
Closed diamonds: galenas from the Kidd Creek massive sulfide deposit, Ont. (Franklin et al., 1983).
Open diamonds: galenas from the Kidd Creek deposit (Tilton, 1983).
1: geochron at 2685 m.y. according to the two-stage model (Stacey and Kramers, 1975).
2: geochron at 2685 m.y. according to the Superior model (Thorpe, 1982).
$\mu 1$: growth-curve of the source reservoir of the porphyries, $\mu 1 = 8.64$ and 8.71 according to the two-stage model (Stacey and Kramers, 1975) and the Superior model (Thorpe, 1982), respectively.
Frac.: mass dependent isotope fractionation error.
204: error of measurement of the ^{204}Pb isotope.

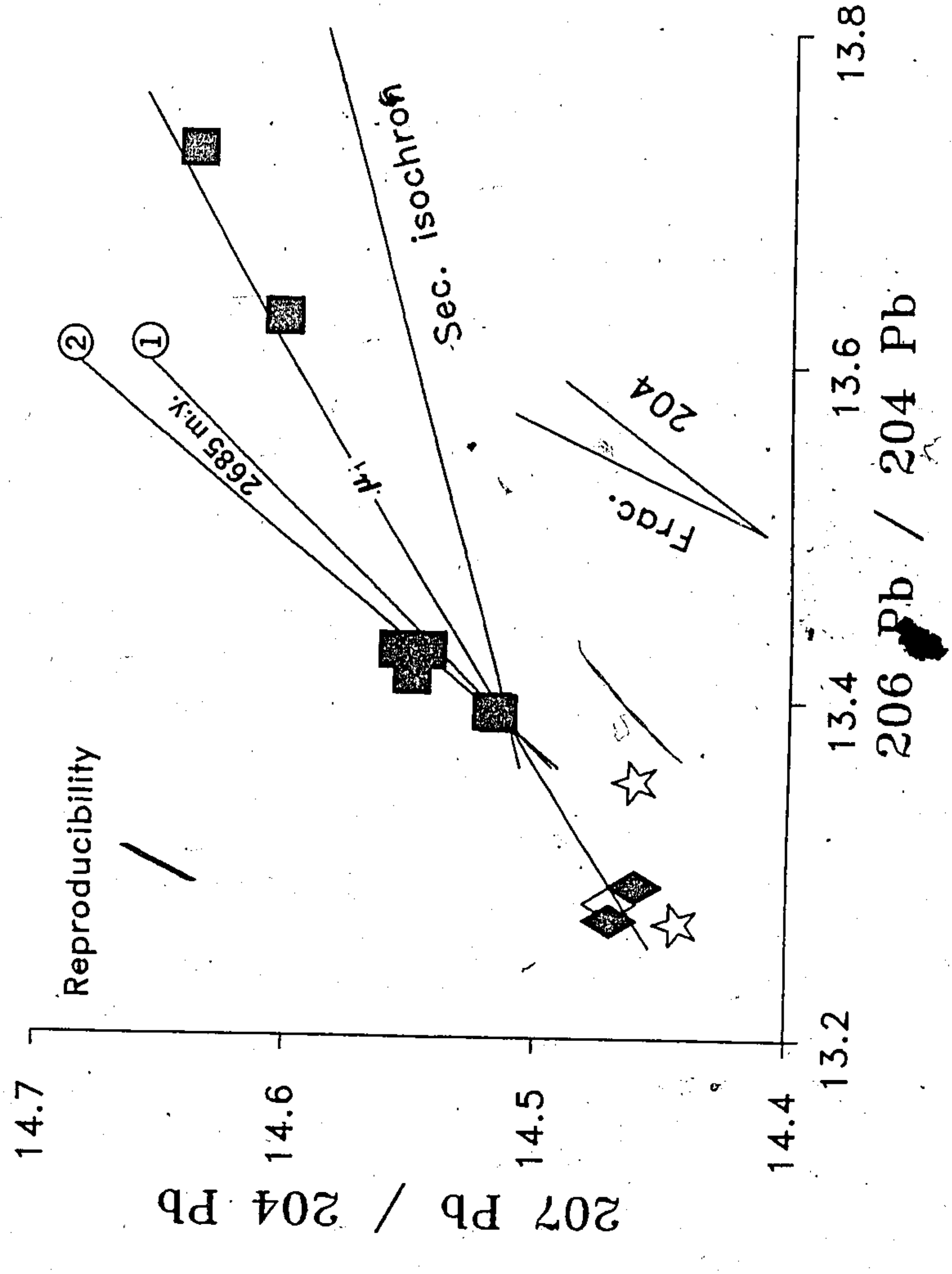
207 Pb / 204 Pb
14.7
14.6
14.5
14.4
206 Pb / 204 Pb
13.2
13.4
13.6
13.8
Reproducibility
②
①
2685 m.y.
μ
Sec. isochron
Frac.
204

attributed to error in measuring ^{204}Pb, and to mass dependent isotopic fractionation.

The similar lead isotope composition of the galenas and the initial ratio of the porphyries from the Dome Mine environment may be interpreted as evidence of a genetic affiliation between both. Alternatively, this pattern may be fortuitous with the porphyries and the galenas being of the same age but not from the same source.

It was noted above that various source reservoirs may not have developed significantly different μ values, thus rendering it difficult to recognize lead derived from different reservoirs. Possible sources include an upper mantle or a lower crustal reservoir, a fluid generated by metamorphic outgassing of a volcanic pile composed chiefly of basalts and komatiites, or the local intrusives. However, the fairly uniform lead composition of the six galenas from the main cluster suggests an isotopically well homogenized source.

Two galena samples have "anomalous" lead compositions with respect to the main galena cluster. The two "anomalous" samples and the main galena grouping are colinear. This linear array has a slope of 0.33 ± 0.07 (York, 1969).

The process which generated this line can be approximated by a mixing model, with the main galena cluster as one end member and a radiogenic crustal component as the other. It is possible to determine approximately when this contamination event occurred by making a few sound assumptions. The closest source for radiogenic lead are the adjacent volcanic and sedimentary rock sequences. The Tisdale volcanism lasted about 22 m.y. (Nunes and Pyke, 1980, 1981). The length of the volcanism which generated the rocks of the Deloro Group is not so well constrained. However, for the sake of argument let us attribute a comparable duration of approximately 22 m.y. to the Deloro volcanism. In this case, deposition of the volcanic pile lasted from about 2750 to 2703 m.y.. For convenience of calculation the beginning of radiogenic lead accumulation is time-averaged at 2725 m.y. Using this reasonable age, and the slope of the linear galena array, the time of addition of radiogenic lead from the adjacent volcanic pile to the galenas from the QFV can be calculated as $1970 \pm^{510}_{720}$ m.y. ago (Fig. 8-3). It is entirely possible that more than one contamination event took place.

Independent evidence for a possible alteration of the lead isotopic system in the time span established above is given by Masliwec et al. (1986), who recognize in model $^{40}Ar/^{39}Ar$ age spectra of the Dome Mine fuchsites a significant disturbance 2450 m.y. ago and a second milder perturbation 1800 m.y. ago.

Several thermal episodes could have caused the remobilization of lead from nearby volcanic and sedimentary

Figure 8-3. Mixing responsible for the generation of "anomalous" galenas in the Quartz-Fuchsite vein.

Black squares: galenas from the Quartz-Fuchsite vein.
Stippled curved line: growth curve of the source of the porphyries.
1 and 2: geochron at 2685 m.y. in the two-stage model (Stacey and Kramers, 1975) and the Superior model (Thorpe, 1982), respectively.
3 and 4: geochron at 1970 m.y. in the two-stage model and the Superior model, respectively.
M and N: composition of the radiogenic lead from the Timmins area volcanic and sedimentary sequences 1970 m.y. ago in the two-stage model and the Superior model, respectively.

The "anomalous" galenas are the result of mixing of lead from the Quartz-Fuchsite vein galenas (main galena cluster) and radiogenic lead from the surrounding rock sequences (points M and N) 1970 m.y. ago (time-averaged).

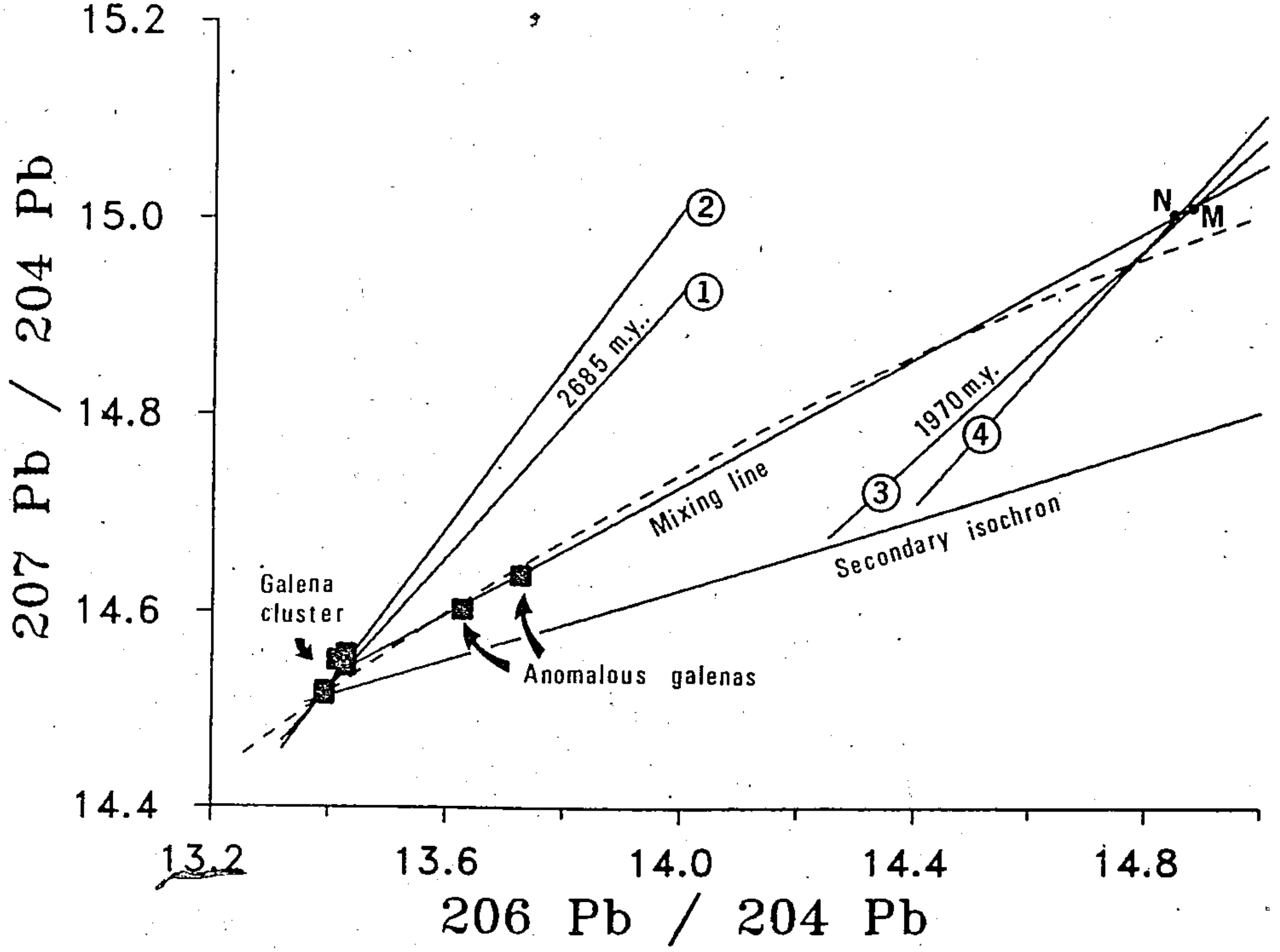

207 Pb / 204 Pb
206 Pb / 204 Pb
15.2
15.0
14.8
14.6
14.4
13.2
13.6
14.0
14.4
14.8
②
①
2685 m.y.
N
M
1970 m.y.
④
③
Mixing line
Secondary isochron
Galena cluster
Anomalous galenas

strata, and conceivably the perturbations in the argon age spectra. For instance, the Kenoran and Hudsonian orogenies occurred at 2480 m.y. and 1735 m.y., respectively (Stockwell et al., 1976). Additionally, diabase dikes intruded this part of the Abitibi belt. Measured or inferred ages range from Early to Late Precambrian (Leech in Ferguson et al., 1968; Pyke, 1982). In a comprehensive study, Franklin et al. (1983) found very similar "anomalous" lead isotope patterns in many gold deposits from the Abitibi greenstone belt. They attribute the distribution of the "deviant" leads to Kenoran metamorphic events, and possibly to the Nipissing diabase intrusion event, which took place 2170 m.y. ago (Krogh and Davis, 1974). The above-mentioned thermal events might also explain the scatter shown by the porphyry lead ratios.

8.5. CONCLUSIONS

The aim of the present lead isotope study of the galenas from the QFV and various lithologies from the Dome Mine was to determine the source of lead, and by association the source of gold. Carbonatized komatiitic rocks from the immediate vicinity of the QFV have been ruled out as a major source of lead, and by inference gold. The similarity between the lead isotopic composition of the galenas and the initial lead ratio of the porphyries may suggest a genetic association between the gold mineralization in the QFV and local porphyries. Alternatively, the porphyries and the galenas may be of roughly the same age but not from the same source. It is possible that different lead source reservoirs had similar μ values, which cannot be distinguished by current techniques. The present investigation has shown that lead isotopes alone probably cannot distinguish lead, and by inference gold, from the upper mantle and/or lower crust, from local felsic intrusives, or from a fluid generated by metamorphic outgassing. Any of these sources is possible. This finding contrasts with conclusions reached by Browning et al. (1987), that lead and gold from Archean lode deposits of Western Australia were derived from basalts and komatiites by devolatilization of a greenstone pile during regional metamorphism.

Nevertheless, the lead composition of the galenas demonstrates that the bulk of lead was derived from an isotopically well homogenized source about 2685 m.y. ago. After deposition of the galenas, one or more contamination events took place broadly between 1250 and 2480 m.y. ago. This conclusion is compatible with the disturbances found in the argon age spectra from Dome Miñe fuchsites (Masliwec et al., 1986), which remained unexplained so far.

The scatter of the whole rock data is due either to alteration of the uranium-lead ratios after their formation, or to primary lead isotopic variations in the source of the porphyries. Despite the non-linearity of the data, the lead evolution of the porphyries can be approximated by a two-stage model confirming the conclusions reached by McAuley (1983) and Kerrich and Fryer (1979), that the porphyries are cogenetic, and that the slates are genetically related to the porphyries. Low µ values for the sources of the galenas and the porphyries indicate, that both were derived from an uranium-depleted reservoir.

CHAPTER 9

SULFUR ISOTOPES

9.1. INTRODUCTION

A limited sulfur isotope study was undertaken to gain complementary information about the source of sulfur in the mineralization of the QFV, and to further characterize the nature of the ore-bearing fluid and the processes of ore deposition.

9.2. RESULTS AND DISCUSSION

Sulfur isotope results are displayed in figure 9-1. $\delta^{34}S$ values for pyrite from the host rocks and the QFV lie in the range of 0 to 10‰, that is typical of Archean lode gold deposits (Colvine et al., 1984; Kerrich, 1987).

Galenas from the QFV have lighter sulfur isotope compositions than pyrites from the QFV, with averages of $\delta^{34}S$ of 1.1 and 3.4, respectively (Fig. 9-1). The lighter sulfur isotopic composition of galena relative to pyrite is consistent with the experimental data of Kajiwara and Krouse (1971), who showed that galena coprecipitated in equilibrium with pyrite has a lighter sulfur isotopic composition. However, application of the isotopic

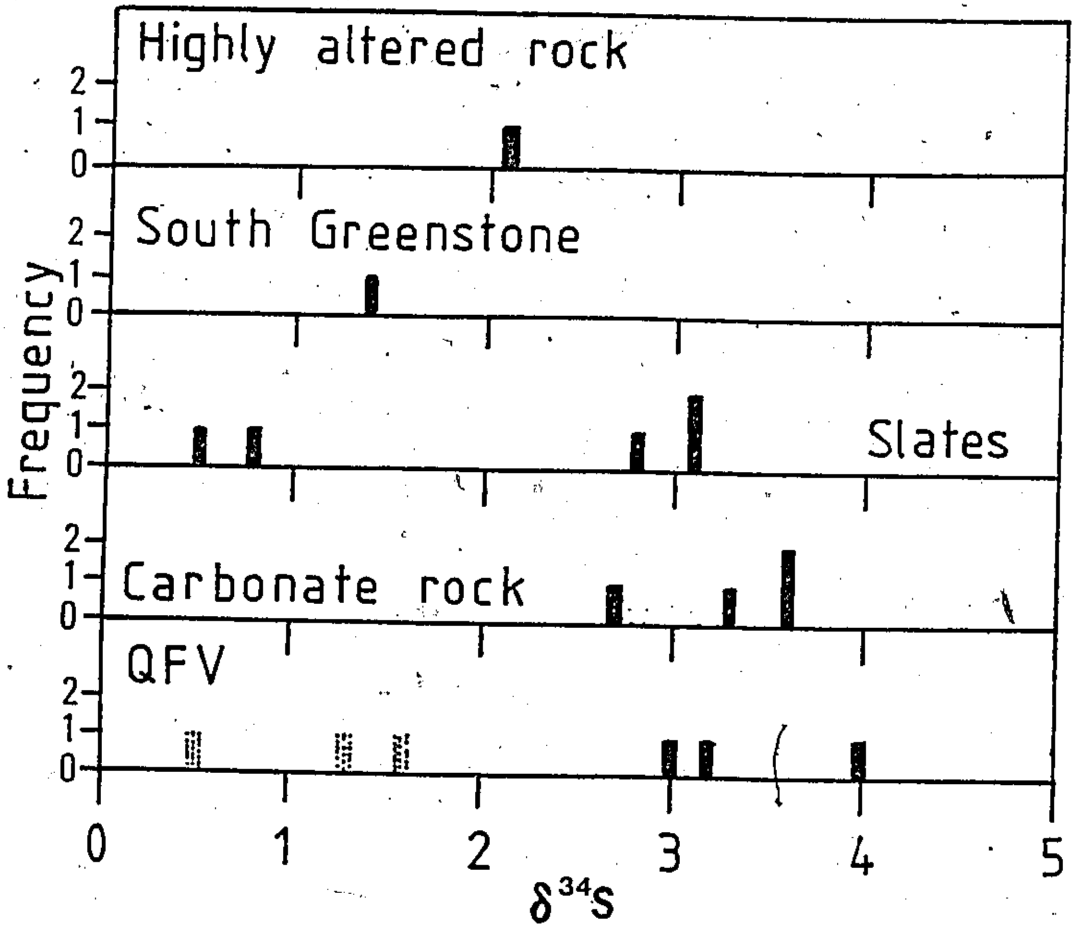

Figure 9-1. $\delta^{34}S$ of pyrites (solid lines) and galenas (dotted lines) from the Quartz-Fuchsite vein and its host rocks.

thermometer for the pyrite-galena pair given by Ohmoto and Rye (1979, table 10-2, p.518) yields a temperature of 393° ± 26°C. This temperature does not agree with the temperature range of 250° to 300°C obtained from microthermometric studies of the fluid inclusions (Chapter 7). It is believed that the temperature range gained from the fluid inclusion study is probably a better estimate of the temperature of the ore-bearing fluid, unless deformation of the QFV has severely altered the homogenization temperatures. This preference is based on the following reasons :

1) Fluid inclusion bulk homogenization temperatures from the QFV is in better agreement with the usual range of 200° to 400°C found in other Archean lode gold deposits (Section 7.2.). The temperature gained from isotope geothermometry lies at the extreme upper range.

2) $\delta^{34}S$ from galena and pyrite often give temperatures that are discrepant with respect to estimates gained by other methods (Ohmoto and Rye, 1979). Discrepancies may result if both sulfides are not in equilibrium, or were not precipitated contemporaneously, or were precipitated from fluids with different chemical states.

It is quite possible that pyrite and galena were not in equilibrium, since they are never found in grain boundary contact. Galena is found in association with gold and tellurides, often in the quartz layers of the banded parts from the QFV whereas pyrite is usually located in the phyllosilicate layers of the QFV.

Pyrites from the QFV and pyrites from the carbonate wall rock have almost identical $\delta^{34}S$ values averaging 3.4 and 3.3, respectively (Fig. 9-1). Therefore, it is possible that both pyrites were deposited from the same hydrothermal fluid with identical chemical properties before crack-seal vein growth took place. This is consistent with the conclusions reached in chapters 5 and 6, where it was argued that the banding in the QFV represents slivers of the wall rock that were incorporated in the vein during crack-seal. Pyrites in the QFV might be part of such wall rock slivers. In contrast, galena was probably deposited with gold and tellurides during crack-seal vein growth, whereby pH and fO_2 of the hydrothermal fluid were increased (Chapter 7). However, this later point might be subject to discussion, since there is no textural evidence of such a paragenetic sequence.

Although sulfides are not predominant minerals in the QFV, an estimate of the $\delta^{34}S$ of the ore-bearing fluid can be obtained from galena and pyrite. At temperatures below 400°C, H_2S and SO_4^{2-} are the two important aqueous species which control the distribution of sulfur isotopes. The high CH_4 content in the fluid inclusions probably reflects the reducing nature of the ore-bearing fluid. Therefore, it can be assumed that SO_4^{2-} was present in negligible concentrations, and that $\delta^{34}S$ of H_2S is similar to the bulk $\delta^{34}S$ of the hydrothermal fluid. Since $\delta^{34}S$ of galena and of pyrite are lower by 2°/∞ and higher by 1°/∞, respectively, than $\delta^{34}S$ of the hydrothermal fluid at temperatures around 300°C (Fig. 10-3, p. 515 in Ohmoto and Rye, 1979), it is probable that the ore-bearing fluid had a $\delta^{34}S$ value in the range of 0 to 5°/∞. Such an isotope signature is consistent with sulfur derived from a magmatic source, or by leaching from volcanic rocks. Moreover, the initial isotopic composition of the ore-bearing fluid might have been altered by interaction with the adjacent slates, which could have contributed some light sulfur. Thus, it is difficult to attribute a unique source to the sulfur now present in the QFV, particularly in the galenas associated with gold.

9.3. CONCLUSIONS

The isotopic signature of pyrites from the QFV and its host rocks is similar to that found in other Archean lode gold deposits.

Galenas and pyrites from the QFV have $\delta^{34}S$ compositions which are higher than homogenization temperatures of fluid inclusions. This may be due to disequilibrium, or non-contemporaneous deposition. The second possibility is likely if pyrite was deposited during carbonatization of the host komatiites, and galena was deposited together with gold and tellurides as the ore-bearing fluid experienced a shift in pH and fO_2 during crack-seal vein growth. During the same event, pyrite in slivers from the wall rock was incorporated into the QFV.

The sulfur isotope composition of both pyrites and galenas may reflect the composition of the ore-bearing fluid. $\delta^{34}S$ of the fluid between 0 and 5‰ is compatible with either a magmatic source or sulfur derived by leaching of a volcanic rock pile in the course of metamorphism. Some light sulfur might have been added from the adjacent slates, although this is difficult to evaluate.

CHAPTER 10

GENESIS OF THE QUARTZ-FUCHSITE VEIN

In order to understand the genesis of the gold-bearing QFV of the Dome Mine, the main conclusions of the previous chapters need to be considered:

1) Alteration of the host rocks of the QFV is centered around the porphyry lens present in the zone of carbonatized and altered rocks, rather than around the vein.

2) Intensity of country rock fracturing, quartz veining, fuchsite and pyrite development increases towards the porphyry lens.

3) Most of the major and trace elements introduced into the komatiites during alteration were probably derived from the immediate neighboring lithologies which are mainly porphyries, and to a lesser extent, slates.

4) It seems unlikely that the carbonatized komatiites supplied any gold to the QFV, since they are enriched in gold as well.

5) Both the porphyries of the Dome Mine and the QFV were

emplaced before the regional compressional event labelled as D_1 (Roberts et al., 1978; Roberts, 1981).

6) Quartz precipitated in cracks formed during hydraulic fracturing in a regime of low stress difference and high pore fluid pressure régime that developed at the carbonate rock - slate contact.

7) Two types of quartz vein materials were deposited : massive barren quartz precipitated during prolonged episodes of fracture growth, opening and crystallization; and, banded ore-bearing quartz deposited during repetitive brief periods of crack-seal vein growth.

8) The characteristic banding of the QFV formed as a consequence of numerous repeated increments of microcrack opening. During this accretionary vein growth process, wall rock slivers were isolated and mechanically incorporated in the vein concomitant with quartz deposition from the hydrothermal fluid responsible for hydraulic fracturing.

9) The consistent association of gold with banded quartz suggests a genetic link; specifically, that gold and quartz were deposited from a hydrothermal fluid, which may have precipitated them in response to pressure decrease caused by a crack-seal mechanism operating in conjunction with hydraulic fracturing.

10) Fuchsite and melonite, two minerals associated with gold in the banded parts of the QFV, formed probably during crack-seal vein growth by reaction of the ore-bearing

hydrothermal fluid with wall rock slivers as they were incorporated in the QFV.

11) Deposition of gold probably occurred as a consequence of unmixing of a low-salinity, CH_4-rich H_2O-CO_2 fluid, whereby partitioning of CO_2 and CH_4 to the vapor phase resulted in a shift of fO_2 and pH towards higher values of the residual fluid.

12) Fluid destabilization was generated by the crack-seal mechanism which produced the small pressure drops necessary for unmixing of the parent fluid into a liquid phase and a vapor phase.

13) The parent fluid was probably a low-salinity H_2O-CO_2 fluid that acquired its high CH_4 content by interaction with slates at the contact with the carbonate rocks.

14) Massive and non-banded veins were a less favorable environment for fluid unmixing, since fluid pressure had to be high to hold the walls of the fracture open.

It was also concluded that the QFV did not form as result of quartz deposition along a shear zone concomitant with the development of foliation in the wall rock. The shear zone model commonly applied to the emplacement of Archean lode gold deposits does not adequately explain the genesis of the Dome Mine QFV.

Some of these conclusions suggest a genetic link between the QFV and the porphyry lens found in the zone of carbonatized rocks. Lateral fluid migration in the carbonate rocks towards the contact with the slates, that is necessary to generate a zone of high pore fluid pressure, is fully compatible with the textural, mineralogical and geochemical zonation centered around the porphyry lens. The fluid that progressively altered the carbonate rocks adjacent to the porphyry lens moved towards the contact with the slates where it was hindered from further migration. As a consequence, a high pore fluid regime developed that resulted in hydraulic fracturing of the carbonate rock. Thus, in the case of the QFV, a genetic model linking emplacement of porphyries and gold ore development is preferred. The carbonate rock - slate contact and the porphyry lens are probably the two fundamental ingredients that created the favorable environment for the development of the gold-bearing QFV.

The emplacement of intrusions is known to generate thermal anomalies, and to impose a stress field in the country rocks (Burnham and Ohmoto, 1980; Knapp and Norton, 1981). Transport of heat from the intrusions into the host rocks leads to an increase in pore fluid pressure (Knapp and Knight, 1977). Magma bodies in the crust cause a radial and concentric stress field in which the maximum principal stress is in the radial position, and the minimum principal stress is in the concentric position (Knapp and Norton, 1981). As a consequence, intense fracturing is developed around and inside the intrusions. The orientation of the fractures is a function of the stress field prevailing at the time of their formation.

In the case of the QFV environment, intrusion of the porphyry lens, or dike, explains the intense rock fracturing centered around that lens. The thermal gradient generated by the porphyry lens drove the hydrothermal fluid circulation from the center of the carbonate rock zone towards its margins, and it also increased pore fluid pressure in the country rocks. Pore fluid pressure was increased furthermore at the slate - carbonate rock interface, since fluid migration was hindered. Hydraulic extension failure occurred when fluid pressure was greater than the combined least principal stress and tensile strength of the wall rock ($P_F > \sigma_3+T$). The orientation of the quartz veins that form in such an environment are a function of both preexisting fractures and the prevalent stress field. In the case of the QFV, σ_1 was probably subvertical, and σ_3 was subhorizontal. This is reflected in the subvertical orientation of the QFV, and many quartz veins in the wall rock in the vicinity of the gold-bearing vein. The strataboubd character of the QFV is a consequence of the control that the slates played on the localization of hydraulic fracturing.

The low K/Rb ratio of fuchsite from the banding in the QFV reflects the residual composition of the ore-bearing fluid probably emanating from the porphyry lens.

This fluid initially interacted with the carbonate rocks to produce the fuchsite alteration around the porphyry lens, whereby the Rb content of the hydrothermal fluid was increased relative to K. This relative increase of Rb with respect to K was accentuated by interaction with the slates. Hence, the hydrothermal fluid that deposited fuchsite along the wall rock slivers as crack-seal proceeded had a relatively low K/Rb ratio. The probable dependence of fuchsite development to K derived from the porphyries is strongly inferred from the distribution of fuchsite within the QFV. In the western part of the vein, which is closer to the main porphyry bodies of the Dome Mine, the banding is rich in fuchsite, whereas in the eastern portion of the vein further from the main porphyry bodies the banding is predominantly composed of chlorite.

Based on field and thin section evidence, the following sequence of alteration and depositional events can be suggested:

1) Initially, carbonatization of the original komatiites occurred. During this event some silica was probably removed from the original protolith. According to oxygen isotope geothermometry, this carbonatization event is estimated to have taken place at 300° to 400°C in the Dome Mine (Kerrich and Fryer, 1979).

2) Fuchsite developed subsequently around the porphyry lens.

3) Interaction of the hydrothermal fluid with the slates resulted in K and Rb depletion, and in formation of CH_4 in the ore-forming fluid.

4) Hydraulic fracturing of the carbonate rocks at the slate contact resulted in quartz veining and fuchsite development along slivers of wall rock, and in deposition of gold, tellurides and galena. Silica removed in a first instance from the original komatiites during carbonatization was redeposited in the fractures formed at this stage. Fluid inclusion microthermometry suggests that this event occurred at 250° to 300°C.

The hydrothermal activity which was active around the porphyry lens probably resulted in the redistribution of many elements in the environment of the QFV. Extraneous elements in the carbonate rocks such as Zr, Y, K, Rb, Ca, LEE, and Eu were probably derived mainly from the porphyries, and to a lesser extent from the adjacent slates.

The lead and sulfur isotope data are in full agreement with such a genetic evolution of the QFV. In particular, lead isotopes suggest a genetic link between the porphyries of the Dome Mine environment and the gold-bearing QFV.

By analogy to other Archean quartz vein gold deposits, the parent fluid which transported gold was a low salinity H_2O-CO_2 fluid. It is assumed that gold was transported as a bisulphide complex. However, due to the relatively high abundance of tellurides consistently associated with gold in the QFV it is possible that, as suggested by Seward (1973), telluro-gold species may have been important in this hydrothermal fluid.

The evidence of a genetic relationship between the QFV and the emplacement of a porphyry lens into the zone of the carbonatized komatiites, does not imply that the ultimate source of the ore components in the QFV is this particular porphyry lens. It is only suggested that the porphyry lens caused ground preparation, in particular fracture the country rock that facilitated fluid motion, and the generation of a thermal anomaly that drove the hydrothermal system and that increased fluid pressure in the wall rock. The ultimate source of the ore-bearing fluid and the gold must be found at depth, rather than in the local environment. The data and observations obtained in the present study do not allow a discussion of this aspect of the genetic problem on an objective basis. However, as stated in the Introduction one can attempt to relate the geological environment of the QFV to various conceptual Archean gold deposit models.

It appears unlikely that the entire depositional environment of the QFV can be related to metamorphic dehydration and focusing of a fluid flow along a regional shear zone as suggested by Groves and Phillips (1987) for deposits from the Western Australian shield, or by Kerrich and Fryer (1979) for the Dome Mine. Although the QFV has undergone deformation after its emplacement, the gold in this vein is an integral part of the original depositional process in the setting formed by the porphyry lens and the slates. It cannot be related to a complex and multistage remobilization ore genesis mechanism as advocated by Hutchinson and Burlington (1984). The gold present in the large deposits from the Timmins area can probably not be realistically derived from the immediate felsic porphyries, unless these were highly enriched in gold initially. However, the felsic stocks present in this mining camp might be the upper visible apophyses of larger magmatic bodies present at depth. Recently, it has been suggested that gold in Archean lode deposits might be derived from felsic magmas with fairly high fO_2 that were rich in CO_2 (Cameron and Hattori, 1987; Hattori, 1987). This is suggested in part by analogy to younger examples of gold-rich porphyry copper deposits (Sillitoe, 1979). CO_2-rich aqueous fluids emanating from such intrusions at depth could have transported gold to the Dome Mine environment, where the local porphyry lens and the slates created a favorable environment for gold deposition. An alternative source of ore fluid might be the lower crust, where granulite formation accompanied by streaming of a CO_2-rich fluid incorporated large ion lithophile elements and gold, that were transported to higher crustal levels (Fyon et al., 1983; Colvine et al., 1984; Fyon, 1986; Cameron, 1988). The lead isotope signature of galenas consistently associated with gold in the QFV suggests a genetic link between the gold mineralization in the vein and local porphyries of the Dome Mine. However, further interpretation of this data, to decide whether a close underlying magma body or the lower crust is a more favorable source would be highly speculative.

CHAPTER 11

CONCLUSIONS

The QFV vein of the Dome Mine is an Archean gold vein deposit that is genetically related to local felsic porphyry intrusives, in particular to a small porphyry lens present in a zone of carbonatized and altered rocks. Intrusion of porphyry dikes into komatiites bounded on one side by slates created a favorable environment for ore formation. This intrusion generated a thermal gradient that drove a hydrothermal system, fractured the country rock, and it increased the pore fluid pressure in the latter. The slates acted as a trap that inhibited further fluid migration and ultimately caused hydraulic fracturing. Numerous crack-seal events are responsible for the development of ore-bearing banded quartz, whereby wall rock slivers were mechanically incorporated in the QFV. Drops in fluid pressure inside the cracks favored unmixing of the mineralizing fluid. This resulted in an increase of fO_2 and pH of the remaining fluid. As a consequence, gold, tellurides, and galena were precipitated, and fuchsite formed by reaction of the destabilized hydrothermal fluid with wall rock selvages. Gold ore formation probably took place at the culmination of a sequence of intrusion, alteration, and fracturing events, that are :

1) Intrusion of the porphyry lens (dike).

2) Carbonatization of this lens and of the komatiites at temperatures between 300° and 400°C (Kerrich and Fryer, 1979).

3) Fuchsite (sericitization) and pyrite development in the country rock immediately adjacent to the porphyry lens.

4) Hydraulic fracturing at the slate - carbonate rock contact, with quartz vein formation and deposition of gold, galena, tellurides, and fuchsite at temperatures between 250° and 300°C.

It is suggested that the source of the mineralizing low salinity H_2O-CO_2 fluid and of the gold is a deeper seated magma (Cameron and Hattori, 1987; Hattori, 1987), or the lower crust (Fyon, 1986; Cameron, 1988).

Both local intrusives of the Dome Mine and the QFV were emplaced before the regional compressional deformation event labelled as D_1 (Roberts et al., 1978; Roberts, 1981). The geological setting and evolution of the QFV is inconsistent with a metamorphic remobilization model as advocated by Kerrich and Fryer (1979) or Groves and Phillips (1987), whereby gold would be deposited in shear zones. The QFV acquired its present fault-like configuration only after the D_1 deformation event. The geological setting of the QFV is rather similar to the gold-rich porphyry model suggested by Mason and Melnik (1986a,b) for the Pearl Lake porphyry in the nearby McIntyre-Hollinger mine. Thus, the other gold ore bodies in the Dome Mine should be reinvestigated to understand their possible genetic relationship to the felsic porphyry bodies of the mine, in particular the major Preston and Paymaster porphyries.

The results and conclusions of the present research also have the following practical applications:

1) Felsic intrusions should be selected as prime targets for gold exploration. As mentioned in the introduction, porphyries have been appreciated by prospectors as a key to locating new gold deposits.

2) Once such an intrusion has been delineated, relatively impermeable rock lithologies that would bar hydrothermal fluid migration outwards from the intrusions into the country rock should be defined. Such traps would create favorable environments for hydraulic fracturing and gold deposition.

3) Zones of intense deformation might be good ore guides, since strain would be concentrated along heterogeneities such as ore bodies and, to a lesser extent intrusions, in a regional rock sequence that underwent compressional deformation. However, a shear zone is probably not a sufficient criteria by itself to locate an ore body, since

shear zones might form in areas devoid of any ore bodies or intrusions.

In the course of the present study it was noted that high gold ore grades are often a function of the presence of banded quartz. It is possible that the model of ore deposition developed in the present case study is applicable to other Archean and younger deposits. The combination of high pore fluid pressure, and episodic crack-seal events may be optimum conditions to form high ore grade bodies such as the QFV. The crack-seal mechanism is probably the trigger necessary for unmixing of a hydrothermal ore fluid that is sensitive to slight pressure variations, whereby its chemical state might be altered and ore-complexes destabilized.

This research has also shown that a lead isotope study alone might be meaningless and not sufficient to define a unique ore source in the case of Archean lode gold deposits. The reason is that various lead source reservoirs in the Archean may not have developed significantly different U-Pb ratios. Lead isotope investigations should be integrated in the complete geological framework that can be defined for an ore body. It is only in such a context that lead isotopes may permit a genetic link between a given mineralization and given lithologies to be ascertained.

From a methodological point of view, this study has pointed out that the presence of gold mineralization within a shear or fault zone does not necessarily imply that the latter controlled the mineralization. It must be recognized whether vein material precipitation and deformation are processes that took place independently in time, or if both are essentialy coincident in time. Gold is often thought to be one of the latest phases that precipitate in the paragenetic sequence of a mineralized vein. This conclusion would be reached for the QFV, if the sequence of precipitation and deformation was not fully understood. The occurrence of gold, and other ductile minerals such as galena, along fractures and quartz grain boundaries is a natural consequence of deformation that may follow deposition of the vein material. Thus, the common description of "late" gold in Archean ore-bearing veins should be used cautiously, particularly where the timing of ore deposition and deformation is not known with certainty.

REFERENCES

Agiorgitis G., and Wolf R. (1978). Aspects of osmium, ruthenium and iridium contents in some Greek chromites. Chem. Geol., 23, 267-272.

Andrews A.J., Hugon H., Durocher M., Corfu F., and Lavigne M.J. (1986). The anatomy of a gold-bearing Greenstone belt: Red Lake, Northwestern Ontario, Canada. In Macdonald A.J., ed., Proceedings of Gold'86, an international Symposium on the Geology of Gold: Toronto, 1986, pp. 3-22.

Anoshin G.N., and Perezhogin G.A. (1976). Determination of gold, silver and tantalum in the new USGS standards by neutron activation analysis. U.S. Geol. Surv. Prof. Paper, 840, 185-187.

Arden J.W., and Gale N.H. (1974). New electrochemical technique for the separation of lead at trace levels from natural silicates. Anal. Chem., 46, 2-9.

Armbrust G.A., and Gannicott R.A. (1980). K/Rb ratios as a source indicator for hydrothermal fluids at the Seneca volcanogenic massive sulfide deposit, British Columbia. Econ. Geol., 75, 466-470.

Arndt N.T. (1986). Differentiation of komatiite flows. J. Petrol., 27, 279-301.

Arndt N.T., and Nisbet E.G. (1982). What is a komatiite ? In Arndt, N.T., and Nisbet, E.G., eds., Komatiites, Allen and Unwin, London, pp. 19-27.

Arndt N.T., Naldrett A.J., and Pyke D.R. (1977). Komatiitic and iron-rich tholeiitic lavas of Munro Township, Northeastern Ontario. J. Petrol., 18, 319-369.

Augé T. (1985). Platinum-group-mineral inclusions in ophiolitic chromitite from the Vourinos Complex, Greece. Can. Mineral., 23, 163-171.

Augé T. (1986). Platinum-group-mineral inclusions in chromitites from the Oman ophiolite. Bull. Minéral., 109, 301-304.

Babcock R.S. (1973). Computational models of metasomatic processes. Lithos, 6, 279-290.

Barnes S.-J., Naldrett A.J., and Gorton M.P. (1985). The origin of the fractionation of platinum-group elements in terrestrial magmas. Chem. Geol., 53, 303-323.

Bean R.E., and Titley S.R. (1981). Porphyry copper deposits. Part II. Hydrothermal alteration and mineralization. Econ. Geol., 75th anniversary vol., 235-269.

Bernasconi A. (1985). Archaean gold mineralization in Central Eastern Brazil: a review. Mineral. Deposita, 20, 277-283.

Beswick A.E. (1982). Some geochemical aspects of alteration, and genetic relations in komatiitic suites. In Arndt, N.T., and Nisbet E.G., eds., Komatiites, London, Allen and Unwin, pp. 283-308.

Beswick A.E. (1983). Primary fractionation and secondary alteration within an Archean ultramafic lava flow. Contrib. Mineral. Petrol., 82, 221-231.

Beswick A.E., and Soucie G. (1978). A correction procedure for metasomatism in an Archean Greenstone belt. Precamb. Res., 6, 235-248.

Blais S., Auvray B., Jahn B.-M., and Taipale K. (1987). Processus de fractionnement dans les coulées komatiitiques archéennes: cas des laves à spinifex de la ceinture de roches vertes de Tipasjärvi (Finlande orientale). Can. J. Earth Sci., 24, 953-966.

Bowers T.S., and Helgeson H.C. (1983a). Calculation of the thermodynamic and geochemical consequences of nonideal mixing in the system H_2O-CO_2-NaCl on phase relations in geologic systems: Equation of state for H_2O-CO_2-NaCl fluids at high pressures and temperatures. Geochim. Cosmochim. Acta, 47, 1247-1275.

Bowers T.S., and Helgeson H.C. (1983b). Calculation of the thermodynamic and geochemical consequences of nonideal mixing in the system H_2O-CO_2-NaCl on phase relations in geologic systems: metamorphic equilibria at high pressures and temperatures. Am. Mineral., 68, 1059-1075.

Boyle R.W. (1979). The geochemistry of gold and its deposits (together with a chapter on geochemical prospecting for the element). Geol. Surv. Canada, Bull. 280, 584 pp.

Brevart O., Dupré B., and Allègre C.J. (1986). Lead-lead age of komatiitic lavas and limitations on the structure and evolution of the Precambrian mantle. Earth Planet. Sci. Lett., 77, 293-302.

Brisbin D.I., and Mason R. (1987). Hydrothermal alteration and fabric development in Tisdale Township - Timmins. In Geoscience Research Seminar and Open House, Abstracts, Dec. 15-16 1987, Toronto, Ontario Geol. Surv., p. 4.

Browning P., Groves D.I., Blockley J.G., and Rosman K.J.R. (1987). Lead isotope constraints on the age and the source of gold mineralization in the Archean Yilgarn Block, Western Australia. Econ. Geol., 82, 971-986.

Brügman G.E., Arndt N.T., Hofmann A.W., and Tobschall H.J. (1987). Noble metal abundances in komatiite suites from Alexo, Ontario, and Gorgona Island, Colombia. Geochim. Cosmochim. Acta, 51, 2159-2169.

Burnham C.W., and Ohmoto H. (1980). Late-stage processes of felsic magmatism. Mining Geology, Spec. Issue No.8, 1-11.

Burrows D.R., and Spooner E.T.C. (1986). The McIntyre Cu-Au deposit, Timmins, Ontario, Canada. In Macdonald, A.J., ed., Proceedings of Gold'86, an international Symposium on the Geology of Gold; Toronto, 1986,pp. 23-39.

Burrows D.R., Wood P.C., and Spooner E.T.C. (1986). Carbon isotope evidence for a magmatic origin for Archaean gold-quartz vein ore deposits. Nature, 321, 851-854.

Burruss R.C. (1981). Analysis of phase equilibria in C-O-H-S fluid inclusions. In Hollister L.S., and Crawford M.L., eds., Short course in fluid inclusions: applications to petrology. Calgary, May 1981. Mineral. Assoc. Canada, pp. 39-74.

Butler J.C. (1986). The role of spurious correlation in the development of a komatiite alteration model. J. Geophys. Res., 91, B13, E275-E280.

Cameron E.M. (1988). Archean gold: relation to granulite formation and redox zoning in the crust. Geology, 16, 109-112.

Cameron E.M., and Hattori K. (1987). Archean gold mineralization and oxidized hydrothermal fluids. Econ. Geol., 82, 1177-1191.

Canil D. (1987). The geochemistry of komatiites and basalts from the Deadman Hill area, Munro Township, Ontario, Canada. Can. J. Earth Sci., 24, 998-1008.

Chace F.M. (1949). Origin of the Bendigo saddle reefs with comments on the formation of ribbon quartz. Econ. Geol., 44, 561-597.

Chauvel C., Dupré B., Arndt N.T., and Hofmann A.W. (1987). Composition of the Archean mantle: evidence from Pb and Nd isotopes. Geol. Assoc. Canada - Mineral. Assoc. Canada, Program with Abstracts, 12, p. 31.

Cherry M.E. (1983). The association of gold and felsic intrusions - Examples from the Abitibi belt. In Colvine A.C., ed., The geology of gold in Ontario. Ontario Geol. Surv., Miscellaneous Paper 110, pp. 48-55.

Clark M.E., Archibald N.J., and Hodgson C.J. (1986). The structural and metamorphic setting of the Victory Gold Mine, Kambalda, Western Australia. In Macdonald A.J., ed., Proceedings of Gold'86, an international Symposium on the Geology of Gold: Toronto, 1986, pp. 243-254.

Collins P.L.F. (1979). Gas hydrates in CO_2-bearing fluid inclusions and the use of freezing data for estimation of salinity. Econ. Geol., 74, 1435-1444.

Colvine A.C. (1983). The geology of gold in Ontario. Ontario Geol. Surv., Miscellaneous Paper 110, 278 pp.

Colvine A.C., Andrews A.J., Cherry M.E., Durocher M.E., Fyon A.J., Lavigne Jr. M.J., Macdonald A.J., Soussan Marmont, Poulsen K.H., Springer J.S., and Troop D.G. (1984). An integrated model for the origin of Archean lode gold deposits. Ontario Geol. Surv., Open file report 5524, 98pp.

Condie K.C., and Martell C. (1983). Early Proterozoic metasediments from north-central Colorado: metamorphism, provenance, and tectonic setting. Geol. Soc. Amer. Bull., 94, 1215-1224.

Conolly H.J.C. (1936). A contour method of revealing some ore structures. Econ. Geol., 31, 259-271.

Cornet F.H. (1982). Etude de la propagation des fractures hydrauliques dans les roches imperméables. Ann. Geophys., 38, 211-224.

Coveney Jr. R.M. (1981). Gold quartz veins and auriferous granite at the Oriental Mine, Alleghany district, California. Econ. Geol., 76, 2176-2199.

Cox S.F., and Etheridge M.A. (1983). Crack-seal fibre growth mechanism and their significance in the development of oriented layer silicate microstructure. Tectonophysics, 92, 147-170.

Cox S.F., Etheridge M.A., and Wall V.J. (1987). The role of fluids in syntectonic mass transport and the localization of metamorphic vein-type ore deposits. Ore Geol. Reviews, 2, 65-86.

Crawford M.L. (1981a). Phase equilibria in aqueous fluid inclusions. In Hollister L.S., and Crawford M.L., eds., Short course in fluid inclusions: applications to petrology. Calgary, May 1981. Mineral. Assoc. Canada, pp.75-100.

Crawford M.L. (1981b). Fluid inclusions in metamorphic rocks - Low and medium grade. In Hollister L.S., and Crawford M.L., eds., Short course in fluid inclusions: applications to petrology. Calgary, May 1981. Mineral. Assoc. Canada, pp. 157-181.

Crocket J.H. (1979). Platinum-group elements in mafic and ultramafic rocks: a survey. Can. Mineral., 17, 391-402.

Crocket J.H. (1981). Geochemistry of the platinum-group elements. In Cabri L.J., ed., Platinum Group Elements: Mineralogy, Geology, Recovery. CIM Spec. Vol. 23, pp. 47-64.

Crocket J.H., and MacRae W.E. (1986). Platinum-group element distribution in komatiitic and tholeiitic volcanic rocks from Munro Township, Ontario. Econ. Geol., 81, 1242-1251.

Crocket J.H., Keays R.R., and Hsieh S. (1968). Determination of some precious metals by neutron activation analysis. J. Radioanal. Chem., 1, 487-507.

Davies J.F. (1977). Structural interpretation of the Timmins mining area, Ontario. Can. J. Earth Sci., 14, 1046-1053.

Davies J.F. and Luhta L.E. (1978). An Archean "porphyry-type" disseminated copper deposit, Timmins, Ontario. Econ. Geol., 73, 383-396.

Deer W.A., Howie R.A., and Zussman J. (1962). Rock forming minerals. Volume three: sheet silicates. Longmans, Green and Co. Ltd, London, 270 pp.

Doe B.R., Hedge C.E., and White D.E. (1966). Preliminary investigation of the source of lead and strontium in deep geothermal brines underlying the Salton Sea geothermal area. Econ. Geol., 61, 462-483.

Drummond S.E., and Ohmoto H. (1985). Chemical evolution and mineral deposition in boiling hydrothermal systems. Econ. Geol., 80, 126-147.

Dubessy J. (1984). Simulation des équilibres chimiques dans le système C-O-H. Conséquences méthodologiques pour les inclusions fluides. Bull. Minéral., 107, 155-168.

Dunbar W.R. (1948). Structural relations of the Porcupine ore deposits. In Structural geology of Canadian ore deposits. CIM Spec. Vol., pp. 442-456.

Dupré B., and Arndt N.T. (1987). Pb isotopes in Archean komatiites, basalts and sulfides. Terra Cognita, 7, 272.

Eckstrand O.R. (1975). The Dumont serpentinite : a model for control of nickeliferous opaque mineral assemblages by alteration reactions in ultramafic rocks. Econ. Geol., 70, 183-201.

Etheridge M.A., Wall V.J., and Cox S.F. (1984). High fluid pressures during regional metamorphism and deformation: implications for mass transport and deformation mechanisms. J. Geophys. Res., 86, B6, 4344-4358.

Faure, G. (1986). Principles of isotope geology. Second edition, John Wiley and Sons, 589 pp.

Ferguson S.A., Buffam B.S.W., Carter .F., Griffis A.T., Holmes T.C., Hurst M.E., Jones W.A., Lane H.C., and Longley C.S. (1968). Geology and ore deposits of Tisdale Township, District of Cochrane. Ontario Dept. Mines, Geological report 58, 177 pp. Accompanied by map 2075, scale 1:12'000 or 1 inch to 1000 feet.

Fournier R.O. (1985). The behavior of silica in hydrothermal solutions. In Berger B.R., and Bethke P.M., eds., Geology and geochemistry of epithermal systems. Reviews in economic geology, vol. 2, pp. 45-61.

Franklin, J.M., Roscoe S.M., Loveridge W.D., and Sangster D.F. (1983). Lead isotope studies in Superior and Southern Provinces. Geol. Surv. Canada, Bull. 351, 60 pp.

Fryer B.J., Kerrich R., Hutchinson R.W., Peirce M.G., and Rogers D.S. (1979). Archean precious-metal hydrothermal systems, Dome Mine, Abitibi Greenstone belt. 1. Patterns of alteration and metal distribution. Can. J. Earth Sci., 16, 421-439.

Fyon J.A. (1986). Field and stable isotopic characteristics of carbonate alteration zones, Timmins area. Unpublished Ph.D. thesis, McMaster University, Hamilton, Ontario, Canada, 399 pp. Accompanied by 5 microfiches.

Fyon J.A., and Crocket J.H. (1981). Volcanic environment of carbonate alteration and stratiform gold mineralization, Timmins area. In Pye E.G., and Roberts R.G., eds., Genesis of Archean, volcanic-hosted gold deposits. Ontario Geol. Surv., Miscellaneous Paper 97, pp. 47-58.

Fyon J.A., and Crocket J.H. (1982). Gold exploration in the Timmins district using field and lithogeochemical characteristics of carbonate alteration zones. In Hodder R.W., and Petruk W., eds., Geology of Canadian gold deposits. CIM Spec. Vol. 24, 113-129 pp.

Fyon J.A., Crocket J.H., and Schwarcz H.P. (1983a). The Carshaw and Malga iron formation-hosted gold deposits of the Timmins area. In Colvine A.J., ed., The geology of gold in Ontario. Ontario Geol. Surv., Miscellaneous Paper 97, pp. 98-110.

Fyon J.A., Crocket J.H., and Schwarcz H.P. (1983b). Magnesite abundances as a guide to gold mineralization associated with ultramafic flows, Timmins area. J. Geochem. Explor., 18, 215-266.

Fyon J.A., Schwarcz H.P., and Crocket J.H. (1984). Carbonatization and gold mineralization in the Timmins area, Abitibi Greenstone belt: genetic links with Archean mantle CO_2-degassing and lower crustal granulitization. Geol. Assoc. Canada - Mineral. Assoc. Canada, Program with Abstracts, 9, p. 431.

Gamond J.F. (1983). Displacement features associated with fault zones: a comparison between observed examples and experimental models. J. Struct. Geol., 5, 33-45.

Gariépy C., and Allègre C.J. (1985). The lead isotope geochemistry and geochronology of late-kinematic intrusives from the Abitibi Greenstone belt, and the implication for late Archaean crustal evolution. Geochim. Cosmochim. Acta, 49, 2371-2383.

Gariépy C., Allègre C.J., and Lajoie J. (1984). U-Pb systematics in single zircons from the Pontiac sediments, Abitibi Greenstone belt. Can J. Earth Sci., 21, 1296-1304.

Garnett R.H.T. (1966). Relationship between tin content and structure of lodes at Geevor mine, Cornwall. Trans. Instn. Mining Metall., 75, B1-B22.

Glasson M.J., and Keays R.R. (1978). Gold mobilization during cleavage development in sedimentary rocks from the auriferous Slate Belt of Central Victoria, Australia: some important boundary conditions. Econ. Geol., 73, 496-511.

Govindaraju K. (1984). 1984 compilation of working values and sample description for 170 international reference samples of mainly silicate rocks and minerals. Geostandard Newsletters, VIII, Spec. Issue, 3-16, accompanied by 4 appendices.

Grant J.A. (1986). The isocon diagram - A simple solution to Gresens' equation for metasomatic alteration. Econ Geol., 81, 1976-1982

Gratier J.P. (1982). Approche expérimentale et naturelle de la déformation des roches par dissolution-cristallisation, avec transfert de matière. Bull. Minéral., 105, 291-300.

Gresens R.L. (1967). Composition-volume relationship of metasomatism. Chem. Geol., 2, 47-65.

Gromet L.P., Dymek R.F., Haskin L.A., and Korotev R.L. (1984). The "North American Shale Composite": its compilation, major and trace element characteristics. Geochim. Cosmochim. Acta, 48, 2469-2482.

Groves D.I., and Phillips G.N. (1987). The genesis and tectonic control on Archaean gold deposits of the Western Australia Shield - A metamorphic replacement model. Ore Geol. Reviews, 2, 287-322.

Groves D.I., Phillips G.N., Ho, S.E., and Houstoun, S.M. (1985). The nature, genesis and regional controls of gold mineralization in Archaean Greenstone belts of the Western Australian shield: a brief review. Trans. Geol. Soc. South Afr., 88, 135-148.

Groves D.I., Golding S.D., Rock N.M.S., Barley M.E., and McNaughton N.J. (1988). Archaean carbon reservoirs and their relevance to the fluid source for gold deposits. Nature, 331, 254-257.

Guha J., Gauthier A., Vallée M., Descarreaux J., and Lange-Brard F. (1982). Gold mineralization patterns at the Doyon mine (Silverstack), Bousquet, Québec. In Hodder R.W., and Petruk W., eds., Geology of Canadian gold deposits. CIM Spec. Vol. 24, pp.50-57.

Gulson B.L. (1986). Lead isotopes in mineral exploration. Development in Economic Geology, Elsevier, 23, 245 pp.

Gustafson J.K., and Miller F.S. (1937). Kalgoorlie geology re-interpreted. Econ. Geol., 32, 285-317.

Haimson B.C. (1981). Large scale laboratory testing of hydraulic fracturing. Geophys. Res. Lett., 8, 715-718.

Häkli T.A., Hänninen E., Vuorelainan Y., and Papunen H. (1976). Platinum-group minerals in the Hitura nickel deposit, Finland. Econ. Geol., 71, 1206-1213.

Hancock P.L. (1985). Brittle microtectonics: principles and practice. J. Struct. Geol., 7, 437-457.

Harte B., and Graham C.M. (1975). The graphical analysis of greenschist to amphibolite mineral assemblages in metabasites. J. Petrol., 16, 347-370.

Haskin L.A., Haskin M.A., Frey F.A., and Wildeman T.R. (1968). Relative and absolute terrestrial abundances of the rare earths. In Ahrens L.H., ed., Origin and distribution of the elements. Pergamon, Oxford, pp.

889-911.

Hattori K. (1987). Magnetic felsic intrusions associated with Canadian Archean gold deposits. Geology, 15, 1107-1111.

Hendel E.M., and Hollister L.S. (1981). An empirical solvus for CO_2-H_2O-2.6 wt% salt. Geochim. Cosmochim. Acta, 45, 225-228.

Hedenquist J.W., and Henley R.W. (1985). The importance of CO_2 on freezing point measurements of fluid inclusions: evidence from active geothermal systems and implications for epithermal ore deposition. Econ. Geol., 80, 1379-1406.

Henderson J.F. (1948). Structural control of ore deposits in the Canadian Shield between Great Slave Lake and Great Bear Lakes. In Structural geology of Canadian ore deposits, CIM Spec. Vol., pp. 238-243.

Henderson P., and Pankhurst R.J. (1984). Analytical chemistry. In Henderson P., ed., Rare earth element geochemistry. Developments in geochemistry, Elsevier, vol. 2, pp. 467-499.

Henley R.W. (1973). Solubility of gold in hydrothermal chloride solutions. Chem. Geol., 11, 73-87.

Heyen G., Ramboz C., and Dubessy J. (1982). Simulation des équilibres de phases dans le système CO_2-CH_4 en-dessous de 50°C et de 100 bar. Application aux inclusions fluides. Comptes Rendus Acad. Sci. Paris, 294, série II, 203-206.

Ho S.E., Groves D.I., and Phillips G.N. (1985). Fluid inclusions as indicators of the nature and source of ore fluids and ore depositional conditions for Archaean gold deposits of the Yilgarn Block, Western Australia. Trans. Geol. Soc. South Afr., 88, 149-158.

Hobbs B.E. (1987). Principles involved in mobilization and remobilization. Ore Geol. Reviews, 2, 37-45.

Hodgson C.J. (1983). The structure and geological development of the Porcupine camp - A re-evaluation. In Colvine A.C., ed., The geology of gold in Ontario. Miscellaneous Paper 110, pp. 211-225.

Hodgson C.J. (1986). Place of gold ore formation in the geological development of the Abitibi Greenstone belt, Ontario, Canada. Trans. Instn. Min. Metall., 95, B183-B194.

Hodgson C.J., and MacGeehan P.J. (1982). Geological characteristics of gold deposits in the Superior Province of the Canadian Shield. In Hodder R.W., and Petruk W., eds., Geology of Canadian gold deposits. CIM Spec. Vol. 24, pp. 211-229.

Hollister L.S. (1981). Information intrinsically available from fluid inclusions. In Hollister L.S., and Crawford M.L., eds., Short course in fluid inclusions: applications to petrology. Calgary, May 1981. Mineral. Assoc. Canada, pp.1-12.

Hollister L.S., and Burruss R.C. (1976). Phase equilibria in fluid inclusions from the Khtada Lake metamorphic complex. Geochim. Cosmochim. Acta, 40, 163-175.

Hollister L.S., and Crawford M.L. (1981). Short course in fluid inclusions: applications to petrology. Calgary, May 1981. Mineral. Assoc. Canada, 304 pp.

Holloway J.R. (1976). Fluids in the evolution of granitic magmas: consequence of finite CO_2 solubility. Geol. Soc. Am. Bull., 87, 1513-1518.

Holloway J.R. (1981). Compositions and volumes of supercritical fluids in the earth's crust. In Hollister L.S., and Crawford M.L., eds., Short course in fluid inclusions: applications to petrology. Calgary, May 1981. Mineral. Assoc. Canada, pp. 13-38.

Holloway J.R. (1984). Graphite-CH_4-H_2O-CO_2 equilibria at low-grade metamorphic conditions. Geology, 12, 455-458.

Holmes A. (1946). An estimate of the age of the earth. Nature, 157, 680-684.

Holmes T.C. (1968). Dome Mines Limited. In Ferguson S.A., and associated geologists, eds., Geology and ore deposits of Tisdale Township. Ontario Dept. Mines, Geological report 58, pp. 82-98.

Houtermans F.G. (1946). Die Isotopenhäufigkeiten in natürlichen Blei und das Alter des Urans. Naturwissenschaften, 33, 185-186, 219.

Hower J., Eslinger E.V., Hower M.E., and Perry E.A. (1976). Mechanism of burial metamorphism of argillaceous sediment: 1. Mineralogical and chemical evidence. Geol. Soc. Amer. Bull., 87, 725-737.

Hudson D.R. (1986). Platinum-group minerals from the Kambalda nickel deposits, Western Australia. Econ. Geol., 81, 1218-1225.

Hurst M.E. (1935). Vein formation at Porcupine Ontario. Econ. Geol., 30, 103-127.

Hutchinson R.W. (1987). Metallogeny of Precambrian gold deposits: space and time relationships. Econ. Geol., 82, 1993-2007.

Hutchinson R.W., and Burlington J.L. (1984). Some broad characteristics of greenstone belt gold lodes. In Foster R.P., ed., Gold'82: The geology, geochemistry and genesis of gold deposits. Balkema, Rotterdam, pp. 339-372.

Hynes A. (1980). Carbonatization and mobility of Ti, Zr and Y in Ascot Formation metabasalts, SE Quebec. Contrib. Mineral. Petrol., 75, 79-87.

Jacobs J.W., Korotev R.L., Blanchard D.P., and Haskin L.A. (1977). A well-tested procedure for instrumental neutron activation analysis of silicate rocks and minerals. J. Radioanl. Chem., 40, 93-114.

Jensen L.S. (1976). A new cation plot for classifying subalkalic volcanic rocks. Ontario Div. Mines, Miscellaneous Paper 66, 22 pp.

Johannes W. (1969). An experimental investigation of the system $MgO-SiO_2-H_2O-CO_2$. Am. J. Sci., 267, 1083-1104.

Jolly W.T. (1978). Metamorphic history of the Archean Abitibi belt. Geol. Surv. Canada, Paper 78-10, pp. 63-77.

Jolly W.T. (1980). Development and degradation of Archean lavas, Abitibi area, Canada, in light of major element geochemistry. J. Petrol., 21, 323-363.

Jolly W.T. (1982). Progressive metamorphism of komatiites and related Archaean lavas of the Abitibi area, Canada. In Arndt N.T., and Nisbet E.G., eds., Komatiites, Allen and Unwin, London, pp. 247-266.

Kajiwara Y., and Krouse H.R. (1971). Sulfur isotope partitioning in metallic sulfide systems. Can. J. Earth Sci., 8, 1397-1408.

Karvinen W.O. (1982). Geology and evolution of gold deposits, Timmins area, Ontario. In Hodder R.W, and Petruk W., eds., CIM Spec. Vol. 24, Geology of Canadian gold deposits, pp. 101-112.

Keays R.R. (1982). Palladium and iridium in komatiites and associated rocks: application to petrogenetic problems. In Arndt N.T., and Nisbet E.G., eds., Komatiites, Allen and Unwin, London, pp. 435-457.

Keays R.R. (1984). Archaean gold deposits and their source rocks: the upper mantle connection. In Foster R.P., ed., Gold'82 The geology, geochemistry and genesis of gold deposits. Balkema, Rotterdam, pp. 17-51.

Keays R.R. (1987). Principles of mobilization (dissolution) of metals in mafic and ultramafic rocks - The role of immiscible magmatic sulfides in the generation of hydrothermal gold and volcanogenic massive sulphide deposits. Ore Geol. Reviews, 2, 47-63.

Kerrich R. (1976). Some effects of tectonic recrystallization on fluid inclusions in vein quartz. Contrib. Mineral. Petrol., 59, 195-202.

Kerrich R. (1987). The stable isotope geochemistry of Au-Ag vein deposits in metamorphic rocks. In Kyser T.K., ed., Short course in stable isotope geochemistry of low temperature fluids, Saskatoon, May 1987. Mineral. Assoc. Canada, vol. 13, pp. 287-336.

Kerrich R., and Allison I. (1978). Vein geometry and hydrostatics during Yellowknife mineralisation. Can. J. Earth Sci., 15, 1653-1660.

Kerrich R., and Fryer B.J. (1979). Archean precious metal hydrothermal systems, Dome Mine, Abitibi Greenstone belt. II. REE and oxygen isotope relations. Can. J. Earth Sci., 16, 440-458.

Kerrich R., and Fyfe W.S. (1981). The gold-carbonate association: source of CO_2, and CO_2 fixation reactions in Archean lode deposits. Chem. Geol., 33, 265-294.

Kerrich R., Fryer B.J., King R.W., Willmore L.M., and van Hees E. (1987). Crustal outgassing and LILE enrichment in major lithosphere structures, Archean Abitibi greenstone belt: evidence on the source reservoir from strontium and carbon isotope tracers. Contrib. Mineral. Petrol., 97, 156-168.

Knapp R.B., and Knight J.E. (1977). Differential thermal expansion of pore fluids: fracture propagation and microearthquake production in hot pluton environment. J. Geophys. Res., 82, 2515-2522.

Knapp R.B., and Norton D. (1981). Preliminary numerical analysis of processes related to magma crystallization and stress evolution in cooling pluton environments. Am. J. Sci., 281, 35-68.

Kosterin A.V. (1959). The possible modes of transport of the rare earths by hydrothermal solutions. Geochemistry, 4, 381-387.

Kramers J.D., and Foster R.P. (1984). A reappraisal of lead isotope investigations of gold deposits in Zimbabwe. In Foster R.P., ed., Gold'82 The geology, geochemistry and genesis of gold deposits. Balkema, Rotterdam, pp. 569-582.

Kreulen R. (1987). Thermodynamic calculations of the C-O-H system applied to fluid inclusions: are fluid inclusions unbiassed samples of ancient fluids ? Chem. Geol., 61, 59-64.

Krogh T.E., and Davies G.L. (1974). The age of the Sudbury nickel irruptive. Geophysical Laboratory; Geochemistry; Radiometric Geochronology, Carnegie Institute, Washington, Yearbook, 73, 567-569.

Kwong Y.T.J., and Crocket J.H. (1978). Background and anomalous gold in rocks of an Archean Greenstone assemblage, Kakagi Lake area, Northwestern Ontario. Econ. Geol., 73, 50-63.

LaKind J.S. (1984). Geochemical study of gold-quartz veins, Red Lake gold camp, Northwest Ontario. Unpublished M.Sc. thesis, University of Wisconsin-Madison, USA, 69 pp.

Lamb W.M., and Valley J.W. (1985). C-O-H fluid calculations and granulite genesis. In Tobi A.C., and Touret J.L.R., eds., The deep Proterozoic crust in the North Atlantic Provinces. D. Reidel Publishing Company, pp. 119-131.

Lambert R. St. J. (1985). Lead isotopes in Archean rocks and the evolution of the mantle. In Ayres L.D., Thurston P.C., Card K.D., and Weber W., eds., Evolution of Archean supracrustal sequences. Geol. Assoc. Canada, Spec. Paper 28, pp. 49-53.

Leroy J. (1979). Contribution à l'étalonnage de la pression interne des inclusions fluides lors de leur décrépitation. Bull. Minéral., 102, 584-593.

Ludden J.N., and Gélinas L. (1982). Trace element characteristics of komatiites and komatiitic basalts from the Abitibi metavolcanic belt of Québec. In Arndt N.T., and Nisbet E.G., eds., Komatiites, Allen and Unwin, London, pp. 331-346.

Ludden J.N., Daigneault R., Robert F., Taylor R.P. (1984). Trace element mobility in alteration zone associated with Archean Au lode deposits. Econ. Geol., 79, 1131-1141.

Macdonald A.J. (1983). The iron formation - gold association: evidence from the Geraldton area. In Colvine A.C., ed., The geology of gold in Ontario. Ontario Geol. Surv., Miscellaneous Paper 110, pp. 75-83.

Macdonald A.J. (1984). Gold mineralization in Ontario, I: the role of banded iron formation. In Guha J., and Chown E.H., eds., Chibougamau - Stratigraphy and mineralization. CIM Spec. Vol. 34, pp. 412-430.

Malcolm W. (1929). Gold fields of Nova Scotia. Geol. Surv. Canada, Memoir 156, 253 pp.

Marchand M. (1973). Determination of Rb, Sr, and Rb/Sr by XFR. Tech. Memo. 73-2, Dept. of Geology, McMaster University, Hamilton, Ontario, Canada.

Marmont S. (1983). The role of felsic intrusions in gold mineralization. In Colvine A.C., ed., The geology of gold in Ontario. Ontario Geol. Surv., Miscellaneous Paper 110, pp. 38-47.

Masliwec A., McMaster D., and York D. (1986). The dating of Ontario's gold deposits. Ontario Geol. Surv., Miscellaneous Paper 130, 107-114.

Mason R., and Brisbin D.I. (1987). The geological setting of gold deposits in the Porcupine mining camp. Ontario Geol. Surv., Miscellaneous Paper 136, 215-233.

Mason R., and Melnik N. (1986a). The anatomy of an Archean gold system - The McIntyre Hollinger complex at Timmins, Ontario, Canada. In Macdonald A.J., ed., Proceedings of Gold'86, an international Symposium on the geology of gold, Toronto: 1986, pp. 40-55.

Mason R., and Melnik N. (1986b). The McIntyre-Hollinger investigation, Timmins, Ontario: a gold dominated porphyry copper system. In Current Research, Part B, Geol. Surv. Canada, Paper 86-1B, 577-583.

Mawer C.K. (1987). Mechanics of formation of gold-bearing quartz veins, Nove Scotia, Canada. Tectonophysics, 135, 99-119.

McAuley J.B. (1983). A petrographic and geochemical study of the Preston, Preston West and Paymaster Porphyries, Timmins, Ontario. Unpublished M.Sc. thesis, Laurentian University, Sudbury, Ontario, Canada, 118 pp.

McKinstry H.E., and Ohle Jr. E.L. (1949). Ribbon structure in gold-quartz veins. Econ. Geol., 44, 87-109.

Merriman R.J., Bevins R.E., and Ball T.K. (1986). Petrological and geochemical variations within the Tal y Fan intrusion: a study of element mobility during low-grade metamorphism with implications for petrogenetic modeling. J. Sediment. Petrol., 27, 1409-1436.

Mitchell R.H., and Keays R.R. (1981). Abundances and distribution of gold, palladium and iridium in some spinel and garnet lherzolites: implications for the nature and origin of precious metal-rich intergranular components in the upper mantle. Geochim. Cosmochim. Acta, 45, 2425-2442.

Moorbath S., and Taylor P.N. (1981). Isotopic evidence for continental growth in the Precambrian. In Krõner A., ed., Precambrian plate tectonics, Elsevier, chap. 20, pp. 491-525.

Murphy J.B., and Hynes A.J. (1986). Contrasting secondary mobility of Ti, P, Zr, Nb and Y in two metabasaltic suites in the Appalachians. Can. J. Earth Sci., 23, 1138-1144.

Naldrett A.J., and Smith I.S.E. (1980). Mafic and ultramafic volcanism during the Archean. In Basaltic volcanism of the terrestrial planets. Pergamon Press, Inc., New-York, pp. 5-29.

Naldrett A.J., Hoffman E.L., Green A.H., Chou C.-L., Naldrett S.R., and Alcock R.A. (1979). The composition of Ni-sulfide ores, with particular reference to their content of PGE and Au. Can. Mineral., 17, 403-415.

Nesbitt R.W., and Sun S.-S. (1976). Geochemistry of Archean spinifex-textured peridotites and magnesian and low-magnesian tholeiites. Earth Planet. Sci. Lett., 31, 433-453.

Nesbitt R.W., Sun S.-S., and Purvis A.C. (1979). Komatiites: geochemistry and genesis. Can. Mineral., 17, 165-186.

Neuerburg G.J. (1975). A procedure, using hydrofluoric acid, for quantitative mineral separations from silicate rocks. J. Res. U.S. Geol. Surv., 3, 377-378.

Norrish K., and Hutton J.T. (1969). An accurate X-ray spectrographic method for the analysis of a wide range of geological samples. Geochim. Cosmochim. Acta, 33, 431-453.

Nunes P.D., and Jensen L.S. (1980). Geochonology of the Abitibi metavolcanic belt, Kirkland Lake area-Progress report. In Pye E.G., ed., Summary of geochronology studies 1977-1979. Ontario Geol. Surv., Miscellaneous Paper 92, pp. 40-45.

Nunes P.D., and Pyke D.R. (1980). Geochronology of the Abitibi metavolcanic belt, Timmins - Matachewan area-Progress report. In Pye E.G., ed., Summary of geochronology studies 1977-1979. Ontario Geol. Surv., Miscellaneous Paper 92, pp. 34-39.

Nunes P.D., and Pyke D.R. (1981). Time-stratigraphic correlation of the Kidd Creek ore body with volcanic rocks south of Timmins, Ontario, as inferred from zircon U-Pb ages. Econ. Geol., 76, 944-951.

Ohmoto H., and Rye R.O. (1979). Isotopes of sulfur and carbon. In Barnes H.L., ed., Geochemistry of hydrothermal ore deposits. Second edition, John Wiley and Sons, New York, pp. 509-567.

Oshin I.O., and Crocket J.H. (1982). Noble metals in Thetford Mines ophiolites, Quebec, Canada. Part I: distribution of gold, iridium, platinum, and palladium in the ultramafic and gabbroic rocks. Econ. Geol., 77, 1556-1570.

Patterson C.C. (1956). Age of meteorites and the earth. Geochim. Cosmochim. Acta, 10, 230-237.

Pearce T.H. (1987). The identification and assessment of spurious trends in Pearce-type ratio variation diagrams: a discussion of some statistical arguments. Contrib. Mineral. Petrol., 97, 529-534.

Pécher A. (1981). Experimental decrepitation and re-equilibration of fluid inclusions in synthetic quartz. Tectonophysics, 78, 567-583.

Pécher A., and Boullier A.M. (1984). Evolution à pression et température élevées d'inclusions fluides dans un quartz synthétique. Bull. Minéral., 107, 139-153.

Phillips G.N. (1985). Archaean gold deposits of Australia. Inform. Circ., Econ. Geol. Res. Unit, University of Witwatersrand, Johannesburg, 41 pp.

Phillips G.N., Groves D.I., and Martyn J.E. (1984). An epigenetic origin for Archean banded iron-formation-hosted gold deposits. Econ. Geol., 79, 162-171.

Phillips W.J. (1972). Hydraulic fracturing and mineralization. J. Geol. Soc. London, 128, 337-359.

Pichavant M., Ramboz C., and Weisbrod A. (1982). Fluid immiscibility in natural processes : use and misuse of fluid inclusion data. I. Phase equilibria analysis - A theoretical and geometrical approach. Chem. Geol., 37, 1-27.

Platt J.P., and Vissers R.L.M. (1980). Extensional structures in anisotropic rocks. J. Struct. Geol., 2, 397-410.

Potter II R.W., Clynne M.A., and Brown D.L. (1978). Freezing point depression of aqueous sodium chloride solutions. Econ. Geol., 73, 284-285.

Pyke D.R. (1976). On the relationship of gold mineralization and ultramafic volcanic rocks in the Timmins area, Northeastern Ontario. CIM Bull., 69, 79-87.

Pyke D.R. (1981). Relationship of gold mineralization to stratigraphy and structure in Timmins and surrounding areas. In Pye E.G., and Roberts R.G., eds., Genesis of Archean, volcanic-hosted gold deposits. Ontario Geol. Surv., Miscellaneous Paper 97, pp. 1-15.

Pyke D.R. (1982). Geology of the Timmins area, District of Cochrane. Ontario Geol. Surv., Report 219, 141 pp. Accompanied by map 2455, scale 1:50'000, 3 charts, and 1 sheet microfiche.

Ramboz C. (1980). Problèmes posés par la détermination de la composition des fluides carboniques complexes, à l'aide des techniques microthermométriques. Comptes Rendus Acad. Sci. Paris, 290, sérle D, 499-502.

Ramboz C., Pichavant M., and Weisbrod A. (1982) Fluid immiscibility in natural processes: use and misuse of fluid inclusion data. II. Interpretation of fluid inclusion data in terms of immiscibility. Chem. Geol., 37, 29-48.

Ramsay J.G. (1980a). The crack-seal mechanism of rock deformation. Nature, 284, 135-139.

Ramsay J.G. (1980b). Shear zone geometry: a review. J. Struct. Geol., 2, 83-99

Ramsay J.G., and Graham R.H. (1970). Starin variation in shear belts. Can. J. Earth Sci., 7, 786-813.

Ramsay J.G., and Huber M.I. (1983). The technique of modern structural geology. Volume 1: strain analysis. Academic Press, London, 307 pp.

Ramsay J.G., and Huber M.I. (1986). The technique of modern structural geology. Volume 2: folds and fractures. Academic Press, London, 391 pp.

Razin L.V., and Khomenko G.A. (1969). Accumulation of osmium, ruthenium, and the other platinum-group metals in chrome spinel in platinum-bearing dunites. Geochem. Intern., 6, 546-557.

Read J.J., and Meinert L.D. (1986). Gold-bearing quartz vein mineralization at the Big Hurrah Mine, Seward Peninsula, Alaska. Econ. Geol., 81, 1760-1774.

Reading D.J., Roberts R.G., and Fritz P. (1982). Geology and isotope geochemistry of the ankerite units, Dome Mine, Timmins. Geol. Assoc. Canada - Mineral. Assoc. Canada, Program with Abstracts, 7, p. 75.

Rees C.E. (1978). Sulphur isotope measurements using SO_2 and SF_6. Geochim. Cosmochim. Acta, 42, 383-389.

Richards J.R. (1986). Lead isotopic signatures: further examination of comparisons between South Africa and Western Australia. Trans. Geol. Soc. South Afr., 89, 285-304.

Robert F., and Brown A.C. (1986a). Archean gold-bearing quartz veins at the Sigma Mine, Abitibi Greenstone belt, Quebec: Part I. Geologic relations and formation of the vein system. Econ. Geol., 81, 578-592.

Robert F., and Brown A.C. (1986b). Archean gold-bearing quartz veins at the Sigma Mine, Abitibi Greenstone belt, Quebec: Part II. Vein paragenesis and hydrothermal alteration. Econ. Geol., 81, 593-616.

Robert F., and Kelly W.C. (1987). Ore-forming fluids in Archean gold-bearing quartz veins at the Sigme Mine, Abitibi Greenstone belt, Quebec, Canada. Econ. Geol., 82, 1464-1482.

Robert F., Brown A.C., and Audet A.J. (1983). Structural control of gold mineralization at the Sigma Mine, Val d'Or, Québec. CIM Bull., 76, 72-80.

Roberts R.G. (1981). The volcanic-tectonic setting of gold deposits in the Timmins area, Ontario. In Pye E.G., and Roberts R.G., eds., Genesis of Archean, volcanic-hosted gold deposits. Ontario Geol. Surv., Miscellaneous Paper 97, pp. 16-28.

Roberts R.G. (1987). Ore deposit models # 11: Archean lode gold deposits. Geoscience Canada, 14, 37-52.

Roberts R.G., and Reading D.J. (1981). Volcanic-tectonic setting of gold deposits in the Timmins district-Carbonate-bearing rocks at Dome Mine. Ontario Geol. Surv., Miscellaneous Paper 98, 222-232.

Roberts R.G., Carnevalli J., and Harris J.D. (1978). The volcanic-tectonic setting of gold-quartz vein systems in the Timmins district, Ontario. In Current Res., Part B, Paper 78-1B, Geol. Surv. Canada, 187-190.

Robin P.-Y.F. (1979). Theory of metamorphic segregation and related processes. Geochim. Cosmochim. Acta, 43, 1587-1600.

Roedder E. (1984). Fluid inclusions: Mineral. Soc. Am., Reviews in Mineralogy, vol.12, 644 pp.

Rogers D.S. (1982a). Diamond drilling as an aid in ore definition at the Dome Mine. CIM Bull., 75, 98-104.

Rogers D.S. (1982b). The geology and ore deposits of the #8 shaft area, Dome Mine. In Hodder R.W., and Petruk W., eds., Geology of Canadian gold deposits. CIM Spec. Vol. 24, pp. 161-168.

Rollinson H.R., and Roberts C.R. (1986) Ratio correlations and major element mobility in altered basalts and komatiites. Contrib. Mineral. Petrol., 93, 89-97.

Rosholt J.N., Zartman R.E., and Nkomo I.T. (1973). Lead isotope systematics and uranium depletion in the Granite Mountains, Wyoming. Bull. Geol. Soc. Am., 84, 989-1002.

Saager R., and Köppel V. (1976). Lead isotopes and trace elements from sulfides of Archean greenstone belts in South Africa - A contribution to the knowledge of the oldest known mineralizations. Econ. Geol., 71, 44-57.

Santosh M. (1986). Ore fluids in the auriferous Champion Reef of Kolar, South India. Econ. Geol., 81, 1546-1552.

Schwartz M.O. (1986). Interpretation of the Conolly contour diagram of fault-related veins. Mineral. Deposita, 21, 1-11.

Schwarz L.J., and Barker J.L. (1976). Gold content of USGS standard rocks. U.S. Geol. Surv. Prof. Paper, 840, 71-72.

Seward T.M. (1973). Thio complexes of gold and the transport of gold in hydrothermal ore solutions. Geochim. Cosmochim. Acta, 37, 379-399.

Seward T.M. (1984). The transport and deposition of gold in hydrothermal systems. In Foster R.P., ed., Gold'82: The geology, geochemistry and genesis of gold deposits. Balkema, Rotterdam, pp. 165-181.

Shaw D.M. (1954). Trace elements in pelitic rocks. Part I. Geol. Soc. Amer. Bull., 65, 1151-1166.

Shaw D.M. (1956). Geochemistry of pelitic rocks. Part III: major elements and general geochemistry. Geol. Soc. Amer. Bull., 67, 919-934.

Shaw D.M. (1969). Evaluation of data; part I: analytical errors and related topics in geochemistry. In Wedepohl K.H., ed., Handbook of geochemistry, Springer Verlag, Berlin, pp. 325-332.

Shirey S.B., and Carlson R.W. (1987). Pb and Nd isotope evolution of the Archean crust and mantle. Terra Cognita, 7, 272.

Sillitoe R.H. (1979). Some thoughts on gold-rich porphyry copper deposits. Mineral. Deposita, 14, 161-174.

Smith T.J., Cloke P.L., and Kesler S.E. (1984). Geochemistry of fluid inclusions from the McIntyre-Hollinger gold deposit, Timmins, Ontario, Canada. Econ. Geol., 79, 1265-1285.

Spooner E.T.C., Wood P.C., Burrows D.R., Thomas A.V., and Noble S.R. (1985). Geological, fluid inclusions, and isotopic (carbon and sulphur) studies of Au-quartz-carbonate-pyrite-scheelite vein mineralization and intrusion-hosted Cu-(Au-Mo) mineralization in the Hollinger-McIntyre system, Timmins, Ontario. Ontario Geol. Surv., Miscellaneous Paper 127, 229-246.

Spooner E.T.C., Bray C.J., Wood P.C., Burrows D.R., and Callan N.J. (1987). Au-quartz vein and Cu-Au-Ag-Mo-Anhydrite mineralization Hollinger-McIntyre mines, Timmins, Ontario: $\delta^{13}C$ values (McIntyre), fluid inclusion gas chemistry, pressure (depth) estimation, and H_2O-CO_2 phase separation as a precipitation and dilation mechanism. Ontario Geol. Surv., Miscellaneous Paper 136, 35-56.

Sprunt E.S., and Nur A. (1977). Destruction of porosity through pressure solution. Geophysics, 42, 726-741.

Stacey J.S., and Kramers J.D. (1975). Approximation of terrestrial lead isotope evolution by a two-stage model. Earth Planet. Sci. Lett., 26, 207-221.

Steiger R.H., and Jäger E. (1977). Subcommission on geochronology : convention on the use of decay constants in geo- and cosmochronology. Earth Planet. Sci. Lett., 36, 359-362.

Sterner S.M., and Bodnar R.J. (1984). Synthetic fluid inclusions in natural quartz I. Compositional types synthesized and applications to experimental geochemistry. Geochim. Cosmochim. Acta, 48, 2659-2668.

Stockman H.W., and Hlava P.F. (1984). Platinum-group minerals in alpine chromitites from Southwestern Oregon. Econ. Geol., 79, 491-508.

Stockwell C.H., McGlynn J.C., Emslie R.F., Sanford B.V., Norris A.W., Donaldson J.A., Fahrig W.F., and Currie K.L. (1976). Geology of the Canadian Shield. In Douglas R.J.W., ed., Geology and economic minerals of Canada, Part A (Chap. I-VII). Econ. Geol., Report No. I, Geol. Surv. Canada, Dept. Energy, Mines and Resources, pp. 43-150.

Sun S.-S., and Nesbitt R.W. (1978). Petrogenesis of Archean ultrabasic and basic volcanics: evidence from REE. Contrib. Mineral. Petrol., 65, 301-325.

Takenouchi S., and Kennedy G.C. (1965). The solubility of carbon dioxide in NaCl solutions at high temperatures and pressures. Am. J. Sci., 263, 445-454.

Tatsumoto M., Knight R.J., and Allègre C.J. (1973). Time differences in the formation of meteorites as determined from the ratio of lead-207 to lead-206. Science, 180, 1279-1283.

Taylor R.G. (1966). Distribution and deposition of cassiterite at South Crofty Mine, Cornwall. Trans. Instn. Mining Metall., 75, B35-B49.

Taylor R.P., and Fryer B.J. (1982). Rare earth element geochemistry as an aid to interpreting hydrothermal ore deposits. In Evans A.M., ed., Metallization associated with acid magmatism. Wiley and Sons Ltd., pp. 357-365.

Taylor S.R., and McLennan S.M. (1985). The continental crust: its composition and evolution. Geoscience Text. Blackwell Scientific Publications, Oxford. 312 pp.

Tchalenko J.S. (1968). The evolution of kink bands and the development of compression textures in sheared clays. Tectonophysics, 6, 159-174.

Thode H.G., and Rees C.E. (1971). Measurement of sulphur concentrations and the isotope ratios $^{33}S/^{32}S$, $^{34}S/^{32}S$ and $^{36}S/^{32}S$ in Apollo 12 samples. Earth Planet. Sci. Lett., 12, 434-438.

Thode H.G., Monster J., and Dunford H.B. (1961). Sulphur isotope geochemistry. Geochim. Cosmochim. Acta, 25, 159-174.

Thomas L.J. (1978). An introduction to mining. Methuen of Australia, 471 pp.

Thompson G., and Bankston D.C. (1970). Sample contamination from grinding and sieving determined by emission spectrometry. Applied Spectrometry, 24, 210-219.

Thomson J.E. (1948). Regional structure of the Kirkland Lake - Larder Lake area. In Structural geology of Canadian ore deposits. CIM Spec. Vol., pp. 627-632.

Thomson M.L. (1986). Petrology of the Crixas gold deposit, Brazil: evidence for gold associated with hydrothermal alteration subsequent to metamorphism. In Macdonald A.J., ed., Proceedings of Gold'86, an international Symposium on the geology of gold, Toronto: 1986, pp. 284-296.

Thorpe R.I. (1982). Lead isotope evidence regarding Archean and Proterozoic Metallogeny in Canada. Revista Brasileira de Geociências, 12, 510-521.

Thorpe R.I., Guha J., and Cimon J. (1981). Evidence from lead isotopes regarding the genesis of ore deposits in the Chibougamau region, Quebec. Can. J. Earth Sci., 18, 708-723.

Tihor S.L. (1978). The mineralogical composition of the carbonate rocks of the Kirkland Lake - Larder Lake gold camp. Unpublished M.Sc. thesis, McMaster University, Hamilton, Ontario, Canada, 93 pp.

Tilling R.I., Gottfried D., and Rowe J.J. (1973). Gold abundances in igneous rocks: bearing on gold mineralization. Econ. Geol., 68, 168-186.

Tilton G.R. (1983). Evolution of depleted mantle: the lead perspective. Geochim. Cosmochim. Acta, 47, 1191-1197.

Touret J. (1976). The significance of fluid inclusions in metamorphic rocks. In Fraser D.G., ed., Thermodynamics in geology. D.Reidel Publishing Company, Nato Advanced Study Institutes Series, vol. 30, pp. 203-227.

Touret J. (1981). Fluid inclusions in high grade metamorphic rocks. In Hollister L.S., and Crawford M.L., eds., Short course in fluid inclusions: applications to petrology, Calgary, May 1981. Mineral. Assoc. Canada., pp. 182-208.

Travis G.A., Woodall R., and Bartram G.D. (1971). The geology of the Kalgoorlie Goldfield. In Clover J.E., ed., Spec. Publ. Geol. Soc. Aust., pp. 175-190.

Vearncombe J.R. (1986). Structure of veins in a gold-pyrite deposit in banded iron formation, Amalia Greenstone belt, South Africa. Geol. Mag., 123, 601-609.

Walker R.J., Shirey S.B., and Stecher O. (1988). Comparative Re-Os, Sm-Nd and Rb-Sr isotope and trace element systematics for Archean komatiite flows from Munro Township, Abitibi Belt, Ontario. Earth Planet. Sci. Lett., 87, 1-12.

Wendlandt R.F., and Harrison W.J. (1979). Rare earth partitioning between immiscible carbonate and silicate liquids and CO_2 vapor: results and implications for the formation of light rare earth-enriched rocks. Contrib. Mineral. Petrol., 69, 409-419.

Werre Jr. R.W., Bodnar R.J., Bethke P.M., and Barton Jr. P.B. (1979). A novel gas-flow fluid inclusion heating/freezing stage. Geol. Soc. Am., Program with Abstracts, 11, 539.

Whitford D.J., and Arndt N.T. (1978). Rare earth element abundances in a thick, layered komatiite lava flow from Ontario, Canada. Earth Planet. Sci. Lett., 41, 188-196.

Whitemore D.R.E., Berry L.G., and Hawley J.E. (1946). Chrome micas. Am. Mineral., 31, 1-21.

Wilkins R.W.T., and Barkas J.P. (1978). Fluid inclusions, deformation and recrystallization in granite tectonites. Contrib. Mineral. Petrol., 65, 293-299.

Wood P.C., Burrows D.R., Thomas A.V., and Spooner E.T.C. (1986a). The Hollinger-McIntyre Au-quartz vein system, Timmins, Ontario, Canada: geologic characteristics, fluid properties and light stable isotope geochemistry. In Macdonald A.J., ed., Proceedings of Gold'86, an international Symposium on the geology of gold: Toronto, 1986, pp.56-80.

Wood P.C., Burrows D.R., and Spooner E.T.C. (1986b). Au-quartz vein and intrusion-hosted Cu-Au-Ag-Mo mineralization, Hollinger-McIntyre mines, Timmins, Ontario: geological characteristics, structural examination, igneous and hydrothermal alteration geochemistry, and light stable isotope (hydrogen and oxygen) geochemistry. Ontario Geol. Surv., Miscellaneous Paper 130, 115-137.

Woods T.L., Bethke P.M., Bodnar R.J., and Werre Jr. R.W. (1981). Supplementary components and operation of the U.S. Geological Survey gas-flow heating/freezing stage. U.S. Geol. Surv., Open File Report, 81-954, 12 pp.

Wronkiewicz D.J., and Condie K.C. (1987). Geochemistry of Archean shales from the Witwatersrand Supergroup, South Africa: source-area, weathering and provenance. Geochim. Cosmochim. Acta, <u>51</u>, 2401-2416.

York, D. (1969). Least-square fitting of a straight line with correlated errors. Earth Planet. Sci. Lett., <u>5</u>, 320-324.

Zartman R.E., and Doe B.R. (1981). Plumbotectonics - The model. Tectonophysics, <u>75</u>, 135-162.

Zielinski R.A., Peterman Z.E., Stuckless J.S., Rosholt J.N., and Nkomo I.T. (1981). The chemical and isotopic record of rock-water interaction in the Sherman Granite, Wyoming and Colorado. Contrib. Mineral. Petrol., <u>78</u>, 209-219.

Zindler A. (1982). Nd and Sr isotopic studies of komatiites and related rocks. <u>In</u> Arndt N.T., and Nisbet E.G., eds., Komatiites, Allen and Unwin, London, pp. 399-420.

APPENDIX I

CONOLLY CONTOUR DIAGRAM

A detailed description on the construction and the use of Conolly contour diagrams can be found in Conolly (1936), Garnett (1966), Taylor (1966), and Schwartz (1986). The method of construction is presented in figure I-1.

This graphical method consists of selecting an arbitrary reference plane, which is placed behind the lode to be contoured. The attitude of the reference plane approximates the average strike and dip of the vein. Measurements of the horizontal distance between the plane and the lode at set intervals are transferred as raw data to their corresponding positions on a vertical projection plane, which is placed in front of the lode. Hence, when looking at the projection plane from the front, the vein is located between the projection plane and the reference plane. The figure on the projection plane, when contoured, presents a visual picture of the shape of the lode. The result is akin to a topographical map showing such structural trends as changes in slopes, "crests", and "valleys".

Figure I-1. Method of constructing the Conolly contour diagram. See text for explanation.

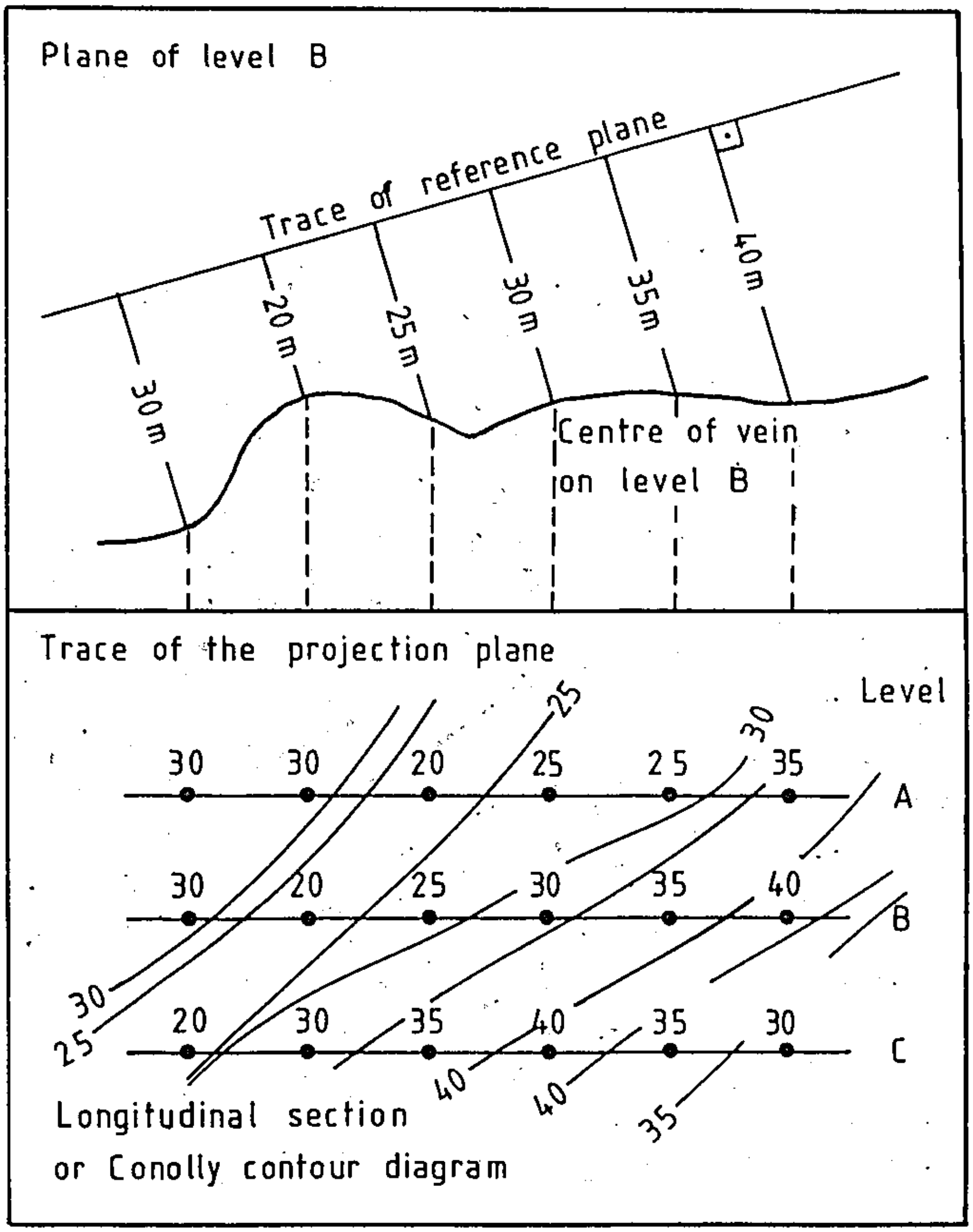
Plane of level B
Trace of reference plane
30 m
20 m
25 m
30 m
35m
40 m
Centre of vein on level B
Trace of the projection plane
Level
A
B
C
30
30
20
25
25
35
30
20
25
30
35
40
20
30
35
40
35
30
25
30
30
25
40
40
35
Longitudinal section or Conolly contour diagram

APPENDIX II

ANALYTICAL ERRORS

II.1. XRF analysis

Replicate analyses of different pellets of the same sample were carried out to evaluate the precision of the data. Analytical results for the three main rock types run in triplicate for major and some trace elements are given in tables II-1 and II-2. The coefficient of variation for most oxides falls within the acceptable range of 0.5 to 5.0% suggested by Shaw (1969) (Table II-1). The exceptions are K_2O and P_2O_5 for the carbonate rocks, and MnO and P_2O_5 for the slate. The precision of Na_2O cannot be expressed for the carbonate rocks due to abundances below the limit of detection (see below). Trace elements have coefficient of variations lying below 15% as recommended by Shaw (1969) (Table II-2). Exceptions to that are Nb and Cu.

Accuracy of analyses was evaluated by analyzing standard samples of known composition. Standard rocks analyzed are: SCo-1, JB-1, JG-1, PCC-1, NIM-P, NIM-N, NIM-D, Mica-Fe, and Mica-Mg. There is a good agreement between most of the results obtained in the course of the

Fuchsite-bearing carbonate rock: #12507

	1	2	3	Mean	SD	CV %
SiO2	30.57	30.31	30.57	30.48	0.12	0.40
Al2O3	4.55	4.38	4.44	4.46	0.07	1.52
Fe2O3	16.66	16.39	16.54	16.53	0.11	0.67
MgO	33.13	34.12	33.56	33.60	0.40	1.20
CaO	13.15	12.75	13.06	12.99	0.17	1.33
Na2O	0.24	<0.20	<0.20	-	-	-
K2O	0.92	1.10	0.95	0.99	0.08	7.87
TiO2	0.41	0.44	0.41	0.42	0.01	3.28
MnO	0.30	0.30	0.30	0.30	-	-
P2O5	0.07	0.10	0.12	0.10	0.02	18.71
Total	100.00	100.00	100.00			

Carbonate rock: #12530

	1	2	3	Mean	SD	CV %
SiO2	44.22	44.03	44.31	44.18	0.12	0.26
Al2O3	6.94	6.87	7.00	6.94	0.05	0.78
Fe2O3	11.52	11.55	11.48	11.51	0.03	0.24
MgO	29.26	29.50	29.23	29.33	0.12	0.40
CaO	7.22	7.24	7.12	7.20	0.05	0.71
Na2O	<0.20	<0.20	<0.20	-	-	-
K2O	<0.05	<0.05	0.09	-	-	-
TiO2	0.31	0.31	0.31	0.31	-	-
MnO	0.24	0.25	0.23	0.24	0.01	4.54
P2O5	0.17	0.17	0.19	0.18	0.01	3.54
Total	100.00	100.00	100.00			

Slate: #12534

	1	2	3	Mean	SD	CV %
SiO2	67.96	67.99	67.87	67.94	0.05	0.08
Al2O3	16.58	16.50	16.44	16.51	0.06	0.34
Fe2O3	6.37	6.33	6.47	6.39	0.06	0.95
MgO	2.86	2.78	2.85	2.83	0.04	1.30
CaO	0.23	0.23	0.23	0.23	-	-
Na2O	2.64	2.78	2.61	2.68	0.07	2.67
K2O	2.60	2.62	2.75	2.66	0.06	2.40
TiO2	0.62	0.62	0.66	0.63	0.02	3.07
MnO	0.06	0.06	0.05	0.06	0.005	8.32
P2O5	0.08	0.09	0.07	0.08	0.01	10.21
Total	100.00	100.00	100.00			

Table II-1. Precision of major elements based on triplicate analyses of two carbonate rock samples and one slate sample from the Dome Mine.

SD: one standard deviation.
CV %: coefficient of variation.

Carbonate rock: #12506

	1	2	3	Mean	SD	CV %
Rb	21	20	18	20	1	6.34
Sr	291	288	298	292	4	1.43
Y	13	11	12	12	1	6.80
Zr	27	25	28	27	1	4.68
Nb	4	2	5	4	1	34.02
Ni	1330	1336	1320	1329	7	0.50
Cr	2220	2170	2180	2190	22	0.99
V	113	115	116	115	1	1.09
Zn	59	51	63	58	5	8.65
Cu	5	5	3	4	1	21.76
Pb	10	11	12	11	1	7.42

Fuchsite-bearing carbonate rock: #12523

	1	2	3	Mean	SD	CV %
Rb	15	14	16	15	1	5.44
Sr	474	479	476	476	2	0.43
Y	17	17	17	17	-	-
Zr	37	39	38	38	1	2.15
Nb	<2	4	4	-	-	-
Ni	674	657	673	668	8	1.17
Cr	1420	1430	1430	1427	5	0.33
V	64	65	64	64	0.5	0.73
Zn	39	53	46	46	6	12.42
Cu	17	17	16	17	0.5	2.83
Pb	9	8	8	8	0.5	5.66

Slate: #12534

	1	2	3	Mean	SD	CV %
Rb	72	70	69	70	1	1.77
Sr	86	91	93	90	3	3.27
Y	21	25	24	23	2	7.28
Zr	156	161	164	160	3	2.06
Nb	5	9	6	7	2	25.50
Ni	71	78	77	75	3	4.10
Cr	141	142	145	143	2	1.19
V	126	128	122	125	2	1.99
Zn	75	81	74	77	3	4.03
Cu	23	27	24	25	2	6.89
Pb	21	18	15	18	2	13.61

Table II-2. Precision of some trace elements based on triplicate analyses of two carbonate rock samples and one slate sample from the Dome Mine.

SD: one standard deviation.
CV %: coefficient of variation.
All data in ppm.

	SCo-1		JB-1			JG-1			PCC-1	
	1	2	1	2	1	1	2	1	1	2
SiO2	68.56	67.91	52.85	53.32	73.77	72.32	72.75	44.02	44.39	44.24
Al2O3	15.03	14.68	14.58	14.85	14.46	14.37	14.29	0.69	0.81	0.78
Fe2O3	5.66	5.59	8.94	9.17	1.94	2.13	2.15	8.79	8.65	8.82
MgO	2.98	2.96	7.99	7.90	0.26	0.73	0.74	45.56	45.45	45.60
CaO	2.91	2.83	9.32	9.49	1.98	2.21	2.19	0.70	0.50	0.54
Na2O	0.97	1.02	3.02	2.85	2.95	3.69	3.41	0.05	0.05	0.01
K2O	2.97	3.02	1.56	1.45	4.25	4.08	3.97	0.04	0.01	0.004
TiO2	0.64	0.66	1.30	1.37	0.24	0.28	0.26	0.01	0.01	0.02
MnO	0.06	0.05	0.16	0.16	0.06	0.07	0.06	0.15	0.13	0.13
P2O5	0.23	0.24	0.28	0.27	0.09	0.12	0.10	0.01	0.01	0.002
Total	100.00	100.00	100.00	100.00	100.00	100.00	100.00	100.00	100.00	100.00
Rb										
Sr										
Y										
Zr										
Nb										
Ni			139	139		8	6		2450	2339
Cr			396	405		59	53		2810	2730
V			222	211		21	24		27	30
Zn			79	84		38	41		43	36
Cu			60	56		4	1.5		9	11.3
Pb										

		NIM-P		NIM-N		NIM-D		Mica-Fe		Mica-Mg	
	1	1	2	1	2	1	2	1	2	1	2
SiO2	52.37	52.61	51.28					35.17	35.28	39.96	39.28
Al2O3	4.07	4.31	4.19					20.06	20.00	16.08	15.53
Fe2O3	13.43	13.08	12.80					26.56	26.31	10.04	9.70
MgO	26.40	26.35	25.42					4.66	4.67	21.28	20.92
CaO	2.74	2.68	2.67					0.39	0.44	0.05	0.08
Na2O	0.36	0.46	0.37					0.45	0.31	0.16	0.12
K2O	0.11	0.09	0.09					9.27	8.97	10.49	10.26
TiO2	0.21	0.19	0.20					2.61	2.56	1.71	1.67
MnO	0.26	0.20	0.22					0.35	0.36	0.23	0.27
P2O5	0.03	0.02	0.02					0.49	0.46	0.01	0.01
Total	100.00	100.00	100.00					100.00	100.00	100.00	100.00
Rb	7	8	5	8	6	1	-				
Sr	34	33	32	254	260	3	3				
Y	8	6	5	8	7	5	-				
Zr	34	8	30	20	23	27	20				
Nb	3	0.4	-	2	2	0.3	-				
Ni											
Cr											
V											
Zn											
Cu											
Pb	8					5	7				

Table II-3. Accuracy of major and selected trace element determinations of reference standards.
1: present study, 2: Govindaraju (1984).

Fusion pellets (major elements)	wt%	Powder pellets (trace elements)	ppm
SiO2	0.25	Rb	5
Al2O3	0.10	Sr	2
Fe2O3	0.10	Zr	5
MgO	0.10	Nb	2
CaO	0.10	Ni	3
Na2O	0.20	Cr	10
K2O	0.10	V	2
TiO2	0.01	Zn	3
MnO	0.05	Cu	3
P2O5	0.01	Pb	6

Table II-4. Lower detection limit of XRF for major and trace elements. (O.Murdoch, pers. communication, 1985).

present study and the concentrations proposed or recommended by Govindaraju (1984) (Table II-3).

The lower detection limits for major elements and selected trace elements are listed in table II-4. These values are specific for the XRF equipment used in the present study.

II.2. Instrumental NAA

Duplicate analyses of different aliquots of the same sample were carried out to evaluate the reproducibility of Au, As, Sb, and REE. Results are listed in tables II-5A and II-6A. Reproducibility is good for As and Sb. Precision is poor for the REE at the low abundance levels present in the carbonate rocks from the Dome Mine, and in particular for the mineral separates from the QFV (Table II-6A). If the rock standard STM-1 is used as an unknown sample, it is recognized that at higher REE concentrations the reproducibility is much better (Table II-6B). Inhomogeneous Au distribution in the same sample is indicated by the large variations that exist between some of the duplicate analyses (Table II-5A).

Accuracy was estimated by analyzing the rock standards SGR-1 and SCo-1 for Au, As, and Sb; and STM-1 for REE and comparing them to values from the literature (Tables II-5B and II-6B). There is a very good agreement for As and REE. Sb is systematically higher in analyses

	807		12504		12508		12513		13002	
	#1	#2	#1	#2	#1	#2	#1	#2	#1	#2
Au	41	32	62	50	46	102	393	493	127	101
As	47	46	634	636	1464	1386	73	69	1532	1583
Sb	6	6	8	7	12	13	3	3	25	25

Table II-5A. Duplicate analyses of carbonate rocks and one komatiite sample (807) for As (ppm), Sb (ppm), and Au (ppb).

	SGR-1					SCo-1			
	#1	#2	#3	Litt.	Ref.	#1	#2	Litt.	Ref.
Au	25	93	63	8.9 & 10.8	1 & 2	5	23	2.11 & 2.72	1 & 2
As	70	66	65	65	3	13	13	15	3
Sb	7	6	7	3.5	3	5	5	2.5	3

Table II-5B. Analyses of standards for Au (ppb), As (ppm), and Sb (ppm).
#1,#2,#3: this study. Litt.: values found in literature.
Ref.1: Schwarz and Barker (1976). Ref.2: Anoshin and Perezhogin (1976).
Ref.3: Govindaraju (1984).

2

	17002CFU		12506		120196CHL	
	#1	#2	#1	#2	#1	#2
La	ND	ND	0.07	0.12	ND	0.44
Ce	5.11	ND	0.43	1.13	ND	0.13
Nd	4.41	0.38	ND	1.31	2.56	3.62
Sm	0.34	0.25	0.21	0.16	ND	0.26
Eu	0.15	0.22	0.20	0.17	0.05	0.25
Tb	0.08	ND	0.12	0.19	0.04	0.19
Tm	0.49	0.19	0.14	0.16	ND	ND
Yb	0.65	0.29	0.40	0.65	0.18	0.36
Lu	0.06	0.11	0.40	0.04	0.04	0.17

Table II-6A. Duplicate analyses for low REE-content rock material. ND: not detected. All data in ppm. 17002CFU: fuchsite banding. 120196CHL: chlorite banding. 12506: carbonate wall rock.

	#1	#2	#3	Ref.
La	153	160	153	150
Ce	259	251	259	260
Nd	90	78	78	78
Sm	14	14	14	13
Eu	3.6	3.5	3.6	3.7
Tb	2.7	2.8	2.5	1.6
Tm	2.4	3.4	3.0	-
Yb	4.0	4.3	4.0	4.3
Lu	0.7	1.0	0.7	-

Table II-6B. Replicate analyses of the STM-1 standard for REE compared to REE-concentrations recommended in the literature. Reference: Govindaraju (1984). All data in ppm.

from the present study. Au shows highly discrepant concentrations between measurements in the present study and abundances obtained previously by other authors. Moreover, reproducibility between each set of Au-analyses is very poor. Au-concentrations obtained in the present study are considered to be unreliable, and were not used. Discussion of the distribution of gold in the QFV environment is based on muck sample analyses provided by the Dome Mine Geology Department.

II.3. Lead isotope analysis

Reproducibility of lead isotopes ratios ~~is~~ very good for galenas (see duplicate analyses in table 8-4), and acceptable for whole rocks (Table 8-2). Replicate analyses of the standard NBS SRM 981 obtained in the course of the entire study are in good agreement with the recommended value for NBS SRM 981 (Table II-7), thus indicating a good accuracy of the Pb isotopic measurements.

The two main errors that affect lead isotope analyses are mass dependent isotopic fractionation in the mass spectrometer and the uncertainty in measurement of the least abundant isotope ^{204}Pb. Both errors yield theoretical error lines in a $^{207}Pb/^{204}Pb$ vs $^{206}Pb/^{204}Pb$ diagram (Doe et al., 1966), which have slopes of 1.37 for mass fractionation and 0.91 for inaccuracy in ^{204}Pb measurement.

Date	206Pb 204Pb	207Pb 204Pb	208Pb 204Pb
01/08/87	16.907	15.459	36.598
01/08/87	16.859	15.403	36.428
04/01/87	16.920	15.475	36.627
04/01/87	16.933	15.498	36.693
04/20/87	16.898	15.460	36.558
04/20/87	16.918	15.480	36.622
04/20/87	16.929	15.486	36.662
07/31/87	16.908	15.465	36.606
07/31/87	16.932	15.490	36.661
09/09/87	16.911	15.483	36.647
09/09/87	16.865	15.429	36.467
09/09/87	16.894	15.458	36.549
Recommended value:			
	16.937	15.461	36.721

Table II-7. Lead isotope compositions obtained in the present study for the standard NBS SRM 981. Ionization took place at 1240 degrees C.

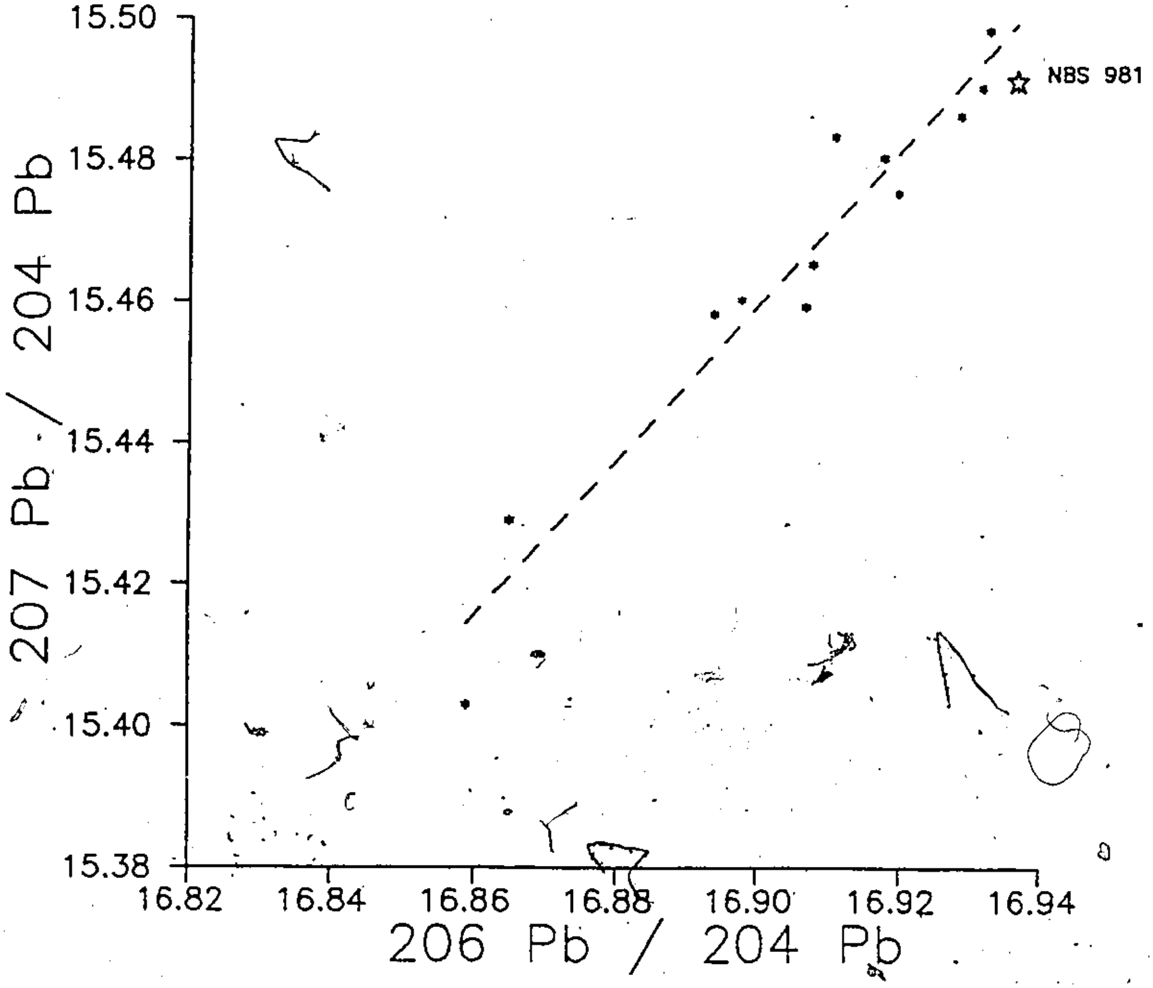

Figure II-1. Experimental error line defined by replicate analyses of the standard NBS SRM 981.

Small black dots: measurement of NBS SRM 981 in the present study.
Open star: recommended lead isotope composition of the standard NBS SRM 981.

The replicate analyses of NBS SRM 981 also define an array in a $^{207}Pb/^{204}Pb$ vs $^{206}Pb/^{204}Pb$ diagram (Fig. II-1). This "error line" has a slope of 1.08, which is intermediate between the two theoretical error lines, thus indicating that lead isotope measurements have been affected more or less equally by both analytical errors. Both errors explain the spread found in galena compositions in figure 8-2.

All data have been corrected for mass isotopic fractionation using the following procedure:

corrected composition=(measured composition)/(1-F x n/100), where F corresponds to the percentage of fractionation per atomic mass unit, and n to the mass spread of the ratio which is considered in the correction procedure, for instance for the $^{208}Pb/^{204}Pb$ ratio n=4. The percentage of fractionation per atomic mass unit can be deduced from comparison between the measured and the recommended lead composition of the standard. In the present study this was found to be 0.06% in the average.

II.4. Fluid inclusion microthermometry

The operation of the U.S. Geological Survey gas-flow heating-freezing stage, device used in the present research are described in detail by Woods et al. (1981) and Roedder (1984, chap.7). Measurements of temperature are carried out with a thermocouple that rests directly on the sample under study. The thermocouple is attached to a trendicator which indicates the value of the temperature.

The temperature scale has been adjusted following the two procedures suggested by the instruction manual provided by Fluid Inc. System. These are:

1) The thermocouple attached to a thermometer has been immerged into an ice bath. When the temperature stabilized at 0.0°C, the trendicator was set to read this temperature as well.

2) Approximately 3 lbs of triply distilled mercury contained in a sealed 125 ml wash bottle were placed into an empty 1-2 liter insulated dewar. The thermocouple was inserted all the way into the straw protruding from the wash bottle. Liquid N_2 was poured into the dewar until the trendicator indicated approximately -50°C. At this temperature the mercury was frozen. Temperature slowly increased until it reached the invariant melting point of mercury at -38.9°C. The trendicator was then set to yield the mercury melting temperature.

Points 1 and 2 were alternatively repeated until both temperatures 0.0°C and -38.9°C were obtained without having to make any further adjustments. This scale adjustment was carried out every time when the thermocouple was changed, or when the power of the trendicator was shut off.

Accuracy of temperature measurements was evaluated by using "home-made" standards and with synthetic fluid inclusions purchased from Fluid Inc. System. The type of synthetic fluid inclusions used in the present study is described by Sterner and Bodnar (1984). Four types of inclusions are suggested to be used as reliable standards, since they exhibit phase transitions that are sufficiently uniform throughout the sample:

1) Melting of solid CO_2 in H_2O-CO_2 inclusions, containing 25 mole % CO_2, that occurs at -56.6°C.

2) Final melting of ice in 10 wt% NaCl aqueous inclusions, which occurs at -6.6°C.

3) Melting of ice in pure aqueous inclusions, which takes place at 0.0°C.

4) Homogenization of pure aqueous inclusions to the critical temperature whcih occurs at 374.1°C.

"Home-made" standards were prepared according to the sealed glass capillary method described by Roedder (1984, pp.204-206). The liquids and solids used in the present study as standards were selected among the materials suggested by Roedder (1984, table 7-4, pp.208-210). These are: n-hexane (melting point:-95.0°C), n-heptane (-90.6°C), n-decane (-29.7°C), triple distilled H_2O (0.0°C), azobenzene (+68.0°C), sulfur (+112.8°C), sodium nitrate (+306.8°C), and tellurium (+449.5°C).

Melting temperatures were repeatedly measured in the course of the present study. All phase transitions were measured on the heating cycle, at a heating rate less than 2°C/minute, and when possible at 0.5°C/minute. The differences between melting points given in the literature and melting temeperatures obtained in the present study are represented in figure II-2. The agreement between recommended melting temperatures and temperatures measured herein is very good at freezing temperatures. The difference between both experimental and recommended temperatures is less than 1°C, in particular in the range of 0° to −56.6°C it is less than 0.5°C. The largest discrepancy is obtained for azobenzene and sulfur at +68°C and +112.8°C. At high temperatures over 300°C the agreement is within 2°C, which is also acceptable. The temperature discrepancy for both azobenzene and sulfur may be attributed to impurities in the standards, small thermal gradients, moisture in the sample. Thus, temperature of phase changes obtained on the samples from the QFV are reported without any correction.

Figure II-2. Temperature difference between theoretical melting temperatures and measured melting temperatures of selected standard solutions.

SFI: synthetic fluid inclusion.
$\Delta T = T_{theoretical} - T_{measured}$.

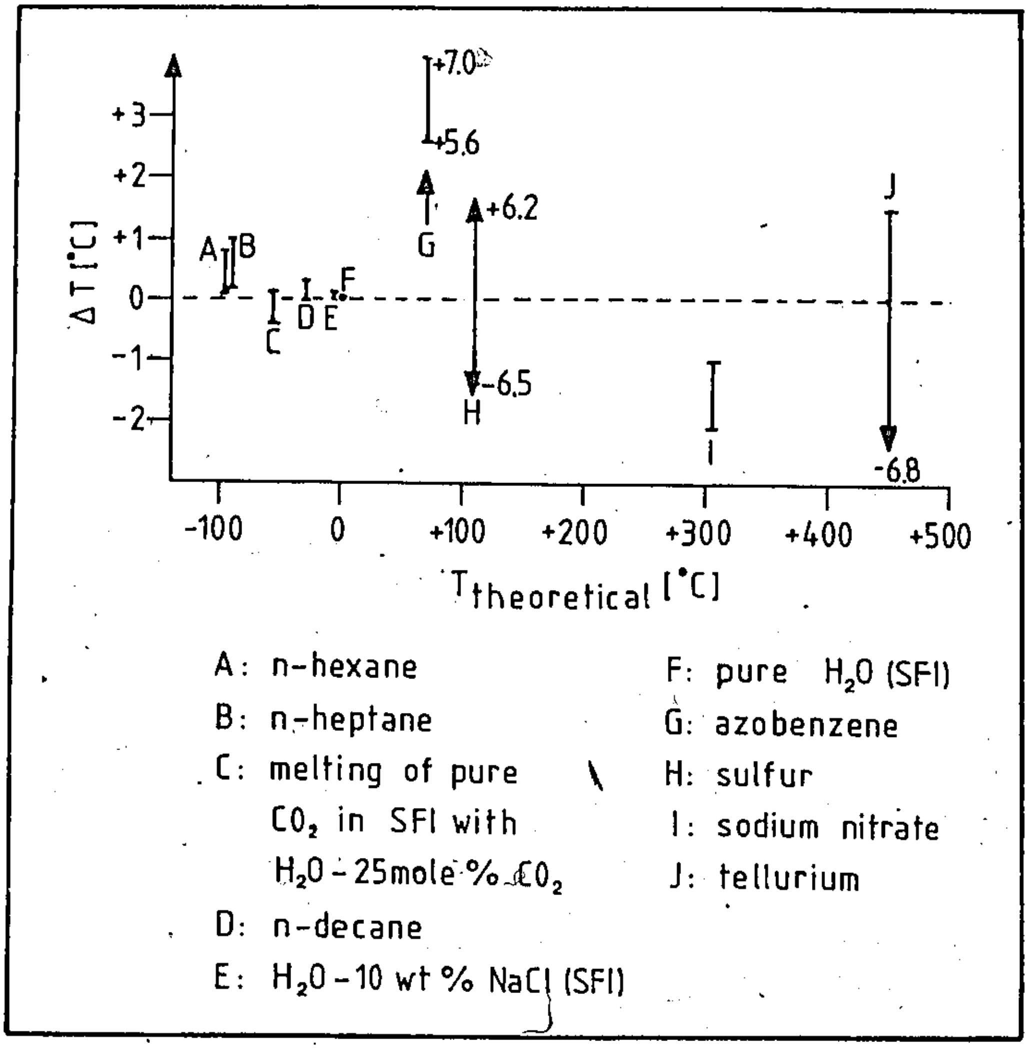
+7.0
+5.6
+6.2
-6.5
-6.8
+3
+2
+1
0
-1
-2
ΔT [°C]
A
B
C
D
E
F
G
H
I
J
-100
0
+100
+200
+300
+400
+500
T theoretical [°C]
A: n-hexane
B: n-heptane
C: melting of pure CO_2 in SFI with H_2O - 25mole % CO_2
D: n-decane
E: H_2O - 10 wt % NaCl (SFI)
F: pure H_2O (SFI)
G: azobenzene
H: sulfur
I: sodium nitrate
J: tellurium

Date	Melting point [°C]	Operator
02/21/86	-56.5	3
02/21/86	-56.5	3
03/09/86	-56.6	1
03/09/86	-56.5	1
04/13/86	-56.8	2
04/13/86	-56.7	2
04/17/86	-56.8	3
04/17/86	-56.6	3
07/11/86	-56.8	3
07/11/86	-56.7	3
08/27/86	-57.0	3
08/27/86	-56.8	3
08/27/86	-56.8	3

Table II-8A. Replicate measurements of melting temperature of pure CO_2 in synthetic inclusions. Melting of pure CO_2 should occur at -56.6 °C.

Date	Melting point [°C]	Operator
02/12/86	0.0	3
03/11/86	0.0	1
03/11/86	0.0	1
03/12/86	0.1	1
03/12/86	0.1	1
04/09/86	0.0	2
04/20/86	0.0	2
08/27/86	0.0	3
08/27/86	0.0	3

Table II-8B. Replicate measurements of melting temperature of pure H_2O in synthetic inclusions and "home-made" standards. Melting of pure H_2O should occur at 0.0 °C.

Operators are: 1 - J.Inman. 2 - B. McInnes. 3 - R.Moritz.

Date	Melting point [°C]	Operator
03/15/86	375.5	1
03/15/86	375.2	1
03/16/86	375.1	3
03/16/86	375.2	3
03/16/86	375.3	3
03/16/86	375.4	3
03/16/86	375.5	3
03/16/86	375.4	3
03/16/86	375.4	3
03/16/86	375.7	3
03/16/86	375.7	3
03/16/86	375.8	3

Table II-9. Replicate measurements of critical homogenization phenomena of pure H_2O inclusions. Theoretically, critical homogenization of H_2O should take place at 374.1°C.
Operators are : 1 - J.Inman. 3 - R.Moritz.

Precision of measurements has been estimated by repeated runs of three synthetic fluid inclusions obtained from Fluid Inc. System, and described by Sterner and Bodnar (1984). Replicate melting temperature measurements of CO_2 and H_2O, and critical homogenization temperatures are listed in tables II-8 and II-9. It appears that results are reproducible within ±0.3°C from -60° up to about +400°C.

APPENDIX III

LEAD MODEL CALCULATIONS

III.1. Constants and symbols used in the Pb-Pb age and model calculations

Constants and symbols are listed in table III.1. It must be noted that constants vary from one lead evolution model to the other. The single-stage model that implies constant unperturbated production of radiogenic lead since the earth was formed sets the start of the evolution of any radiogenic component at 4.55 x 10^9 years, the age of the Earth (Patterson, 1956), and uses the primeval lead isotope ratios of the Earth (Tatsumuto et al., 1973) to model any radiogenic lead evolution. Whereas Stacey and Kramers (1975) suggested that 3.7x10^9 years ago the U/Pb ratio of the source reservoir was drastically modified by geochemical differentiation, thus setting a new starting time and new initial lead isotope ratios for the modeling of radiogenic lead. Recently, Thorpe (1982) proposed on the basis of lead minerals associated with Superior Province syngenetic and syn-volcanic deposits a source age of 4.06 x 10^9 years (T^*), with initial $^{206}Pb/^{204}Pb$ and $^{207}Pb/^{204}Pb$ ratios which are respectively 10.242 and 11.9556.

SYMBOL	MEANING	VALUE	REF.
λ_1	Decay constant for ^{238}U	1.55125×10^{-10}/year	1
λ_2	Decay constant for ^{235}U	9.8485×10^{-10}/year	1
k	Present $^{238}U/^{235}U$ ratio	137.88	
μ	Present $^{238}U/^{204}Pb$ ratio	variable	
a_o	Primeval $^{206}Pb/^{204}Pb$	9.307	2
b_o	Primeval $^{207}Pb/^{204}Pb$	10.294	2
T	Age of the earth	4.55×10^9 years	3
T'	Date of geochemical differentiation in Stacey's and Kramers' model (1975)	3.7×10^9 years	
a'	Initial $^{206}Pb/^{204}Pb$ in Stacey's and Kramers' model (1975)	11.152	
b'	Initial $^{207}Pb/^{204}Pb$ in Stacey's and Kramers' model (1975)	12.998	
T^*	Date of source age in in Thorpe's model (1982)	4.06×10^9 years	
a^*	Initial $^{206}Pb/^{204}Pb$ in Thorpe's model (1982)	10.242	
b^*	Initial $^{207}Pb/^{204}Pb$ in Thorpe's model (1982)	11.9556	
m	slope of a secondary isochron		
i	intercept of a secondary isochron and the $^{207}Pb/^{204}Pb$ axis		

Table III-1. Constants and symbols used in the Pb-Pb age and model calculations. Ref.: 1 - Steiger and Jäger, 1977. 2 - Tatsumoto et al., 1973. 3 - Patterson, 1956.

III.2. Calculation of the secondary isochron fitting the distribution of the lead isotope ratios of the porphyries and the slates

If a sample of Pb passed through two U-bearing systems characterized by different $^{238}U/^{204}Pb$ ratios (μ_1 and μ_2), then the $^{206}Pb/^{204}Pb$ and $^{207}Pb/^{204}Pb$ ratios of that sample are :

$$(^{206}Pb/^{204}Pb) = a_o + \mu_1(e^{\lambda_1 T} - e^{\lambda_1 t_1}) + \mu_2(e^{\lambda_1 t_1} - e^{\lambda_1 t_2}) \qquad \text{(III.1.)}$$

$$(^{207}Pb/^{204}Pb) = b_o + (\mu_1/k)(e^{\lambda_2 T} - e^{\lambda_2 t_1}) + (\mu_2/k)(e^{\lambda_2 t_1} - e^{\lambda_2 t_2}) \qquad \text{(III.2.)}$$

where t_1 is the time when Pb was removed from system 1 and transferred to system 2, and t_2 is the time when Pb was removed from system 2 after which its isotopic composition remained constant. $t_2 = 0$, since Pb evolution continues up to the present, when the isotopic composition is determined. T that corresponds to the Single-Stage model, can be exchanged with T' or T^* depending on the model which is preferred. Moreover, we simplify the initial first stage component of equations III.1. and III.2. with A and B respectively. Thus, we obtain :

$$({}^{206}Pb/{}^{204}Pb) = A + \mu_2(e^{\lambda_1 t_1} - 1) \qquad (III.3.)$$

$$({}^{207}Pb/{}^{204}Pb) = B + (\mu_2/k)\ (e^{\lambda_2 t_1} - 1) \qquad (III.4.)$$

Both equations can be combined to eliminate μ_2 :

$$m = \frac{({}^{207}Pb/{}^{204}Pb) - B}{({}^{206}Pb/{}^{204}Pb) - A} = \frac{1}{k}\frac{(e^{\lambda_2 t_1} - 1)}{(e^{\lambda_1 t_1} - 1)} \qquad (III.5.)$$

This is the equation of a family of straight lines passing through a point with A and B as coordinates, and whose slopes are given by :

$$m = \frac{1}{k}\frac{(e^{\lambda_2 t_1} - 1)}{(e^{\lambda_1 t_1} - 1)} \qquad (III.6.)$$

In other words, a two-stage Pb lies on a secondary isochron that passes through a point on the growth curve of system 1 and whose slope depends only on the interval of time t_1-t_2 during which the lead resided in system 2. In the present case, t_1-t_2= 2.685 x 10^9 years. This latter value and equation III.6. were used to calculate the slope of the secondary isochron fitting the distribution of the lead isotopic composition from the porphyries and the slates. This slope has a value of 0.1835.

III.3. Calculation of the μ value of the source reservoir of the porphyries

The $^{206}Pb/^{204}Pb$ and $^{207}Pb/^{204}Pb$ ratios of the porphyry and slate samples lying along the secondary isochron are related to each other by an equation in the form of :

$$(^{207}Pb/^{204}Pb) = i + m\ (^{206}Pb/^{204}Pb) \qquad \text{(III.7.)}$$

The lead isotope ratios of the porphyry and slate samples and the slope m can be used to determine i. The average value obtained for i is 12.029. Thus, i represents the intercept between the secondary isochron and the $^{207}Pb/^{204}Pb$ axis.

The 2.685 x 10^9 years isochron, the secondary isochron with a slope m = 0.1835 and the growth curve of the porphyry source reservoir must have a common intercept. If the lead in the source reservoir of the porphyries had a single stage history before it was incorporated in the intrusions, then its isotopic composition can be written as follows:

$$^{206}Pb/^{204}Pb = a + \mu\ (e^{\lambda_1 T} - e^{\lambda_1 t}) \qquad \text{(III.8.)}$$

$$^{207}Pb/^{204}Pb = b + (\mu/k)\ (e^{\lambda_2 T} - e^{\lambda_2 t}) \qquad \text{(III.9.)}$$

We can use equations III.7., III.8. and III.9. to determine the μ_1 value of this reservoir. It has to be noted that a, b, and T can be the primordial parameters of any of the models presented in part III.1. Equations III.9. and III.7. can be combined in the form of :

$$i + m\,({}^{206}Pb/{}^{204}Pb) = b + (\mu/k)\,(e^{\lambda_2 T} - e^{\lambda_2 t}) \qquad \text{(III.10.)}$$

Equations III.8. and III.10. in turn can be combined as follows :

$$i + m\,[a + \mu\,(e^{\lambda_1 T} - e^{\lambda_1 t})] = b + (\mu/k)\,(e^{\lambda_2 t} - e^{\lambda_2 t}) \qquad \text{(III.11.)}$$

μ_1 can be obtained from this latter equation III.11., since μ remains as the sole unknown.

III.4. Calculation of the time of addition of radiogenic lead to the galenas from the Quartz-Fuchsite vein

This type of calculation is similar to the one for the fitting of the secondary porphyry isochron. The difference is that lead evolution stopped in time, since no radiogenic lead could from in galenas.

The line that fits the distribution of the anomalous galenas has a slope of 0.33. Following an identical demonstration as in point III.2., the slope can be expressed by:

$$m \simeq 1/k \frac{(e^{\lambda_2 t_r} - e^{\lambda_2 t_s})}{(e^{\lambda_1 t_r} - e^{\lambda_1 t_s})} \qquad \text{(III.12.)}$$

t_r represents the time when radiogenic lead started to accumulate, and t_s the time when this radiogenic lead was added to an earlier formed sulfide.

APPENDIX IV

CHEMICAL ANALYSES OF CARBONATE ROCKS

Analyses are given in weight % for the major elements in ppm for the trace elements, and ppb for Ir. All analyses are by XRF unless stated otherwise (NAA, RNAA). Rocks are: carb - carbonate rock, HA - highly altered (carbonate rock rich in fuchsite), kom - komatiite, and talcsch - talc schiste. ND: not detected, blank: element was not analysed for this particular sample.

	606 Carb	801B Kom	807 Kom	8002G Carb	8006Ha Carb	8010A Carb	10015C Carb	12008B Carb	12008D Talcsch	12502 HA
SiO2	22.26	43.05	43.15	28.80	14.59	31.78	28.64	31.81	32.57	38.78
Al2O3	2.49	5.29	4.43	9.88	8.69	5.70	9.33	4.47	4.56	7.01
Fe2O3	6.14	11.42	9.89	9.94	9.05	9.01	15.50	7.83	7.99	7.74
MgO	23.39	25.30	29.99	18.26	20.64	19.97	20.77	16.01	19.61	15.16
CaO	13.12	8.47	4.72	10.62	17.14	11.64	7.33	14.22	11.60	10.17
Na2O	<0.20	<0.20	<0.20	<0.20	<0.20	<0.20	<0.20	<0.20	<0.20	0.63
K2O	<0.10	<0.10	<0.10	0.17	0.19	0.17	<0.10	<0.10	<0.10	0.16
TiO2	0.16	0.39	0.32	0.53	0.40	0.25	0.56	0.29	0.23	0.24
MnO	0.16	0.14	0.15	0.16	0.25	0.20	0.13	0.26	0.15	0.16
P2O5	0.01	0.03	0.07	0.01	0.01	0.17	0.02	0.02	0.02	0.04
LOI	32.25	5.87	7.15	21.45	28.99	21.05	17.70	25.02	23.24	19.91
TOTAL	100	100	100	100	100	100	100	100	100	100
CO2	32.35	0.91	0.22	16.06	25.38	17.08	16.29	18.84	20.41	16.53
S	0.01	0.02	0.06				1.93	0.05	0.03	0.03
Rb	<5	<5	<5	5	5	5	<5	<5	<5	5
Sr	494	19	15	195	500	213	339	399	550	475
Y	9	9	9	14	12	11	12	9	9	9
Zr	38	38	37	39		25	43	38	39	34
Nb	2	<2	4	8	5	4	<2	4	3	<2
Ba (NAA)	22	28	1			ND	46	22	9	39
Th (NAA)	ND	0.1	ND			0.1	ND	ND	ND	ND
Hf (NAA)	0.2	0.7	0.8			0.3	0.7	0.4	0.5	0.4
Cs (NAA)	ND	0.8	0.4			ND	ND	ND	0.4	0.5
Ta (NAA)	0.2	ND	ND			0.3	0.2	0.3	2.5	0.3
Ni	1376	1329	1531	825	1428	1011	523	840	766	1060
Ni (NAA)	1151	1146	1625			1350	547	1066	813	931
Cr	1658	2370	2460	3753	3557	2528	3200	2070	1790	2143
Cr (NAA)	1303	3263	2298			2046	2616	2011	1626	1865
Sc (NAA)	17	34	28			29	61	27	27	26
V	53	35	134	192	137	113	176	120	97	95
Pb	<6	<6	8	24	27	16	7	21	9	9
Zn	27	100	49	139	110	83	83	58	40	51
Cu	5	34	19	9	14	10	132	3	22	13
Au (NAA)		17	32			141	152	150		40
As (NAA)		1	47			1482	258	1812		731
Sb (NAA)	2	1	6			11	3	15		8
Ir (RNAA)			2.98							
La (NAA)	0.80	1.21	0.74			ND		ND		
Ce (NAA)	1.59	1.94	1.60			2.89		1.53		
Nd (NAA)	ND	3.00	ND			ND		ND		
Sm (NAA)	0.33	0.78	0.65			0.60		0.49		
Eu (NAA)	0.23	0.35	0.24			0.50		0.61		
Tb (NAA)	0.06	0.21	ND			0.21		0.15		
Tm (NAA)	ND	ND	ND			ND		ND		
Yb (NAA)	0.52	0.59	0.72			0.67		0.54		
Lu (NAA)	0.09	0.10	0.10			0.12		0.07		

	12504	12506	12507	12508	12521	12523	12526	12527	12528	12530
	HA	HA	HA	HA	HA	HA	HA	HA	HA	Carb
SiO2	34.30	27.48	20.58	30.27	31.03	27.20	31.54	35.52	35.21	33.19
Al2O3	4.31	2.97	3.01	3.28	5.16	1.96	6.05	5.31	4.90	5.24
Fe2O3	9.83	8.32	11.16	10.33	10.07	8.00	10.25	9.52	9.60	8.62
MgO	18.61	22.88	22.69	20.00	14.53	14.03	22.89	19.33	21.93	22.05
CaO	7.34	6.23	8.77	7.50	14.05	17.86	3.74	6.63	3.05	5.38
Na2O	0.28	0.48	<0.20	0.33	0.32	<0.20	<0.20	<0.20	<0.20	<0.20
K2O	0.15	0.74	0.67	0.22	0.20	0.57	0.14	0.15	0.23	<0.10
TiO2	0.26	0.17	0.29	0.22	0.32	0.19	0.32	0.28	0.30	0.23
MnO	0.16	0.13	0.20	0.15	0.20	0.33	0.18	0.13	0.17	0.17
P2O5	0.07	0.06	0.07	0.06	0.03	0.01	0.15	0.09	0.05	0.13
LOI	24.70	30.34	32.47	27.63	24.09	29.66	24.65	22.90	24.51	24.89
TOTAL	100	100	100	100	100	100	100	100	100	100
CO2	22.86	30.13	33.29	27.00	23.03	30.70	22.32	21.20	22.83	22.66
S	0.04	0.05	0.05	0.03	0.06	0.23	0.03	0.05	0.05	0.04
Rb	<5	18	19	6	<5	15	<5	5	6	<5
Sr	430	330	475	395	457	558	186	308	152	268
Y	8	12	10	10	12	15	11	11	12	12
Zr	35	27	36	32	36	38	23	30	23	
Nb	<2	<2	<2	3	3	3	2	2	3	2
Ba (NAA)	0	82	58	10	ND	27	ND	31	27	50
Th (NAA)	ND	ND	ND	0.1	ND	ND	ND	ND	ND	ND
Hf (NAA)	0.4	0.3	0.4	0.4	0.4	0.3	0.7	0.4	0.6	0.2
Cs (NAA)	ND	0.7	0.3	0.2	ND	0.2	ND	0.1	0.1	0.1
Ta (NAA)	0.3	0.6	0.4	0.4	0.3	0.5	0.2	0.3	0.3	0.4
Ni	930	1329	980	810	677	668	1073	895	1080	1079
Ni (NAA)	773	1446	1242	990	829	769	945	816	1204	1210
Cr	2552	2190	2590	2270	2070	1427	3257	2520	2880	2670
Cr (NAA)	1968	1556	1924	1654	1865	1421	2260	1988	2069	2000
Sc (NAA)	30	20	26	23	31	26	33	30	30	29
V	129	115	144	123	143	64	206	147	177	189
Pb	8	11	16	9	9	8	10	10	10	8
Zn	63	58	68	70	61	46	68	45	63	71
Cu	12	4	14	16	4	17	14	13	9	4
Au (NAA)	51		81	61	395	97	36	98	82	89
As (NAA)	635		1744	1425	1140	1071	110	666	1822	1157
Sb (NAA)	7	9	17	13	9	9	1	12	15	20
Ir (RNAA)	1.48						1.94	1.26		3.53
La (NAA)		0.71					0.71	0.42	0.73	0.23
Ce (NAA)		1.30					1.78	1.43	2.74	2.38
Nd (NAA)		ND					ND	ND	ND	ND
Sm (NAA)		0.33					0.53	0.42	0.35	0.37
Eu (NAA)		0.14					0.13	0.22	0.22	0.22
Tb (NAA)		0.08					0.20	0.16	0.13	ND
Tm (NAA)		ND					ND	ND	ND	0.07
Yb (NAA)		0.32					0.50	0.71	0.51	0.67
Lu (NAA)		0.05					0.13	0.13	0.13	0.09

	13002 Carb	16001F Carb	17002B Carb	10001D Carb	10001E Carb	10001F Carb	10001O Carb	10001P Carb	10001Q Carb	10006A Carb
SiO2	26.56	29.24	30.42	29.88	34.60	33.49	30.25	30.00	35.56	32.45
Al2O3	3.82	6.25	4.10	6.89	4.70	4.31	4.70	5.71	5.03	3.70
Fe2O3	6.64	10.56	8.74	10.10	9.25	8.34	9.68	11.01	9.66	8.29
MgO	18.22	19.24	22.57	18.15	19.17	17.78	20.99	21.36	20.08	20.90
CaO	15.91	11.15	6.87	10.19	7.01	9.83	4.42	5.70	4.97	6.93
Na2O	<0.20	<0.20	<0.20	<0.20	<0.20	<0.20	<0.20	<0.20	<0.20	<0.20
K2O	<0.10	<0.10	<0.10	0.12	0.11	0.11	0.11	0.12	0.10	0.10
TiO2	0.20	0.37	0.19	0.31	0.26	0.22	0.26	0.29	0.27	0.15
MnO	0.26	0.18	0.13	0.29	0.15	0.16	0.14	0.16	0.12	0.15
P2O5	0.01	0.01	0.02	0.01	0.01	0.01	0.01	0.01	0.01	0.01
LOI	28.34	22.92	26.90	23.98	24.70	25.71	25.00	25.61	24.10	27.24
TOTAL	100	100	100	100	100	100	100	100	100	100
CO2	26.56	21.21	25.37	21.35	22.70	24.11	22.78	23.06	21.88	25.73
S	0.06	0.46	0.04							
Rb	<5	<5	<5	5	5	5	5	5	5	5
Sr	384	346	266	414	244	375	173	273	213	225
Y	14	14	11	12	13	11	9	15	14	11
Zr										
Nb	<2	3	<2	8	8	6	4	9	9	10
Ba (NAA)	21	36	13							
Th (NAA)	ND	ND	ND							
Hf (NAA)	0.4	0.7	0.5							
Cs (NAA)	0.4	ND	0.1							
Ta (NAA)	0.2	0.8	0.4							
Ni	879	501	682	1212	905	860	1278	1141	1089	1018
Ni (NAA)	1066	567	986							
Cr	1710	1945	2089	3560	2791	2234	2915	3156	2907	1769
Cr (NAA)	1613	1654	1634							
Sc (NAA)	24	41	24							
V	82.	140	99	129	113	106	113	150	129	71
Pb	9	10	10	13	8	12	7	11	8	47
Zn	52	70	73	98	73	66	80	106	70	73
Cu	28	24	17	70	16	43	17	10	27	10
Au (NAA)	99	100	29							
As (NAA)	1558	430	1492							
Sb (NAA)	25	6	11							
Ir (RNAA)										
La (NAA)	1.46	0.61	ND							
Ce (NAA)	6.20	4.71	1.22							
Nd (NAA)	3.78	ND	0.78							
Sm (NAA)	1.36	0.79	0.38							
Eu (NAA)	2.36	0.45	0.24							
Tb (NAA)	0.55	ND	0.17							
Tm (NAA)	ND	ND	ND							
Yb (NAA)	0.79	0.85	0.73							
Lu (NAA)	0.19	0.16	0.16							

	10006E	10007A	10007E
	Carb	Carb	Carb
SiO2	33.47	35.19	35.09
Al2O3	4.68	4.30	4.80
Fe2O3	10.42	8.53	8.35
MgO	19.36	17.45	18.83
CaO	6.67	9.26	7.81
Na2O	<0.20	<0.20	<0.20
K2O	0.11	0.10	0.11
TiO2	0.32	0.23	0.26
MnO	0.16	0.14	0.13
P2O5	0.02	0.01	0.02
LOI	24.70	24.74	24.40
TOTAL	100	100	100
CO2	22.42	22.67	22.12
S			
Rb	5	5	5
Sr	195	288	256
Y	13	12	10
Zr			
Nb	7	6	7
Ba (NAA)			
Th (NAA)			
Hf (NAA)			
Cs (NAA)			
Ta (NAA)			
Ni	1284	955	928
Ni (NAA)			
Cr	2833	2105	2647
Cr (NAA)			
Sc (NAA)			
V	127	103	106
Pb	11	6	15
Zn	72	52	64
Cu	11	41	45
Au (NAA)			
As (NAA)			
Sb (NAA)			
Ir (RNAA)			
La (NAA)			
Ce (NAA)			
Nd (NAA)			
Sm (NAA)			
Eu (NAA)			
Tb (NAA)			
Tm (NAA)			
Yb (NAA)			
Lu (NAA)			